IRREVERSIBLE BREAKDOWN OF HIV-1 BY PEPTIDE TRIAZOLE THIOLS AND MULTIVALENT GOLD NANOPARTICLE CONJUGATES

A Thesis

Submitted to the Faculty

of

Drexel University

by

Arangassery Rosemary Bastian

in partial fulfillment of the

requirements for the degree

of

Doctor of Philosophy

May 2014

Dedications

To my papa and mummy – A.F Sebastian and Gracy Sebastian,

For constantly giving me the inspiration, support and love to move forward and succeed

To my brother, sister in law– Pradeesh Bastian and Sona Pradeesh,

For keeping me on track, listening to my scientific thoughts with patience and supporting me through my PhD

To my little nephews - Ryan Pradeesh and Ethan Pradeesh,

For all their love and always reminding me to think like a child

To my husband – Abin Sebastian Thayil,

For his support, patience and unconditional love

Acknowledgements

I would like to express my gratitude to my Advisors Dr. Irwin Chaiken and late Dr. Elisabeth Papazoglou for giving me the support and constantly supporting my intellectual curiosity in every way and giving me inspiration to go through this PhD. I would like to especially thank Dr. Elisabeth Papazoglou for having faith in me, accepting me into the program, always giving me inspiration and love and having faith in me to success every time. I would like to provide my deepest gratitude for Dr. Irwin Chaiken for supporting and guiding me through my highs and lows and always having faith in me.

Special thanks to my advisory committee Dr. James Hoxie, Dr. Adrian Shieh, Dr. Andres Kriete, Dr. Kenneth Barbee, Dr. Jeffrey Jacobson and Dr. Cameron Abrams for their constructive criticisms and constant feedback through my PhD.

I am thankful to Dr. Hoxie's lab especially Beth Haggarty who opened her lab for me and helped me conduct work in a BSL2 plus facility. I am thankful for Dr. Farida Shaheen for helping me in the University of Pennsylvania CFAR. I am grateful for Dr. Kevin Freedman for helping me with electron microscopy.

I am thankful to my colleagues and friends Dr. Rachna Arora, Lauren Baily, Ramalingam Venkat Kalyana Sundaram, Ali Emileh, Aakansha Nangarlia, Charles Ang, Dr. Mark Contarino, Dr. Kantharaju, Armin Darvish, Caitlin Duffy, Dr. Karyn McFadden, Andrew Holmes, Pamela Kubinski, Dr. Diogo Moreira, Dr. Umashankara Muddagowda, Dr. Srivats Rajagopal, Dr. Ferit Tuzer, Yu-Hung Huang, Kevin Lam,

Amanda Hoffman, Dr. Chetana Sunkari, Dr. Nachiket Vaze, John Alamia and Thao Nguyen for guidance, sharing resources, insightful discussions and feedback.

Table of Contents

List of Tables

List of Figures

Abstract

Irreversible Breakdown of HIV-1 by Peptide Triazole Thiols and Multivalent Gold Nanoparticle Conjugates
Arangassery Rosemary Bastian

The HIV entry is a critical multi-stage process which leads to attachment to the cell receptor followed by co-receptor binding leading to a conformation change in the HIV envelope spike leading to membrane fusion. The peptide triazoles developed in the Chaiken lab has previously been established to function as dual antagonists of the binding of gp120 at its host cell receptor binding sites for both CD4 and CCR5/CXCR4 and have shown to have broad neutralization In Vitro. In this work we showed that a representative member of this class, peptide triazole thiol, led to HIV inhibition but also leads to irreversible lysis and complete inactivation of cell-free HIV-1. Further to improve the potency of these peptide triazole thiol inhibitors, I created multivalent displays of KR13 on gold nanoparticles that led to a drastic potency increase in inhibition of HIV-1.

My research is focused on understanding the mechanism of action of the peptide triazole thiol and its gold nanoparticle conjugates that lead to the virolysis action of HIV-1. In order to study this intriguing breakdown of HIV-1, my studies focused on kinetic and thermodynamic studies. This included understanding the fate of several important viral proteins, including gp120, gp41 and p24, time dependent inhibition of viral entry into host cells and the morphological and biological state of the residual virus. Further the molecular, physical and functional transformations of the gold nanoparticle peptide

conjugates and how these properties affect their virolytic function were tested. From these studies it is conclusive that the peptide triazole thiol virolysis event does follow a time-dependent breakdown pathway of the viral machine that eventually leads to complete disruption of the virus. A clear correlation between peptide triazole thiol dependent HIV-1 virolysis and HIV-1 – host cell fusion was observed. Gold nanoparticle peptide triazole conjugate studies showed that the gold nanoparticle inhibitor virolysis works by a different mechanism all together. We further showed that increasing size of the nanoparticle and density of peptide coverage led to an inhibitor with almost 2000 fold enhancement of its anti-viral potency. These studies therefore have led to two major findings; one, the discovery of an innovative class of HIV-1 inhibitors that that lead to complete irreversible breakdown of the virus by hijacking the virus-cell fusion mechanism and two, the proof of concept model of nanoparticle-inhibitor constructs that have opened up the field to the rules required for development of highly potent nanoparticle inhibitor constructs that irreversibly lyse the virus. These findings have thereby given the HIV-1 field as well as the nanomedicine field an innovative approach that can be further developed and nurtured.

Summary

The human immunodeficiency virus which is the viral precursor that is responsible for the disease that is still a challenge and an epidemic, AIDS [4-6]. Several top physicians as well as scientists in the field have been trying to combat this virus and trying to inhibit the infection and spread of the disease. Due to the constant mutation tendencies of the HIV virion it has become a big challenge to target this virus and eradication of the virus infection all together [7]. Our group at Drexel University College of medicine has developed several inhibitors that target the virus directly that not only leads to very potent entry inhibitors but further have gone a step further to create microbicides that target the virion Env and lead it to irreversible self-destruction[8-10]. This innovative approach has led to the development of a class of microbicides that can be used at several stages of AIDS progression which include, initial entry, reduction of new virus production as well as cell-cell transmission of the virion leading to complete virus abolition of the disease progression.

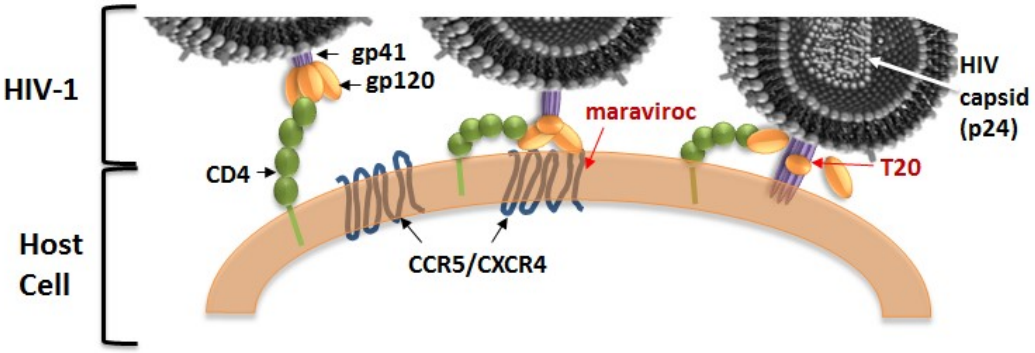

Figure 1: Fusion of HIV-1 with host cell. The HIV proteins gp120 and gp41, together known as the HIV-1 spike interacts with the receptor CD4 and coreceptor CCR5 or CXCR4. The gp120 sheds off the spike and the gp41 is exposed on the cell surface. Gp41 follows a 6-helix bundle formation and the virus and cell surface fuse and the capsid is released. The inhibitors that are currently approved for therapy that target HIV-1 fusion with cell are indicated in red with maraviroc that targets the co-receptor, CCR5 binding to gp120 and T20 (enfurvitide) that targets gp41 blocking 6-helix bundle formation and therefore fusion of the two membranes.

Host cell infection by HIV-1 is mediated by cell receptor interactions with trimeric envelope glycoprotein (Env) spikes that are exposed on the virus membrane surface. Env is the only virus-specific protein on the virion surface, and is essential for cell receptor interactions and subsequent virus-cell fusion [11-13] (**Figure 1**). Hence, Env presents an obvious target to attack the virus directly in order to block the cascade of integrated binding and conformational change steps that lead to host cell infection. Env-specific inhibitors that could inactivate the virus before receptor encounter would hold great promise of preventing AIDS transmission and progression. The proteins of the HIV-1 Env include gp120 and gp41 on the viral envelope spike and the cell surface receptors include CD4 and a chemokine receptor, either the CCR5 or CXCR4. The fusion inhibitor T20[14], and the CCR5 inhibitor maraviroc[15] are approved drugs used currently for salvage therapy in HIV-infected patients, though trials are ongoing to assess their addition to first line regimen (**Figure 1**). T20 targets the N-terminal heptad repeat region of gp41, blocking gp41 conformational changes essential for 6-helix bundle formation and membrane fusion. This inhibitor however has a relatively short time window to act on the transiently exposed N-helix of gp41 at the cell-virus synapse. In addition, T20 is logistically difficult to administer, as it can only be given parentally, and adverse reactions at sites of injection are common. Maraviroc only blocks R5-tropic HIV-1 and its use requires that CXCR4-tropic viruses are not present [15]. While there are other small molecule entry inhibitors[16, 17], peptidomimetics[18, 19] and anti-CD4 antibodies[20, 21] that block or interfere with proteins at the cell-virus interface, they are still not advanced to clinical use as a first line regimen.

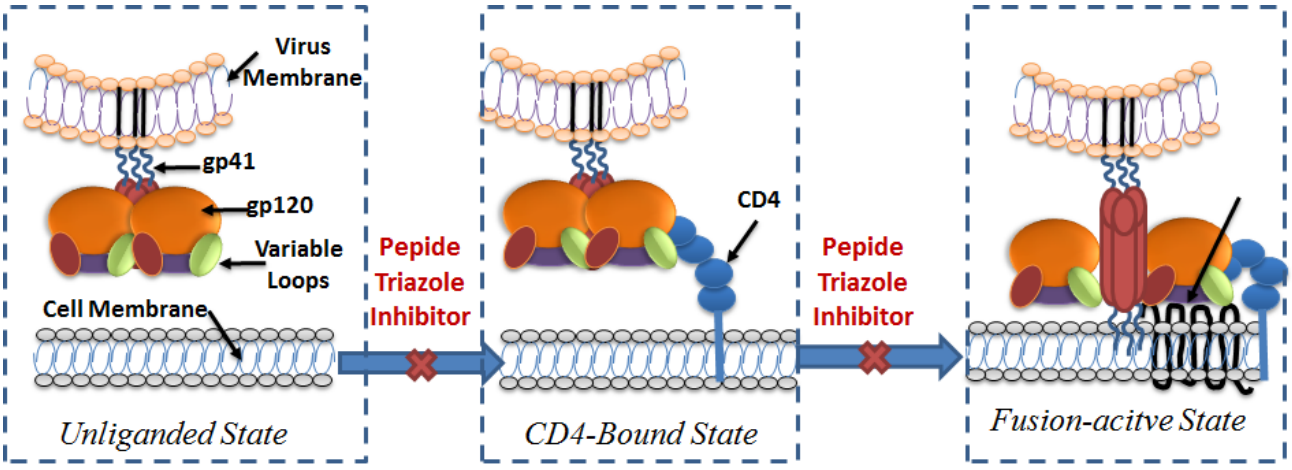

Figure 2: The schematic representation of the peptide triazole mode of action. It is an allosteric diverter that puts the gp120 protein in an inactive state that is insensitive to CD4 and CCR5 binding leading to complete inhibition of HIV fusion and therefore entry of the virion into the host cell.

These groups of microbicides are called peptide triazole inhibitors, made with amino acids just like proteins in the body and hence they are very biocompatible[22]. They have been engineered by using a technology called click chemistry to create a pharmacophore [22] that binds close the CD4 binding pocket, which is a highly conserved region among the several drug resistant mutants strains of the virus that are currently present. The peptide triazoles compete with the CD4 as well as co-receptor binding site which therefore inhibits the virus from initial contact with the host cell, blocking its entry [9, 23-25]. The peptide triazoles revert gp120 to an alternate inactivate state which will not proceed towards CD4 or coreceptor binding, hence blocking virus cell fusion as shown in **figure 2**. This class of peptides was further developed to create the virolytic class of the peptide triazole inhibitors called peptide triazole thiols [6, 8]. These virolytic peptides have an additional characteristic in addition to entry inhibition, which is the cell-free virolysis. This unique effect of the peptide triazole thiol is still under investigation but we have shown that the cysteine in the C-terminus is very crucial for this lytic effect[6]. Further we also have demonstrated that this effect follows a similar pathway as regular virus fusion with the host cell. This was proven by showing that peptide induced virus breakdown followed a similar time-line as virus fusion as demonstrated in Bastian et al. 2013 [6]. Also further the fusion inhibitor, T20 that targets HIV-1 spike protein gp41 and blocks the 6 helix bundle formation of the virion, also inhibits the peptide induced virus breakdown. These two striking results have led to exploration of how the peptide triazole thiols are hi-jacking the virus fusion machinery and mocking the virion to think it is fusing with a cell but instead leading to complete release of the protein (p24) that is in the virus nucleus into the surrounding environment. One additional component that makes

there peptides very unique is that they can target multiple clades of the HIV-1 virus including the founder viruses. Several inhibitors that are currently in the pipeline have very few specific clades that they are more active against, and therefore are limited to their inhibitory action. The results of these are elaborated in the Bastian et al. 2013 paper [6].

This novel finding is not only creating a new class of virus targeted inhibitors but also can answer some unknown questions about virus fusion with a host cell that is yet to be answered. We have also led to several discoveries juxtapositioning this finding that can lead to the creation of inhibitors that can completely and irreversible destruct the virion at the site of initial contact with the host. Our current research is focused on several aspects of this potent class of virus disrupting inhibitors. We had previously shown that multivalent display of this virolytic peptide triazole thiols lead to a 20 fold enhancement of the antiviral effects making it a much more potent inhibitor [8]. But recently we found that if we use nanotechnology to present an increased local concentration of this virolytic inhibitor on a single virion we can lead to nearly 200 fold potency enhancement of virolysis compared to peptide alone and also further we saw that this leads to disruption of the infected cells that act as a virus producing factory.

Therefore **figure 3** summarizes the effects of peptide triazole inhibitors as well as their multivalent gold nanoparticle conjugates and shows how they target different stages of the virus infection as well as how they act as a multi level process that can be used as microbicides to exterminate the disease completely. This therefore is a innovative approach that can be developed further for longer bioavailability as well as microbicidal

preparations in order to create a multi-process inhibitor that can target the virus and lead to pre-infective inactivation and complete breakdown of the virus.

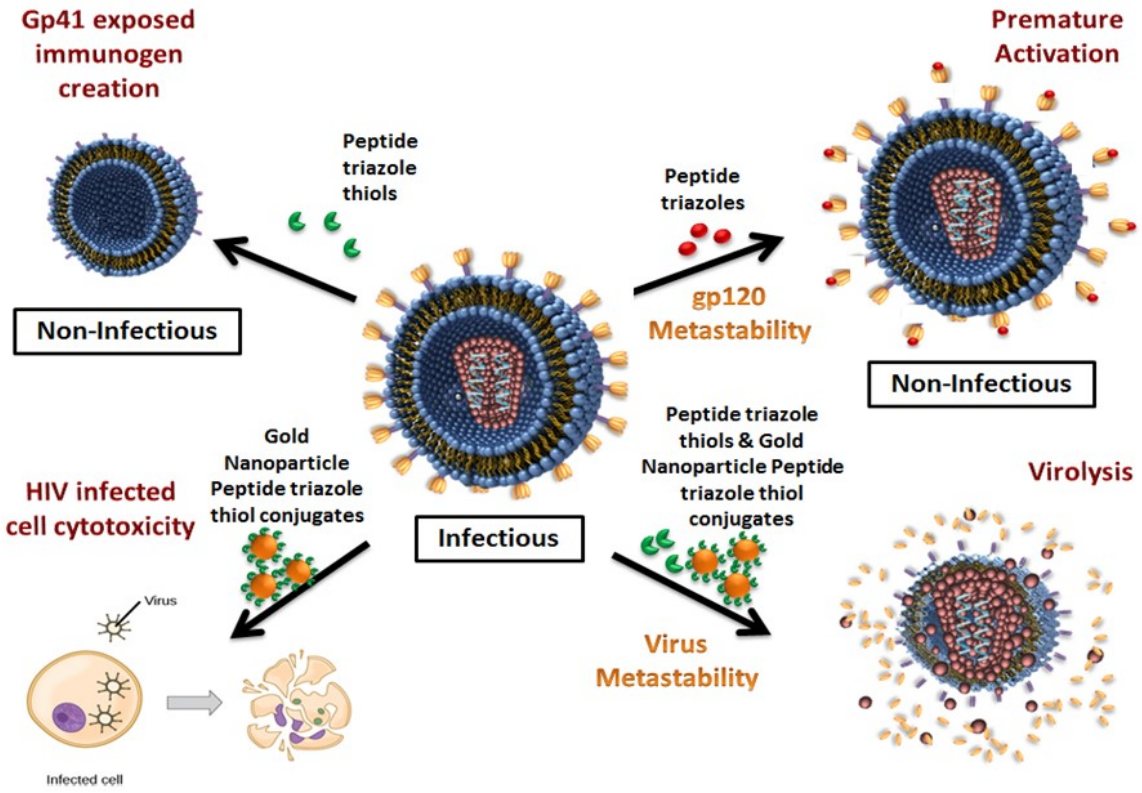

Figure 3: Schematic representation of the different effects of peptide triazoles and its conjugates. It summarizes the different stages of HIV infection

Specific Aims

My overall aim is to study these very intriguing phenomena of irreversible HIV-1 breakdown induced by peptide triazole and its multivalent conjugates and to understand the mechanism of this action. There is an urgent need for antiretroviral agents to combat the spread of HIV-1 [26]. With the exception of the recently approved fusion inhibitor enfuvirtide (T20), most of the currently approved HIV drugs target viral enzymes, in particular reverse transcriptase, protease and recently integrase [27-29]. In contrast, current first-line therapies include no antagonist that targets the entry process and remains a compelling and yet elusive means to prevent infection and spread of the virus. Entry is dependent on the ability of the virus envelope protein spike to interact with specific cell receptors in a multistage process that triggers conformational rearragements in Env and consequent fusion of virus and cell membrane to deliver virus contents to the host. Agents that could either block virus Env – host cell receptor interactions or inactivate the Env spike before cell encounter would be powerful tools for AIDS prevention and treatment. The HIV-1 envelop (spike) is known to be metastable in its native form and becomes much more conformationally stable post CD4 receptor binding [30]. A peptide triazole (PT) class of entry inhibitors has been identified previously and found to be able to bind to HIV-1 gp120 with close to nanomolar affinity, to suppress protein ligand interactions of the Env protein at both its CD4 and co-receptor binding sites and to inhibit cell infection by a broad range of virus subtypes[10, 22, 31, 32].

The HIV-1 virion envelop has been shown previously to be metastable in its native state [30, 33, 34]. Once gp120 binds to CD4 on the host cell, the envelope becomes very stable and following the coreceoptor binding leads to the trigger of the remaining cascade structural changes in the envelope that eventually leads to fusion[35-38]. Previously, Emileh et al. has demonstrated that the peptide triazoles put the gp120 env protein in an altered confirmation that stabilizes the inactive state. This therefore stops the cascade conformational changes of the envelope required for fusion to occur[24, 39]. The figure below demonstrates the structural changes the HIV-1 Env goes through post CD4 binding and also post peptide triazole binding (Figure 4). This led me to the development of my thesis development and hypothesis;

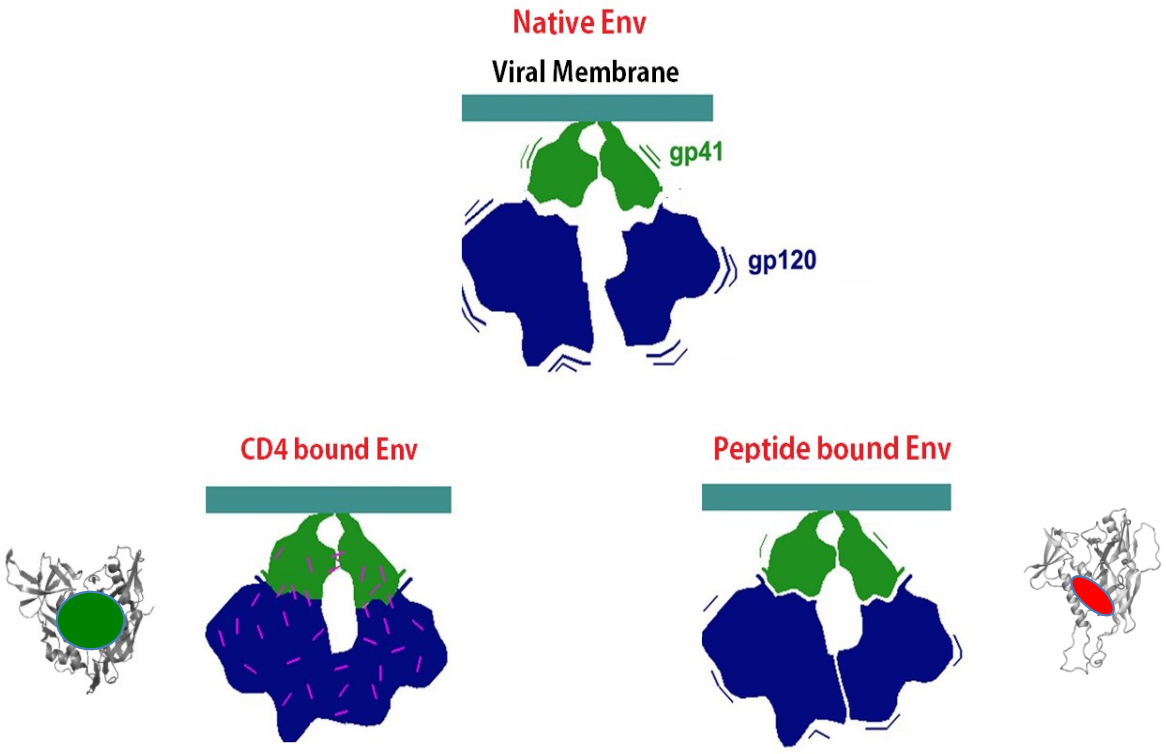

Figure 4: Schematic showing the state of the HIV-1 env post CD4 binding (bottom left) and peptide triazole binding (bottom right). The structures shown for the gp120 are adapted and modified from Emileh et al. 2013.

The metastability of the HIV-1 envelope protein provides a target for irreversible inactivation of HIV-1 and suppression of host cell entry. There is a need to create an agent that combines, for the first time, two functionalities uniquely suited to attacking HIV as soon as it presents itself in the host body. (1) strong and selective binding to the HIV envelope spike glycoprotein gp120, and (2) destabilize the virus membrane leading to complete HIV breakdown. The rationale behind this design objective is based on the idea that is to destabilize the HIV membrane either by using protein structural modifications or physical membrane stress to disrupt the membrane integrity and enhance inhibitory potency sufficiently to cause irreversible leakage of viral contents, rendering the virus noninfectious. This work can help identify HIV-1-specific virucidal agents to use in AIDS treatment and prevention by promoting cell-free virus destabilization and inactivation of HIV-1.

4 specific aims for this project include:

Aim 1. Characterize the irreversible inactivation by peptide triazole thiol and the relationship of this peptide induced virolysis to the virus-cell fusion process: Using coordinated virus infection and study of viral content release, the effects of peptide triazole thiol (PTT) on the virion. To better understand the intrinsic mechanism of PTT induced virolysis, the effects of the virolytic PT on molecular and physical transitions that occur in the metastable HIV-1 virion, including gp120 shedding (ELISA), release of intraviral components (ELISA for p24), gp41 on the residual virion, loss of membrane

integrity (TEM) and loss of cell infection activity will be measured. Specific focus on understanding the mechanism of PTT induced virolysis will be tested by comparing PTT induced virolysis relation to virus-cell fusion.

Aim 2. Develop multivalent nanoparticle constructs of the virolytic peptide triazole, understand the mechanism of action of these nanoparticle conjugates and determine the rules necessary to create highly potent nanoparticle conjugates. To increase the potency of the virolytic PTT action on HIV-1, gold nanoparticle conjugates of PTT will be constructed. The mechanism of action of these nanoparticle conjugates, on the metastable HIV-1 will be conducted by testing the release profiles of viral proteins and morphological analysis of the treated virion. From these studies, rules required to create a nanoparticle construct will be established and also a model of the gold nanoparticle – PTT conjugate and HIV-1 interface will be created.

Aim 3: Determine the effects of virolytically active peptide triazole thiols and nanoparticle conjugates on new virus formation and proliferation. Peptide triazoles are known to target the HIV-1 entry, but due to its known unique function, the virolytic peptide triazoles ability to inhibit viral production and infected cells was tested. Virus harvested in the presence of peptide triazoles and gold nanoparticle peptide triazole conjugates will be tested for infectivity, p24 content, gp120 release and gp41 recognition patterns.

Aim 4: Understand the mechanism of PTT induced virolysis by testing stabilizing viral capsid mutants and immature virus particles and development of an immunogen using residual post PTT treatment. In order to better understand the mechanism of the virolytic breakdown by PTT, the effect of PTT on stabilized p24 core

mutant HIV-1 as well as immature HIV-1 will be tested. The residual virion post PTT treatment will be used as an immunogen to develop antibodies against viral envelope protein gp41.

Overall, this work will derive principles for designing virolytic agents that specifically target HIV-1. The functional and molecular transitions of the virolytic process will give more insight towards understanding the viral fusion mechanism. The NP's will help expand understanding of the extent to which the Env metastability that is critical for pathogenic host cell entry can be hijacked for therapeutic and microbicide functions. The results will provide precedent for how other gp120 inhibitor compositions can be devised for HIV-1 virus inactivation as well as how ligand-specific pathogen rupture can potentially be achieved for other viruses, such as influenza, ebola and dengue, that contain metastable prefusion surface protein complexes.

CHAPTER 1: INTRODUCTION

1. Introduction

Acute immunodeficiency syndrome or AIDS is caused by the Human immunodeficiency virus (HIV-1) [40, 41]. Since the first reported case of AIDS in the US, it has been nearly 30 years and the progress that has been made to understand and treat the disease is exceptional[41]. In the 30 years since the discovery of the HIV virus, 31 medicines have been approved to treat HIV infection, and a 20 year old diagnosed with HIV can expect to live 50 years. With nearly 90 medicines in development for the treatment of HIV/AIDS, promising treatment gains are on the horizon. All this started with the introduction of highly active antiretroviral therapy (HAART) in 1996[42, 43]; this changed the outlook of treatment for this epidemic and had an exponential improvement of treatment regimens. HAART lead to 70% drop in mortalities and this lead to a ray of hope for this deadly disease [41, 44]. Although HAART therapy has progressed very well and has resulted in a drastic decrease of the new infections as well as reducing the number of deaths resulting from AIDS, it is still not a cure for this disease. The HAART therapy although leading to success does come with baggage, as in, people getting treatment are more prone to creating new resistant variants of the virus making the virus much more difficult to tackle [40, 45]. Currently, according to the 2013 UNAIDS Global report, there are currently 33.3 million people living with HIV globally and 2.6 million newly infections. Although the HAART therapy coverage is improving exponentially, it is till limited because the number of new infections outweighs the treatment availability

[40, 41]. Therefore, there is a huge requirement for the development of novel drugs, drug targets and/or vaccine that can control and eventually eradicate the AIDS epidemic [40, 41]. In order for the development of novel drug and drug targets, it is important to study the structure/configuration of the virus itself and further understand how the epidemic has evolved and what drugs and drug targets is currently used to target the virus or the virus infection. Further we will explore focus on the microbicides that target virus entry specifically because we believe that this is one of the most important areas of the HIV lifecycle to focus on for drug development in order to eliminate the disease progression.

1.1 Structure and Lifecycle of the virus

1.1.1 Structure of the Virus

HIV-1 is an enveloped retrovirus that is slowly replicating and hence specifically belongs to the lentivirus genus [46]. It is approximately 100-120 nm diameter and mostly is spherical in shape[47]. The structure can be simply stated as a collection of fifteen proteins and an RNA encapsulated by a lipid bilayer [46, 47]. There are twelve of these proteins present in the viral particle: The four Gag proteins MA (matrix), CA/ p24 (capsid), NC (nucleocapsid) and p6 plus the two Env proteins gp120 and gp41 are the structural components of the virus. The three Pol proteins PR (protease), RT (reverse transcriptase) and IN (integrase) provide essential enzymatic functions and along with the accessory proteins Vif, Vpr and Nef, are packaged into the virion [46]. The three other HIV-1 encoded proteins Tat, Rev and Vpu are gene

regulatory proteins that help with the HIV infection and lifecycle. The lipid bilayer that encapsulates the virus is taken from the membrane of the hot cell when a new virion buds off the host cell. The lipid bilayer of the virus has a higher level of several lipids compared to the human t-cell membrane with composition percentages similar to a lipid raft on a host cell lipid membrane [48-50].

HIV-1 is very highly genetically variable due to its ease to mutate in order to survive and become resistant. There are three groups of HIV-1 based on the differences in the envelope (env) region: M, N, and O [51]. Group M is the most prevalent and is subdivided into eight subtypes (or clades), based on the whole genome, which are geographically distinct. The most prevalent are subtypes B (found mainly in North America and Europe), A and D (found mainly in Africa), and C (found mainly in Africa and Asia); these subtypes form branches in the phylogenetic tree representing the lineage of the M group of HIV-1[52, 53]. Because most of this divergence and mutations arise in the env of the HIV it is important to study the envelope and develop drugs that target this very vulnerable yet important protein of the virus.

Structure of the HIV Envelope:

The envelope glycoprotein (Env) is presented as a trimer on the viral envelope and it is the only virally encoded antigen on the surface of HIV-1[54]. This is the first trigger that leads to viral entry into host cells, and is the region of the virus that morphs itself in order to survive in the cell environment [52, 54-56]. The trimer is composed of heterodimers of gp120/gp41 complexes and the two proteins are

attached to each other through a non-covalent association [57]. The gp120 glycoprotein must be flexible to allow conformational change, yet retain sufficient contact with gp41 to maintain the integrity of the unliganded trimer and, after CD4 binding, to arrest gp41 transitions at a prehairpin intermediate stage. The shedding of gp120 from the trimer and functional inactivation of the CD4-bound spike are well documented consequences of missteps in this demanding process. Various structures of components of gp120 and gp41, alone and in complex with different ligands have been determined [12, 58].

Gp120 is a heavily glycosylated protein with up to 50% of its molecular weight contributed by carbohydrates [59, 60]. The gp120 sequence contains five conserved regions (C1-C5) interspersed with five variable loops (V1-V5) as shown in **Figure 5** [57]. It has been shown by very extensive studies that the five conservative regions make up the core and the variable loops extend out of it. Most of the literature depicts the gp120 architecture to be thought as a series of domains/layers that move according to the binding with receptor and co-receptor. **Figure 5A and 5B** demonstrate how these layers move respect to each other post ligand/receptor binding [1, 57]. And **Figure 5C** demonstrates the first crystal structure showing gp120 presented as a structural complex of gp120 with sCD4 and 17b for crystallization purposes. 17b is an antibody that binds to the coreceptor binding site on gp120 and thus acts like a coreceptor surrogate for structural studies [61].

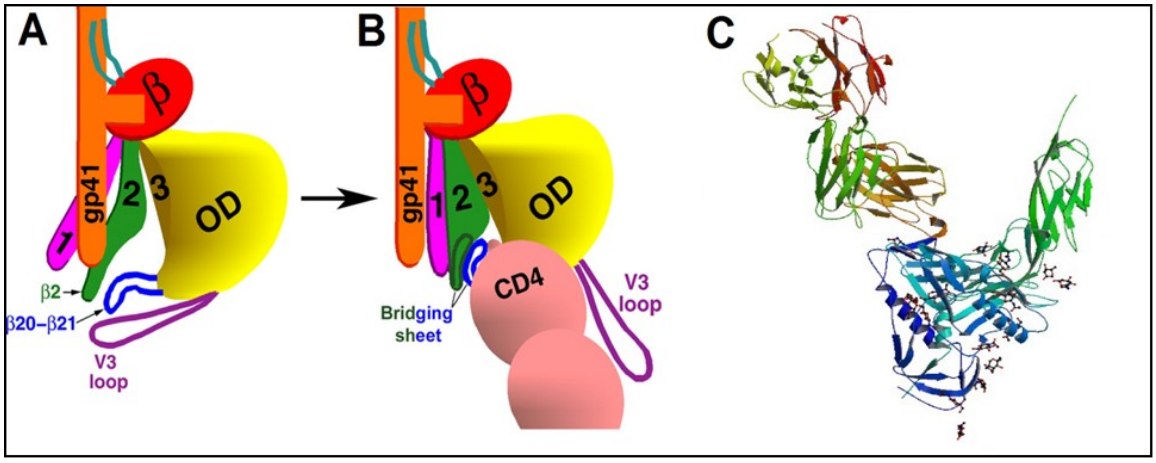

Figure 5: A. Model of the conformational changes in the HIV-1 gp120 monomer induced by CD4 binding (B) (Image adopted from Xiang etl al. 2010)[1]. The viral membrane is on the top of the image. The gp120 outer domain (OD) is yellow. The HIV-1 gp120 inner domain consists of a β-sandwich (red) and loops that form three topological layers (layer 1 [magenta], layer 2 [green], and layer 3 [yellow]). B. Changes in the V3 loop and the β 20 – β 21 which form the bridging sheet post CD4 binding to expose gp120 for coreceptor binding. Image adapted from Xiang et al. 2010[1]. C. The crystal structure revealing the complex of gp120 (HXBC-2), sCD4 and 17b (a coreceptor surrogate antibody), PDB: 1G9M.

Although this structure presented in **figure 5C** did lack the variable loops, the protein was modified to contain no N and C-termini, deglycosylated and in complex with CD4 and 17b for crystallization purposes, this finding revealed several potential inhibitor development against gp120 [61-63]. Several structural studies have been conducted in the past 16 years resulting in a more complete picture of this state of gp120 by adding other components like the V3 and V4 loops and the N and C-termini[57, 64, 65]. In 2013, for the first time ever using cryo electron tomography the 6-Å structure of the membrane bound fully glycosylated, HIV-1 Env trimer was revealed in its uncleaved and unliganded stage (**Figure 6**) [2]. This was further demonstrated also by several groups in the same year using the cryo- EM methodology as described by Mao et al. 2013 [66-70]. This lead to a giant leap in the field which lead to several discoveries of antibodies, conservative binding sites in the native trimer, as well as new inhibitor target sites on the HIV env. Further one of the greatest and most encouraging rewards of last year to the field was the crystal structure of the native cleaved trimer (SOSIP) – pdb structure 4NCO [54]. This has led to the discovery of several key sites on the HIV-1 env that is highly immunodominant and immunoactive which brings an HIV vaccine creation closer to reality [71-73].

Gp41 is a 41 amino acid glycoprotein that contains three domains, the extracellular domain (ED), the transmembrane domain (TMD) as well as the cytoplasmic domain (CD). The extracellular domain consists of a fusion peptide (FP), a N- heptad repeat (NHR), a loop region, a C- heptad repeat (CHR) as well as the membrane proximal external region (MPER) (**Figure 6**) [74-78]. In the currently accepted model, HIV-1

fusion cascade begins with the binding of surface subunit gp120 to target cell receptors. Activation of the fusion leads to structural rearrangements of the gp41 ectodomain leading to a final structure that as shown in **Figure 6** and which was crystallographically resolved in 1997 as the 6-helix bundle[49, 79]. These structural rearrangements include the reorientation of the NHR and CHR and collapse into a folded 6 helix bundle with the fusion peptide anchored to the cell membrane and the TMD to the viral membrane. In this 6 helix bundle structure the carboxyl-terminal helices arrange in the reverse direction against hydrophobic grooves outside the coiled coil, so that the amino- and carboxyl-termini are placed at the same end of the molecule. This therefore is speculated to result in both the membranes moving closer to each other and leading to lipid mixing [80, 81]. Following the lipids start mixing between both the membranes that lead to a hemi-fusion intermediate and eventually complete fusion [82-85].

The HIV-1 env structural information has advanced due to the new structures that have evolved over the past 10 years and this has brought new insight into building new targets for inhibition as well as immunogen creation. The **Figure 6**, is from the recent paper by Kwong et al. 2012, shows us how the cryo-EM structure of the Env trimer is giving us information on developing new target sites for antibodies. Especially recent advances towards the PGT antibodies that target the V3 loop glycans are becoming increasing interesting due to their broad neutralization activity [86-90].

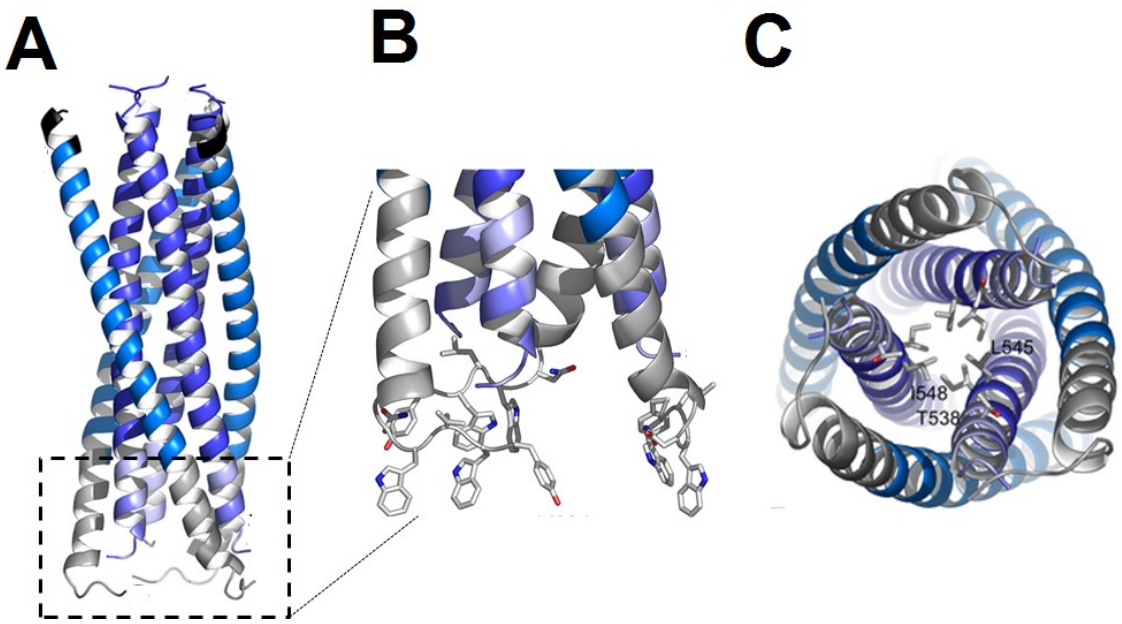

Figure 6: Currently available crystal structure at 2°A resolution of gp41 6 helix bundle. Figure on the left (A) shows the 6 helix bundle structure including the membrane proximal external region (MPER) and fusion peptide proximal region (FPPR). The dark blue is the HR1 (NHR) andlight blue is HR1 (CHR). B. Close up of the MPER (grey) and FPPR (light blue) region showing hydrophobic interactions. C. Showing the bottom view of the 6 helix bundle. For the 6-helix bundle core, the structure used is the modified version of pdb 1AIK and the MPER structure is pdb 1P5A. The figure is a modified figure from Buzon et al. 2010[4].

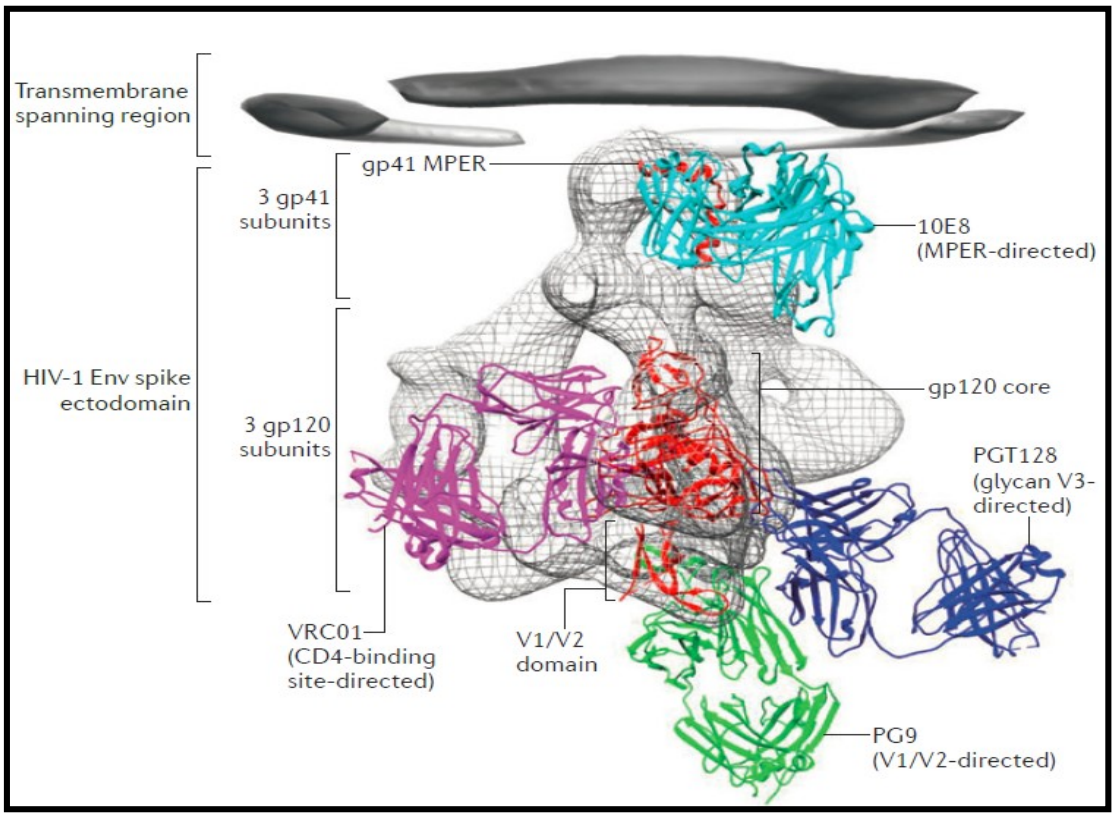

Figure 7: A. Sites of HIV‑1 vulnerability to neutralizing antibodies. The HIV‑1 envelope spike is the cryo EM structure of the uncleaved trimer obtained by Mao et al. 2013[2].

1.1.2 HIV Life cycle

The HIV virus is a sexually transmitted virus that enters the body through sexual contact that lead to fluid exchange or other forms of fluid exchange like breast feeding, blood transfusions or needle sharing [82, 91-93]. The HIV lifecycle is split into six major parts, these includes, (a) virus entry, (b) reverse transcription, (c) integration, (d) transcription, assembly, and (e) budding and maturation[94]. HIV-1 infects cells that display the CD4 receptor on their surface (CD4+) along a mandatory coreceptor, a member of the chemokine receptor family, either CCR5 or CXCR4 [95]. These cells include immune cells present in our body such as the $CD4^{+ve}$ T-cells (lymphocytes), macrophages and microglial cells [96]. Further HIV-1 is known to latch on to dendritic cells that assist with spread of infection [97]. The virus lifecycle can be summarized as follows; The HIV-1 Env protein gp120 binds to the receptor (CD4) and then the coreceptor. Following, gp120 is shed off exposing the gp41 that inserts its fusion peptide into the cell membrane. The gp41 protein undergoes conformational changes that lead to virus-cell membrane fusion and allow the virion core, composed of MA, RT, IN, Vpr and RNA, to enter the cell [46]. This complex is transported to the cell nucleus where the viral genetic code encoding RNA is transcribed into DNA by RT and integrated into the host genome by IN [46, 95]. At this point, the cell becomes a HIV protein production factory and is ready to produce more viral proteins. These viral proteins are then transported to the cell surface membrane and assembled and budded off. Post budding, the immature virion goes through a protease digestion of the capsid in order to create a fully mature infectious virion, and continue the virus life cycle by infecting other targets. Because my project

focused on developing inhibitors that target the first interaction in the HIV lifecycle, the HIV-1 entry, it is important to understand this step in more detail.

HIV-1 Entry:

The HIV-1 entry is an elusive target for drug development because it's the first step in the HIV-1 lifecycle that leads to infection. One of the first steps of the entry process is the interactions of the positively charged domains on gp120 with negatively charged proteoglycans on the surface of the cell [98, 99]. This is an important step but is not critical for the processes that follow during viral entry. The entry process happens as a sequence of events which are schematically illustrated in **Figure 2**. Next is one of the most crucial steps for entry, the interaction of Env glycoprotein gp120 with the T cell co-receptor CD4 [37, 100-103]. CD4 binding results in extensive conformational changes within gp120 that induces a greater exposure of gp41 and the formation of the co-receptor binding site [37, 104-106]. This is structurally described as two sets of beta sheets brought together by CD4 binding to form a 4 stranded beta sheet called the bridging sheet and also movement and exposure of the V1/V2 and V3 loops structures which in turn exposes the co-receptor binding site [88, 106, 107]. Gp120 binding to the coreceptor, CCR5 or CXCR4 depending on the virus tropism, results in further conformational changes in the Env that leads to the exposure of gp41 and insertion of a hydrophobic sequence of residues on its N-terminus called the fusion peptide into the host cell membrane[108-110]. Once

the fusion peptide is inserted into the host cell membrane, the extended conformation of gp41 with its C-terminus in the viral membrane and its N-terminus in the cell membrane is called the “prehairpin intermediate”[109, 111]. Following this short lived state the two heptad repeats of gp41 fold into a hairpin structure which results in an energetically favorable structure known as the six helix bundle[78, 80, 112, 113]. This brings the two membranes together and leads to membrane fusion and insertion of the virion core into the cell, effectively starting the infection[114]. The 6 helix bundle formation have two distinct depictions as shown is **figure 8, Figure 8A** shows that for efficient fusion and virus-cell membrane fusion you require two spikes to be triggered, while **Figure 8B** shows that for fusion you require only one spike trigger. Both these theories have been proved with evidence, and so it is very much debated to whether we require more than one spike for efficient fusion and hence HIV infection [85, 115].

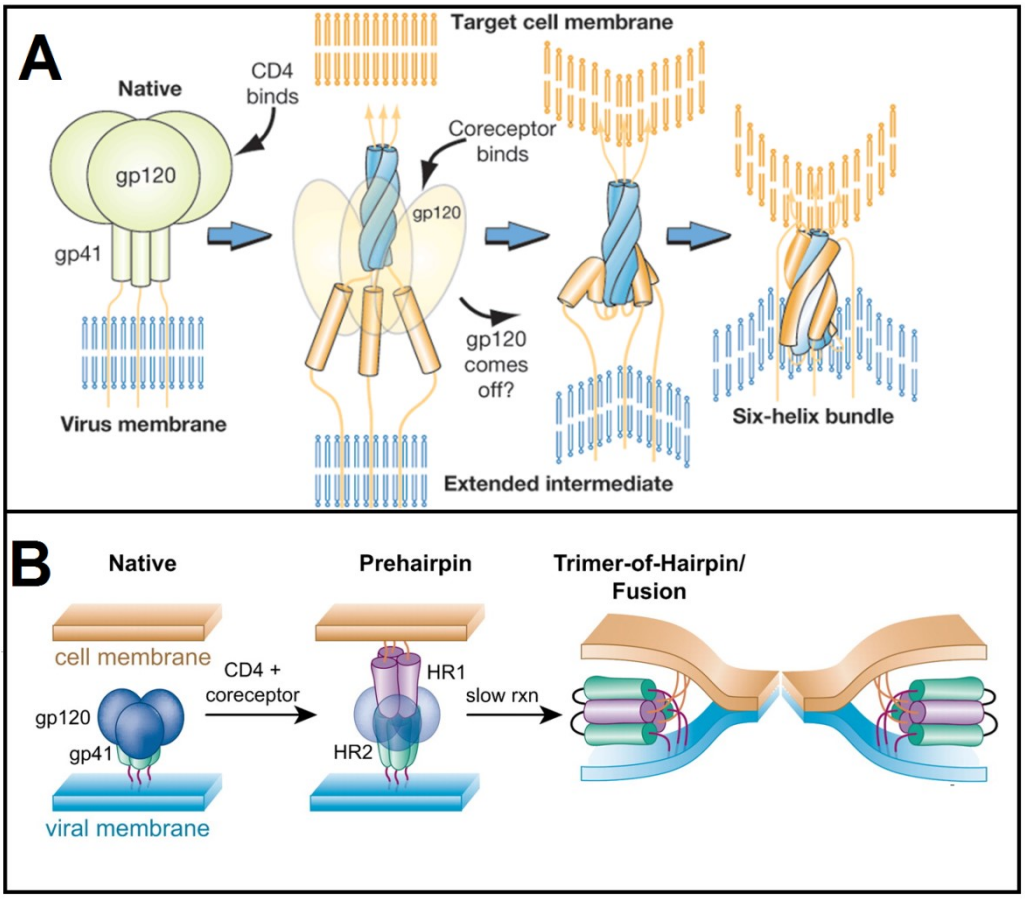

Figure 8: Schematic diagram of gp41 function during HIV fusion. A. The model adapted from Dr.Salzwedel in which he demonstrates the 6 helix bundle formed with one spike and folded perpendicular to the viral membrane. The gp41 HR1 and HR2 regions are depicted in blue and yellow, respectively. B. The 6- helix bundle formation adapted from adapted from Chan and Kim [116]. The gp41 HR1 and HR2 regions are depicted in purple and green, respectively.

1.2 HIV inhibitors

There are several inhibitors currently in market as well as currently in clinical trials and in preliminary development that targets several stages of the virus lifecycle. It is important to develop these inhibitors that target different stages of the virus life cycle so that they can be used in combination as well as individually. Further the UNAIDS and other global health initiatives are funding the development of HIV inhibitors in order to get closer to the eradication of this epidemic and reduce the number of deaths. Further it is important to create inhibitors that are easy to produce in large quantities at low rates so that this can be served as a drug for a globally spreading disease. Highly active antiretroviral therapy (HAART) was initiated in the 1970s when the virus was very less known. This was mostly done by several independent researchers and biologists trying to understand the virus and the disease better [117]. But the first known treatment used and also known as the initial HAART therapy was in 1986 in a double blind study. They used azidothymidine (AZT) to treat AIDS symptoms showing individuals [118]. In 1996, the introduced using the combination therapy for AIDS treatment and this resulted in a decline of deaths and hospitalizations from 60% to 80% [43, 119]. Now more than a decade later HAART therapy has brought down the deaths from AIDS to nearly 85%. Further there are more than 30 FDA approved HIV drugs that can be used in several combination HAART [117, 120]. This wonderful progress has led to hope of survival increasing and also our hope of completely eradicating the disease is becoming reality. The UNAIDS last year has come up with a complete eradication initiative called “Getting

to Zero", and this is a combination of patient and people awareness, treatment approach, treatment breadth around the world and a very important factor, new drug development[41]. A report by UNAIDS showed that a record 9.7 million people living with HIV were accessing treatment in 2012 compared to just over 8.1 million in 2011—an increase of 1.6 million in one year alone. This is mostly due to the increased availability and also the increased awareness and rapid free HIV testing that is provided around the world. Hence it is important to know the overview of the current drugs used in HAART therapy and what are the challenges faced [2, 121].

1.2.1 Current Inhibitors in the market

There are currently over 30 inhibitors that are approved by FDA for HAART therapy. These inhibitors are divided into six different classes. These include; nucleoside reverse transcriptase inhibitors (NRTIs, nonnucleoside reverse transcriptase inhibitors (NNRTIs), protease inhibitors (PIs), integrase inhibitors (IIs), fusion inhibitors (FIs) and Chemokine receptor antagonists (CRAs). The inhibitors that are in each class target a different step in the virus life cycle and therefore HAART used a minimum of two inhibitors in combination[122, 123]. The regimens of HAART are decided based on several factors that have been a learning process and is set up by the WHO in collaboration with the UNAIDS committee and FDA [121, 124-126]. These factors include the ease of use, the allergies of patients, the stage of infection based on the CD4 counts and largely by the availability and clinical preferences in developing countries [126-128].

There are several challenges that are faced during HAART; the first and the most challenging is the resistance to the drug. A study was conducted recently in order to assess why there was failure in HAART first line therapy and one of the main reasons was resistant mutants of the virus developing very quickly [129]. The other challenging include adverse side effects specific to different patients, pregnant women having limited treatment and hence disease spread and co-infection with hepatitis B or C virus or tuberculosis which makes it very difficult to maintain treatment[129-134].

1.2.2 Inhibitors that target HIV entry in HAART

There are currently only two FDA approved inhibitors that target HIV fusion and entry, these include T-20 or enfurvitide, which targets the pre-fusion intermediate gp41 N-termini, and maraviroc, which targets the co-receptor CCR5, present on the host cell [135, 136]. Both of these inhibitors are only used salvage therapy during HAART treatment due to several reasons and challenges which are detailed in this section.

T-20:

Enfuvirtide also marketed under the name FUZEON, is a synthetic peptide inhibitor that is 36-amino acid long and targets gp41[137]. T20 is a peptide from the gp41 protein extending from Tyr638 in the middle of the C-HR to Phe673 in

the Trp-rich membrane proximal external region (MPER) that before the TMD[137]. Therefore tis gp41 C-HR peptide targets the gp41 N-terminal heptad repeat region (N-HR), blocking gp41 conformational changes essential for the entry process. But as we know from above, during the fusion process, the N-HR is exposed from 10-20 minutes and hence the time of action of T-20 is very limited[138]. There are several mutants on the N-HR that have developed as resistant/escape mutants of T20 which reduce the binding affinity of the inhibitor nearly 40-80 fold [139-142]. One of the major mutants includes V38A, N34D as well as I37K and these have different range of resistance but do not affect HIV-1 fusion and infection[14, 141]. This therefore is one of the reasons why T20 is not used in the first line regimen of HAART. The other reasons include the allergies, diarrhea and skin irritation and rash in region of delivery [143, 144]. T20 is usually administered by subcutaneous injection at a dose of 90 mg (1 ml) twice-daily and a paediatric dose of 2 mg/kg to provide comparable exposure to the adult 90 mg dose independent of age group, pubertal stage, body weight or body surface area[136, 145, 146]. And other limitation of use of T20 in first line therapy include the availability, the expenses of production as well as the amount of social awareness because it is still new to HAART[136, 147].

Maraviroc:

Marviroc is the product of a high-throughput screen conducted by Pfizer in order to identify an imidazopyridine CCR5 ligand [148, 149]. The CCR5 belongs to a

G-protein coupled receptor superfamily and is the co-receptor that is required by most HIV-1 clades for complete fusion [150, 151]. Further CCR5 is a very compelling target for therapeutic intervention because of its natural absence in the Δ32 homozygous genotype populations and hence are also protected greatly from HIV-1 infection [152, 153]. The crystal structure of maraviroc with CCR5 was solved by Tan et al. in 2013, pdb No. 4MDS and from this it is observed that maraviroc binds specific to the extracellular loop -2 of CCR5 [154]. Maraviroc was FDA approved in 2007 for use as an antiretroviral but its use was limited to special cases of patients for salvage therapy [155, 156]. Maraviroc blocks R5-tropic but not X4-tropic HIV-1; thus, clinical use requires co-receptor tropism assays to be performed prior to initiating treatment [16, 155, 157, 158]. In addition there are challenges that rise with the use of the drug, which is administered orally at 600 mg/day, such as rash, dizziness, and upper respiratory infections. In addition overdose or patients with hepatic abnormalities will be subjected to severe adverse effects due to its toxicity [155, 159, 160]. Resistance of the drug has been reported with resistant variants of the virus developing with mutations in the v3 loop [161].

From the above it is clearly observed that there is a huge necessity and huge gap in the advance of fusion and entry inhibitors of HIV. Therefore it is important for us, the scientific community to conduct a major therapeutic intervention advancing the development of inhibitors that target HIV fusion and entry.

1.2.3 Microbicides that target HIV virus entry

There are currently several inhibitors as well as antibodies that are currently in the pipeline that target different stages of HIV-1 entry into host cells. The following section will conduct a review of the current entry and fusion inhibitors that are in either phase I, II or III clinical trials and also the new inhibitors that are in early development. The inhibitors currently in development will be listed based on different stages of the HIV-1 entry.

The gp120 and CD4 interaction:

There are several inhibitors that target this interaction, either that bind to gp120 or the CD4. This is a very critical stage due to its importance in initial contact with the host cell. CD4 is a single transmembrane protein with four extracellular domains from which the 3rd and 4th domains seem to be crucial for gp120 binding, especially the beta hairpin that contains the Phe 43 residue [162]. Further years of biochemical and mutational analysis have revealed that the Phe 43 and Arg 59 on CD4 are important for binding to gp120[163, 164]. In 1998 Kwong et al. derived the crystal structure of gp120 bound to CD4 and showed that there are several interactions that are important for the CD4 and gp120, where CD4 binds to a region on gp120 between the inner and outer domains[61, 164, 165]. This area on

gp120 was later on known to be the phe 43 cavity and contains amino acids that are nearly 98-99% conserved in a glycoprotein that is highly mutated [61-63].

This important interaction is a very attractive one but has not given very many success stories. Although they are very many inhibitors in the pipeline very few have managed to surpass several factors and reach to a stage of clinical trials. One of the first attempts was the development of soluble CD4 protein in order to target the virus prior to host cell encounter and thus resulting in blockade of the phe 43 cavity necessary for the CD4 receptor binding. Although this showed good potency of inhibition in vitro there was limited success in patients in clinical trials due to high resistance to the drug by primary isolates[166]. Following this the crystal structure of the gp120-CD4 became available and there were many attempts to develop small molecule inhibitors that targeted the phe 43 cavity. These included a class of BMS compounds specifically BMS 378806, BMS 448043 and BMS 626529[167]. These compounds mostly did not process any further than phase 2 clinical trials due to its poor pharmacokinetics although they did have very potent inhibition IC_{50}s[18]. The BMS compounds mostly appear to stabilize gp120 in a conformation that is incapable of binding to CD4 but some also show to interfere with conformational changes in gp120[168, 169]. Following these attempts there was an era of the CD4 mimetics, in which there were screens conducted in order to find small molecules that fit/bind deep into the phe 43 pocket of gp120. These included M33 peptide, the NBD group of compounds as well other small molecule inhibitors. The main problem that arose from these compounds was the conformational entrapment of gp120 by these

compounds resulted in increased coreceptor binding which led to enhancement of infection at lower concentrations [64, 168, 170-173].

There were also antibodies that targeted this interaction that was developed both through screen studies as well artificial creations. Ibalizumab (TNX-355) is an antibody that binds to CD4 D1-D2 domain, this does not directly block the CD4-gp120 interaction but stops the interactions that follow [174, 175]. There are antibodies that have evolved that conformational entrap gp120 in a state where the phe 43 pocket is either sterically hindered or no longer accessible, these include, F105, b12, and the VRC group of antibodies which is currently going into human clinical trials, trial -VRC-HIVMAB060-00-AB [176-182]. One of the most recent and hyped antibody developments is the PGT group of antibodies that target the glycans of gp120 specifically close to the V3 loop region [86, 183]. These are similar to 2G12 which was one of the first glycan antibodies that target the glycans on gp120 [184]. But these PGT antibodies are much more specific and have a specific region of binding which has been mapped out on the native trimer using PG9 antibody through cryo tomography[185]. Although there are very potent antibodies against the binding of CD4 to gp120, they are still very expensive to mass produce and resistant mutants are very easy to develop [182, 186]. But these antibodies are heading in a vaccine direction due to their stability and biocompatibility for patients at risk and currently there are many attempts that are being made in the direction of vaccine development [89, 187, 188].

The gp120 and coreceptor engagement:

There are several chemokines in the body that include CCL3 (MIP-1α), CCL4 (MIP-1β), and the most studied RANTES [189]. These induce internalization of the coreceptor CCR5 for a brief period but it is not an irreversible action, the CCR5 is recycled back onto the cell surface [190]. There have been several different types RANTES derivatives that have been developed to improve its function and have also been used as topical microbicides [191-193]. The limitation is the dual effect of the chemokines and also that it works more efficiently with CCR5 and not CXCR4 [193]. The next category is the small molecule inhibitors, which are the newer versions of marviroc such as viciviroc, aplaviroc and cenicriviroc. These inhibitors are developing still and cenicriviroc has an additional property of being anti-inflammatory which might be beneficial due to the immune activation by HIV [194-197]. These inhibitors however have cell toxicity issues and severe side effects which might be challenging to overcome and still produce an affordable inhibitor[194, 195]. Several drugs have also been developed against CXCR4 coreceptor specifically such as AMD3100 but have not proceeded to clinical trials due to its medical complications and poor pharmacokinetics [198]. The other direction of approach is the antibody development against the coreceptor interaction with gp120 and the top antibodies developed include 17b, 2D7 and PA14 [199, 200]. Although these antibodies, also known as CD4 induced antibodies, do have a low nano molar inhibitory

concentration, they are specific to CCR5 [21, 187]. And also they act in a short time window of action and hence cannot be used as a microbicide efficiently.

The fusion of HIV and host cell membrane:

As seen in **figure 6** and **figure 8,** the last step of HIV entry is the exposure of gp41, insertion of the FP into the cellular membrane and following the 6 helix bundle formation both the membranes fuse together and result in complete fusion and virus entry. This step of HIV entry is one of the most developed and oldest areas where inhibitor development is focused. These have been mostly been conducted by peptide sequences that have been developed from heptad repeats that could bind to their respective partner heptad repeats blocking the major step in fusion, the 6 helix bundle formation [79, 137]. These inhibitors include the inhibitors that are peptides from the CHR of gp41 which include T20, C34, T1249 and sifuvirtide [163, 201, 202]. There are also peptides from the NHR of gp41 which include N36, NCCG41, 5 helix and T21 [201, 203, 204]. These inhibitors target the fusion process but their time of action is very limited to the fasted step in HIV-1 entry which is the pre-fusion intermediate of gp41 [76]. Although these C-peptides described above have a very high clearance rate due to their vulnerability to proteases present in the cell. Hence recent developments have been on developing other more biocompatible and bioavailable fusion inhibitors. These include the D-peptide inhibitors that bind the N-HR pocket with high affinity and potently inhibit viral entry [205, 206]. These d-peptides are also

known to be active against resistant mutants of the 5-helix and T20, making it more broadly active [205, 207]. The progress of these inhibitors is progressing slowly and lately multivalent versions are being created [208]. Once again the limiting factor is the time window of action, which is during the pre-fusion intermediate state of gp41, which is very short lived [114, 157, 209-211].

1.2.4 Virucidal agents that lead to virus disruption

Virucidal agents are microbicides that lead to destruction of the virus particles upon contact. These agents differ from the regular microbicides due to the fact that they act directly or indirectly on the viral membrane leading to irreversible or reversible lysis [212, 213]. The current virucides are small molecules and peptides that target the viral membrane directly. These inhibitors are used as preventatives due to its early on action on the virus leading to damage of the virus to proceed towards infection. The virucides include surfactants like nonoxynol-9, [214] which is a spermicidal molecule [215]. Others include bile salts derivatives that can target the virus using a surfactant mechanism [212]. These surfactants are effective virucides but they have very adverse effects on the other cells in the body due to their surfactant mechanism. This was shown during the pharmacokinetic test of nonoxynol-9 in a vaginal gel, they showed severe damaging effects on the epithelial linings of the female vagina [215]. There are other multivalent conjugated virucides such as polyamide nucleic acid-membrane transducing peptide conjugates lead not only to HIV-1 replication

inhibition but also have virucidal properties [216]. The dendrimer microbicide SPL7013 is a broad spectrum inhibitor that targets not only HIV but also Herpes simplex virus (HSV) and human papillomavirus. These have also shown to have virucidal properties leading to rupture of virus [217, 218]. Although these inhibitors have good virucidal properties they have drawbacks such as their limited knowledge of mechanism of action, specificity and also the risk of cell toxicity [218, 219].

1.3 A Unique HIV-1 Entry Inhibitor

From the above group of inhibitors it is clearly evident that there is a need for HIV entry inhibitors that are non-toxic, have low clearance rate and are specific the HIV inhibition. Further the inhibitors that are currently in market for HIV fusion and entry are limited due to their availability, expense of production, specificity to receptor/target and finally resistant mutations developing in the virus. This therefore led us to the search for a potent inhibitor that is novel and could target the gp120-CD4 interaction which is one of the first stages of virus and host cell encounter.

We have discovered a family of peptide triazoles (PTs) that function as dual receptor site antagonists of HIV-1 Env gp120 by targeting a conserved functional site that overlaps the CD4 binding region of the Env protein[9, 22]. High affinity PTs were found to bind to HIV-1 gp120 with nano molar affinity, suppress protein ligand interactions of the Env protein at both the CD4 and co-receptor binding sites, and to

stabilize a partially structured conformational state, suggesting allosteric aspects of the inhibitory mode of action (**Figure 9**) [23]. The parent peptide of PTs was 12p1 which is a peptide that as obtained from a random phage library screen to identify peptides targeting gp120 [220]. 12p1 was one of the most potent peptides in the screen with a gp120 binding affinity of 3.7 μM K_d value, and showed good specificity [221]. In order to understand the mechanism of action of 12p1, alanine scanning mutants and truncations of the peptide were produced. From this it was found out that 2-8th residues of 12p1 was important for activity and importantly the proline-tryptophan cluster was important for binding and mimicked the Phe43 of CD4[9, 23]. Following this our lab modified 12p1 by adding an azidoproline group to substitute the proline group on 12p1 in order to create the first generation of peptide triazoles. This enhanced the potency of inhibition nearly two orders of magnitude and also had an additional feature of dual antagonism [23, 221]. Further a ferrocene group was added on the azidoproline ring in order to enhance potency. This addition was conducted by click chemistry on the peptide which had an azidoproline substitution in order to add the ferrocenyl group [221]. This generated the second generation of PTs with HNG156 being the most studied PT (**Figure 9**). It was important to understand the mechanism of action of this unique PT and this led us to a series of peptide truncations and residue substitutions [32]. This showed that the c-terminal was important for activity and also the isoleucine, azidoproline and tryptophan (IXW) in that order is important for function(**Figure 9**) [32]. Further it was important to understand the binding site of the peptide, for this we used the truncated version, UM15 and UM24 as the ligand and alanine mutations in gp120 in order to map out

the binding site. From this we saw that the residues close to the phe 43 cavity of gp120 is important for PT binding, namely, D474, T257, M475 and E370[25]. These residues are highly conserved in gp120 and are present overlapping the phe 43 cavity (**Figure 9**) [222, 223]. Further, the lab has been converting the peptide to its D-peptide variants for increased stability in physiological conditions, one of the variants are shown in **figure 9** – KR42 [224]. This therefore demonstrates a unique and novel approach to microbicide development.

Further modifications on the PT are presented in this thesis to make it a much more modified and improved inhibitor. These include modification of the AA in the PT and creation of multivalent constructs of PT in order to increase the local concentration of the inhibitor on the virus.

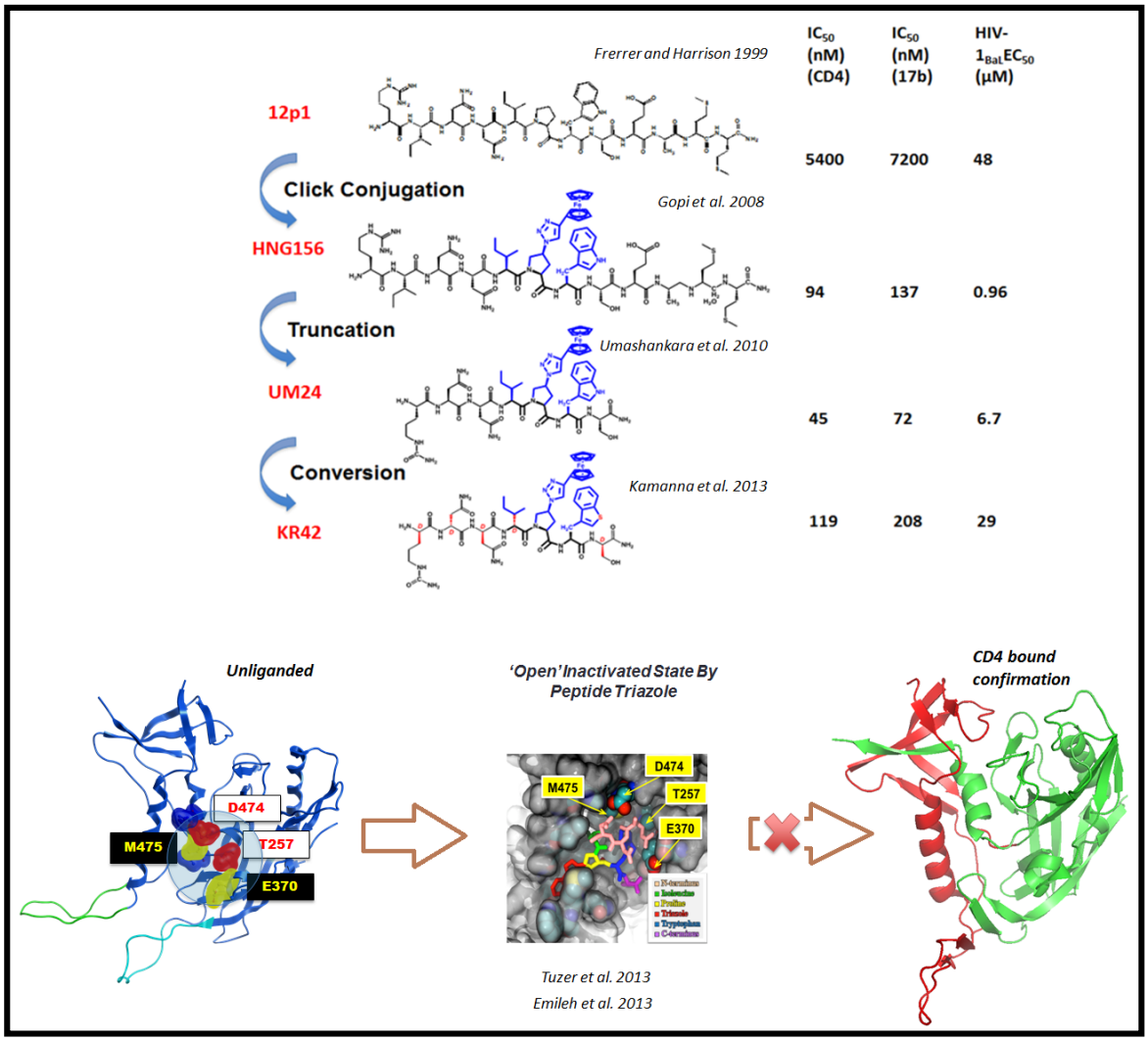

Figure 9: Summary figure showing the generations and characteristics of peptide triazoles. The figure above shows the modifications made to the parent peptide 12p1 structurally and the increase in potency of CD4 and 17b competition to gp120 monomer binding and the HIV-1 BaL-01 pseudotyped infection inhibition by these PTs. The blue highlighted are on the structures show the active pharmacophore of PTs. The figure below shows how the PTs transition the unliganded gp120 to an open activated state which is a conformational entrapment of gp120 from proceeding to the CD4 bound state.

1.4 Nanoparticles and HIV-1

There have been several developments that have been conducted over the years in order to generate nanocarriers of anti-hiv drugs. There have been many types including polymeric nanoparticles, non-polymeric nanoparticles as well as biological carriers such as viral vectors (**Figure 10**) [225, 226]. Most of these have been developed to increase stability of the drug in vivo as well as enhance their targeted delivery in order to make the drug long lasting[227]. Targeted delivery of some drugs to very difficult regions of the human body (especially the central nervous system) are easily achieved using nanoparticle carriers with drug mostly loaded in the particle lumen and the nanoparticle membrane mostly hydrophobic such as liposomes (**Figure 10**) [225, 228-230]. In a recent study based on polymeric systems, nanosuspensions (200 nm) of the drug rilpivirine stabilized by polyethylene-polypropylene glycol and PEGylated tocopheryl succinate ester (TPGS 1000) were studied [231]. One of the most recent development by GSK which is becoming great success as a long-acting single dose injectable is the GSK-1265744 which is an analogue of the HIV integrase inhibitor dolutegravir. This crystalline active drug is then milled to an average nanoparticle size of 200 nm with 100% active drug with surfactant, polymer, tonicity agent and water for injection (ViiV healthcare). The pharmacokinetics are very promising and the drug is available in sera for more than 30 days with only one injection at 200mg/ml [232, 233].

Another category of nanocarriers is nanoparticle conjugations of low potency anti-HIV inhibitors to enhance their potency. The two studies that inspired me to use gold nanoparticles are the Bowman et al. study of conjugating a derivative TAK779 on a gold nanoparticle and the study by Elechiguerra et al. that used naked silver nanoparticles to target cell-free virus and lyse them prior to cell encounter[234, 235]. Bowman et al. showed that by conjugating SDC-1721 a derivative of TAK779 with a very low antiviral activity was conjugated onto 2 nm diameter AuNPs. There was approximately 2000 fold increase in potency and thus proving that nanoparticle conjugation increases local concentration of the drug on the virion surface making it highly active antivirals[235]. Therefore this was an inspiration to creating AuNP-peptide triazole conjugates in this study. However bowman et al. used 2 nm AuNP which might have non-specific cellular uptake as shown previously[236]. The silver nanoparticles were approximately 20 nm to avoid non-specific cellular uptake, and this showed that there was sulfur interaction with the silver nanoparticle surface lysing the virion. But this also led to slight cell-toxicity which might be a limiting factor in its development and the specificity is low[234].

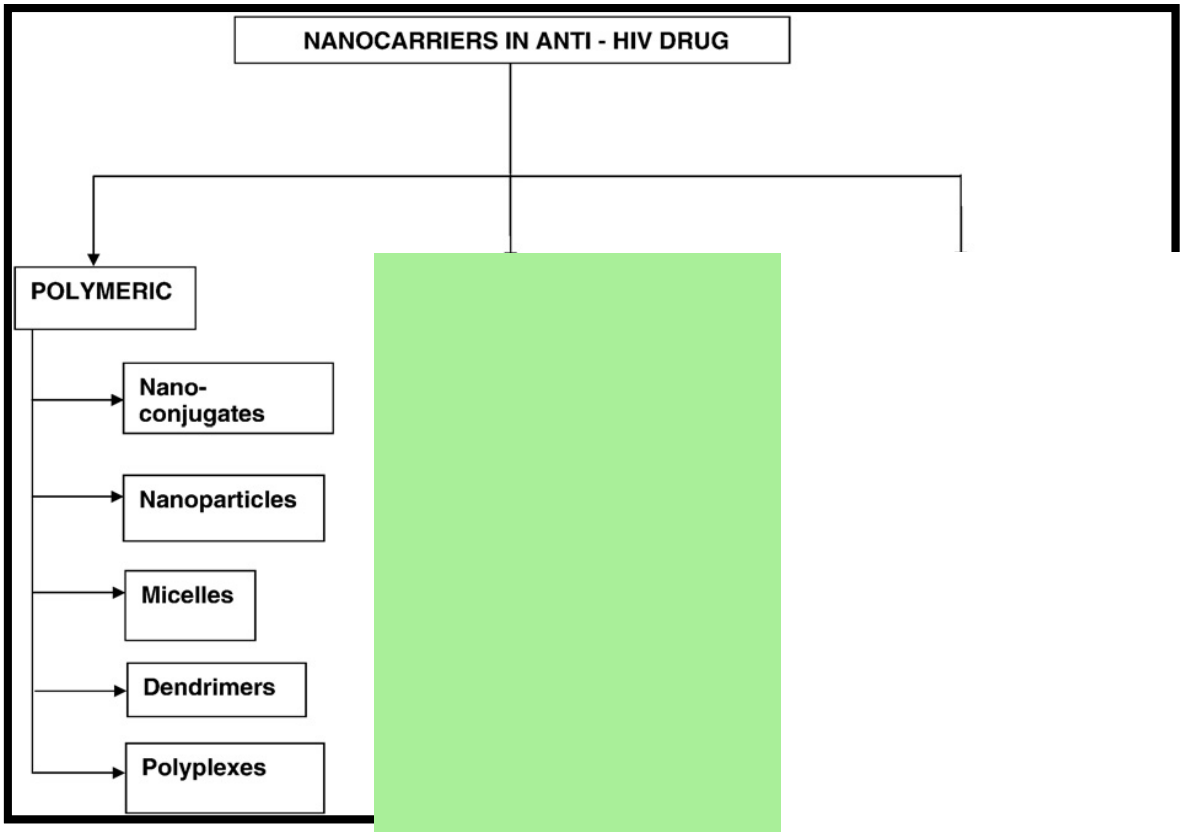

Figure 10: Schematic representing the different nanocarriers currently used in HIV-1 field

CHAPTER 2: SYNTHESIS AND ANTIVIRAL ACTIVITIES OF THE FIRST GENERATION OF VIROLYTIC AGENTS

2. Introduction

There is an urgent need for antiretroviral agents to combat the spread of HIV-1[41]. Other than T20 and maraviroc used in salvage therapy, there is limited first-line anti-HIV drugs target the entry process [14, 16, 28, 237, 238]. The fusion inhibitor enfuvirtide (T20) [14] and the CCR5 inhibitor maraviroc [15] are the only currently approved HIV entry drugs for both first-line and salvage therapy [16, 157, 158]. T20 targets the N-terminal heptad repeat region of gp41, blocking gp41 conformational changes essential for 6-helix bundle formation and membrane fusion [14]; however, T20 has a relatively short time window to act on the transiently exposed N-helix of gp41 at the cell-virus synapse [239]. In addition, T20 is logistically difficult to administer, as it can only be given parentally, and adverse reactions at sites of injection are common [16, 240]. Maraviroc blocks R5-tropic but not X4-tropic HIV-1; thus, clinical use requires co-receptor tropism assays prior to initiating treatment [16, 155, 157, 158]. Other small molecule entry inhibitors in development include: small molecules against gp120, gp41 and co-receptor [16-18, 241-244]; monoclonal antibodies targeting CD4 [20] and CCR5 [245, 246]; and neutralizing antibodies targeting the virion [21, 89, 247]. However, none of these latter agents have as yet advanced to first-line clinical use [248-250]. Therefore initial entry of HIV-1 into host cells remains a compelling and yet elusive target for developing agents to prevent infection[238]. This step is mediated by a sequence of interactions of a trimeric gp120/gp41 envelope (Env) protein complex with host cells, including initial gp120 encounter with the cellular receptor CD4 and a chemokine co-receptor usually either CCR5 or CXCR4[116].

Since gp120 is the first viral protein to interact with the host cell, it is an attractive target for inhibiting infection. We previously identified a peptide triazole class of HIV-1 Env gp120 inhibitors that are highly active on R5-and X4-tropic viruses and exhibit remarkable breadth among different HIV-1 subgroups [10, 32]. This inhibition is mediated by binding to a region of gp120 that partially overlaps the CD4 binding site [9, 10, 22-25, 32, 224]. The peptide triazole inhibitors appear to function mechanistically by trapping gp120 in an inactive conformation that is distinct from either the flexible, unliganded conformation or the highly structured, CD4-activated state [9, 10, 22-25, 32, 224]. This conformational entrapment serves to prevent entry prior to virion attachment to CD4 or coreceptor on target cells [9, 23]. In this study we report the first ever peptide triazole derivative that is virucidal leading to irreversible disruption of the viral particle. Following the discovery, we more elaborately characterize the mechanism of action of these unique and novel PTs and its relation to HIV-1 fusion with host cell. This therefore will showcase the first ever virucide that is not toxic to cell, broadly action and acts on the virus by hijacking the virus-cell fusion mechanism for complete irreversible lysis of the virus particle. We herein report this unexpected finding, which has significant implications for both prevention and therapeutic applications.

We found that, while all peptide triazoles tested induced shedding of gp120, only those containing a C-terminal sulfhydryl group induced p24 release. The apparent poration of virions leading to p24 release occurred on replication competent HIV-1 as well as on pseudoviruses bearing an HIV-1 Env. Remarkably, the lysis activity of the peptide triazole thiols (PTTs) was completely inhibited by fusion inhibitors that target gp41 such

as T20, C34, 5 Helix and N36. This desensitization by the fusion inhibitors suggested that the disruption of viral membranes was coupled to physiological activation of gp41 and formation of the 6-helix bundle post initial binding of gp120 to CD4 during HIV entry to host cells. We also defined kinetic and biochemical differences between inhibition of viral infectivity and phases of virion disruption. Our findings strongly suggest that the novel virolytic effect induced by KR13 is related to physiological triggering of fusion machinery on the envelope glycoprotein trimer, which in the absence of CD4 or coreceptor engagement leads to disruption of the viral membrane and potent, irreversible viral inhibition.

2.1 Production and validation of the virolytic peptide triazole thiol, KR13

2.1.1 Materials

All Fmoc-protected α- and β-amino acids, O-Benzotriazole-N,N,N',N'-tetramethyl- uranium-hexafluoro-phosphate (HBTU), 1-Hydroxybenzotriazole (HOBt), Rink amide resin (4-(2',4'-Dimethoxyphenyl-Fmoc-aminomethyl) phenoxy resin) with a 0.55 mmol/g substitution, N,N- dimethylformamide (DMF), Pyridine and N,N-Diisopropylethylamine (DIPEA) were purchased from Chem-Impex International Inc, Ethynylferrocene and Cu(I)I was purchased from Sigma-Aldrich and used without further purification. Fmoc- cis-4-azidoproline was synthesized starting with commercially available trans-Hyp-OH. Monomeric YU2 gp120 and sCD4 were produced in-house in

293F cells following a previously established protocol [10, 25]. Ten mM phosphate buffer was prepared using monosodium phosphate, monohydrate and disodium phosphate heptahydrate to reach pH 7.2. All other materials were obtained from Fisher Scientific.

2.1.2 Synthesis of Peptide Triazole and peptide triazole thiol Inhibitors

Peptide triazole and peptide triazole thiol (KR13) were synthesized by manual solid phase synthesis using Fmoc chemistry on a Rink amide resin at 0.25mmol scale. The [3 + 2] cyclo addition of azide and ethynylferrocene was carried out by copper catalyzed, on resin method [22]. Once the synthesis was complete, the peptide was removed from solid-phase resin using a cleavage cocktail mixture of 95:2:2:1 trifluoroacetic acid (TFA)/1, 2- ethanedithiol/water/thioanisole for 3 h. Crude peptide was isolated by precipitation into 20 volumes of cold ether and purified by reverse-phase HPLC (Beckmann Coulter) on a C18 column with a linear gradient of 5-95 % of acetonitrile/water in 0.1% TFA (**Figure 11A**). The final purified peptide was confirmed by MALDI-TOF-MS, m/z of KR-13: 2084.79 [M+H] + (Mcal = 2083.5 Da) (**Figure 11B**). The sequences of the main peptides produced are; HNG156 (RINNIXWSEAMM-$CONH_2$) and KR13 (RINNIXWSEAMMβAQβAC-$CONH_2$), where X is ferrocenyltriazole-Pro, were synthesized by manual solid phase synthesis using Fmoc chemistry on a Rink amide resin at a

0.25 mmol scale (**Figure 12**) [8, 22]. Control peptide triazoles, KR13s and KR13b were also prepared and validated as described above (**Figure 12**). Purity of produced peptides was confirmed by RP-HPLC and MALDI-TOF. Prior to cellular assays using peptide triazoles, we tested for their possible effects on cell viability with HOS $CD4^{+ve}$ $CCR5^{+ve}$ cells after 24 hours of inhibitor exposure. The cell viability was measured using the tetrazolium salt premix reagent, WST-1 from Takara Bio Inc. following the manufacturer's protocol. The formazan product was measured using the micro plate reader at absorbance wavelength 460 nm (Molecular Devices).

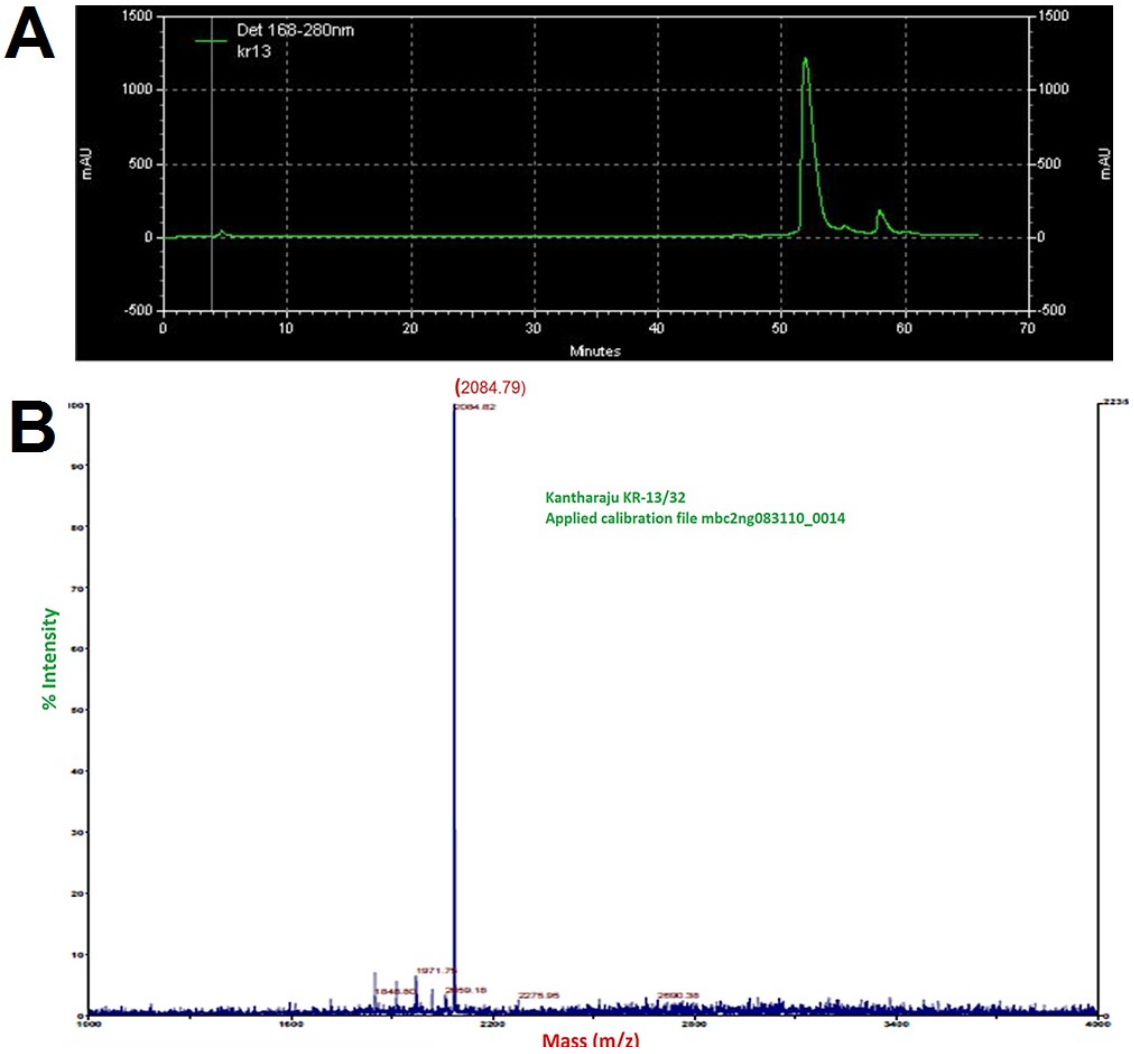

Figure 11: Validation of the lab synthesized KR13. A. HPLC profile of KR13: VYDAC-C18 analytical column: 5-95% Acetonitrile/water in 0.1%TFA. B. MALDI-TOF spectrum of KR13; m/z Obs : 2084.79 [M+H]+ (Mcal = 2083.5 Da) (data from Wistar Inc.)

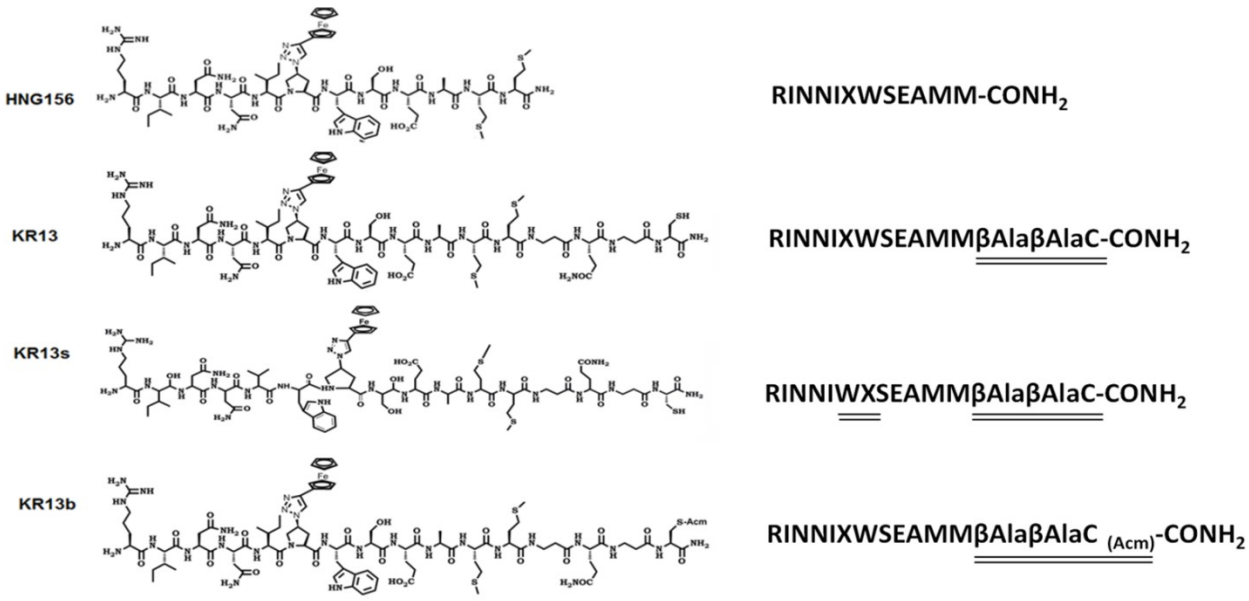

Figure 12: Chemical structures (left) and sequences (right) of the peptide triazoles HNG156, KR13, KR13s and KR13b. The chemical structures were generated in Chemdraw Pro 13.0. The underlined residues in the one letter coded sequences on the right denote the changes made to the parent peptide triazole (HNG156) to derive the three additional peptide triazoles investigated in this paper. X = ferrocenyl-triazole-Pro and Acm = Acetamidomethyl.

2.1.3 Peptide Characterization and Optical Biosensor Binding Assays

The effects of the synthesized PTs on gp120 binding of sCD4 and mAb 17b were screened by competition ELISA (Enzyme Linked Immunosorbent Assay), **Figure 12**.

In a typical assay, HIV-1YU-2 gp120 (100 ng) was immobilized on a 96-well microtiter plate overnight at 4 °C, followed by three times washing with PBST buffer (1x PBS with 0.1 % Tween-20 v/v) and blocked with 3 % BSA (Bovine Serum Albumin) in 1× PBS for 2 h. Serial dilution peptide (5uM to down 0.001 μ M) was premixed with 0.1μg/ml sCD4 and the mixture was added to the plate in triplicate (65μ/well) and incubated for 1 hour. The plate was washed three times with PBST followed by 1 hour incubation with biotinylated anti-CD4 antibody at 65μl/well (eBioscience). The PBST wash step was repeated followed by 1 hour incubation with streptavidin-bound horseradish peroxidase (AnaSpec) at 1:3000 dilution and 65μl/well. The above experiment was repeated using Serial dilution peptide (5uM to down 0.001 μ M) mixed mAb 17b (protein A purified) at 0.1 μg/ml. After 1 h incubation followed by washing three times, goat-anti-human-HRP antibody (Chemcon) was added and incubated for 1 h. The extent of HRP conjugate binding was detected in both assays by adding 200 μl o-phenylenediamine (Sigma–Aldrich) reagent for 30 min followed by measuring optical density (OD) at 450 nm using a micro plate reader (Molecular Devices). All incubation was done at room temperature unless otherwise mention and the samples were loaded in triplicate.

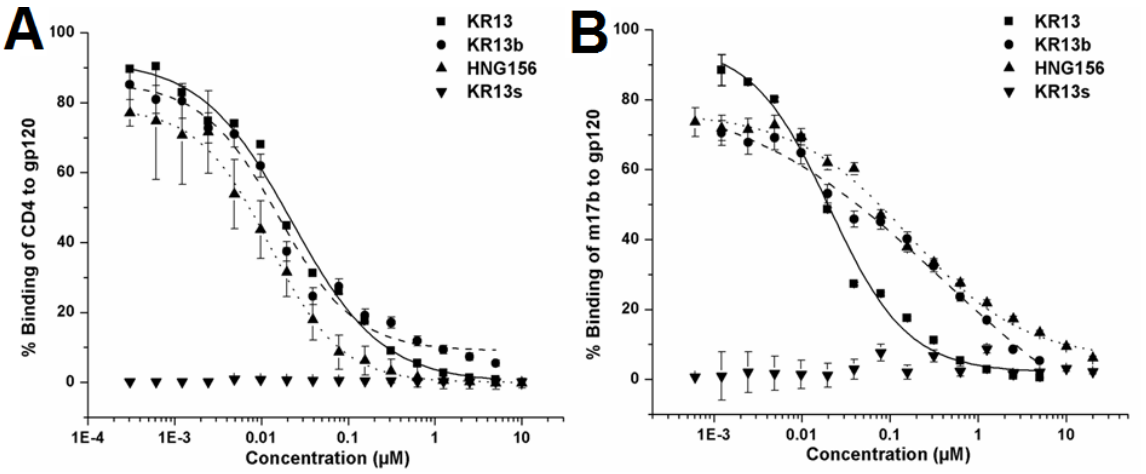

Figure 13: ELISA-derived competition of sCD4 (a) and m17b (b) binding to plate-immobilized gp120 by KR13, HNG156, KR13s, and KR13b. The optical density values obtained for sCD4 and 17b binding to the gp120 in the absence of peptide were taken as 100% binding controls. The IC50 values calculated for sCD4 competition by KR13, KR13b, HNG156 and KR13s were 22.2 ± 3.2 nM, 15.8 ± 2.9 nM, 12.4 ± 1.2 nM and undetected. The IC50 values calculated for 17b competition by KR13, KR13b, HNG156 and KR13s were 20.5 ± 3.5 nM, 415.8 ± 22.9 nM, 165.7 ± 27.6 nM and undetected. Error bars represent the standard deviation of the mean, n > 3.

Surface Plasmon resonance (SPR) interaction analyses were performed on a Biacore 3000 optical biosensor (GE Healthcare) (**Figure 14)** at 25°C using standard 1× PBS, pH 7.3, with 0.005% Tween-20. A CM5 sensor chip was derivatized by amine coupling by using N-ethyl-N-(3-dimethylaminopropyl) carbodiimide /N-hydroxysuccinimide-1 with HIV-1YU-2 gp120 (Fc2 cell) and as a control surface, mAb 2B6R (antibody to human IL-5 receptor α, Fc1 cell). For direct binding experiments, HIV-1YU-2 gp120 was immobilized on the sensor surface (~5500 RU); peptide analyte in PBS buffer (concentration range of 125nM to 0.98 nM) was passed over the surface at a flow rate of 50 μL min−1 with a 5 min association phase and a 5 min dissociation phase. Regeneration of the surface was achieved by a single 5 second pulse of 10 mM glycine, pH 1.5. Data analysis was performed using BIAEvaluation 4.0 software (GE). A double reference subtraction was performed for each data set to account for non-specific binding. The steady state affinity analysis was performed by plotting data of association equilibrium value selected from 10 sec before dissociation phase for each concentration v/s peptide concentration (**Figure 14**).

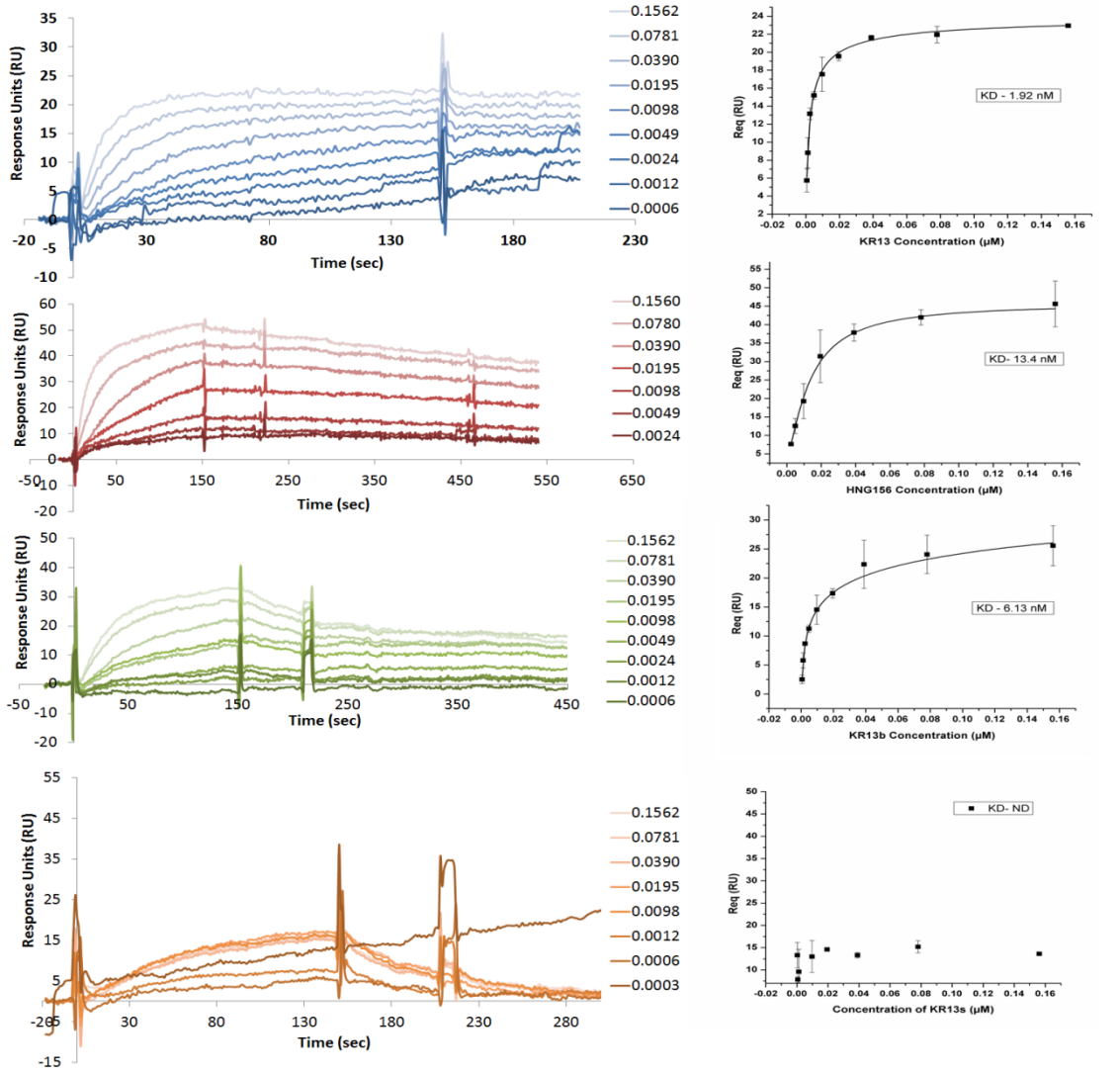

Figure 14: Sensorgrams obtained from SPR analysis of direct binding of KR13, HNG156, KR13b and KR13s to gp120. The peptides at concentrations ranging from 0.0003 µM to 0.156 µM were injected at a constant flow rate of 100 µl/min with 250 µl injection volume onto the surface of immobilized YU2 monomeric recombinant gp120. YU2 monomeric recombinant gp120 produced in 293F cells was immobilized on a Biacore CM5 chip at surface density of 2500 RU using EDC/NHS chemistry explained in detail in the Supplementary Text section. The graphs on the left show the sensorgrams obtained post double reference subtraction using the BiaEvaluation software. The graphs

on the right show steady state fit analysis of the R_{eq} values for each peptide concentration. The R_{eq} values were calculated using the BiaEvaluation software, with separate k_{on} and k_{off} fit analysis using the Langmuir equation described in Supplementary Text section. Error bars represent standard deviation of the mean, n = 3.

2.1.4 Cell viability analysis in presence of peptide triazoles

Viability of cells in the presence of peptides KR13, HNG156, KR13b and KR13s was assessed using the tetrazolium salt premix reagent, WST-1, from Takara Bio Inc. following the manufacturer's protocol (**Figure 15**). HOS CD4+ve CCR5+ve cells were treated with increasing concentrations of each peptide ranging from 0.1 μM to 250 μM and incubated overnight at 37°C. Following media change, 10 μl of the tetrazolium salt was added to each sample and incubated for 30 minutes at 37°C. The formazan product was measured using the micro-plate reader at absorbance wavelength 460 nm (Molecular Devices).

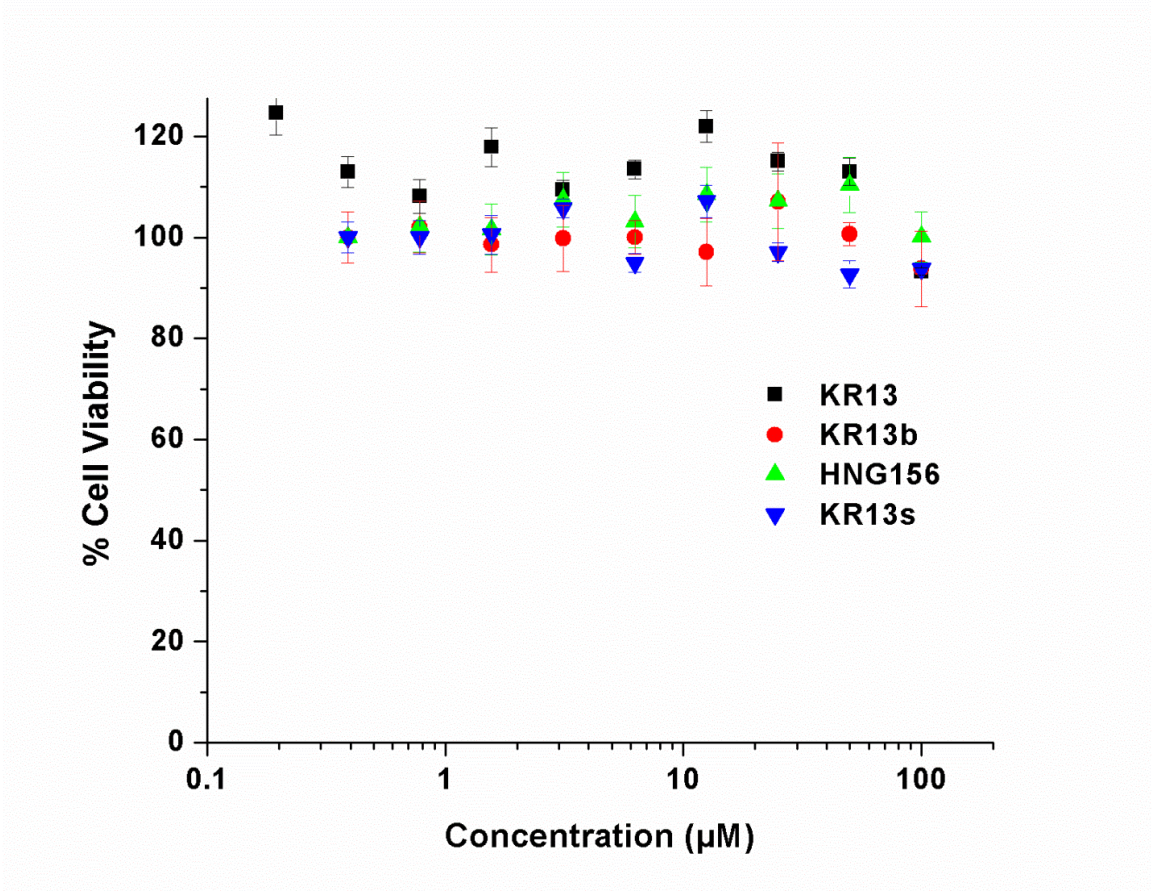

Figure 15: Cell Viability of HOS CD4+ve CCR5+ve cells in the presence of HNG156, KR13, KR13b and KR13s. The samples were tested using the WST-1 assay following manufacturer's protocol. The viability of HOS CD4+ve CCR5+ve cells in the absence of inhibitor was the 100% control.

2.1.5 Results

The synthesis of the virolytic peptide triazole is the same as the regular peptide triazole with the same pharmacophore (shown in blue in **Figure 11**). Except the scrambled sequence of KR13 (KR13s) the other PTs compete with both CD4 and 17b binding to gp120 monomer showing that these peptides are dual acting, blocking both CD4 and 17b interaction (**Figure 13**). Peptide binding to gp120 was determined using surface plasmon resonance (SPR) interaction analysis, with K_d values for KR13, KR13b, and HNG156 found to be 2.71nM, 6.13 nM, and 13.4 nM, respectively (**Figure 14**). Binding analysis of KR13s by SPR direct analysis yielded low and inconsistent dose dependent signals, and no K_d was determined in this case. The K_d values were determined using BiaEvaluation software using the steady state affinity model. It was also confirmed that the peptide triazoles in this study did not induce any significant cell toxicity by testing viability of HOS CD4+ve CCR5+ve cells exposed to these inhibitors for 24 hours at 37 °C (**Figure 15**).

2.2 Antiviral functions of peptide triazoles and the peptide triazole thiol

The antiviral functions of the peptide triazole variants were tested both on the virus-host cell interaction as well as on the cell-free virus. This is important to test

so that when these peptides are transitioned into microbicides we can target on different stages of the virus lifecycle depending on their anti-viral functions observed.

2.2.1 Materials

Modified Human Osteosarcoma Cells (HOS $CD4^{+ve}$ $CCR5^{+ve}$) engineered to express CD4 and CCR5, receptor and co-receptor respectively, as well as pNL4-3.Luc R-E- backbone DNA, were obtained from Dr. Nathaniel Landau[251]. The HOS $CD4^{+ve}$ $CCR5^{+ve}$ cells were grown in DMEM supplemented with 10% FBS, 2.5% HEPES, 1% Penicillin- Streptomycin, 2% L-Glutamine and 1 mg of puromycin. 293T cells were obtained from American Type Culture Collection and grown in the same culture medium as the HOS $CD4^{+ve}$ $CCR5^{+ve}$ cells except without puromycin. The plasmids for HIV-1 BaL-01 gp160 and VSV-G Env DNA were gifts from Dr. Julio Martin-Garcia. The antibodies mouse anti-p24, rabbit anti-p24, and the protein p24, were from Abcam. Monomeric YU2 gp120 and sCD4 were produced in-house in 293F cells following a previously established protocol [10, 25]. Fully Infectious HIV-1 (BaL) was a gift from Dr. Michele Kutzler and obtained from Penn Center For AIDS Research (CFAR). The protein gp120 monomer was produced using already-established protocols [25], anti-gp120 was from Alto chemicals. Gp41 protein, enfuvirtide (T20) and anti-gp41 antibodies 4E10, 2F5 and 98-6 were from NIH AIDS Research and Reference Reagent Program (ARRRP). Enhanced chemiluminescence western

blot detection system was from Amersham. O-phenylenediamine (OPD) was from Sigma Aldrich. All other materials were from Fisher Scientific.

2.2.2 Pseudoviral infection assay

2.2.2.1 Production of single-round recombinant luciferase producing HIV-1 virus like particles (VLPs):

The recombinant virus consisted of (1) the pro-viral envelope plasmid sequence corresponding to the CCR5 targeting HIV-1BaL strain or a VSV (Vesicular Stomatitis Virus) pseudotype and (2) the backbone sequence corresponding to an envelope-deficient pNL4-3-Fluc+env– provirus developed by N. Landau[252]. 4 μg of envelope and 8 μg of backbone DNA were co-transfected into 293T cells using FuGene 6 as the transfection reagent [253]. Fourteen hours post-transfection, the medium was changed, and subsequently the VLP-containing supernatants were collected at 48 hours post transfection. The VLP-containing supernatants were cleared using a 0.45 μm syringe filter and purified further by spinning the sample on an iodixanol gradient, using a Hoefer continuous gradient maker, ranging from 6 - 20 % iodixanol, at 30,000 rpm for 2 hours at 4 °C (**Figure 16**). The collected fractions were validated for p24 content using capture ELISA and for gp120 content using western blot detection as described in the main text. Virions purified on the 6-20% iodixanol gradient exhibited a characteristic distribution

profile of p24 and gp120 content (**Figure 16**), enabling viral (18-19.2% iodixanol) and soluble protein (6-8% iodixanol) fractions to be isolated. The purified virus samples were collected between the 18.2%-19% iodixanol fractions on the gradient, aliquoted and stored at -80°C until further use (**Figure 16**).

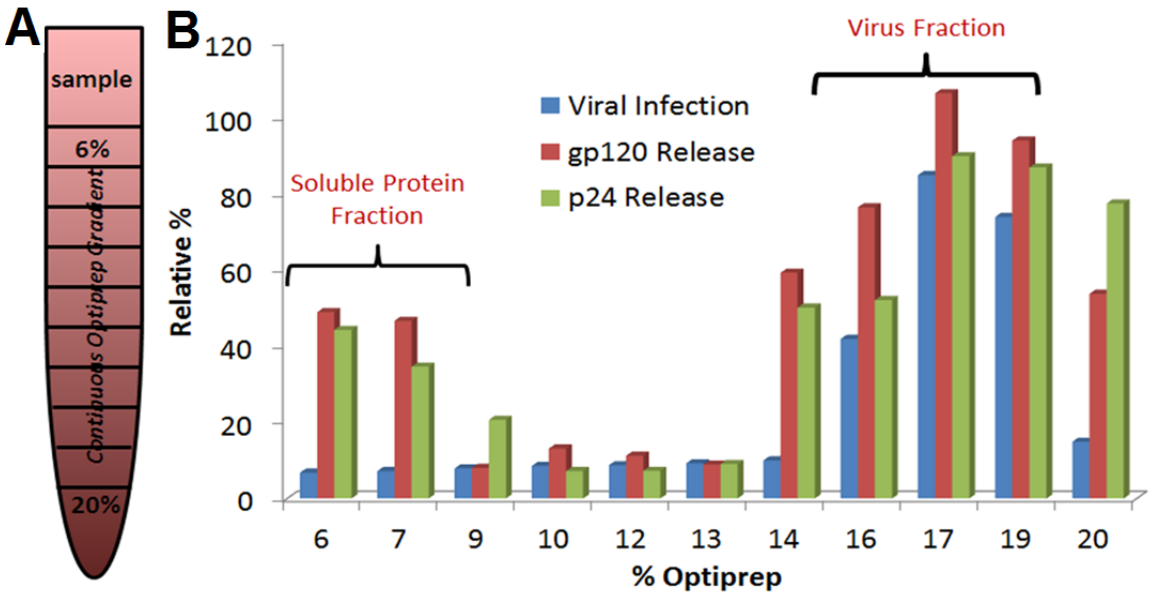

Figure 16: Scheme depicting method of purification of intact virus and peptide-triazole derived virus breakdown products by gradient centrifugation. (A) Scheme of location of sample loading and the positions of the 20% and the 6% optiprep fractions after centrifugation. (B) Plot of the virus infection, gp120 release and p24 release activities for the iodixanol fractions collected from the gradient post KR13 (1 μM) treatment. The soluble protein fraction corresponded to 6-8% iodixanol, and the treated virus fraction to the 16-18% fraction, based on the presence respectively of freely soluble p24 and gp120 in the former and viral infection activity in the latter. The controls include virus treated with PBS (intact virus) and virus treated with 1% triton X and boiled for 5 min at 95°C before gradient purification (solubilized proteins).

2.2.2.2 Luciferase reporter assay:

A luciferase reporter assay was used to monitor cell infection activity of pseudovirion preparations as well as the inhibition of infection. For the infection profiles, 8,000 cells per well in a 96 well plate were incubated for 24 hours followed by addition of serial dilutions of the gradient purified virus fractions. Forty-eight hours post infection, luciferase activity was measured [8]. Cells were lysed with 50 µl of Passive Lysis Buffer (Promega) per well for 5 minutes followed by quick freeze/thaw cycles. Luciferase assay was performed using 1 mM D-luciferin salt (Anaspec) as substrate and detected on a 1450 Microbeta Liquid Scintillation and Luminescence Counter (Wallac and Jet). For inhibition of infection assays with the peptide triazoles, infectious dilutions (1 million RLU (Relative Luminescence Units)) of the pre-tested purified virions were pre-incubated with serial dilutions of the inhibitor for 30 minutes at 37°C. HOS $CD4^{+ve}$ $CCR5^{+ve}$ cells, seeded at 8,000 cells per well in a 96 well plate, were incubated for 24 hours followed by addition of the pre-incubated inhibitor-virus complex. Forty eight hours post infection, luciferase activity was measured as explained above [8]. The same method was used in order to measure the effect of the peptides, KR13 and HNG156, on the HOS $CD4^{-ve}$ $CCR5^{+ve}$ cells in order to check for possible enhancement of infection (**Figure 16**). Non-linear regression analysis was used with Origin Pro.8 (Origin Lab) to determine IC_{50} values. All experiments were performed at least in triplicate, and results were expressed as

relative infection with respect to cells infected with virus in the absence of inhibitor (taken as 100% infection).

2.2.3 P24 Release assay

Serial dilutions of peptide triazole starting from 50 μM were incubated for 30 minutes with working dilution of the purified pseudotyped HIV-1 BaL virus. Control samples included (1) PBS with virus and (2) 1% Triton X-100 with virus. Ten 1 ml fractions were collected from the gradient. Each fraction was tested for p24 content using capture ELISA. High binding polystyrene ELISA plates were coated overnight at 4°C with 50 ng of mouse anti-p24 and blocked with 3% BSA. The blocked plate was rinsed 3 times with PBS-T (PBS and 0.05% Tween 20), and 1 ml gradient fractions were loaded onto the plate using a 1:10 dilution factor with 0.5% BSA in triplicate. After two hour incubation, rabbit anti-p24 was added to the plate for 1 hour, following PBST rinse (3 times, 5 minutes each), and then anti-rabbit IgG fused to horseradish peroxidase (HRP) was added to the plate and incubated for another hour. Following further PBST rinse, o-Phenylenediamine (OPD) was added to the plate and incubated in the dark for 30 minutes. The optical density (OD) was measured at 450 nm using a micro plate reader (Molecular Devices).

2.2.4 Gp120 shedding assay

The HIV-1 BaL pseudovirions were treated with the peptide triazole of interest for 30 minutes at 37 °C, and the fractions were collected from centrifugation in a 6-20% iodixanol gradient. Fractions were boiled with SDS loading buffer for 5 minutes and proteins separated on a 12% SDS non-reducing polyacrylamide gel (NuPAGE – Invitrogen). As a control in the gels, YU2 recombinant gp120 monomer produced in 293F cells was used at 500ng/ml. This control usually runs as a lower molecular weight species compared to the BaL virus gp120. We surmise that this is due to an altered glycosylation pattern for the cell type (293F) used to express the recombinant protein versus the cells (293T) used to produce the BaL virus. The 293T cells produced gp120 runs approximately at 100 kDa while the gp120 from 293F cells runs approximately at 120 kDa (data shown in bastian et al. 2013)[6]. The separated proteins in the gels were electrophoretically transferred onto (Polyvinylidene Fluoride) PVDF membrane at 100 mV for 1 hour. The blotted membrane was blocked with 5% skimmed milk in PBST for 1 hour at room temperature. After washing the membrane with PBST, sheep gp120 antibody (D3724) diluted in 5% skimmed milk was added and incubated for 1 hour at room temperature. The bound antibodies were detected by horseradish peroxidase-conjugated anti-sheep IgG secondary antibody followed by the enhanced chemiluminescence detection system (Amersham) according to the manufacturer's protocol.

2.2.5 Viral infection inhibition and viral breakdown of fully infectious HIV-1 by peptide triazoles

Virions were purified using 6-20% iodixanol gradient and p24 content measured using ELISA. The $TCID_{50}$ was determined using Origin Pro.8 (Origin Lab). The working dilution of virus was pre-treated with a serial dilution of KR13 or HNG156 starting from 100 μM for 30 min at 37 °C. HOS $CD4^{+ve}$ $CCR5^{+ve}$ cells seeded, at 8,000 cells per well in a 96 well plate, were incubated for 24 hours followed by addition of pre-incubated inhibitor-virus mixture. After 48 hours infection, p24 content of virions in the supernatant was measured in order to determine the IC_{50} value of viral inhibition. Further, the peptide triazole and cell-free virus were pre-incubated for 30 min at 37°C followed by spinning for 2 hours at 13,600 rpm in a table top centrifuge (Eppendorf) at 4°C. Supernatant was separated and p24 content determined using the p24 capture ELISA explained above. The extents of viral inhibition and p24 release from fully infectious HIV-1 BaL were also evaluated for control peptide HNG156.

2.2.6 Results of the antiviral effects of peptide triazoles

2.2.6.1 Separation of virus components derived from HIV-1 breakdown induced by peptide triazoles:

To probe the effects of peptide triazoles on HIV-1, gradient-purified viral pseudotype particles containing the HIV-1 BaL Env were treated with various peptide triazole variants and then fractionated using iodixanol gradient centrifugation [254]. The density gradient enabled separation of the solubilized proteins from the residual virion fraction. Each gradient fraction was tested for viral infectivity and protein content. Proteins released from virus particles were present in the 6-8% Optiprep fraction (soluble protein fraction), while the intact virions were present in the 18.2-19% Optiprep fraction (residual virion fraction). Solubilized protein and residual virion fractions were evaluated for infectivity and for p24, gp120 and gp41 content (**Figure 16**).

2.2.6.2 Dose dependence and specificity of KR13-induced virus breakdown:

We compared the effects of KR13 and control peptides on HIV-1 infectivity and structure. Peptides included KR13b (KR13 with the thiol blocked with an acetamidomethyl (ACM) group); KR13s, which contains a WX scrambled KR13 amino acid sequence in the gp120-binding IXW pharmacophore [10, 22, 32]; and the parent peptide triazole HNG156, which contains no free thiol group [22] (**Figure 12**). These peptides were chemically synthesized using previously established methods [22, 23, 31, 32]. Anti-viral effects of the peptide triazoles were initially measured using HIV-1 BaL pseudotyped virions. As shown in **Figure 17A**, peptides KR13, KR13b, and HNG156 each inhibited infection, with KR13 and KR13b exhibiting the greatest potency, while the sequence-scrambled peptide control KR13s was inactive. Peptide effects on the contents of the virions were determined by treating gradient-purified pseudotyped particles with increasing concentrations of each peptide and determining gp120 shedding and p24 release. The peptides KR13, KR13b and HNG156, but not the KR13s control, caused gp120 shedding (**Figure 17B; see Appendix Fig. 1 for western blot images**). IC_{50} values for gp120 shedding by the active peptides were comparable (**Table 1**) and similar to IC_{50} values for inhibition of cell infection. In contrast, KR13, but not the other peptide triazoles, induced p24 release (IC_{50} 32 ± 10 nM) (**Figure 17C**). The samples were

normalized to the untreated virus, for which spontaneous p24 release and gp120 shedding were both <5% of the total protein contents as determined by solubilization of the virus particles with 1% triton X treatment (**Appendix Fig. 1**). No inhibition of infection was observed on viruses pseudotyped with either VSV-G or AMLV envelope, indicating that the effects on HIV-1 were highly specific (**Appendix Fig. 2**). All the IC_{50} and EC_{50} values were obtained using sigmoidal plot fit in Origin Pro. 8.

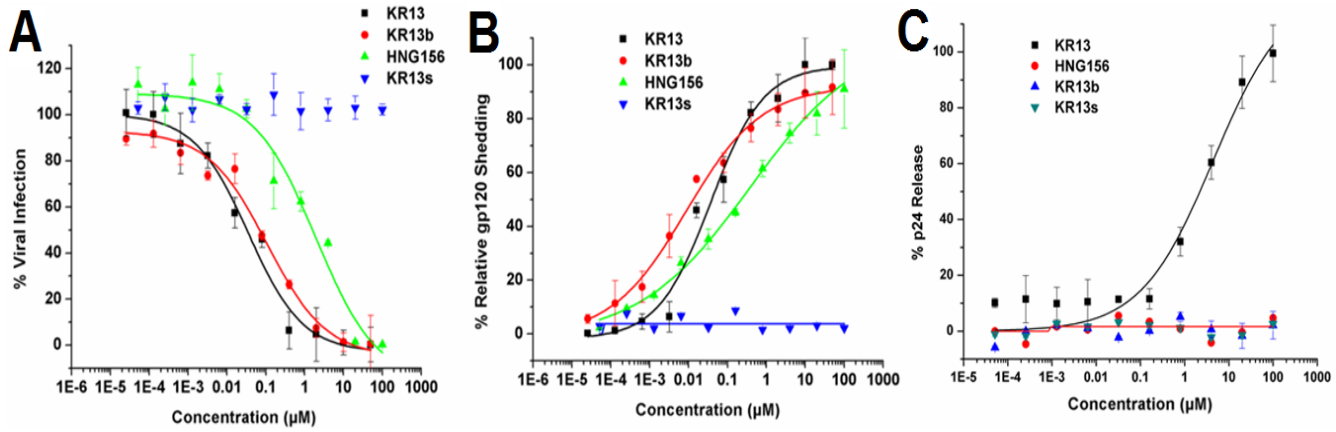

Figure 17: Dose response of the effects of peptide triazoles on HIV-1 BaL pseudovirus. (A) Inhibition of cell infection was measured using a single round infection assay. The EC_{50} values are reported in Table 1. (B) Relative gp120 shedding was determined for the peptides KR13, KR13b, HNG156 and KR13s using western blot analysis. Electrophoretic bands of gp120 in soluble protein and residual virus fractions were quantified using Image J analysis; IC_{50} values obtained are in Table 1. A low level of gp120 shedding (<5%) was observed with the intact virus used as the negative control. Data were normalized to 100% gp120 shedding observed with 1% triton X treated lysed virus. (C) Relative p24 release induced by peptides was measured using ELISA. The data were normalized using untreated virus as negative control (<5% p24 release), and p24 release observed with 1% triton X treated virus was taken as 100% p24 content. The p24 release IC_{50} value for KR13 was 500 ± 80 nM, while the other peptide triazoles exhibited no significant p24 leakage. Sigmoidal curve fits of data were obtained using Origin Pro.8 (Origin Lab). Error bars represent

2.2.6.3 Effects of KR13 on fully-infectious virus:

To determine if the effects of peptide triazoles on pseudotyped HIV-1 BaL particles would also occur on infectious viruses, we performed a dose response analysis for viral infection inhibition and p24 release on fully infectious HIV-1 BaL. As shown in Table 1 and **figure 17**, both HNG156 and KR13 inhibited viral infectivity on HOS $CD4^{+ve}$ $CCR5^{+ve}$ cells (IC_{50} values of 0.53 μM and 5.5 μM, respectively), and caused both gp120 shedding (IC_{50} value of 1.2 μM) and p24 release (IC_{50} value of 4.4 μM) (**Figure 18**). Thus, the virolytic activity induced by KR13 on pseudotyped HIV-1 virions was also seen with replication competent HIV-1. All the IC_{50} and EC_{50} values were obtained using sigmoidal plot fit in Origin Pro. 8.

2.2.6.4 Breadth analysis of peptide triazole thiol induced virolysis

In order to examine if the virolytic effect induced by KR13 occurs broadly with multiple clades of the HIV-1 virus family, we tested several variants from each of clades A, B and C. We also examined transmitted founder viruses prepared from Env plasmids ZM246F.C1G, ZM247Ffs and ZM249M.B10.D4. From the p24 release effects observed (**Figure 19**), it is evident that the virolytic effect induced by KR13 indeed occurs broadly, with IC_{50} values ranging from 0.7 μM to 26 μM. This range of action is

consistent with the viral infection inhibition breadth analysis conducted by McFadden et al. 2011 for the parent peptide HNG156 [10]. The results obtained show that peptide induced virolysis is conserved and inactivates multiple clades of HIV-1.

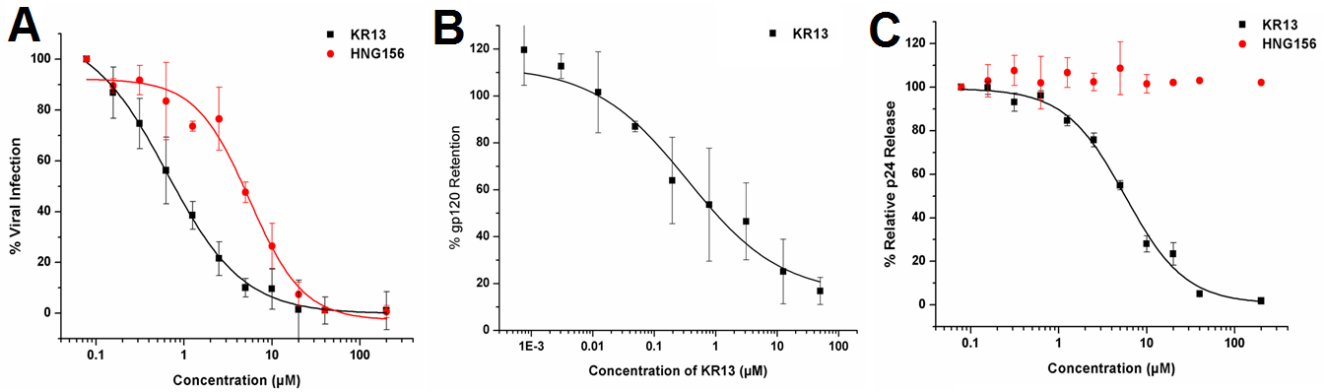

Figure 18: Inactivation (A) and virion breakdown (B and C) of HIV-1 BaL fully infectious virus by KR13 and HNG156. The EC50 values for inhibition of infection by KR13 and HNG156 were 639 ± 68.9 nM and 5.5 ± 0.9 μM, respectively. Gp120 Retention (B) was tested by western blot analysis using D7324 anti-gp120 on the residual gp120 on the virions treated with KR13. The IC50 of KR13 gp120 shedding was 1.2± 0.93 μM. Release of p24 by KR13 and HNG156 (C) was tested with a p24 leakage assay using ELISA as explained in the Materials and Methods section. The IC50 value for KR13 induced virolysis was 4.4 ± 0.7 μM. No p24 release was observed by HNG156 upto at 200 μM. All of the above EC50 and IC50 values were obtained using the Origin Pro. 8 software with sigmoidal fits. Error bars represent the standard deviation of the mean, n = 3.

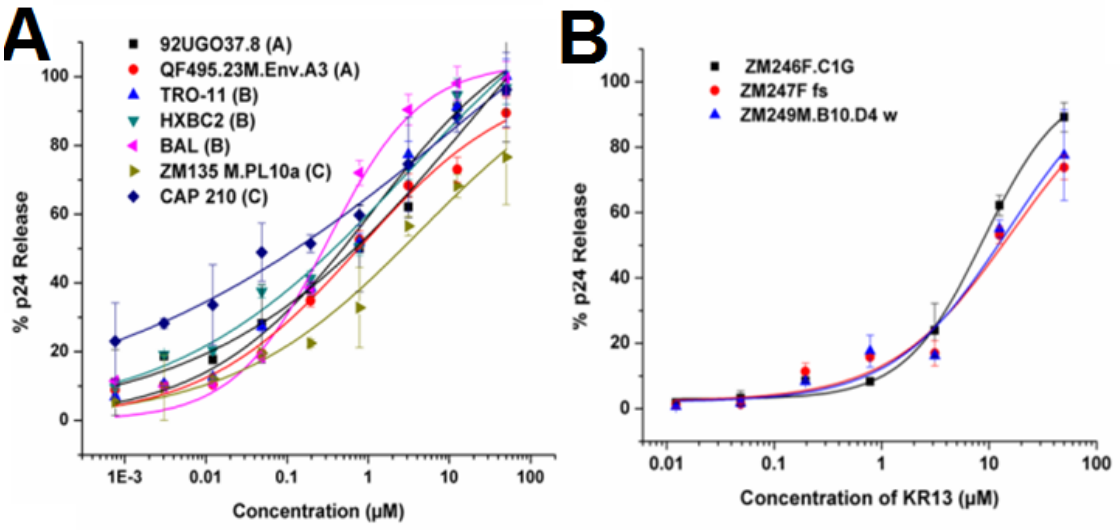

C

Virus	P24 Release IC50 (μM)
92UG037.8 (A)	0.67 ± 0.24
QF495.23M.Env.A3 (A)	3.34 ± 1.14
TRO-11 (B)	1 ± 0.35
HXBC2 (B)	1.89 ± 2.0
BAL-01 (B)	0.8 ± 0.03
ZM135 M. PL10a (C)	1.86 ± 0.86
CAP 210 (C)	25.6 ± 2.31
ZM246F.C1G (founder)	8.8 ± 1.66
ZM247F fs (founder)	16 ± 2.2
ZM249M.B10.D4 W (founder)	15 ± 1.8

Figure 19: Antiviral breadth of KR13 induced virolysis. Dose responses, shown by sigmoidal curve fits, were obtained using Origin Pro. 8 (explained in Materials and Methods section) for p24 release induced by KR13 ranging from 1 nM to 50 μM from several clades of HIV-1 pseudoviruses (A) and transmitted founder viruses (B). (C) Table of the IC50 values obtained from (A) and (B). Error bars represent the standard deviation of the mean, n = 3.

2.3 Mechanism of the peptide triazole thiol virolysis

In order to study in detail the mechanism of the KR13 virolysis, the kinetic breakdown of the lysis, the immunological and morphological characteristics of the residual virus post treatment as well as how fusion inhibitors affect this lytic event was studied. This lead to defining kinetic and biochemical differences between inhibition of viral infectivity and phases of virion disruption. Our findings strongly suggest that the novel virolytic effect induced by KR13 is related to physiological triggering of fusion machinery on the envelope glycoprotein trimer, which in the absence of CD4 or coreceptor engagement leads to disruption of the viral membrane and potent, irreversible viral inhibition.

2.1.4 Kinetic tracking of transitions during peptide-induced viral breakdown

The time course of peptide triazole dependent HIV-1 breakdown was evaluated. The respective peptide triazole was pre-incubated with purified virus at a working concentration for times ranging from 1 min to 24 hour at 37°C. The treated samples were then purified on a 6-20 % iodixanol gradient as explained above. For each time point, purified virions incubated with PBS at 37°C and alternatively with 1% Triton-X 100 was used as negative and positive controls, respectively. Each fraction was collected and quantified for p24 (capsid protein), gp120 and viral infection as explained above.

Based on IC50 values (**Table 1**), a working dilution of gradient-purified pseudotyped HIV-1 particles was exposed to KR13 (1 μM) or HNG156 (100 μM), with incubation times ranging from 1 min to 24 hours at 37 °C. The infectivity of viruses was evaluated, and fractions from post-exposure density gradient fractionation were tested for relative gp120 shedding and p24 release by determining the distribution of protein content between the soluble and virion-containing fractions. As shown in **Figure 20**, infectivity inhibition and gp120 shedding had similar kinetics for both KR13 and HNG156 peptides. However, p24 release was only induced by the KR13 peptide and was delayed kinetically. Thus, p24 release from viral particles was clearly distinct from effects of peptides on infectivity and gp120 shedding. Each time point was normalized to its own negative control, which was the untreated virus, and to 100% release determined by 1% triton X treated virus. The negative controls showed minimal spontaneous p24 release and gp120 shedding of 5 to 15% from 1 min to 24 hours, respectively. All the IC50 and EC50 values were obtained using sigmoidal plot fit in Origin Pro. 8.

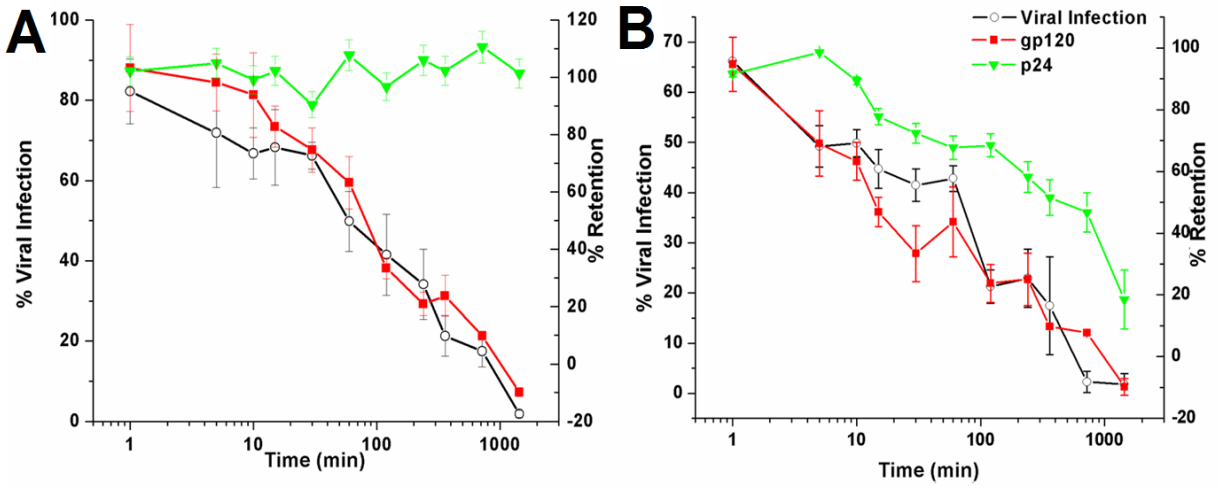

Figure 20: Time-dependence of viral breakdown by HNG156 (a) and KR13 (b) treatments of HIV-1 BaL pseudovirus. The % of cell infection retained after peptide treatment is shown on the left y-axes, and the viral protein gp120 and p24 retained in the virus fraction is shown on the right y-axes. All samples were adjusted to the untreated virus as 100% infection and 100% viral protein retention. Each time point had a control of untreated virus, and this was used to normalize each time point of peptide treatment. The concentrations of KR13 and HNG156 were kept constant for each time point at 1 μM and 100 μM, respectively. Untreated controls showed <5% p24 release and gp120 shedding, and <2% loss of cell infection activity. Error bars represent the standard deviation of the mean, n = 3.

2.1.5 Detection of immunoreactive gp41 on virions post peptide-induced virus breakdown

Residual virus and released protein fractions obtained by gradient purification from KR13 and HNG156 treatments were analyzed for gp41 content. Initially, the presence of gp41 in the treated fractions was detected using western blot analysis with human mAb 98-6 followed by anti-human IgG HRP secondary antibody. Blots were analyzed using the Enhanced Chemiluminescence detection system (Amersham).

We also measured the presence of gp41 epitopes for human mAb's 2F5 and 4E10 using an altered ELISA detection method to minimize virus particle disruption [255]. Pseudovirions were treated for 30 min at 37°C with increasing concentrations of either KR13 or HNG156, and samples spun on a 6-20% iodixanol gradient. Virus fractions were collected and fixed with equal volume of 0.1% paraformaldehyde for 30 minutes at 4°C. The treated virus fractions were spun at 16,000 X g for 2 hours at 4°C in an Eppendorf table top centrifuge. Following PBS wash, fixed virions were coated on an ELISA plate at 50 µl per well and incubated overnight at 4°C. The plate was blocked with 3% BSA, and ELISA was used to detect gp41 epitopes with human gp41 antibodies 2F5 and 4E10 followed by addition of anti-human IgG HRP secondary antibody. This method also was used to assess time-dependent

exposure of gp41 epitopes on the pseudotyped HIV-1 BaL virions induced by KR13 and HNG156 treatment at 1 μM constant concentration.

Initial western blot analysis of KR13 and HNG156 treated HIV-1 BaL pseudotype virions were performed using the human anti-gp41 mAb 98-6, which reacts with a linear epitope at residues 644-663 in the gp41 ectodomain. Following either KR13 or HNG156 treatment, gp41 remained associated with virions (**Appendix Fig. 2**), while gp120 was released into the soluble fraction (**Figures 17 and 120**).

Remarkably, for KR13-treated particles, gp41 was detected only weakly by 98-6 in either soluble or virion-associated fractions. To determine if this effect resulted from a peptide-induced conformational change that blocked exposure of the 98-6 epitope, binding was assessed to conformationally dependent gp41 antibodies 4E10 and 2F5, which react with membrane-associated MPER epitopes at the base of the gp41 ectodomain. To test the antibody binding, the peptide-treated purified virions were fixed using 0.1% paraformaldehyde in order to maintain gp41 conformation. The fixed virions were evaluated by ELISA as described above. On untreated or HNG156-treated virions, MPER epitopes were poorly exposed (**Figure 21**). However, on KR13-treated virions, reactivity to 4E10 and 2F5 increased in a dose-dependent manner and occurred at concentrations comparable to those required to induce gp120 shedding and p24 release (**Figure 21A**). This effect was also time-dependent,

with kinetics similar to that seen for p24 release (**Figure 21B**). Thus, while KR13-treatment induced p24 release, gp41 was clearly retained on virions, but in a conformationally altered state associated with loss of 98-6 epitope and exposure of MPER-associated epitopes.

2.1.6 Analysis of the peptide-treated virions by transmission electron microscopy

Transmission Electron Microscopy (TEM) was conducted to visualize the morphology of the virions treated with KR13. Purified pseudotyped HIV-1 BaL virus and KR13 were pre-incubated from 5-1440 min at 37 °C. Following incubation, samples were fixed with 2% gluteraldehyde for 30 minutes at room temperature, and then embedded in Spur's low viscosity epoxy medium after acetone washes to dry the virions, slices (100 nm thick) were prepared using an ultra-microtome (Leica EM UC6), loaded onto a holey carbon TEM 200 mesh grid (Electron Microscopy Science) and imaged using the JEM 2100 operated at 120 kV (JEOL, Japan). Sixteen images were taken per sample, and the sizes of observed particles were determined, using Image J software to derive average diameters of the virion particles from TEM images measured from 5 angles.

Transmission electron microscopy (TEM) analysis was conducted to assess the morphology of KR13-treated virions before and after p24 release. Pseudotyped HIV-1 BaL was treated with KR13 (1 μM) from 1 min to 24 hours and samples

removed at various time points for TEM imaging. A total of 16 images per sample were taken (**Appendix Fig. 4**), and a probability distribution was plotted to determine the average diameter of the virions pre- and post-KR13 treatment (**Figure 21C**). Following KR13 treatment, virion diameter was reduced by >50% after 24 hours. In addition and in contrast to the pre-incubation time point when cores were typically condensed and clearly observed, the core morphology of KR13-treated virions at 24 hours was substantially different, with a shriveled and disordered appearance. Similar, although less impressive, morphologic changes were observed at 360 minutes, a time point at which a 50% reduction in virion p24 content was observed (**Figure 20**). Thus, consistent with biochemical and immunological changes in KR13-treated virions, striking morphologic differences were also evident.

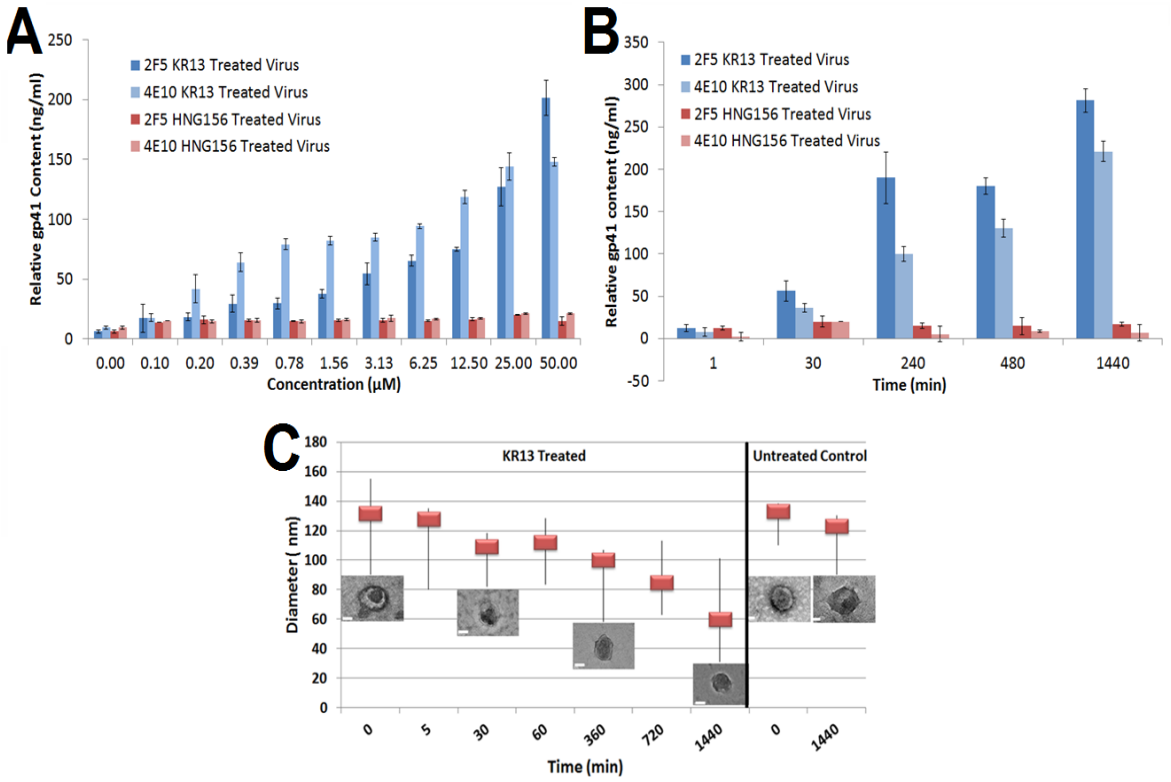

Figure 21: The gp41 content and morphology of residual virions derived from peptide triazole treatments of HIV-1 BaL pseudovirus. (a) Reactivity of residual viruses, from 18.2-19% Optiprep fractions, to gp41 antibodies 2F5 and 4E10 as a function of KR13 and HNG156 concentration. (b). Reactivity of residual viruses to gp41 antibodies as a function of time of treatment with KR13 and HNG156. All samples in (a) and (b) were normalized to total gp41 content on intact virion. Error bars represent the standard deviation of the mean, n = 3. (c) Average diameter of HIV-1 BaL virions untreated and post treatment with KR13 (1 μM) as determined by TEM. The probability distribution box plot shows the average in red and the distribution in bar lines (n=16). The diameter analysis was conducted using Image J Software. Inset: Representative TEM Images obtained at designated time points, with the scale bar representing 50 nm diameter.

2.1.7 Fusion inhibitor enfuvirtide (T20) effects on virolysis

The effect of T20 on virus breakdown by KR13 was assessed. KR13 at 1 μM and serial dilutions of T20 starting at 1 μM were co-incubated with pseudotyped HIV-1 BaL for 30 min at 37°C. Treated virion samples were fractionated on a 6-20% iodixanol gradient (above). Gradient fractions were quantified for p24 using ELISA, and relative p24 release was quantified and plotted using the Origin Pro.8 (Origin Lab). Collected gradient fractions also were analyzed for gp120 shedding using western blot analysis, with detection using primary antibody D7324 and secondary anti-sheep HRP. The bands of the blot were analyzed using Image J software. The IC_{50} values were calculated using Origin Pro.8 (Origin Lab). To further determine whether T20 inhibited peptide-induced virolysis through gp41 interaction, a T20-resistant, gp41-mutated HIV-1 virion was validated and tested for T20 inhibition of KR13-induced virus breakdown. To additionally confirm the specificity of the T20 inhibition, a competition surface plasmon resonance experiment was conducted (Appendix text). Data were analyzed using Biacore 3000 optical biosensor (GE Healthcare) BiaEvaluation software. Steady state analysis was conducted using the method of Morton et al. [256] (**Figure 22**).

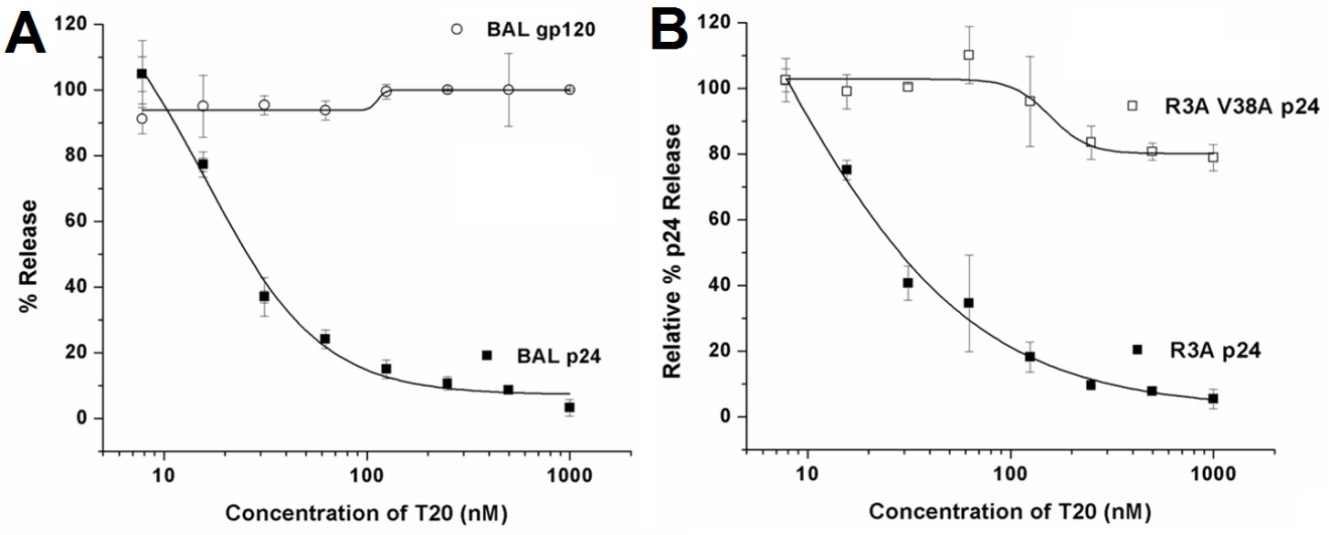

Figure 22: Inhibition of KR13-induced virus breakdown by the gp41-binding fusion inhibitor T20. (A) BaL pseudovirus. Virus was treated with 1 μM KR13 in the absence and presence of serial dilutions of T20 starting from 1 μM. Relative p24 release was measured using p24 ELISA by comparing the residual virion (18.2 - 19% Optiprep) and soluble protein (6-8% Optiprep) fractions. Relative gp120 release was measured using western blot analysis by comparing content of gp120 in the analogous residual virion and soluble protein fractions. Western blot values were obtained using Image J analysis of the protein bands. The IC50 value T20 inhibition of KR13-induced p24 release was 15.9 ± 4.9 nM using Origin Pro .8 (Origin Lab). No significant effect on the gp120 release in the presence of T20. Error bars represent the standard deviation of the mean, n = 3. (B) R3A and R3A V38A pseudoviruses; the latter, mutant virus has been found previously to be resistant to T20 inhibition. Release of p24 was quantified as for BaL pseudovirus in part (a). The IC50 of T20 inhibition of peptide induced p24 release from the virus R3A was calculated to be 21.9 ± 5.9 nM. The mutant virus V38A R3A did not exhibit inhibition of p24 release. Sigmoidal fits were obtained using Origin Pro .8 (Origin Lab). Error bars represent the standard deviation of the mean, n = 3.

2.1.8 Discussion

Previously, we reported that peptide triazole inhibitors of HIV-1 infectivity target gp120 on the HIV-1 virion and allosterically block CD4 and coreceptor (CCR5/CXCR4) binding sites on gp120 [22, 23]. Recently, peptide tirazole containing a C-terminal sulfhydryl group caused irreversible, cell-independent disruption of viral particles, as shown by release of the capsid protein p24 [8]. In the current study, we sought to more fully characterize the underlying mechanism of these effects. We detected multiple molecular transformations during peptide-induced inactivation and disruption of viral particles. The peptide triazole thiol, KR13, was unique in causing both gp120 shedding and p24 release, and this effect was seen with several clades as well as transmitted founder pseudovirions (**Figure 17**), showing the breadth of virolytic inactivation. The virolytic effect induced by KR13 was also observed with replication competent, fully infectious HIV-1 BaL virions (**Figure 18**). Of note, for the fully infectious virions, the IC_{50} values for peptide induced gp120 shedding as well as virolysis were higher. One possible explanation for this difference is the reduced spike density on infectious virion surfaces compared to the pseudotyped virions. From our data, we observed that the pseudovirions used in this study have spike densities ranging from 60-70 spikes per virion, while the fully infectious BAL-01 had approximately 12-15 spikes per virion. The spike densities were calculated from gp120 content determined by western blot analysis of the virus supernatants as described in above.

Gp120 shedding tracked kinetically with loss of cell infection activity, while p24 release occurred more slowly (**Figure 20**). The free sulfhydryl group was required for p24 release but not gp120 shedding, as a non-sulfhydryl peptide triazole (HNG156) induced only gp120 shedding as did the KR13b derivative containing a blocked sulfhydryl group. Strikingly, p24 release was potently inhibited by the entry inhibitor,T20, which specifically blocks formation of the gp41 6-helix bundle, on the Env trimer, that is induced following CD4 and coreceptor engagement by gp120 and required for membrane fusion (**Figure 22**) [14]. Moreover, membrane proximal MPER epitopes on gp41, which are characteristically concealed prior to CD4/coreceptor engagement, became highly exposed on viral particles (Figure 19). Overall, gp120 shedding, 6-helix bundle formation, and perturbations in the viral membrane that cause p24 release and gp41 MPER epitope exposure are analogous to physiological events that occur during viral fusion and entry. These findings are consistent with a model in which peptide triazole thiols trigger native structural programs on the HIV Env trimer that are associated with membrane fusion. This view is depicted schematically in **Figure 23**.

The requirement for the free sulfhydryl group of KR13 in virolysis was demonstrated using synthetic peptide triazole variants. Several peptides in addition to KR13 were examined, including the parent HNG-156 peptide that contained no Cys residue, the KR13b peptide in which the –SH group is blocked and a sequence-scrambled control peptide KR13s (**Figure 12**). Both HNG156

and KR13b bound to gp120 and had strong antiviral activities (**Figure 17 and Table 1**). However, neither of these peptides caused p24 release. Hence, the free Cys-SH group in KR13 is essential for its observed lytic activity. We cannot yet define the mechanistic role of the sulfhydryl group in Env protein disruption. However, Env protein disulfide exchange has been reported to be important in viral entry [257-259]. Hence, it is possible that disulfide exchange may be a component of the KR13-induced gp120 transitions that alter Env spike conformations and, in the absence of a target cell, disrupt the viral membane resulting in breakdown of the virion particle.

We investigated the time dependence of KR13-induced viral disruption by tracking the fate of the viral components gp120, gp41 and capsid protein (p24). We observed (**Figure 20**) a series of breakdown steps, in which gp120 shedding and loss of infectivity occurred at similar rates, while loss of p24 from the viral capsid occurred more slowly. The difference in rates was evident by a loss of 65-70% of gp120 and infectivity at 30 minutes of KR13 exposure, while only 10% loss of p24 occurred at this time. KR13 treatment also caused a time dependent exposure of the MPER epitope as tracked by the antibodies 2F5 and 4E10 (**Figure 20B**). Of note, the membrane-associated MPER epitopes are not well exposed on unliganded viral particles and become transiently exposed during conformational changes associated with entry [260]. Overall, the time dependence of the molecular transitions that occur upon peptide triazole thiol treatment suggests a specific transformation pathway of lytic breakdown that can be related to the

organized molecular structure of the virus and changes in that structure that likely occur during the fusion process in virus cell entry.

The presence of a specific time-dependent pathway of virion disruption also fits with observed changes in the physical structure of the virus. The morphology of KR13-disrupted virions was examined by TEM. From the images obtained at different times of KR13 exposure (**Figure 21C and Appendix Fig. 4**), treated virions were smaller, with a >50% reduction in average diameter compared to untreated virions. These results indicate that, rather than resulting in a non-specific and global fragmentation of viral particles, peptide triazole thiol causes a more limited poration, resulting in an intact, although collapsed, particle that releases p24 capsid but retains membrane-associated gp41.

We further evaluated the possibility that this disruption of viral particles and accompanying changes in gp41 might be related to virus-cell fusion by examining the effect of the fusion inhibitor T20. The latter targets the gp41 N-terminal heptad repeat region (N-HR) and blocks 6-helix bundle formation of gp41, an important Env structural transition state in fusion [239]. Indeed, T20 completely inhibited p24 release with an IC_{50} of 15 ± 4.9 nM comparable to its potency in fusion inhibition [137]. No effect was observed of T20 on the KR13-induced gp120 shedding (**Figure 22**). Suppression of capsid protein (p24) release by T20 strongly suggests that the formation of the 6-helix bundle prefusion complex may be coupled to peptide-induced poration of the viral membrane and virion

inactivation. This possibility was supported by the finding (**Figure 22B**) that no inhibition of p24 release was seen for an HIV-1 Env bearing a mutation (V38A) that confers resistance to T20 [261, 262] . In addition, using surface plasmon resonance analysis, T20 did not interfere with KR13 binding to sensor-immobilized gp120 (**Appendix Fig. 5**), indicating that this effect was not the result of artifactual binding of T20 to the KR13 peptide.

Previous studies have shown that sCD4 [263] and some CD4 mimetic small molecules such as NBD-556 can activate infection in $CD4^{-ve}$ $CCR5^{+ve}$ cells [172]. Since KR13 appears to induce gp41 6-helix bundle formation, and the latter is a required step in cell entry, we evaluated whether KR13 might enhance infection of CD4 negative cells. The same incubation conditions were used as for inhibition of HIV-1 entry into HOS $CD4^{+ve}$ $CCR5^{+ve}$ cells. As shown in **Appendix Fig. 6**, no enhancement of infection was observed under these standard conditions. Interestingly, concerning possible effects of peptide triazoles on Env-expressing cells, we have observed using CHO-K1 cells expressing gp160 that KR13 caused gp120 shedding but did not lyse the cells (results shown in chapter 4). Hence, the virion structure is important for peptide-induced virolysis.

Because peptide triazoles can inactivate virus by targeting the Env spike leading to irreversible virus breakdown, this class of Env inhibitors may be effective in prevention strategies such as microbicides as novel compounds that specifically inactivate viruses before attachment to host cells [10, 264]. In addition, an

attractive though at this stage speculative possibility is that the gp41-antigenic properties of virion particles after peptide triazole thiol treatment may make such a process useful for forming attenuated virus products capable of stimulating a neutralizing immune response.

Previous studies have reported several other agents, including peptide NS5A [265], antibodies 2F5 and 4E10 [266] and sCD4 [267] that lead to HIV-1 breakdown. Peptide triazoles are more HIV-1 specific than NS5A. In addition, viral breakdown triggered by these peptides appears to occur faster than breakdown caused by the antibodies and sCD4 [12, 266]. Overall, the current work reinforces the feasibility of novel pharmacologic approaches that can be applied to specifically disrupt viral particles (**Figure 23**). Furthermore, peptide triazoles can be useful probes to explore poorly understood events, at the viral envelope following CD4 and coreceptor engagement, that lead to alterations of the viral membrane and its fusion to the cell membrane during entry.

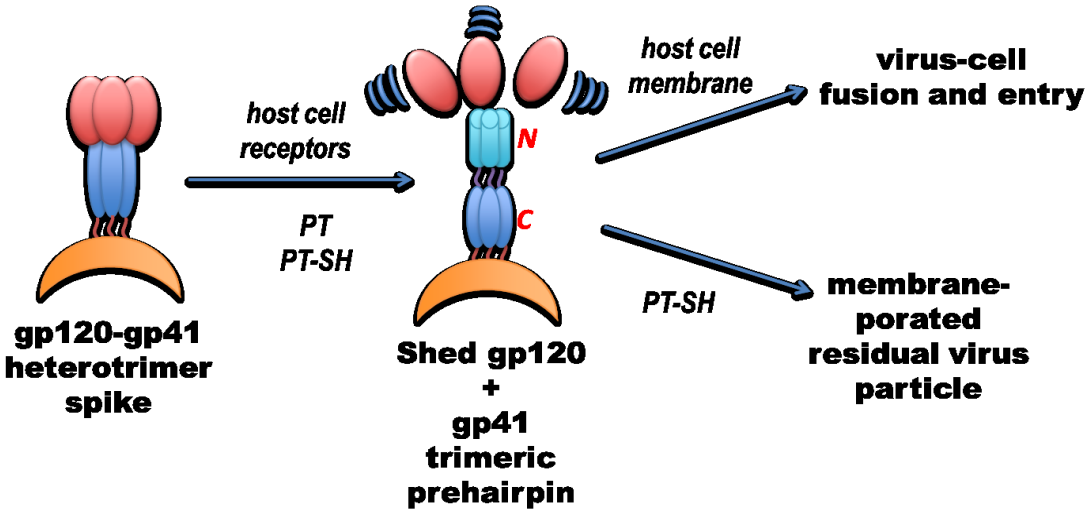

Figure 23: Scheme comparing the HIV-1 deformation steps induced by peptide triazole (PT) and peptide triazole thiol (PT-SH) with gp120 shedding and gp41 trimer prehairpin formation that occurs during cell entry and infection.

2.4 Comparing the peptide triazole thiol virolysis to HIV-1 fusion with the host cell

I showed in this thesis that KR13, a sulfhydryl-containing peptide triazole, can bind to gp120, block CD4 and co-receptor binding, inhibit viral infectivity, and physically disrupt viral particles. Further preliminary studies was conducted in order to characterize the mechanism by which these transformations occur. These results showed that KR13 peptide triazole initially causes viral inactivation through the release of gp120 followed by subsequent interactions with its free sulfhydryl leading to 6-helix bundle formation, viral membrane disruption, and p24 release. Our data are consistent with the conclusion that KR13 triggers structural changes in the HIV-1 trimer typically associated with viral entry and membrane fusion and that, in the absence of target cells, these changes result in irreversible viral inactivation and lysis. Hence it was important to further analyze this relationship between KR13 dependent virolysis and HIV-1 – cell fusion.

Previous studies have showed that the fusion inhibitor, T20, has developed resistant mutants that are no longer sensitive to T20 inhibition of HIV-1 fusion with the host cell. These mutants are mostly on the NHR of gp41, and stops T20 from interacting with the gp41 protein and stopping the 6 helix bundle formation. In this study these mutants were incorporated into the BAL-01 pseudotyped HIV-1 virion and tested to see their effects on T20 inhibition of KR13 induced virolysis. The results showed that these T20 mutants had differential levels of desensitization of the T20 inhibition of the KR13 induced virolysis. The next step to understanding this relationship was to study the differential inhibitory

effects of different already known fusion inhibitors such as 5 helix, N36, C34 and C36 which either bind to the CHR or the NHR of gp41 respectively. The time dependent and concentration dependent inhibition of the fusion inhibitors of KR13 induced virolysis. There were very interesting observations which gave insights into the way in which the 6 helix bundle might be folded post virolysis. Therefore, next the structural confirmation of gp41 on the residual virus post peptide triazole induced virolysis was tested. This led to the speculated model of the gp41 folded to a 6 helix bundle post virolysis as shown in this section. By studying the mechanism of pore formation, 6 helix bundle formation and lysis by KR13 on HIV-1 will provide deep insight into the way an HIV-1 cell fusion occurs. The potent and specific activity of this novel compound and its ability to inactivate virions prior to target cell engagement suggest that KR13 could be highly effective as a microbicide in inhibiting HIV transmission across mucosal barriers as well as a probe to understand biochemical signals required for membrane fusion.

2.4.1 Testing the effects of several T20/enfurvitide mutants on HIV-1 virolysis

Previous studies have shown that there are several resistant mutants have developed over the years for T20 [142]. In this study we will be using the most common and most effective resistant mutants of T20 which are V38A, N43D and I37K. V38A has been shown to have the highest potency, following N43D and I37K [268]. V38A and N43D were obtained from mutations that arose from clinical studies using T20, while I37K was a resistant mutant of C34 peptide but was also tested for T20 [269, 270]. The plasmids of the envelope with the mutant

gp41 regions were obtained as a gift from James Hoxie. The viruses with the mutant gp41 envelopes were synthesized as explained in section 2.2.2.1 using 293T (HEK) cells. The backbone DNA used was the pNL4-3-Fluc+env– provirus developed by N. Landau[252]. Serial dilutions of KR13 starting at 50μM were co-incubated with pseudotyped HIV-1 BaL (WT), V38A, N43D and I37K for 30 min at 37°C. Treated virion samples were fractionated on a 6-20% iodixanol gradient (above). Gradient fractions were quantified for p24 using ELISA, and relative p24 release was quantified and plotted using the Origin Pro.8 (Origin Lab). Also the viral infection inhibition by KR13 and T20 on these HIV-1 mutants was compared by conducting the viral infection inhibition assay as explained in section 2.2.2.2. The starting concentration of T20 and KR13 used was 5 μM and 50 μM respectively. Following, KR13 at 1 μM and serial dilutions of T20 starting at 1 μM were co-incubated with pseudotyped HIV-1 BaL (WT), and the resistant mutant viruses V38A, N43D and I37K for 30 min at 37°C. The samples were then purified in order to separate the residual viruses from the released proteins by spinning at 15,300 rpm for 2 hours at 4°C. The released p24 was assayed by ELISA and quantified compared to positive and negative controls which were the released p24 from viruses treated with 1% triton X and PBS respectively.

Just to confirm the mutant HIV-1 pseudotyped virions were resistant to T20, control viral infection inhibition studies were conducted. The results are summarized in **Appendix Fig. 7**. The results showed that T20 was most resistant

to I37K and it still showed infection inhibition for V38A and N43D. For KR13, the HIV-1 mutant that was inhibited the least for its viral infection was I37K but V38A and N43D both were not that different for the viral infection inhibition (**Appendix Fig. 7**). **Figure 24** summarizes the anti-viral effects of KR13 on these mutant viruses compared to BAL-01 WT virus. From the figure it clearly shows that the p24 release is not that different for V38A compared to WT HIV for KR13 while N43D and I37K were much weaker at releasing. Further, the T20 inhibition of KR13 induced lysis on the mutant viruses was much weaker and there was a differential effect.

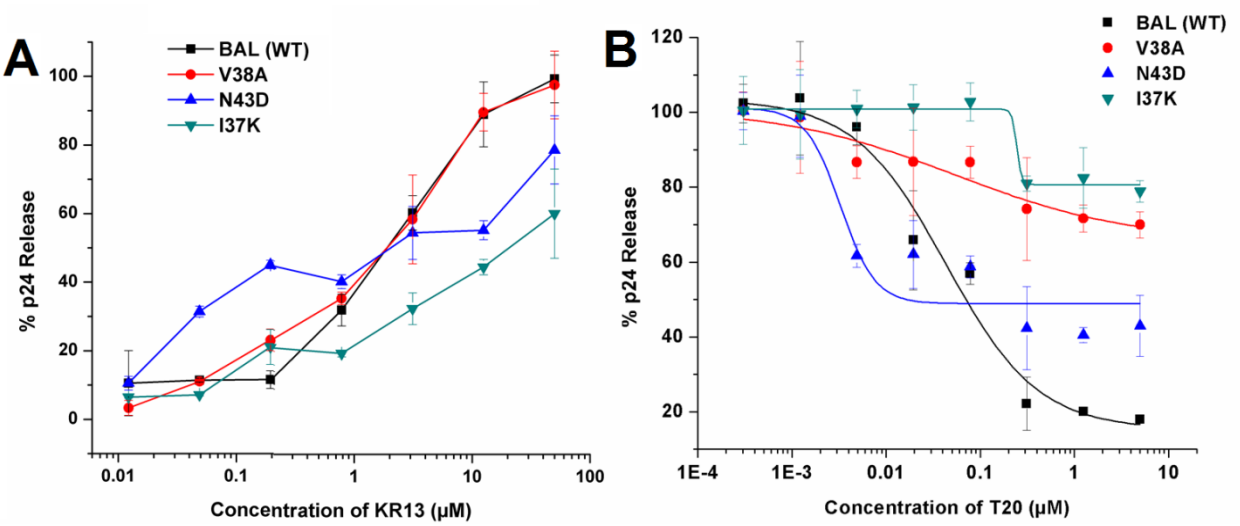

Figure 24: Effects of KR13-induced virus breakdown by the gp41-binding fusion inhibitor T20 on the T20 resistant mutant viruses. (A) P24 release profile induced by KR13 on the T20 resistant viruses versus the Bal-01 virus WT. Relative p24 release was measured using p24 ELISA by comparing the residual virion (18.2 - 19% Optiprep) and soluble protein (6-8% Optiprep) fractions. Error bars represent the standard deviation of the mean, n = 3. (B) Inhibition of p24 release induced by KR13 on the mutant viruses, V38A, N43D and I37K compared to the wildtype control by T20. The IC_{50} of T20 inhibition of peptide induced p24 release from the virus BAL-WT was calculated to be 43.3 ± 5.9 nM. The T20 inhibitory effect of KR13 induced virolysis was desensitized by mutant viruses V38A and I37K while N43D did not affect this inhibitory effect as much compared to BAL-WT. Sigmoidal fits were obtained using Origin Pro .8 (Origin Lab). Error bars represent the standard deviation of the mean, n = 3.

2.4.2 Comparing the effects of different fusion inhibitors that target the virus protein gp41 on the inhibition of peptide triazole thiol virolysis and HIV-1- host cell fusion

In order to biochemically understand the transitions of gp41 during virolysis the inhibitory actions of this effect by fusion inhibitors, which have established binding sites on gp41, were tested. This method therefore helped to breakdown the virolytic process and understand better the conformational changes that gp41 goes through. To achieve this, the most studied and well understood fusion inhibitors which include the CHR inhibitors, 5 Helix and N36, and the NHR inhibitors, T20, C34 and C36 [116, 170, 239, 271]. The NHR inhibitors are shown to bind to the CHR of gp41 and inhibit the 6 helix bundle (6HB) formation at nM affinities [170, 271]. The CHR inhibitors however are shown to be blockers of the 6HB formation and also is involved with inhibition of forming a stable fuseogenic core and the stability of the 6HB [3, 272]. The **Figure 25** shows a summary of the peptides used in this study and also the site on gp41 where they bind. This figure is adapted from the paper by Baldwin and Berkhout, 2008 [3].

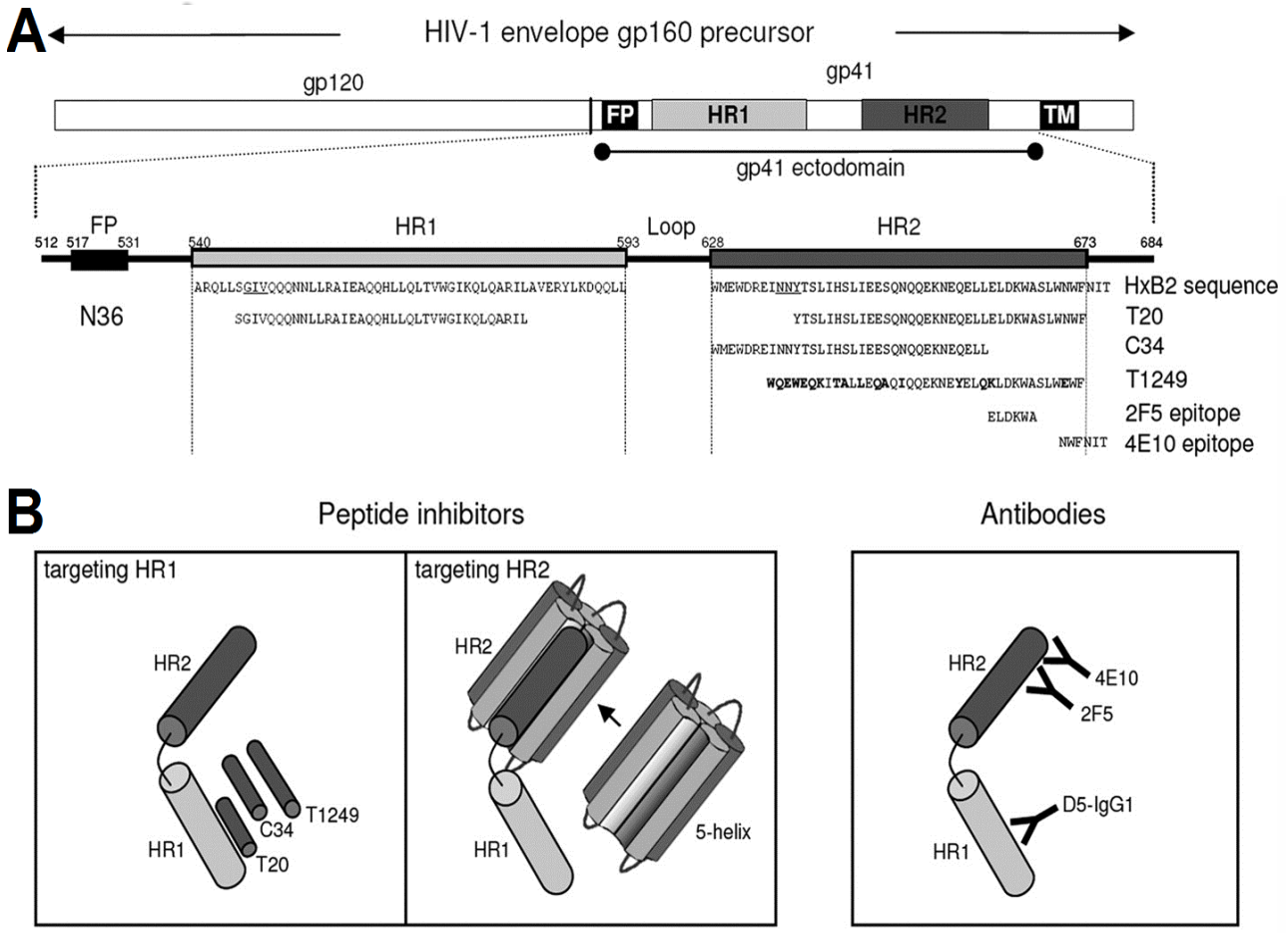

Figure 25: Schematic representation of the gp41 inhibitors and site of action on gp41. (A) The sequences of the CHR (HR2) and NHR (HR1) inhibitors and the regions on the gp41 sequence from which they were derived. This is shown on a gp41 sequence of the HXB2 strain. Further this also shows the gp41 antibodies and the sequence on gp41 that it binds to[3]. (B) Target sites of the different peptide fusion inhibitors and antibodies tested (drawing not to scale). For simplicity, we show only one gp41 molecule instead of the gp41 trimer.

2.1.8.1 Concentration dependent effect of the fusion inhibitors on virolysis

In order to test the effects of these fusion inhibitors on KR13 induced virolysis, KR13 at 1 μM and serial dilutions of the inhibitors starting at 1 μM were co-incubated with pseudotyped HIV-1 BaL (WT) for 30 minutes at 37°C. The samples were then spun on at 15,300 rpm for 2 hours at 4 ºC (Eppendorf Centrifuge 5415R). The supernatant was collected and the p24 content was quantified by p24 ELISA as described in section 2.2.2.3. The relative p24 release was quantified and plotted using the Origin Pro.8 (Origin Lab) compared to the positive and negative controls which were the virus incubated with KR13 alone and the virus incubated with no inhibitor but PBS alone instead. Prior to calculations the background p24 leakage for the inhibitors alone with no KR13 added were tested and validated to be <2% compared to the negative control. The controls were also tested for viral infection inhibition in order to compare their anti-viral effects. In order to test the effects of KR13 on the inhibitory effect of the fusion inhibitors, a serial dilution of the inhibitors starting at 5 μM was incubated with pseudotyped HIV-1 BaL-01 virus in the presence of 500 nM KR13 for 30 minutes at 37°C. The samples were then added to HOS-CD4^{+ve} CCR5^{+ve} cells and the steps for a viral infection inhibition assay were followed as described in section 2.2.2.2. The samples were tested for viral infection using the reported gene assay as described above.

The results are summarized in **Figure 26**. **Figure 26A** shows that in general all these fusion inhibitors also lead to inhibition of KR13 induced virolysis to different degrees. The 5 helix and T20 showing the best inhibition, followed by N36 being an intermediate inhibitor and C37 and C34 affecting virolysis the least. The **Figure 26B** shows that these fusion inhibitors have no non-specific p24 release on its own. The viral infection inhibition assays conducted are summarized in **Figure 26C and 26D**. Compared to **Figure 26D**, in which the viral infection inhibition of the fusion inhibitors alone is shown, the infection inhibition is greatly enhanced for all the 4 inhibitors in the presence of KR13. This therefore shows that KR13 has a synergistic effect with the fusion inhibitors when it comes to HIV-1 BaL pseudotyped infection inhibition. The IC_{50} values are summarized in **table 2**.

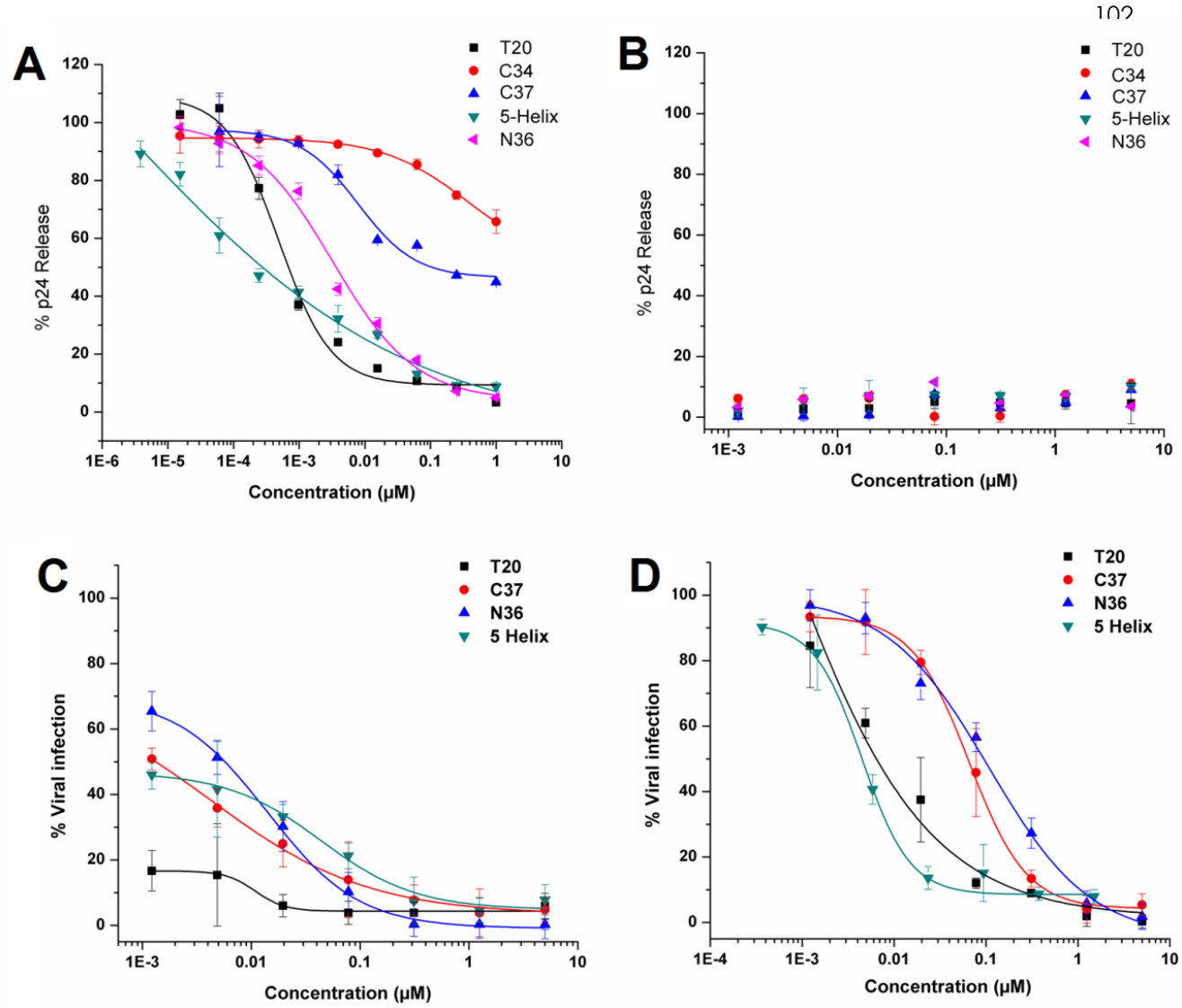

Figure 26: The effects of fusion inhibitors on KR13 induced virolysis. (A) The inhibition of p24 release induced by KR13 (1μM) using fusion inhibitors starting at 5 μM concentration. The IC50 values of the fusion inhibitors' inhibition of KR13-induced p24 release was calculated using Origin Pro .8 (Origin Lab) and summarized in table 2. (B) p24 release from HIV-1 BaL pseudotyped by the fusion inhibitors. (C) Inhibition HIV-1 BaL pseudotyped infection in HOS $CD4^{+ve}CCR5^{+ve}$ cells by fusion inhibitors T20, C37, N36 and 5 Helix in the presence of KR13 (500 nM). (D) Inhibition HIV-1 BaL pseudotyped infection in HOS $CD4^{+ve}CCR5^{+ve}$ cells by fusion inhibitors T20, C37, N36 and 5 Helix. Error bars represent the standard deviation of the mean, n = 3.

2.1.8.2 Time-dependent effect of the fusion inhibitors on KR13 induced virolysis

The time course of peptide triazole dependent HIV-1 breakdown inhibition by the fusion inhibitors T20, C37, N36 and 5 Helix was evaluated. This was a time of addition experiment in order to test upto to what time is the prefusion intermediate exposed on a KR13 treated virion for the fusion inhibitor to bind. Therefore the fusion inhibitor was added either before addition of KR13 to HIV-1 BaL pseudotyped or 0 – 60 minutes after addition of KR13. The samples were then incubated for an additional 30 minutes at 37°C and then spun on a table top centrifuge for 2 hours at 15,300 rpm at 4°C. For each time point, purified virions incubated with PBS at 37°C and alternatively with 1% Triton-X 100 was used as negative and positive controls, respectively. The supernatant was collected and quantified for p24 (capsid protein) using the ELISA described above.

Figure 27 summarizes the results that were observed from the time of addition experiment. Both the 5 helix and N36 surprisingly showed nearly 75% inhibition of the p24 release by KR13 even when added 60 minutes post peptide addition. The C37 and T20 effects reduced from 80% to 20% inhibition when the time of addition was after 10 minutes post peptide addition. This shows evidence that the CHR is much more accessible to the

fusion inhibitors even 60 minutes post KR13 treatment which gives us evidence that the NHR is not as accessible.

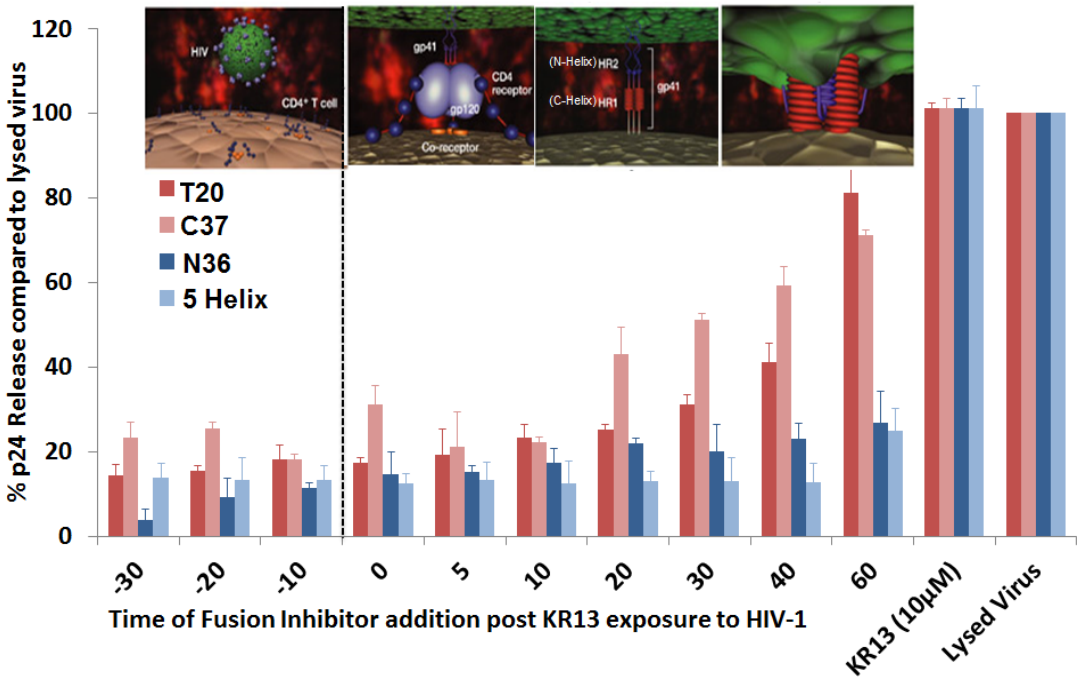

Figure 27: p24 release of the inhibition by fusion peptides T20, C37, N36 and 5 helix. The fusion peptides were added at different times either before addition or after addition of KR13. The relative p24 release measured subtracted from the negative control at each time point with viruses incubated with PBS. The p24 release was quantified using ELISA and the results are averaged from n=3.

2.4.3 Antibody mapping of the residual virion post KR13 virolysis

The gp41 on the residual virion as well as the gp120 that was shed off during virolysis by KR13 was antibody mapped using antibodies with known binding sites on the respective proteins. This analysis would give very specific insights about the confirmation of the gp41 as well as the gp120 post virolysis and hence would give us better understanding about the mechanism of this action. The antibodies used for the gp41 antibody mapping and the gp120 antibody mapping are summarized in table 3 and 4 respectively.

The HIV-1 BaL Pseudovirions were treated for 30 min at 37°C with KR13, HNG156 (1 μM) or PBS as negative control, and samples spun on a 6-20% iodixanol gradient. The released proteins were collected in the 6-8% fractions and pooled together. This released protein fraction was then fixed using equal volume of 0.1% paraformaldehyde and purified on a sephadex G-25 column. The purified protein was then loaded onto an ELISA plate at 100 μl per well and incubated overnight at 4°C. The plate was blocked with 3% BSA, and ELISA was used to detect gp120 epitopes with human gp120 antibodies from table 3 and followed by addition of anti-human IgG HRP secondary antibody. The virus fractions from the iodixanol gradient were collected and fixed with equal volume of 0.1% paraformaldehyde for 30 minutes at 4°C. The treated virus fractions were spun at 16,000 X g for 2 hours at 4°C in an Eppendorf table top centrifuge. Following PBS wash, fixed virions were coated on an ELISA plate at 50 μl per well and

incubated overnight at 4°C. The plate was blocked with 3% BSA, and ELISA was used to detect gp41 epitopes with human gp41 antibodies from table 4 followed by addition of anti-human IgG HRP secondary antibody. This method was used to assess time-dependent exposure of gp41 epitopes on the pseudotyped HIV-1 BaL virions induced by KR13 and HNG156 treatment at 1 μM constant concentration.

Figure 28 shows the results from the antibody mapping studies. **Figure 28A** shows the antibody mapping of the gp120 protein released from the virion post KR13 addition. The CD4 binding antibodies shows reduced binding as expected due to both the peptides, KR13 and HNG156, altering the gp120 confirmation to reduce CD4 and 17b binding as previously shown (**Figure 13 and 14**). F105 however showed good binding to the gp120 post KR13 and HNG156 treatment. However there were clear changes observed in gp120 treated with KR13 compared to HNG156 post CD4 binding site. This is shown especially with 2G12 which showed no binding to gp120 post KR13 treatment while HNG156 had good binding. **Figure 28B** shows the gp41 epitopes exposed on the residual virion post HNG156 treatment or KR13 treatment using antibody mapping. This shows that the HNG156 treated residual virion resembled the untreated virion based on the antibody binding, with increased binding to the HR2 region but mostly linear epitopes. But the KR13 treated residual virion gp41 had very distinctly increased binding to the MPER (membrane proximal external region). This is consistent with the data observed in **Figure 21**, which shows that there is increased MPER exposure with increasing concentration of KR13.

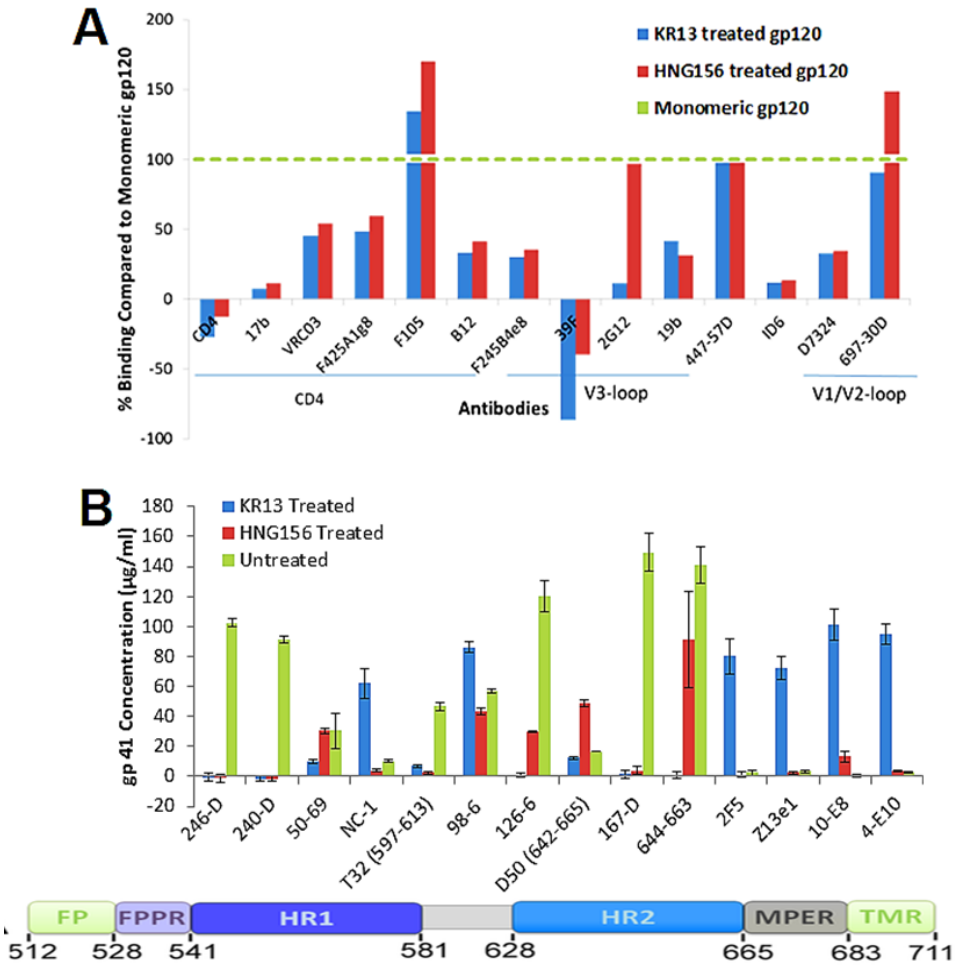

Figure 28: Antibody mapping of the gp120 and gp41 post KR13 and HNG156 treatment on HIV-1 BaL pseudotyped. (A) Antibody mapping of gp120 post KR13 (1 µM) and HNG156 (1 µM) using ELISA analysis. The region where the antibodies are directed to is shown in the bottom of the x-axis. The % binding is compared to the antibody binding to 100 ng/ml monomeric gp120 which is shown as a dotted green line. (B) Antibody mapping of gp41 on the residual virion post KR13 (1 µM) and HNG156 (1 µM) using ELISA analysis. The gp41 concentration on the y-axis is calculated from a standard curve of the antibody binding to soluble gp41 for each antibody. Error bars represent the standard

2.5 Model of the residual virion post peptide triazole thiol virolysis

This study was conducted to focus on what are the conformational changes elicited on the virion during KR13 treatment that leads to virolysis of HIV-1. Previously we have shown that this lytic action follows a time dependent pathway that is similar to HIV-1 fusion, with the rate limiting step being the 6 helix bundle formation and poration action (**Figure 20**) [6]. The first steps of binding and gp120 shedding occur within the first 10 minutes just like in HIV-1 fusion [6, 85, 138, 273]. Following that there was a concentration dependent and time dependent exposure of MPER with KR13 treatment (**Figure 21**). For a typical virus-cell fusion reaction, the MPER site is also exposed during 6 helix bundle formation as shown by several studies both antibody binding and mutational studies [274, 275]. This along with the antibody mapping studies has given me a much better understanding of the conformational changes of gp41 in the virus membrane during the virolytic poration action.

The T20 resistant mutant studies were the first lead on into understanding the conformational alterations in gp41. From this mutant study what we saw is that the KR13 p24 release was least inhibited by T20 in the virus that had the I37K mutation. This mutation was originally discovered as a C34 peptide resistant mutation and was also tested for T20 resistance later on [3, 270]. The I37K mutation is in the hydrophobic pocket in the NHR of gp41 and showed the largest change in the binding energy and led to the collapse of the coiled coil structure 6 helix bundle[14].Following I37K were V38A and N43D that resulted in electrostatic

repulsion also stopping the 6 helix bundle formation and resistance to T20 binding. This was clearly evident in the T20 viral infection inhibition of these mutated virions as seen in **Appendix Fig. 7**. This was also followed through to the inhibition of the peptide dependent virolytic effect by T20 in which the mutant virions followed a desensitization of I37K >> V38A >> N34D. Therefore this also indicates that the T20 inhibitory effect on HIV-1 fusion also had the same effect on KR13 dependent HIV lysis.

Not only did T20 lead to inhibition of the KR13 dependent virolytic effect, but other fusion inhibitors that targeted the 6 helix bundle formation of gp41 also led to inhibition of KR13 induced virolysis. The results summarized in **Figure 26** demonstrated differential effects of the fusion inhibitors effects. The inhibitors that target the CHR had a much more long term effect as demonstrated in **Figure 27**. Although T20 had a better potency of p24 release inhibition compared to N36, this T20 site was no longer available completely post 10-20 minutes of KR13 exposure to the virion. Further it was also observed that KR13 treatment led to the exposure of the fusion inhibitor binding site because the fusion inhibitors had a much better inhibitory effect on HIV-1 infection on HOS $CD4^{+ve}CCR5^{+ve}$ (**Figure 26**). From the time dependent addition experiment we observe that the NHR is hidden post 10 minutes of KR13 treatment on the virus compared to the CHR which is more available even post 60 minutes of KR13 treatment. The results showing that the CHR fusion inhibitors N36 and 5 Helix still have nearly 80% inhibition of p24 release even after 60 minutes of KR13 treatment shows that the 6 helix bundle formed

during virolysis is very similar to the 6HB during fusion. This is shown in literature as the asymmetric deactivation of gp41 which shows exposure of the CHR even post 6HB formation [276].

In order to construct a model of the virion post virolysis the antibody mapping of the residual virion was necessary. From the results summarized in **Figure 28** we observe that the KR13 treated virus has MPER exposed. The binding shows that even the MPER region that is very close to the TMD is also exposed due to the binding of 4E10. The gp120 mapping shows that the 2G12 binding is also lost in the KR13 treated virus gp120, showing that KR13 in addition to the CD4 and coreceptor binding regions also has binding or affects binding near the V3 loop region. From all the data obtained from above and also from the results observed previously the mechanism of KR13 induced virolysis is much more well-defined and shown schematically in **Figure 29**. This figure shows the time dependent virolytic events in part B and the rate limiting step, which is the gp41 conformational changes during the collapse and pore formation, is shown in **Figure 29A** much more in detail. The coiled HR's of gp41 are not to scale but are shown to get a much more realistic visual representation.

The study above shows that there is a very close correlation between HIV-1 cell fusion and KR13 induced HIV-1 irreversible breakdown. **Table 5** summarizes the effects of peptide triazole thiol (KR13) induced virolysis and its similarity to virus-cell fusion. This therefore shows that the peptide hijacks the fusion mechanism and

mocks the virus to think its fusing with a cell. This therefore leads to the cascade action of HIV-1 fusion without a cell present. The 6 helix bundle is formed during virolysis but might not be folded symmetrically which is also possible in regular virus-cell fusion[276]. In order to better define this virolytic mechanism it is important to understand what are the other steps in this cascade therefore future studies will be looking at the effects on the viral

membrane and further how the cytoplasmic tail of gp41 also is involved in lysis and the energy required for poration. The potent and specific activity of this virolytic peptide and its ability to inactivate virions prior to target cell engagement by hijacking the viral fusion mechanism will provide insight to the virus-cell fusion. Further this agent will be highly effective as a microbicide in inhibiting HIV transmission across mucosal barriers as well as a probe to understand biochemical signals required for membrane fusion.

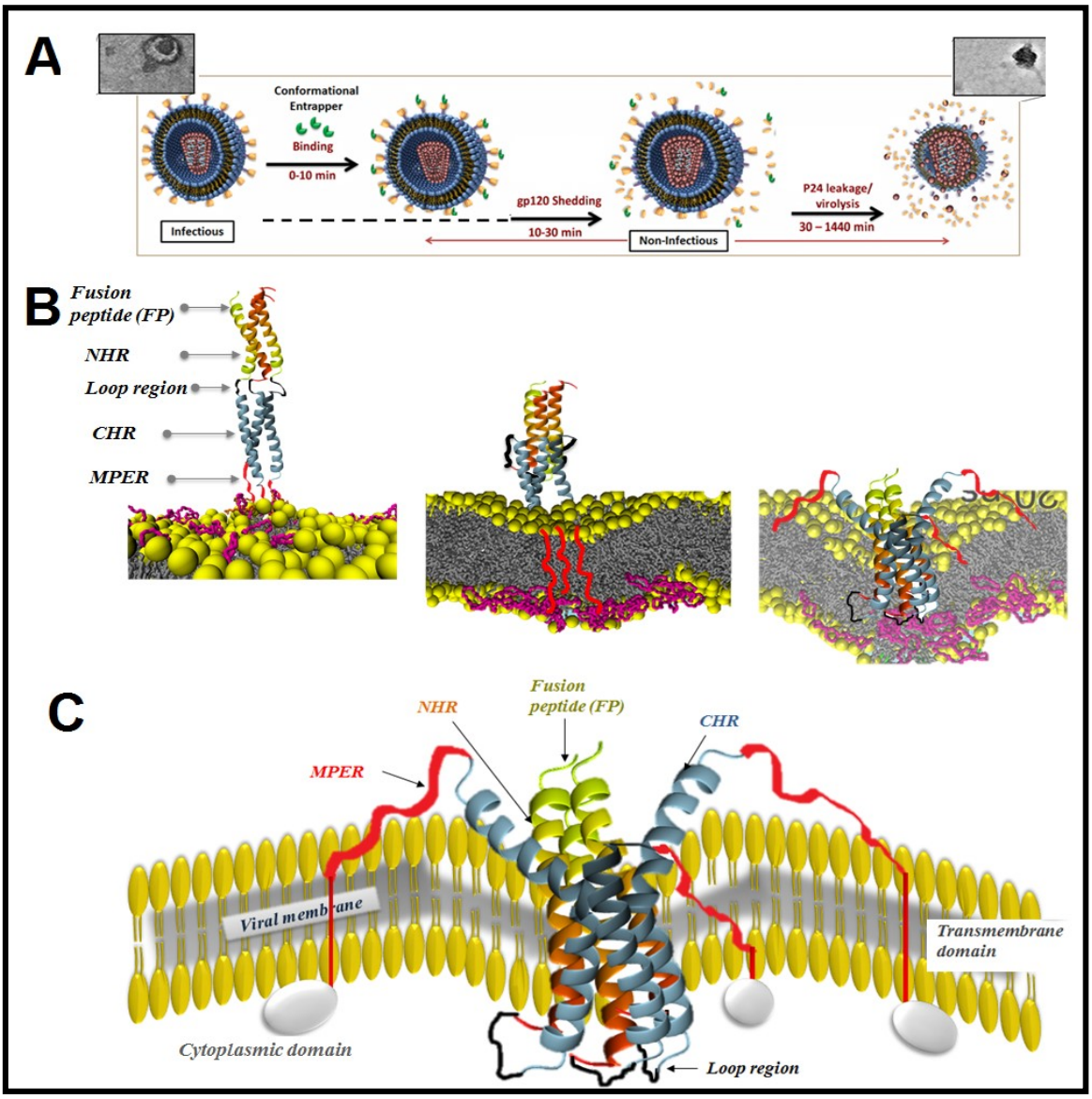

Figure 29: Schematic representation of the KR13 induced virolytic cascade. (A) Kinetic breakdown of the virolytic process, first showing the peptide binding following which the gp120 is shed off and the gp41 is exposed within the first 10 minutes. Following this is the rate limiting step of the pore formation caused by conformational changes in gp41 and eventually p24 release from the viral core. (B) Detailed schematic of the conformational changes of gp41 during virolysis, the loops reach a pre-lysis intermediate following which it is collapsed into a 6 helix bundle with the loop region on gp41 hidden into the viral membrane and MPER region exposed out of the membrane, (C) The zoomed in version of the 6 helix bundle formation schematic drawn based on the experimental results.

CHAPTER 3: MECHANISM OF MULTIVALENT ENCOUNTER FOR POTENCY ENHANCEMENT OF PEPTIDE TRIAZOLE INACTIVATORS OF HIV-1

3 Introduction

There is an urgent need for new antiretroviral agents for the prevention and treatment of HIV-1 infection. Current inhibitors used in most combination antiretroviral therapies target viral enzymes reverse transcriptase, integrase and protease. Although the use of combination antiretroviral therapy has resulted in reducing viremia and HIV related morbidity and mortality, these drugs target the later stages of HIV-1 infection and have significant challenges such as complex regimens and treatment-resistant variants of HIV-1. Currently, there are only two FDA approved antiretroviral drugs targeting the initial entry of the virus into host cells, namely T20 (enfurvitide) and maraviroc, but these are used mainly in salvage therapy due to risks concerning their usage. T20, a fusion inhibitor, targets transient conformations of the virus Env protein, gp41, and hence has a relatively short time window to act during HIV-1 host cell fusion event. Maraviroc, on the other hand, targets the host cell co-receptor, CCR5 and can only block R5-tropic HIV-1 virions from infecting the cell. Hence, this will result in the prevelance of the X4-tropic HIV-1 virus.

Host cell infection by HIV-1 is mediated by cell receptor interactions with trimeric envelope glycoprotein (Env) spikes that are exposed on the virus membrane surface. Env protein is the only virus-specific protein on the virion surface. The external gp120 component of Env is essential for cell receptor (CD4) and coreceptor (usually CCR5 or CXCR4) interactions and subsequent virus-cell fusion. Hence, Env gp120 presents an obvious target to attack the virus directly in order to block the cascade of integrated binding and conformational change steps that lead to host cell infection.

Env-specific inhibitors that could inactivate the virus before receptor encounter would hold great promise in preventing AIDS transmission and progression. In spite of the potential of gp120 antagonists as microbicides, progress has been limited for such agents, due to such factors as, high rate of mutation of gp120 protein leading to development of inhibitor resistance[277-279], low potency of small molecule inhibitors [18, 170, 187], the high cost and potential toxicity of protein inhibitors[159, 194, 280], and the potential risk of infection enhancement with CD4-mimicking ligands[187, 243].

Previously we showed that a family of entry inhibitors, peptide triazoles, bind specifically and with high affinity to HIV-1 Env gp120, antagonize the interactions of Env binding sites for both host cell receptors CD4 and CCR5/CXCR4 and cause gp120 shedding from the virus surface, leading to HIV-1 inactivation before host cell encounter[9, 10, 22, 24, 25, 32]. The most potent compositions of peptide triazole inactivators discovered so far are multivalent forms conjugated to monodisperse gold nanoparticles. The conjugates initially derived were found to have low nanomolar inhibitory values and to act as virucidal agents leading to the irreversible breakdown of the virus before the virus has a chance to engage the host cell[8].

The functional properties of virolytic gold nanoparticle-peptide triazole (AuNP-PT) conjugates make it feasible long term to use this type of agent to inactivate HIV-1 before host cell encounter. In the current work, we sought to investigate the mechanism of cell-free HIV-1 inactivation using the AuNP-PT multivalent nanostructures. Previous literature has shown that using nanoparticles ehanced

antiviral activity of an inhibitor[281, 282]. We evaluated the impact of altering the properties of both the AuNP-PT constructs, by increasing size of the AuNP core and density of the PT coverage, and the HIV-1 virus spike density. The results demonstrate the importance of multivalent contact between nanoparticle and virus surface interaction partners. The results lead to Env-targeting NP designs that take advantage of HIV-1 Env metastability and cause specific and irreversible HIV-1 inactivation. Overall, the investigation demonstrates that the multivalent physical contact approach can be used as a general strategy for antagonizing HIV-1 transmission and proliferation.

3.1 Materials and Methods:

3.1.1 Materials

For peptide triazole synthesis, all fmoc-protected α- and β-amino acids, O-Benzotriazole-*N,N,N',N*'-tetramethyl-uronium-hexafluoro-phosphate (HBTU), 1-Hydroxybenzotriazole (HOBt), Rink amide resin (4-(2',4'-Dimethoxyphenyl-Fmoc-aminomethyl)phenoxy resin) with a 0.55 mmol/g substitution, *N,N*-dimethylformamide (DMF), Pyridine and *N,N*-di-isopropylethylamine (DIPEA) were purchased from Chem-Impex International Inc, Ethynylferrocene and Cu(I)I was purchased from Sigma-Aldrich and used without further purification. Fmoc-cis-4-azidoproline was synthesized starting with commercially available trans-Hydroxyproline-OH[22]. Gold (III) chloride hydrate and citric acid were

obtained from Sigma-Aldrich, Bis (*p*-sulfonatophenyl) phenylphosphine dehydrate dipotassium salt (BSPP) from Strem Chemicals. Citric acid and cysteine used in the conjugation were from Sigma Aldrich. Modified human osteosarcoma cells (HOS.T4.R5) engineered to express CD4 and CCR5, receptor and co-receptor respectively, as well as pNL4-3.Luc R-E- backbone DNA, were obtained from Dr. Nathaniel Landau. The HOS.T4.R5 cells were grown in DMEM supplemented with 10% FBS, 2.5% HEPES, 1% Penicillin-Streptomycin, 2% L-Glutamine and 1 mg of puromycin. 293T cells were obtained from American Type Culture Collection and grown in the same culture medium as the HOS.T4.R5 cells except without puromycin. The plasmids for HIV-1 BaL-01 gp160 and VSV-G Env DNA were from the AIDS Research and Reference Reagent Program (ARRRP). Replication competent HIV-1 BaL-01 virions were obtained from the University of Pennsylvania Center for AIDS Research (Penn CFAR). Mouse anti-p24, rabbit anti-p24 and p24 protein were from Abcam. Fully Infectious HIV-1 (BaL) was a gift from Dr. Michele Kutzler and obtained from the Penn CFAR. The gp120 monomer protein was produced using an already-established protocol[25], anti-gp120 D7324 was purchased from Alto chemicals. Gp41 protein, Enfurvirtide (T20) and anti-gp41 antibodies 4E10 and 2F5 were obtained from from NIH AIDS Research and Reference Reagent Program (ARRRP). Enhanced Chemiluminescence western blot detection system was from Amersham. O-phenylenediamine (OPD) was from Sigma Aldrich. All other materials were from Fisher Scientific.

3.1.2 Peptide Triazoles

To conjugate peptide triazoles on nanoparticles, the peptide triazole KR13 (RINNIXWSEAMMβAQβAC, X=ferrocenyltriazolePro) was synthesized to contain the 12-residue N-terminal sequence of HNG-156 with a C-terminal extension containing a free thiol group. KR13 itself contained the essential peptide triazole pharmacophore, Ile-triazole-Pro-Trp, and not surprisingly was functionally active [6]. The free sulfhydryl group was incorporated to enable direct thiol conjugation to the gold surface of AuNP[8].

3.1.3 Gold nanoparticles

The citrate reduction method developed by Frens et al. [283] was modified in order to synthesize size-controlled, stable and monodisperse AuNPs. The citrate acid concentration was varied to obtain AuNP with various sizes ranging from 13 nm – 123 nm. The citrate reaction solution, initially at 100˚C, was cooled to room temperature and BSPP (18 mg/ml for 20 nm AuNP) was added to the synthesized particles and stirred overnight at room temperature. The resulting particles were further washed with phosphate buffer at pH 7.2 and concentrated using a Millipore 100,000 kDa filter. The particle size was determined by Dynamic Light Scattering (DLS) in the Zetasizer NS90 (Malvern Instruments),

and the particle concentration was calculated using the absorbance at 450 nm and the peak absorbance of the UV spectrum[284]. The AuNP particle morphology was characterized using Transmission Electron Microscopy. Samples were prepared by adding a drop of the AuNP solution onto a lacey carbon grid film and then allowing evaporation. Bright field images were taken with a JEM 2100 camera operated at 200 kV. Further the samples were validated for cell cytotoxicity and stability in physiological conditions prior to cellular assays, the methods and results are elaborated in **appendix Fig. 8A and B**.

3.1.4 Gold nanoparticle-peptide triazole conjugates

Peptide conjugation to the AuNPs was achieved via covalent linkage between the thiol moiety (-SH) on C-terminal cysteine residue and the gold surface of AuNP[8]. A flocculation assay[285] was conducted to determine the ratio of AuNP to KR13 to use for complete peptide conjugation without peptide aggregation following the protocol developed by Xie et al. 2003 (**Appendix Fig. 9**). The BSPP-stabilized AuNP:PT mixtures in phosphate buffer were stirred vigorously for 30 minutes at 25ºC. Excess peptide was removed from the nanoparticle fraction using a 10,000 MW cut-off centrifugation filter. PT content of AuNP-PT preparation was determined using amino acid analysis after acid hydrolysis (Keck Institute, Yale University). To prepare AuNP-PT particles with varying density of KR13, we used 20 nm AuNPs. We mixed different molar ratios of KR13 and L-cysteine during the step of peptide conjugation to AuNP. Both

molecules present a single reactive thiol for covalent attachment to the BSSP-stabilized nanoparticle. However, AuNP-Cys has no virolytic activity (Table 2), and only the KR13 component will bind to HIV Env on the virion surface. Incorporation of KR13 was measured directly by amino acid analysis. We calculated the average density of peptide coverage ($\rho_{coverage}$) by the relationship,

$$\rho_{coverage} = \frac{\left[\frac{C_{peptide}}{C_{AuNP}}\right]}{\pi d^2}$$

where πd^2 is surface area of nanoparticle and $C_{peptide}/C_{AuNP}$ is molar ratio of peptides per nanoparticle. The conjugates were validated for peptide conjugation by testing their change in zeta potential, which was measured by the Zetasizer NS90 (Malvern Instruments) (**Appendix Fig. 10**). Further their monodispersity was assessed using both the DLS (**Figure 29B**) as well as TEM imaging (**Figure 29C**).

3.1.5 HIV-1 Pseudotyped Virions

The recombinant virus consisted of the pro-viral envelope plasmid sequence corresponding to the CCR5 targeting HIV-1BaL strain or a VSV (Vesicular Stomatitis Virus) pseudotype, and the backbone sequence corresponded to an envelope-deficient pNL4-3 luc^+, env^- provirus developed by N. Landau[251, 286]. Four µg of envelope DNA and eight µg of backbone DNA were co-transfected into 293T cells using FuGene 6 as the transfection reagent (Promega). Fourteen hours post-transfection, the medium was changed, and the VLP containing supernatants were collected at 48 hours post transfection.

Protease digestion of pseudovirus was conducted by treating the culture supernatants with a protease cocktail of 1 μg of trypsin, chymotrypsin, subtilisin, and/or proteinase K (Sigma) at 37°C as described by Crooks et al. [287]. Following the enzyme digest, soluble proteins (including Env gp120 and p24) were removed via fractionation on 6-20% iodixanol gradient for 2 hours at 30,000 rpm. The collected fractions were validated for p24 content using capture ELISA as well as gp120 content using the western blot detection. Virions purified on the 6-20% iodixanol gradient exhibited a characteristic distribution profile of p24 and gp120 content, enabling viral fractions (18-19.2% iodixanol) and soluble protein fractions (6-8% iodixanol) to be isolated. The gradient-purified virus samples were collected, aliquoted and stored at -80°C until further use.

3.1.6 Env Spike Presentation on the Virus Surface

To make viruses with varying spike density, HEK293T cells were transfected with backbone vector, pNL4-3.Luc R-E-, and a mixture of active env plasmid (HIV-1 BaL - WT) with a plasmid encoding inactive env gp120 S375W BaL; the S375W mutation has been found previously to cause suppression of PT binding to gp120[222],[24]. Of note, varying density does not in itself eliminate the potential for local clustering, and indeed evidence has been obtained showing that HIV-1 Env spike has the tendency to cluster[288, 289]. Control virions included those with all-active Env (BaL- WT) and all-inactive Env (S375W BaL). Protease digestion of spike-varying viruses was conducted as described

above. Spike density was quantified using western blot analysis of gp120, viral infection and p24 content (ELISA) as explained above (**Appendix Fig. 11**).

3.1.7 Anti-viral functions of AuNP-KR13 conjugates

Dependence of anti-viral effects on the size of AuNP-KR13:

To test the effects of nanoparticle size on viral inhibition and virolytic activity, we synthesized gold nanoparticles (AuNP) with diameters ranging from 10-200 nm as previously described. After AuNP functionalization with the KR13 peptide, we utilized assays for HIV cell infectivity and cell-free leakage of virus contents, p24 and gp41, to correlate nanoparticle diameter and surface area of the AuNP-KR13's with antiviral effects. Purified virus was treated with AuNP-KR13 constructions for thirty minutes at 37°C and spun on a 6-20% iodixanol gradient for 2 hours at 30,000 rpm. The collected virus fraction and the supernatant fraction were tested for infectivity, p24 and g120 content from the virus post treatment. Virus treated with PBS for 30 minutes at 37°C was used as negative control for background signal, and virus incubated for 5 minutes with 2% Triton-X at 98°C was the positive control for p24 and gp120 content.

Modulating nanoparticle surface density of peptide triazoles on AuNP:

Peptide triazole inhibitor coverage on 20 nm diameter Au nanoparticles was varied by mixing different molar ratios of KR13 and L-cysteine during the step of

peptide conjugation to AuNP. Both molecules present a single reactive thiol for covalent attachment to the BSSP-stabilized nanoparticle. However, only the KR13 were expected to bind to HIV envelope glycoproteins on the surface of the virion. AuNP and KR13 were synthesized and functionalized as described above. Cysteine/KR13 molar ratios were varied from 0:1000 to 1000:0 in increments of 50. We calculated the density of peptide coverage (ρ coverage) by the relationship:

$\rho_{coverage} = [C_{peptide}/C_{AuNP}] / 4\pi(d/2)^2$

where $4\pi(d/2)^2$ is surface area of nanoparticle and $C_{peptide}/C_{AuNP}$ is the molar ratio of peptides per nanoparticle. Purified virus was treated with AuNP-KR13 constructions for thirty minutes at 37°C and spun on a 6-20% iodixanol gradient for 2 hours at 30,000 rpm. The collected virus fraction and the supernatant fraction were tested for infectivity and both p24 and g120 contents post treatment.

AuNP-KR13 effects on replication competent HIV-1:

Replication competent HIV-1 BaL virions were obtained from the Penn CFAR, purified using 6-20% iodixanol gradient and p24 content measured using ELISA. The inhibitor concentration that gives 50% reduction of the viral titer in tissue culture (IC_{50}) was determined using Origin V.8.1 (Origin Lab). The working dilution of virus was pre-treated with a serial dilution of AuNP-KR13 (20 nm and 80 nm), starting from 50 μM and 10 μM respectively, for 30 min at 37 °C. HOS.T4.R5 cells, seeded at 8,000 cells per well, were incubated for 24 hours followed by addition of pre-incubated inhibitor-virus mixtures. After 48 hours

infection, p24 content of virions in the supernatant was measured in order to determine the IC_{50} value of inhibition of virus infection. For the latter, the peptide triazole and cell-free replication competent HIV-1 BaL virus were pre-incubated for 30 min at 37°C followed by spinning for 2 hours at 13,600 rpm in a table top centrifuge (Eppendorf) at 4°C. Supernatant was separated and p24 content determined using the p24 capture ELISA as described above. The extents of viral inhibition of, and p24 release from, fully infectious HIV-1 BaL were also evaluated for control peptide KR13 (data shown in Bastian et al. 2013) [6].

3.1.8 Comparisons of anti-viral functions of AuNP-KR13 to KR13 alone

Exposure of gp41 in viruses treated with AuNP-KR13 and KR13:

The HIV-1 BaL pseudotype was incubated with increasing concentration of either KR13 starting at 50μM or AuNP-KR13 starting at 1 μM (KR13 concentration) for 30 minutes at 37°C. The samples were spun at 16,000 rpm for 2 hours at 4°C, and the virion fraction for each sample was collected and fixed using a homemade fixative with 0.1% formaldehyde and 4% gluteraldehyde in PBS. Glycine (0.1 M) was added to stop the crosslinking reaction by the fixative. The virions then were loaded onto an ELISA plate (high protein binding) and incubated overnight on a shaker at 4°C. The plate was blocked with 3% BSA, and ELISA was used to detect gp41 epitopes with human gp41 antibodies 2F5 and 4E10 followed by addition of anti-human IgG HRP secondary antibody.

Effect of fusion inhibitor enfurvirtide (T20) on virolysis induced by AuNP-KR13 and KR13:

T20 was shown previously to effect the 6-helix bundle formation of the HIV-1 virion during fusion with the host cell[14, 239]. Further, T20 was found to specifically inhibit KR13-induced HIV-1 cell-free virolysis [6]. A corresponding experiment was conducted to test whether T20 inhibited virolysis of pseudotyped HIV-1 BaL induced by AuNP-KR13. The AuNP-KR13 was kept at an IC_{80} concentration of 25 nM, and serial dilutions of T20 starting at 1 μM were co-incubated with pseudotyped HIV-1 BaL for 30 min at 37°C. Treated virion samples were fractionated on a 6-20% iodixanol gradient (above). Gradient fractions were quantified for p24 using ELISA, and relative p24 release was quantified and plotted using Origin V.8.1 (Origin Lab).

Time dependence of AuNP-KR13 induced HIV-1 breakdown:

The time dependence of gp120 shedding, p24 release and inhibition of pseudotyped HIV-1 BaL by an IC_{80} concentration of AuNP-KR13 (25 nM) was measured. The AuNP-KR13 was incubated with the virus for different times ranging from 1 min to 24 hours at 37°C, the samples were spun on a 6-20% iodixanol gradient and the gradient fractions were tested for gp120 shedding, p24 release and inhibition of viral infection. For gp120 shedding, the fractions were tested using a western blot analysis with primary anti-gp120 antibody, D7324, and secondary antibody, anti-sheep HRP. For p24 release, the ELISA explained

above was used. For inhibition of viral infection, the luciferase reporter assay was used as explained above[6].

Anti-viral effects of AuNP-KR13 vs. KR13 on HIV-1 pseudovirions with modified env spike presentation on the virus surface:

Comparisons were made of the lytic deformation of viruses by KR13 and AuNP-KR13 with viruses containing a varying proportion of PT-resistant mutant Env spike vs. WT spike density. In the western blot analysis, the amount of loaded virions was normalized using both p24 content from ELISA and total protein content measured using Bradford assay. Antiviral assays included inhibition of infection by KR13 compared to AuNP-KR13 on HOS.T4.R5 cells, and cell-free HIV-1 p24 release.

3.1.9 Morphological Analysis of HIV-1 after AuNP-KR13 conjugate treatments

Transmission Electron Microscopy (TEM) was conducted to visualize the morphology of the virions treated with AuNP-KR13. Purified pseudotyped HIV-1 BaL virus and AuNP-KR13 were pre-incubated from 5-1440 min at 37°C. Following incubation, samples were fixed with 2% glutaraldehyde for 30 minutes at room temperature, and then embedded in Spurr's low viscosity epoxy medium after acetone washes to dry the virions. Slices (100 nm thick) were prepared using an ultra-microtome (Leica EM UC6), loaded onto a holey carbon TEM 200

mesh grid (Electron Microscopy Science) and imaged using the JEM 2100 camera operated at 120 kV (JEOL, Japan). Sixteen images were taken per sample, and the sizes of observed particles were determined, using Image J software to derive average diameters of the virion particles from TEM images measured from 5 angles.

3.2 Results

3.2.1 Monodispersity of Gold Nanoparticle-Peptide Triazole Conjugates

The physical characteristics of gold nanoparticle-peptide triazole conjugates were validated by DLS, TEM and U.V. absorbance. The particle size was obtained by DLS using the Zetasizer NS90 (Malvern Instruments), while the particle concentration was calculated using the UV spectrum as described in the methods section[284]. The DLS data are shown in **Figure 30**, along with representative TEM images of AuNP-KR13 conjugates of various AuNP sizes. **Figure 30A** also shows the comparison between the expected sizes of AuNP using varying concentrations of citric acid as well as the experimentally obtained diameters (DLS). The AuNP-PT conjugates showed good monodispersity as observed by the TEM images in **Figure 30C**. Further, as shown in **Appendix Fig. 10**, zeta potential values for AuNP-KR13 conjugates compared to the AuNP alone verified the successful peptide conjugation to AuNP [290].

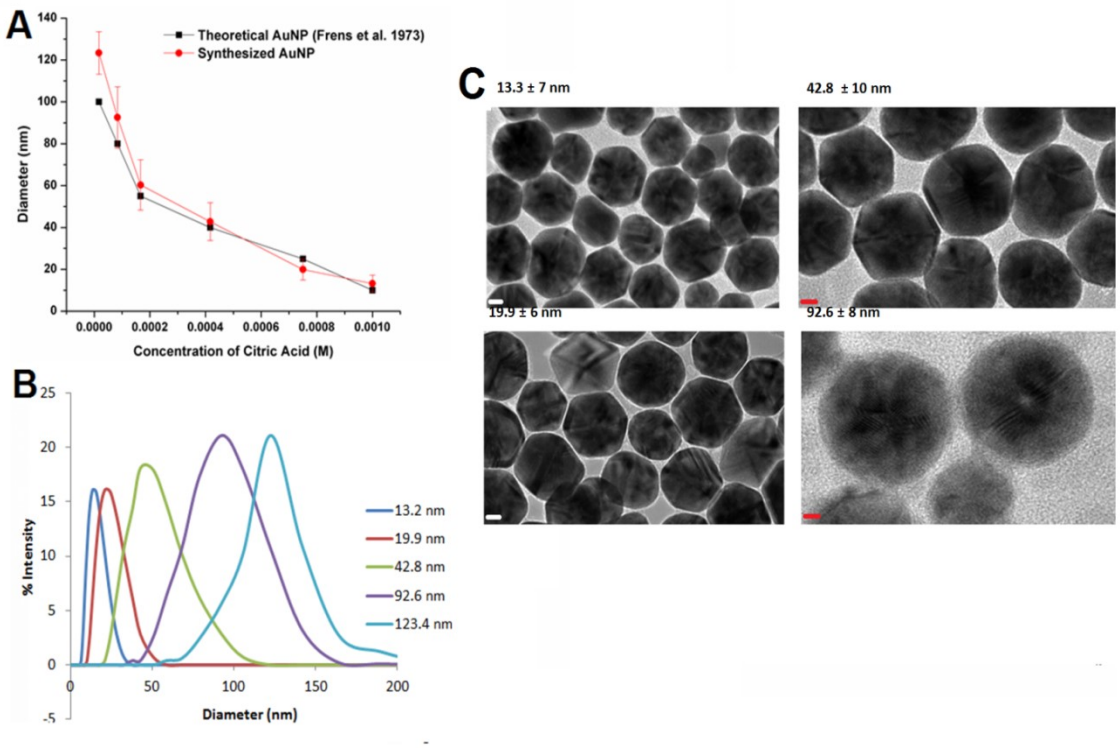

Figure 30: Characterization of the AuNP-KR13 conjugates. (A) Compares the theoretical AuNP diameters, that were expected with increasing concentration of citric acid in the reaction as represented in Frens et al. 1973, to the diameters of the AuNP that were syntehsized as measured using dynamic light scattering (DLS) (n=25). (B) The % intensity of the different diametes of the AuNP-KR13 conjugates as measured on the zetasizer using the dynamic light scattering methodology (n=3). (C) Shows the representative TEM images of the AuNP-KR13 conjugates with diameters 13.3 nm, 19.9 nm, 42.8 nm and 92.6 nm. Error bars represent the standard deviation of the mean, n > 3.

3.2.2 Anti-viral effects of AuNP-KR13 conjugates

Size dependence of the anti-viral functions of AuNP-KR13:

AuNP-KR13 conjugates were tested for both inhibition of HIV-1 BaL pseudotype infection of HOS.T4.R5 cells as well as the cell-free p24 release, in both cases after 30 min exposure of viruses to AuNP-KR13 conjugates. **Figure 31** shows the dose responses of the effects, and IC_{50} values are summarized in **Table 6**. The results are compared to KR13 alone. Strikingly, the anti-viral effects are greatly enhanced with increasing size of the nanoparticle. **Table 6** also shows the number of peptides per nanoparticle calculated from amino acid analysis and the amount of peptide per square nanometer on the AuNP surface. The latter assumes that AuNP is a perfect sphere and that individual molecules of KR13 are equidistant from each other on the NP surface.

To further probe the size dependence of AuNP antiviral effects and to mathematically model the AuNP-PT and virus interface, we prepared nanoparticles in which the number of PT per unit area (PT density) of AuNP surface was kept as similar as possible, by adding sufficient peptide to ensure stability monitored by flocculation assay (Methods) and then adding further peptide determined empirically to equalize density. The antiviral effects of increasing size of AuNP with equal PT density in AuNP-KR13 conjugates are shown in **Figure 32**, and the IC_{50} values obtained from these are summarized in

Table 8. Here, a clear correlation was observed between the effects of AuNP size on inhibition of viral infection and p24 release.

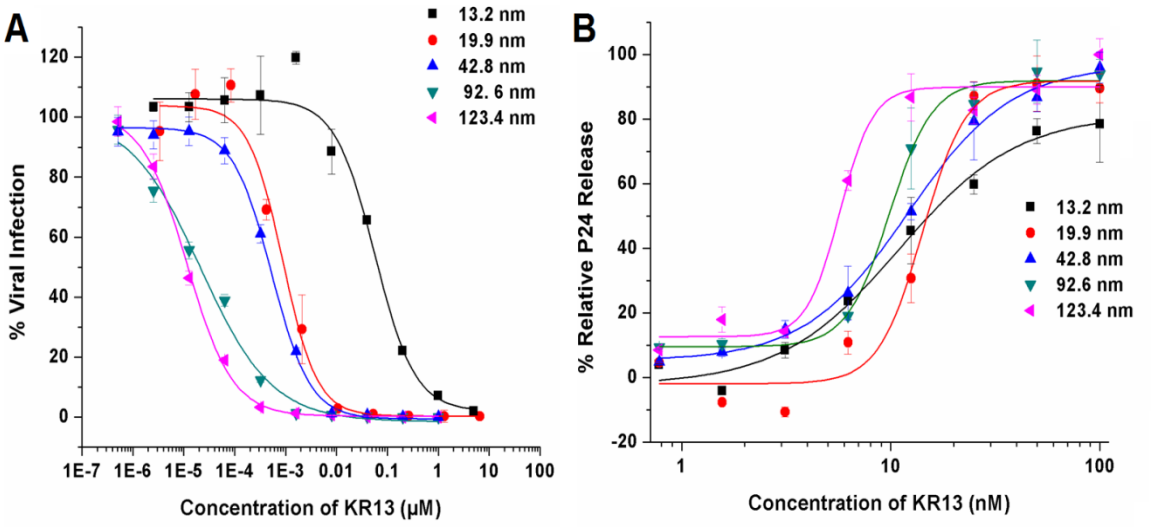

Figure 31: Size dependent anti-viral effects of the AuNP-KR13 conjugates on the HIV-1 BaL pseudovirions. (A) Inhibition of cell infection was measured using a single round infection assay as explained in methods. The IC_{50} values are reported in Table 1. (B) Relative p24 release from the cell-free HIV-1 BaL pseudovirions with increasing concentration of the different diameter AuNP-KR13 conjugates. The EC_{50} values are reported in Table 1. Error bars represent the standard deviation of the mean, n = 3.

Compared to **Figure 31**, **Figure 32** shows a better correlation between the effect of the viral infection inhibition and p24 release. This might be due to the approximately equal number of peptide coverage per square nanometer and which can be used further for AuNP-KR13 and HIV-1 BaL pseudotype spike interface modelling.

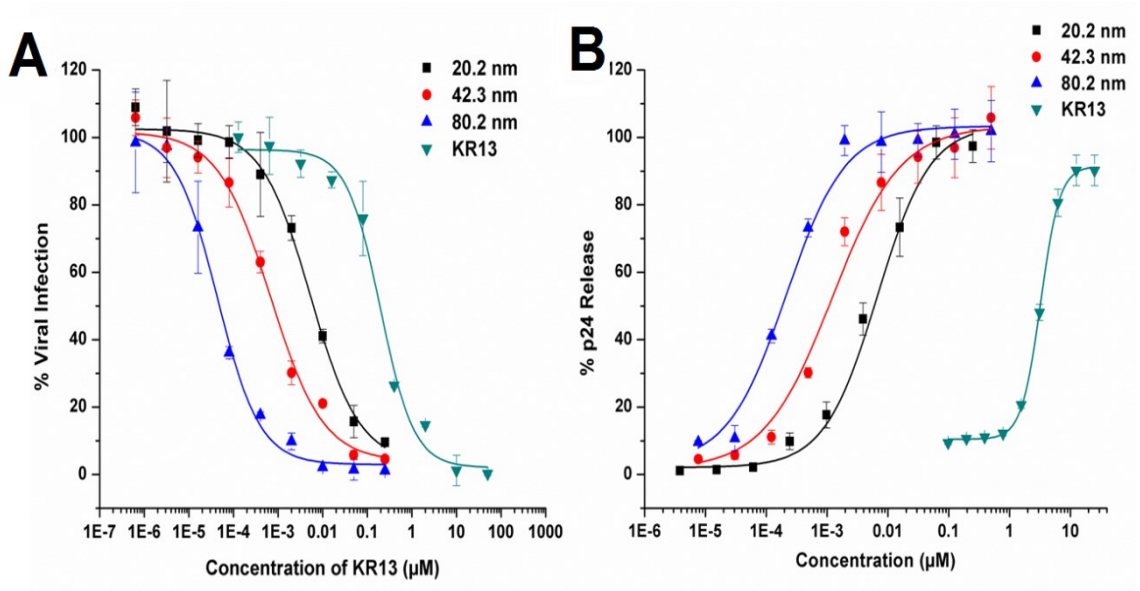

Figure 32: Anti-viral effects of AuNP-KR13 conjugates with increasing diameter of the AuNP with equal density of KR13 coverage per square are on the surface of the AuNP. (A) Inhibition of HIV-1 infection by the AuNP-KR13 conjugates were measured using a single round infection assay as explained in methods. The IC_{50} values are reported in Table 3. (B) Relative p24 release from the cell-free HIV-1 BaL pseudovirions with increasing concentration of the different diameter AuNP-KR13 conjugates. The EC_{50} values are reported in Table 3. Error bars represent the standard deviation of the mean, n = 3.

Impact of density variation of peptide triazoles conjugated on AuNP on anti-viral functions:

AuNP-KR13 conjugates were prepared with varying KR13 densities on 20 nm nanoparticles and tested for both inhibition of HIV-1 BaL pseudotype cell infection with HOS.T4.R5 cells and cell-free p24 release after 30 min of exposure of virus with AuNP-KR13 conjugates. The values computed for KR13 coverage per square nanometer of the AuNP surface assumed that AuNP is a perfect sphere and that individual KR13's are equidistant from each other on the NP surface. As shown in **Figure 33** and **Table 8**, inhibition of both viral infection and p24 release activities were greater with increasing density of KR13 on the AuNP surface. The total number of peptide molecules per AuNP was obtained by amino acid analysis. The AuNP with 0 moles of KR13 have 100% cysteine coverage. As shown in Table 3, the latter non-peptide AuNP exhibited no non-specific anti-viral effects.

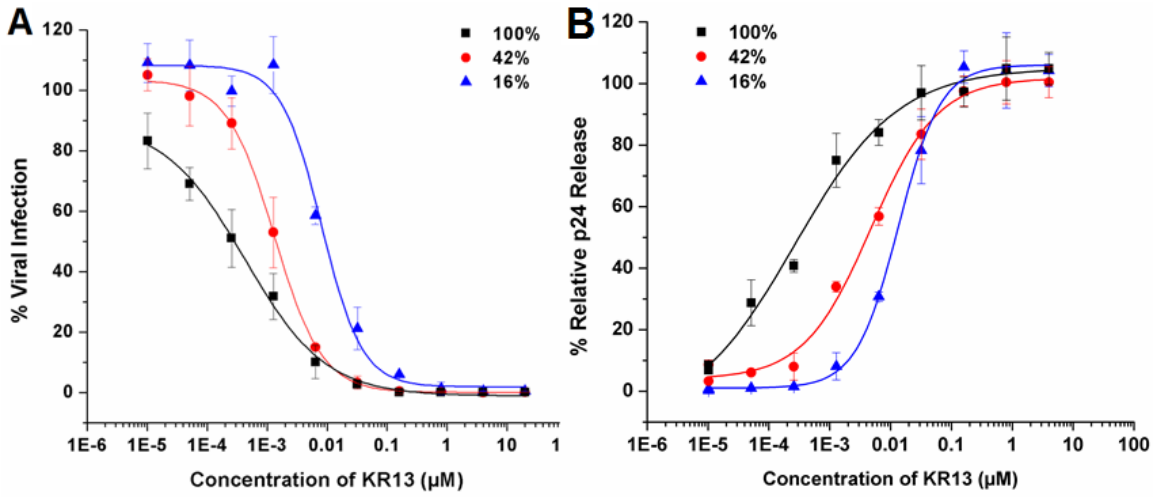

Figure 33: Anti-viral effects of AuNP-KR13 (19.9 nm diameter) with increasing surface desnity coverage of KR13 with 100% being 73 peptides per AuNP as represented in Table 2. (A) Inhibition of cell infection was measured using a single round infection assay as explained in methods. The IC_{50} values are reported in Table 2. (B) Relative p24 release from the cell-free HIV-1 BaL pseudovirions with increasing concentration of the AuNP-KR13 conjugates with decreasing KR13 density coverage. The EC_{50} values are reported in Table 2. Error bars represent the standard deviation of the mean, n = 3.

AuNP-KR13 potencies with replication competent HIV-1:

The anti-viral effects of 20 and 80 nm AuNP-KR13 particles were tested with replication-competent Bal-01 HIV-1, as shown in **Figure 34**. The results demonstrate that the AuNP-KR13 is effective and has a greater potency than KR13 alone (approximately 300 fold greater for the 20 nm AuNP-KR13 and 1400 fold greater for the 80 nm AuNP-KR13 more potent, compared to KR13).

3.2.3 Comparison of the anti-viral functions between AuNP-KR13 and KR13

We previously observed that KR13-induced lysis of HIV-1 embodies virus breakdown properties reminiscent of those occurring during virus-cell fusion. These include exposure of the membrane proximal external region (MPER) of gp41 and inhibition by fusion inhibitor T20. In the current work, we sought to compare AuNP-KR13 lysis for these properties. As shown in **Figure 35A,** AuNP-KR13 treatment does not induce a concentration-dependent exposure of MPER on the residual virion, while treatment with KR13 does. In addition, as seen in **Figure 35B**, the fusion inhibitor, T20, does not lead to the inhibition of AuNP-KR13 induced p24 release, in contrast to the inhibition seen with KR13. **Figure 35C** shows that, like KR13, AuNP-KR13 induced virolysis is accompanied by gp120 shedding. However, for AuNP-KR13, gp120 shedding, p24 release and viral infection inhibition occur simultaneously, all starting within 10 min of incubation with the virus. By comparison, in KR13 virolysis, p24

release occurred with a time lag compared to the gp120 shedding and virus infection inhibition[6]. Hence, from the data shown above, the AuNP-KR13 induced virolysis process appears to be controlled differently than for KR13.

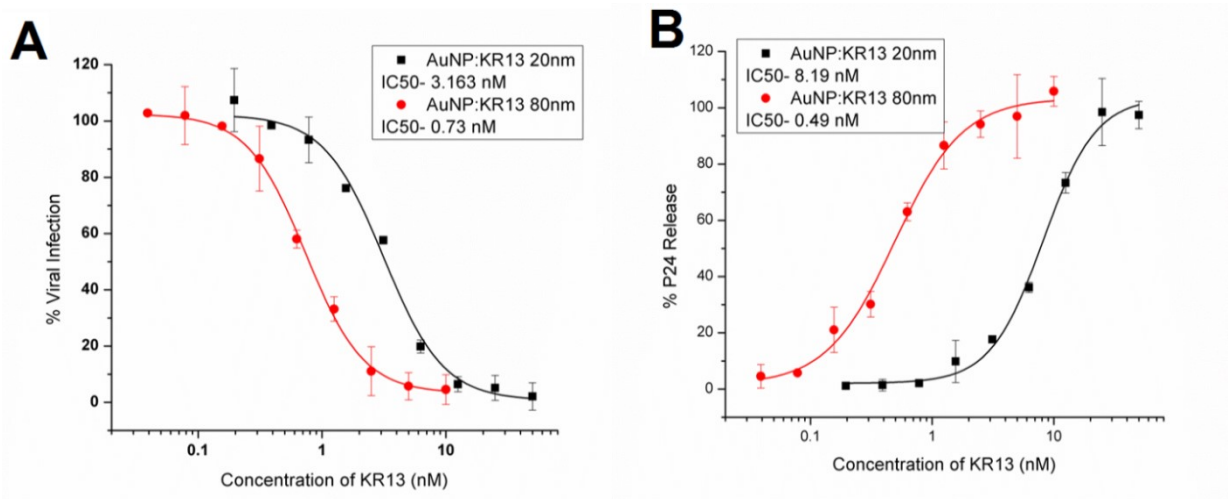

Figure 34: Plots ofAuN: KR13 (20 nm and 80 nm) induced infection inhibition and virus breakdown of replication competent HIV-1 BaL virus. (A) Inhibition of cell infection was measured using a p24 ELISA of the produced virions in the presence of the inhibitor. The IC_{50} values of AuNP:KR13 (20 nm) and AuNP:KR13 (80 nm) to inhibit HIV-1 BaL infection being 3.16 nM and 0.73 nM respectively. (B) Relative p24 release from the cell-free HIV-1 BaL (replication competent) with increasing concentration of the 20 nm and 80 nm diameter AuNP-KR13 conjugates. The EC_{50} values of AuNP:KR13 (20 nm) and AuNP:KR13 (80 nm) to inhibit HIV-1 BaL infection being 8.19 nM and 0.49 nM respectively. Error bars represent the standard deviation of the mean, n = 3.

3.2.4 Impact of Env Spike Presentation on the Virus Surface

We sought to evaluate the importance of simultaneous multi inhibitor-gp120 interactions in AuNP-KR13 induced virolysis. Such encounter could occur by such mechanisms as localized Env spike clustering or multivalent attachment at single spikes. If the AuNP-PT effect were multivalent and required encounter with multiple fully active Env spikes, we expected to observe that reducing active Env density would cause more reduced anti-viral activity with AuNP-KR13 than KR13 alone. To examine this prediction, we compared lytic processes using HIV-1 BaL pseudotype viruses containing different ratios of functional and non-functional gp120. The viruses were produced (see section 4.2) with varying relative amounts of WT and S375W gp120, the latter of which has been found to be ineffective in binding the peptides [25]. Spike variations on the virus, provided by altering the relative abundance of WT vs. mutant S375W gp160 DNA during virus production, led to virions with varying density of WT gp160's on the virion surface. In order to model whether the AuNP-KR13 conjugates work by a multivalent contact mechanism, it was important to know how the mutant (M) and WT (W) monomers were arranged on the spikes (each of which has three monomers[105]) of the virions containing various amounts of mutant DNA. By assuming random protomer assortment, and using i = number of WT protomers,

$$\{W_3\ ,\ W_2M_1,\ W_1M_2, M_3\} = \{W_iM_{3-i}\} \qquad i \in [0,3]$$

$$\propto_i = \frac{3!}{i!\,(3-i)!}\ f^i(1-f)^{3-i}$$

where $f = fraction\ of\ WT\ DNA -$ $proportional\ to\ the\ fraction\ of\ Env\ (WT) expression$

The values for α_0, α_1, α_2 and α_3 for each ratio of WT: S375W DNA were calculated from the formula above, and these values are given in **Figure 38**. The AuNP-KR13 and KR13 effects on these mutated viruses are shown in **Figure 36** and **Table 9.**

Analysis of virus infection inhibition by both KR13 and AuNP-KR13 revealed that, with decreasing WT spike content (4 to 0 μg DNA, while S375W gp120 varied from 0 to 4 □g for total of 4 □g DNA in all cases), there is a decrease in the potency of the inhibitors. However, some significant differences were observed in the response patterns. AuNP-KR13 retained activity even with small abundance of fully active spikes e.g. WT-S375W ratios of 1-3 and 0.5-3.5. In contrast, KR13 activity falls off more dramatically at those conditions (**Figure 36**). This could reflect fundamental differences in how AuNP-KR13 and KR13 encounter the virus to cause lysis.

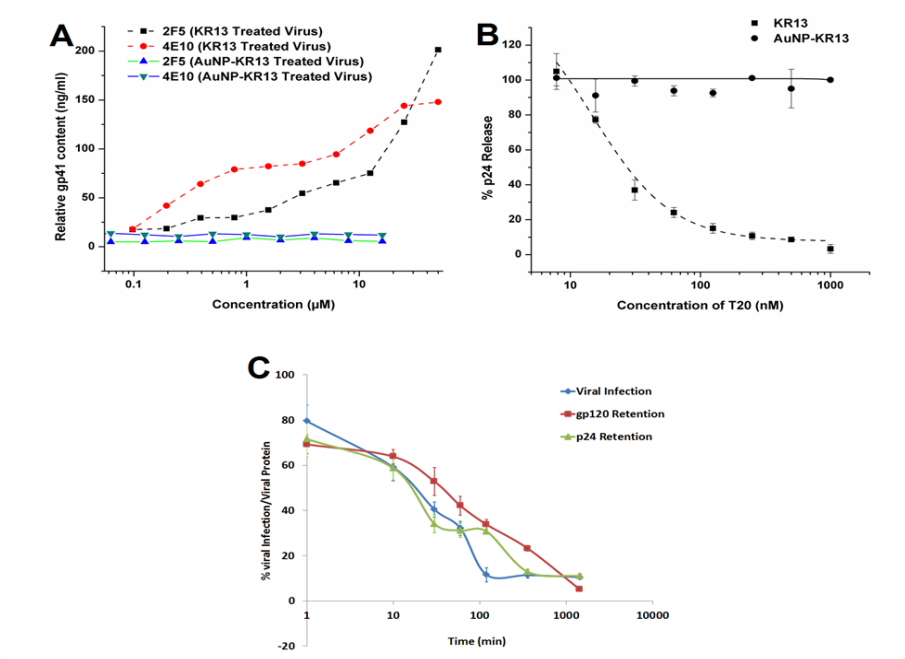

Figure 35: Comparing the anti-viral effects of AuNP-KR13 and KR13 on the HIV-1 BaL pseudotyped virus. (A) Shows the MPER (membrane proximal external region) specific gp41 epitope exposure on the AuNP-KR13 and KR13 alone treated virus by testing MPER specific antibodies (2F5 and 4E10) anbitody binding to HIV-1 BaL pseudotyped virion after 30 minutes of AuNP-KR13 (20 nm diameter) and KR13 repectively. (B) T20 (Fusion Inhibitor) inhibition of AuNP-KR13 (50 nM) and KR13 (1 μM) induced p24 release of HIV-1 BaL pseudotyped, with The IC_{50} value T20 inhibition of KR13-induced p24 release being 15.9 ± 4.9 nM using Origin V.8.1 (Origin Lab). No significant effect on the AuNP-KR13 induced p24 release in the presence of T20. (C) Time dependent anti-viral effects of AuNP-KR13 (20 nm) on the viral infection inhibition p24 and gp120 release. . Time-dependence of viral breakdown by HNG156 (a) and KR13 (b) treatments of HIV-1 BaL pseudovirus. The % of cell infection retained after peptide treatment is shown on the left y-axes, and the viral protein gp120 and p24 retained in the virus fraction is shown on the right y-axes. All samples were adjusted to the untreated virus as 100% infection and 100% viral protein retention . Each time point had controls of untreated virus which was used for normalizing relatively for the each time point peptide treatment. Error bars represent the standard deviation of the mean, n = 3.

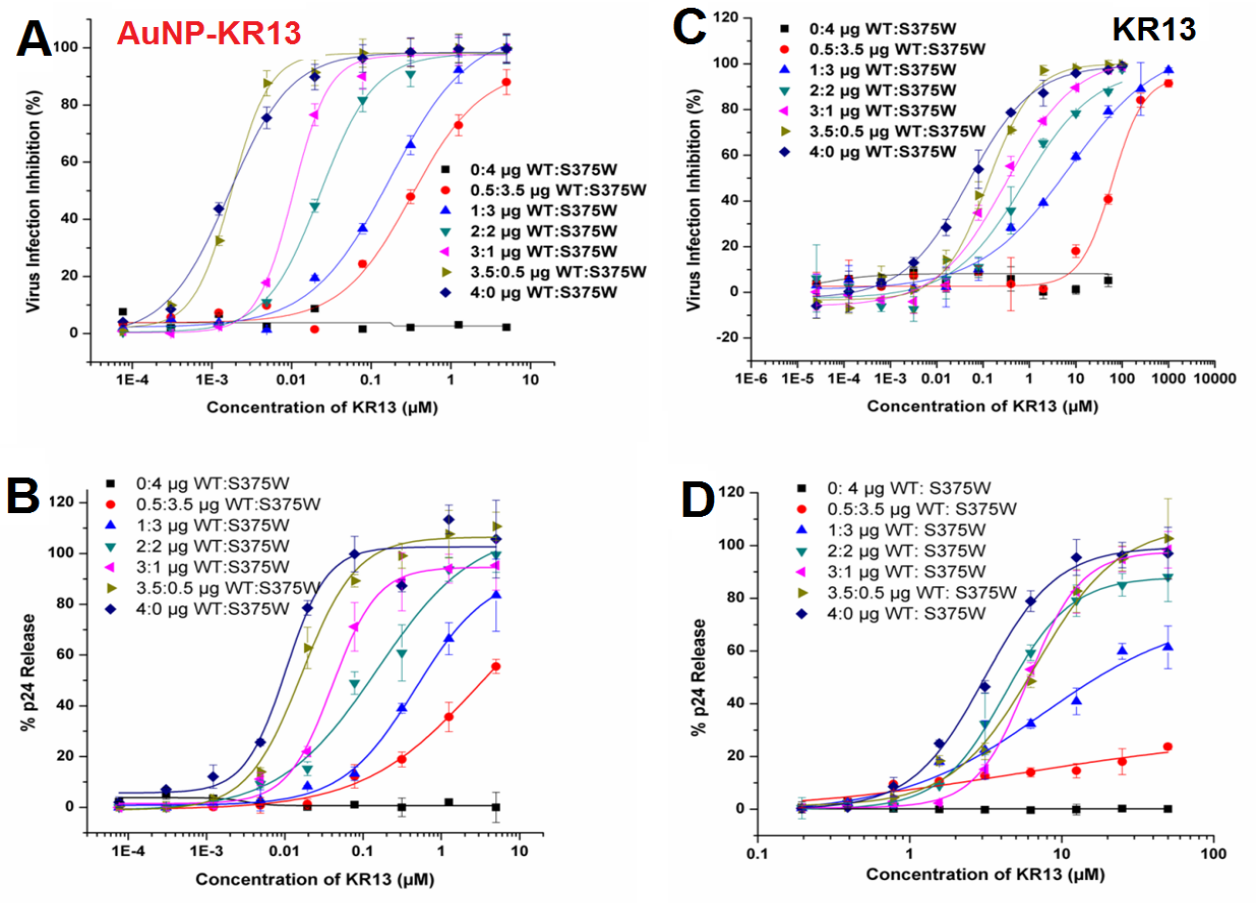

Figure 36: Comparing the antiviral effects which include virus infection inhibiton (A) and p24 release (B) of AuNP-KR13 (20 nm) compared to the virus infection inhibiton (C) and p24 release (D) of KR13 on the HIV-1 BaL pseudovirions with varying concentrations of S375W mutant spikes incorporated. Inhibition of HIV-1 infection was measured using a single round infection assay as explained in methods. The cell-free KR13 and AuNP-KR13 (20 nm) induced p24 release from these virions were measured using the p24 ELISA of the released protein as explained in the methods section. The EC_{50} values are reported in Table 8. Error bars represent the standard deviation of the mean, n = 3.

3.2.5 A continuum mechanics model of the virion-nanoparticle complex

In order to better understand how the AuNP-KR13 conjugates interact with the spikes on the virions, we sought to construct a mathematical model. The surface of AuNP-KR13 particles with varying peptide densities and sizes were modeled as shown **in Figure 37.** The spike dimensions of gp160 were obtained from Mao et al.[106] ,wherein the calculated height and width of the spike was found to be 12 nm and 15.5 nm, respectively, from single particle cryo-electron microscopy. The contact area between the AuNP and virus was modeled by the Hertz contact radius (α) formula using an elastic infinite half space analysis[291],

$$\alpha = \left[\frac{3LR}{4E^*}\right]^{1/3}$$

where L is the applied normal force (load), and the combined Young's modulus and radius of curvature of the two materials 1 and 2 are E* and R, i.e.,

$E^* = \left(\frac{1-{v_1}^2}{E^1} + \frac{1-{v_2}^2}{E^2}\right)^{-1}$, and $R = \left(\frac{1}{R_1} + \frac{1}{R_2}\right)^{-1}$

In the equation above, material 1 is AuNP and the material 2 is the HIV pseudovirus; v_1 and v_2 are the poisson ratios of materials 1 and 2, respectively. The poisson ratio, v_1, and the elastic modulus, E_1, for gold nanoparticle used for the calculation were 0.32 and 100 GPa, respectively[292, 293]. The poisson ratio, v_2, and the elastic modulus, E_2, for the HIV pseudovirus used for the calculation were 0.44 and 440 MPa respectively[294-297]. The load force used was 130 pN, which is the maximum force that can be exerted on the viral membrane that does not fracture the surface[294, 297]. Several assumptions were taken into account

in order to resolve a simplified mathematical model for the contact interface between virion and nanoparticle. These assumptions include: (a) the virus and the AuNP are perfect spheres and (b) the peptides on the AuNP surface have an isotropic arrangement. **Figure 38** depicts the interface of the AuNP and virion surfaces resulting from the above calculations.

3.2.6 Morphological analysis of AuNP-KR13 effects on HIV-1

We sought to image the virus-nanoparticle interface and consequent virus lysis using transmission electron microscopy. Viruses were treated with the AuNP-KR13 (20 nm and 80 nm) conjugates for 10 minutes, and then fixed and loaded on a TEM grid. Uranyl acetate was used as a contrast agent to stain the lipids in order to visualize the virion. Representative images obtained are shown in **Appendix Fig 13**. In the images for both the 20 nm and 80 nm AuNP-KR13, a limited number of AuNP-KR13 particles (average 1-3) were found associated with individual virions, suggesting that a small number of NP's is sufficient to induce virus lysis. The 80 nm AuNP-KR13 appeared to cause a more drastic disruption of the virion compared to the 20 nm AuNP-KR13.

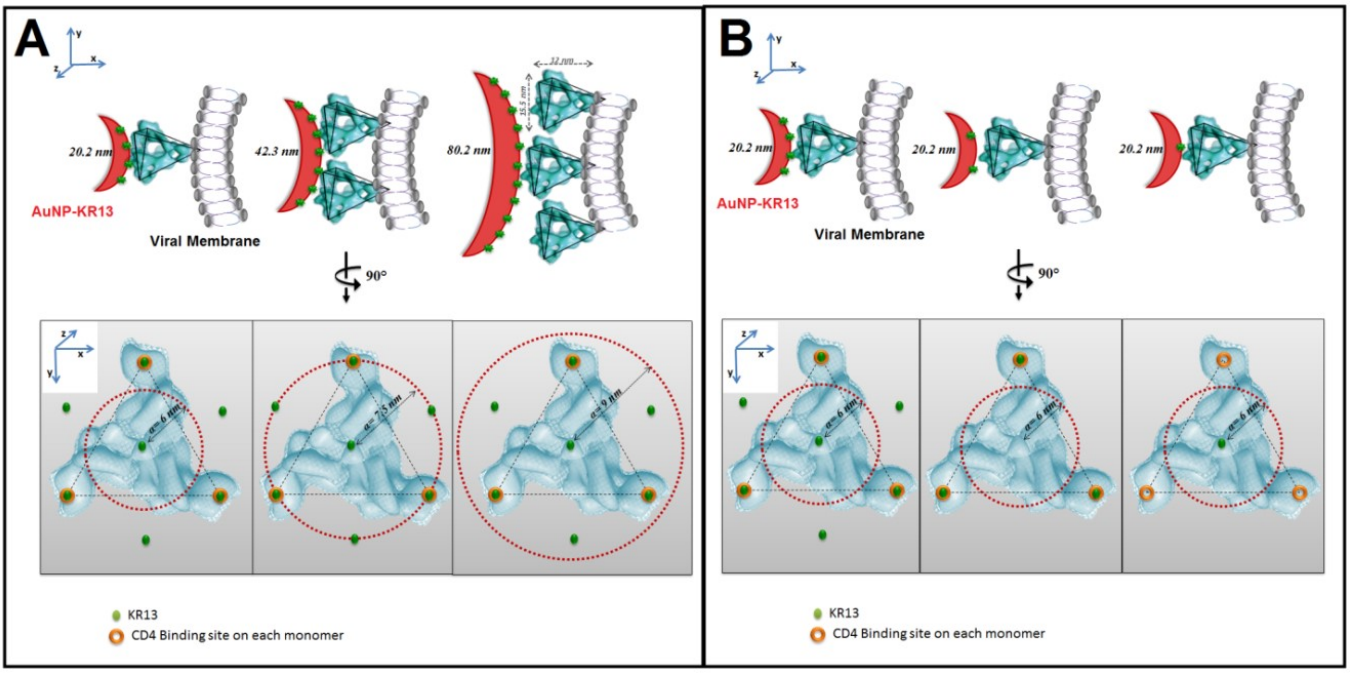

Figure 37: A representative model of the AuNP-KR13 and HIV-1 virus interface. The diameters of the HIV-1 virus as well as the AuNP-KR13 conjugates are taken from the measured values by DLS and TEM respectively. The width and height of a spike was taken from the cryo-TEM modeling from Mao et al. 2012. (A) Shows the interface of the AuNP and virion interface for the size variation of AuNP from figure 30 viewed from a perspective parallel to the viral membrane (top) and viewed from the perspective of the AuNP, at the same contour level (bottom). (B) Shows the interface of the AuNP and virion interface for the density variation of AuNP from figure 31 viewed from a perspective parallel to the viral membrane (top) and viewed from the perspective of the AuNP, at the same contour level (bottom). The contact radius, α, calculated between the AuNP and HIV virion are shown in the bottom images. The model is just representative and has assumptions, one being that the peptides around the AuNP have an isotropic arrangement, two , both the AuNP and HIV-1 virion are perfect spheres and three that the peptide on the AuNP and the spike on the virion are stagnant.

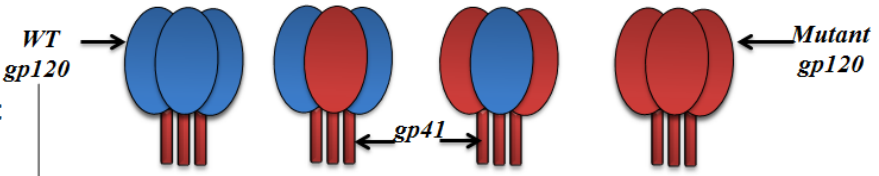

WT DNA-Mutant DNA (µg)	% of spikes			
4-0	100	0	0	0
3.5-0.5	67	29	4	0.2
3-1	42	42	14	2
2-2	12.5	37.5	37.5	12.5
1-3	2	14	42	42
0.5-3.5	0.2	4	29	67
0-4	0	0	0	100

Figure 38: A presentation of how the WT: mutant (S375W) monomers are arranged on the virus spike with different ratios of the WT: mutant DNA concentrations used for virus production. These % of spikes are calculated using the formula which is elaborated in the results section.

3.3 Discussion

This study demonstrated the ability to enhance the anti-HIV-1 potency of peptide triazoles dramatically by gold nanoparticle display and at the same time derived a conceptual model of nanoparticle-virus encounter to account for this enhancement. Previously, we demonstrated that conjugating peptide triazole thiol on AuNP (20 nm) enhanced potency of its anti-viral function[8]. To investigate the limits of this enhancement effect and provide a mechanistic explanation, we altered the size of the AuNP as well as the density of the peptide coverage on the AuNP. Increasing both the size and PT coverage density led to an enhancement in potency of both the viral infection inhibition as well as the cell-free virolysis (**Figures 31, 32 and 33**). Potency enhancement was also observed in replication competent HIV-1 (**Figure 34**).

While prior work had shown that the peptide triazole KR13 alone can causes HIV-1 inactivation and lysis, in this study we show that these antiviral effects are enhanced by AuNP-KR13 conjugates. But there are several observations made in this study (Figure 6) demonstrated that the mechanism by which AuNP-KR13 induces inactivation and lysis is different from KR13 alone. The membrane proximal external region of gp41 on the HIV Env is known to be exposed during the HIV-1 and host cell fusion process, but to be unexposed in the ground (unliganded) state of the virus[274]. For KR13, we previously observed both concentration dependent and time dependent exposure of the MPER epitope on the HIV-1 virion when viruses were treated with KR13[6]. However, in the case of AuNP-KR13, we did not observe MPER epitope exposure (**Figure 35A**). In addition, the data in Figure 6B show that T20, which is a fusion inhibitor that targets the

6-helix bundle formation of gp41 during HIV- fusion with host cell, inhibits KR13-induced p24 release (as reported previously) but does not inhibit such release by AuNP-KR13. Further, the data of Figure 6C show that gp120 shedding, infection inhibition and virolysis induced by p24-release of the HIV-1 BaL pseudotype all had a similar time-dependence for the AuNP-KR13 exposure, versus unequal kinetics for KR13 (for which p24 release lagged compared to gp120 shedding and infection inhibition[6]). Collectively, the characteristics of MPER exposure, T20 sensitivity and time-dependence of antiviral effects observed for KR13 all argue that KR13-induced lysis bore a relationship to the physiological events of virus-cell fusion. In contrast, the lack of these phenotypes (or a similar word) with AuNP-KR13 suggests that the latter responds to different forces (**Figure 35**). **Table 9** summarizes the differences between KR13 induced virolysis and AuNP-KR13 induced HIV-1 virolysis.

Several other differences between KR13 and AuNP-KR13 have emerged during ongoing investigations of KR13-induced lysis (Lauren Bailey, manuscript in preparation). A gp120 antibody, 2G12, that binds to the V3 loop and inhibits KR13 induced virolysis, was found not to inhibit AuNP-KR13 induced virolysis (data not shown) We have also found that DTNB (dithionitrobenzene), a thiol blocking agent that inhibits KR13 induced virolysis, did not affect AuNP-KR13 mediated virolysis (data not shown). These data reinforce the need to consider gold nanoparticle specific mechanisms to explain the virolytic activity of AuNP-KR13.

The responses of potency enhancement to nanoparticle and virus surface properties are consistent with multivalent contact between virus and nanoparticle surfaces as a major driving force for the antiviral effects of AuNP-KR13. A key aspect for multivalent spike

engagement at the virus-nanoparticle interface is the importance of density of both components. As noted above, we observed that the density of peptide on the AuNP surface has a high impact on its anti-viral potency (**Figure 32 and Tables 5 and 7**). In addition, varying the amount of wildtype (active) spikes on the HIV-1 virion surface by replacing the active spikes with the peptide-insensitive mutant spikes, S375W, also had an impact on antiviral activities for AuNP-KR13 and with KR13 alone. By incorporating progressively more mutant vs. peptide-sensitive WT gp120 in the HIV-1 virions, we observed reduced sensitivity to HIV-1 infection inhibition by both KR13 and AuNP-KR13. However, the effect of reduced WT gp120 abundance on p24 release was greater for KR13 than for AuNP-KR13. Correlating with the relative numbers of heterogeneous and homogenous spikes with mutant-WT mixtures (**Figure 38**), we found that, while KR13 induced p24 release required an average of ≥1 fully active spike (containing 3 active WT monomers in individual spikes) per virion, the AuNP-KR13 (20 nm) induced up to 50% p24 release even with an average of 0 fully active spikes.

Based on the above results, we configured a multivalent encounter model based on the previously known dimensions of the virus[61, 106] and the following assumptions: (a) the KR13 on the AuNP are isotropic and equidistant from each other, (b) the virus and AuNP are perfect spheres; and (c) the spikes on the HIV-1 virion are stationary and do not cluster prior to nanoparticle encounter (**Figure 37**). While we recognize that these assumptions are idealized descriptors, they account for the general trends of increased interactions of AuNP-immobilized ligands with multiple spikes and the relative insensitivity of the encounter to the need for fully active spikes.

We speculate that multivalent contact could lead to an elevated stress on the HIV membrane and eventually cause irreversible collapse of the virion particle (**Appendix Fig. 13**). Further investigation is needed to better understand the nature of the virus membrane transformation caused by AuNP-KR13 and how this type of effect compares to membrane transformations triggered by other types of virus-lysing agents [298-300]. Nonetheless, the nanoparticle-virus encounter model could provide a guide to further design inhibitor-NP complexes for HIV-1 and potentially other similar viruses such as influenza virus, sarcoma virus and more.

The work presented here reinforces the potential usefulness of inhibitor display on nanoparticles to improve potency for disease prevention and intervention. While nanocarriers have been used as vehicles for drug delivery, their use for forming therapeutic agents has been more limited[228, 301-303]. Jiang et al. have shown that gold nanoparticles ranging from 2-100 nm in diameter conjugated to multiple trastuzumab antibodies enable targeting and cross-linking of human epidermal growth factor receptor (HER)-2 in human SK-BR-3 breast cancer cells, by causing reduced (HER)-2 receptor expression and inducing receptor mediated endocytosis[304]. Jiang also showed that the anti-cancer potencies were altered by variations of the diameter of the gold nanoparticles, with the larger particles having more protein on its surface and increased avidity, while the smaller particles exhibited greater receptor mediated endocytosis[304]. Nanomedicine design for HIV-1 infection inhibition also has been limited[305]. Gold nanoparticle display has been shown previously to increase the antiviral potency of the HIV-1 inhibitor SDC-1721, a derivative of TAK-779, that targets the cellular coreceptor, CCR5[235, 306]. However, such studies have used very small (2 nm) AuNP that could

be taken up by cells non-specifically[236]. Heterogeneity of the HIV-1 also has been a problem limiting antibody and drug targeting[307]. The current work argues that gold nanoparticle display could help overcome the heterogeneity of Env spikes by enabling multivalent attachment of neighboring partially defective spikes. The current work provides a generalizable approach for nanoparticle drug design not only for HIV-1 but also for other infectious enveloped viruses such as influenza and hepatitis B virus.

‘

CHAPTER 4: USING THE VIRUCIDAL AGENTS TO TARGET OTHER STAGES OF THE HIV-1 LIFECYCLE

4 Introduction

HAART therapy used 2 or more antiretrovirals currently to treat patients with HIV. This form of therapy was chosen so that one can target different stages of the HIV life cycle and hence lead to enhanced inhibitory effect [126]. However, treatment efficacy relies on access to treatment and excellent adherence, which has proven to be a serious challenge to those receiving highly active antiretroviral therapy (HAART) [308]. There is a lot of resistance to most of the drugs used in HAART as well as there is a lot of non-adherence developing in adult populations [309]. Hence it is important to develop new inhibitors that are broadly acting and can target multiple stages of the virus.

Since the over 20 years ago after the discovery of HIV-1, this virus has cause an epidemic disease called AIDS. There have been many attempts to eradicate the disease but somehow the virus finds a way to mutate and protect itself [89, 310]. There have been many attempts made in order to create immunogens that can serve as vaccines against this virus and there have been very few successes[182]. Therefore another venue which needs a lot of research and novel interventions is the vaccine development field.

Hence this study will focus on a novel discovery that the virolytic peptide triazole and its multivalent conjugate to target not only the entry and fusion stage of the lifecycle but also lead to inhibition of new virus production or also known as

vironeogenesis. Further we will elaborate on how the residual virus post KR13 treatment can be the perfect custom made immunogen using the virus that infected the host cell to create neutralizing antibodies against new infections. These novel discoveries will open the phase on multifaceted therapy targeting different stages of the HIV-1 lifecycle using just one agent, making it much more reliable convenient as well as efficient.

4.1 New virus production inhibition by peptide triazoles and gold nanoparticle peptide triazole thiol conjugates

4.1.1 Introduction

HAART therapy has led to a substantial decrease in deaths caused by AIDS, prolonging the life of the infected individual [126]. However, there is a gap in research knowledge in developing singular novel inhibitors that target multiple stages of the virus life cycle as opposed to combination therapy like HAART. Microbicides developed to target viral entry may also be able to target newly produced viruses[311], but unfortunately the bioavailability and stability of these inhibitors are very low, making targeting newly produced virions very difficult, and relegating such drugs to preventative treatments[312].

As the precursor to its presence on newly budded virions, HIV Env glycoprotein must first be constructed and trafficked to the surface of the membrane by standard transcription, translation, and modification cellular machinery, which provides a potential shared target between an infected cell and its daughter virions [313]. Indeed, this has provided other studies with a method of efficiently and specifically killing HIV-infected cells, by conjugating cytotoxic agents to anti-Env antibodies [314, 315]. Furthermore, since the latent population of HIV infected cells has proven to be one of the most difficult stages of the HIV lifecycle to attack [316], and because this latent population is known to express gp120 on their cell membranes when stimulated [317, 318], the strategy of anti-Env immunotoxins has also been shown to kill reactivated modeled latently infected cells (Brooks 2003). However, the risks of broadly cytotoxic agents, combined with Env's variability, and complications with latent reactivation may limit the scope of such approaches.

A peptide triazole (PT) class of entry inhibitors has been identified by our group in prior work and found to be able to bind to HIV-1 Env gp120 with nanomolar affinity, to suppress protein-ligand interactions of the Env protein at both its CD4 and co-receptor binding sites, and to inhibit cell infection by a broad range of virus subtypes[6, 10, 23]. Strikingly, we have recently found that a multivalent form of the peptide triazole KR13 displayed on gold nanoparticles (AuNPs) is able to disrupt virus particles in the absence of host cells, causing

leakage of the internal protein p24 and exhibiting strong antiviral activity as shown in chapter 3 [8].

This study reports on the discovery of other special functions of KR13 and its multivalent gold nanoparticle conjugate. KR13 and AuNP-KR13 were able to inhibit new virus production (vironeogenesis) by HIV-1 infected cells, and AuNP-KR13 additionally exhibited cytotoxicity specific against infected producer cells. Further developments of AuNP-KR13's cytotoxic effect may lead to the capability to target and kill latently infected cells.

4.1.2 Materials and Methods

4.1.2.1 Materials

Modified Human Osteosarcoma Cells (HOS.T4.R5) engineered to express CD4 and CCR5, receptor and co-receptor respectively, as well as pNL4-3.Luc R-E- backbone DNA, were obtained from Dr. Nathaniel Landau. The HOS.T4.R5 cells were grown in DMEM supplemented with 10% FBS, 2.5% HEPES, 1% Penicillin- Streptomycin, 2% L-Glutamine and 1 mg of puromycin. 293T (Human Embryonic Kidney) cells were obtained from American Type Culture Collection and grown in the same culture medium as the HOS.T4.R5 cells except without puromycin. CHO-K1 gp160 +ve cells and regular CHO-K1 cells were obtained from the aids repository and

were grown in DMEM supplemented with 10% FBS and 1% Penicillin-Streptomycin. The plasmids for HIV-1 BaL gp160 and VSV-G Env DNA were gifts from Dr. Julio Martin-Garcia. The antibodies mouse anti-p24, rabbit anti-p24, and the protein p24, were from Abcam. Fully Infectious HIV-1 (BaL) was a gift from Dr. Michele Kutzler and obtained from Penn Center For AIDS Research (CFAR). The protein gp120 monomer was produced using already-established protocols [25], anti-gp120 was from Alto chemicals. Gp41 protein, Enfurvitde (T20) and anti-gp41 antibodies 4E10, 2F5 and 98-6 were from NIH AIDS Research and Reference Reagent Program (ARRRP). Enhanced Chemiluminescence western blot detection system was from Amersham. O-phenylenediamine (OPD) was from Sigma Aldrich. All other materials were from Fisher Scientific.

4.1.2.2 Production of the peptide triazoles and gold nanoparticle peptide triazole conjugate

For this study, we synthesized the peptide triazole denoted KR13, composed of the 12-residue amino acid sequence of the previously identified high potency peptide-triazole HNG156 [319] with a C-terminal extension containing a Cys-SH group. This cysteine-containing derivative was selected because the introduced SH group facilitates conjugation to the AuNP carriers. KR13 was prepared by manual solid phase synthesis using Fmoc chemistry on a Rink amide resin at 0.25 mmol scale [22]. The amino

acid sequence of KR13 is RINNIXWSEAMMβAQβAC-$CONH_2$, where X is ferrocenyltriazole-Pro. As control KR13b was synthesized which is the KR13 amino acid sequence with an acetomethyl group at the C terminus to block the active cysteine (**Appendix Fig. 14**). The KR13 and KR13b was validated for function by conducting a CD4 and 17b competition assay as explained in bastian et al. 2011[8].

The gold nanoparticle was synthesized using the Frenz method of citric acid reduction of $HAuCl_4$ and for this study we produced AuNPs at 20 nm diameter on average . The AuNPs were then stabilized using The synthesized particles will be stabilized using Bis-(p-sulfonatophenyl) phenyl phosphine dehydrate dipotassium salt (BSPP, Strem Chemicals) and transferred into phosphate buffer (pH 7.2) using a Millipore 10,000 MWCO filter. The AuNP was validated using dynamic light scattering and the size was measured as previously explained in Haiss et al. [8, 284]. The KR13 was then conjugated onto the AuNP using the cysteine residue by vigorously stirring a 1000:1 ratio for 30 minutes at room temperature. The conjugate was then stirred at 4°C overnight. The unconjugated peptide was washed off using a 100K filter and the sample was resuspended in phosphate buffer (pH 7.2). AuNP-KR13 coverage density was determined using amino acid analysis (Keck Institute, Yale University).

4.1.2.3 The effect of peptide triazoles and gold nanoparticle peptide triazole thiol on HIV-1 producer cells

The peptide triazoles KR13 and KR13b as well as the AuNP-KR13 conjugate was validated for their antiviral effects by testing their viral infection inhibition as well as their p24 release profiles as previously described in Bastian et al. 2013 and 2011 respectively. Following the effect of these inhibitors on HIV-1 BaL pseudotyped producer cells were tested.

3 million human embryonic kidney cells (293T) were seeded onto a T-75 flask until attached for producing HIV-1 BaL pseudotyped. For recombinant pseudovirus production the pro-viral envelope plasmid sequence used was the CCR5 targeting HIV-1 BaL strain and the backbone plasmid sequence used was an envelope-deficient pNL4-3-Fluc+env– provirus developed by N. Landau [252]. 4 µg of envelope and 8 µg of backbone DNA were co-transfected into 293T cells using FuGene 6 or polyethylenimine as the transfection reagent [253]. Fourteen hours post-transfection, the virus producer cells were washed with PBS and detached using 0.05% trypsin. The cells are re-seeded onto a 24 well plate at 100,000 cells/ml with 2 mls per well. Post 24 hours of re-seeding, the cells were washed with PBS and a serial dilution of the inhibitors KR13, KR13b and AuNP-KR13 were added 1:1 ratio with cell media. The cell supernatants were collected 24 hours post inhibitor addition and spun on a 6-20% iodixanol gradient at 30,000 rpm for

2 hours at 4°C. The virus fraction (16-18%) was collected and tested for p24 content, gp120 content as well as tested for viral infection in HOS $CD4^{+ve}CCR5^{+ve}$ as explained in section 2.2.2.2.

The p24 content was measured using ELISA as explained in section 2.2.3 and the gp120 content was measured using western blot analysis using 1:10 dilution of the virus fraction and primary and secondary antibodies, anti-gp120 D7324 and anti-sheep HRP respectively.

4.1.2.4 Cell viability of the virus producer cells in the presence of the peptide triazoles and gold nanoparticle peptide triazole thiol

The virus producer cells once transferred to a 24 well plate and loaded with inhibitors KR13, KR13b and AuNP-KR13 as explained above, the supernatants were collected and the remainder cells were validated for cell viability. The cells were washed with PBS and loaded with 250 µl of the Pre-mix WST-1 reagent (Takara Bio Inc.). The reagent was incubated with the cells at 37°C for 30 minutes. Following incubation the absorbance was read at 450 nm using a plate reader (Tecan Instruments). The absorbance value at 450 nm corresponds to the mitochondrial activity of the cell. Furthermore, in order to test whether the cytotoxicity observed by AuNP-KR13 is specific to peptide triazole binding, we tested the effect of KR13

and AuNP-KR13 on cells transfected with the infectious, but PT-resistant, envelope mutation S375W [24, 25] (**Appendix Fig. 17**).

4.1.2.5 Effect of the peptide triazoles and gold nanoparticle peptide triazole thiol on cells stably expressing gp160 on the surface

In order to understand the mechanism of action of how these inhibitors lead to virions produced with no activity it was important to understand on a cellular level how they react. In order to test this, CHO-K1 gp160 +ve cells and regular CHO-K1 cells were obtained from the NIH aids repository and grown in their growth media at 100,000 cells per well on a 96 well plate. 24 hours post seeding serial dilution of KR13, KR13b and AuNP-KR13 were added onto the cells and incubated overnight. The cell supernatants were collected and tested for gp120 shedding using western blot analysis as described above. The controls were PBS incubated instead of the inhibitors and also the CHO-K1 cells that has no gp160 expression. The cell viability was also tested post inhibitor addition as explained above using the pre-mix WST-1 reagent.

4.1.2.6 Breadth analysis of new virus formation inhibition by peptide triazoles and gold nanoparticle peptide triazole thiol on replication competent viruses

The virus DNA was obtained from the University of Pennsylvania CFAR as a gift from Farida Shaheen. 293T cells were transfected with the virus DNA in 24 well plates as described above. The variety of viral DNA used was to test for tropism sensitivity as well as clade breadth of this inhibitory effect of these peptides and conjugates which included YU2, JRCSF, NL4-3, HXBC2 and R3A. Three dilutions of the inhibitors KR13, KR13b and AuN-KR13 (10 μM, 1 μM and 0.1 μM) were added to the producer cells post a PBS rinse. The samples were incubated for 24 hours and the cell supernatants were tested for infection on HOS $CD4^{+ve}CCR5^{+ve}$ cells. Since the produced virions have no luciferase reporter gene in their RNA, the following protocol was used for quantification of infection. HOS $CD4^{+ve}$ $CCR5^{+ve}$ cells seeded, at 8,000 cells per well in a 96 well plate, were incubated for 24 hours followed by addition of cell supernatant collected from the 293T cells above. After 48 hours infection, p24 content of virions in the supernatant was measured in order to determine the infection of the produced virions. All these experiments suing replication competent virions were conducted in a BSL-3 facility.

4.1.3 Results

4.1.3.1 Inhibition of vironeogenesis by peptide triazoles and gold nanoparticle peptide triazole thiol

The effect of KR13, KR13b as well as AuNP-KR13 on virus producer cells was tested in order to check whether these novel inhibitors can target multiple stages of the HIV lifecycle. The inhibitors were added to the producer cells and the cell supernatants were purified and tested for p24 content as well as viral infection and gp120 content. As control producer cells treated with PBS alone was used. The viral infection and gp120 content was tested by using normalized virus containing solution from the p24 content analysis in order to confirm we are loading equal amount of virus. Although, the AuNP-KR13 treated cell supernatants had a reduction in p24 content and hence we did not normalize the p24 content for the gp120 and viral infection analysis. **Figure 39** shows the p24 content, viral infection and gp120 content on the virions collected post inhibitor treatment. From this we clearly see that KR13 and AuNP-KR13 lead to virions that are not infectious and also do not contain gp120 on their viral membrane. But the virions still have p24 in their viral lumen showing that the mechanism is not the same as how the KR13 and AuNP-KR13 target produced viruses (**Appendix Fig. 14**). Further even though KR13b does not lead to virions that are non-infectious, it still has reduction of gp120 on the viral surface (**Figure 39C**).

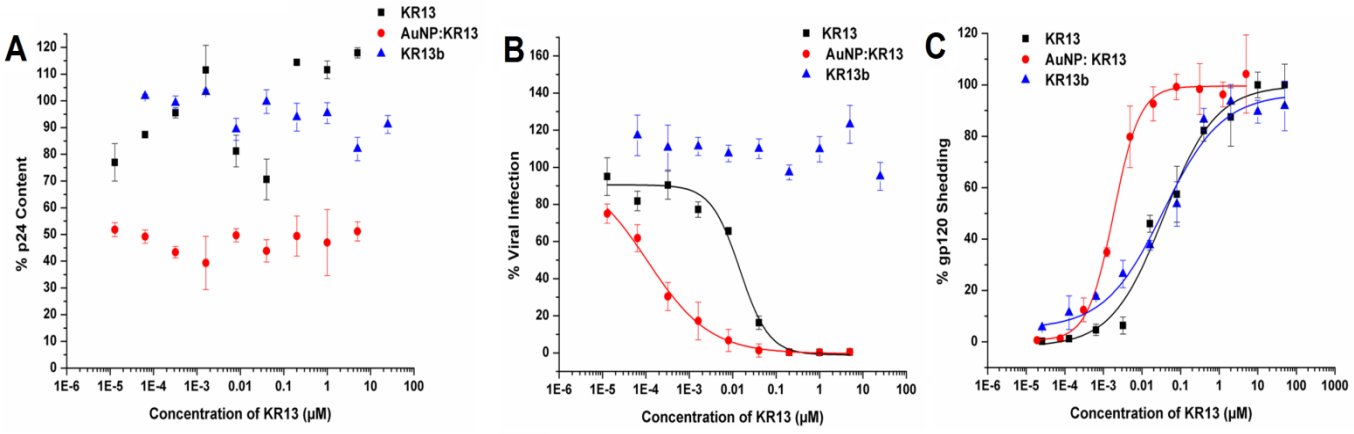

Figure 39: Anti-viral effects by KR13, KR13b and AuNP-KR13 on virus producer cells. (A) Total p24 content in the separated virus fraction from cell supernatants that were treated with KR13 (black), KR13b (blue) and AuNP-KR13 (red). (B) Viral infection and (C) gp120 content of the of the virus fraction collected post inhibitor treatment of the producer cells, the samples were normalized to p24 content prior to addition into HOS $CD4^{+ve}CCR5^{+ve}$ cells and tested for gp120 using western blot analysis respectively. The IC_{50} values for viral infection inhibition of produced virions treated with KR13 and AuNP-KR13 are 25.6 ± 3.5 nM and 1.2 ± 0.05 nM respectively. The EC_{50} of gp120 shedding from the produced virions post KR13, KR13b and AuNP-KR13 treatment are 25.7 ±7.2 nM, 38.7 ± 3.4 nM and 1.8 ± 2 nM respectively. Error bars represent the standard deviation of the mean, n = 3.

4.1.3.2 Cell viability of the virus producer cells in the presence of the peptide triazoles and gold nanoparticle peptide triazole thiol

We tested to see whether the virus producer cells had any toxicity in the presence of the inhibitors, KR13, KR13b and AuNP-KR13. In order to test this we used the WST-1 pre-mix reagent that forms a formazan product based on the metabolic activity of the cells. The results are summarized in **Figure 40**, and show that the cells are nearly 100% viable in the presence of KR13 and KR13b but substantially get affected in the presence of AuNP-KR13. This therefore validates why the p24 content of the virus produced from cells treated with AuNP-KR13 have relatively low amount of p24 (**Figure 39A**). In order to confirm that the AuNP alone had no effects on cell viability, the producer cells were subjected to unconjugated AuNP as well as AUNP conjugated to KR13s a scrambled sequence of KR13 that has no antiviral activity. The results showed that these controls had no effect in cell viability (**Appendix Fig. 15**).

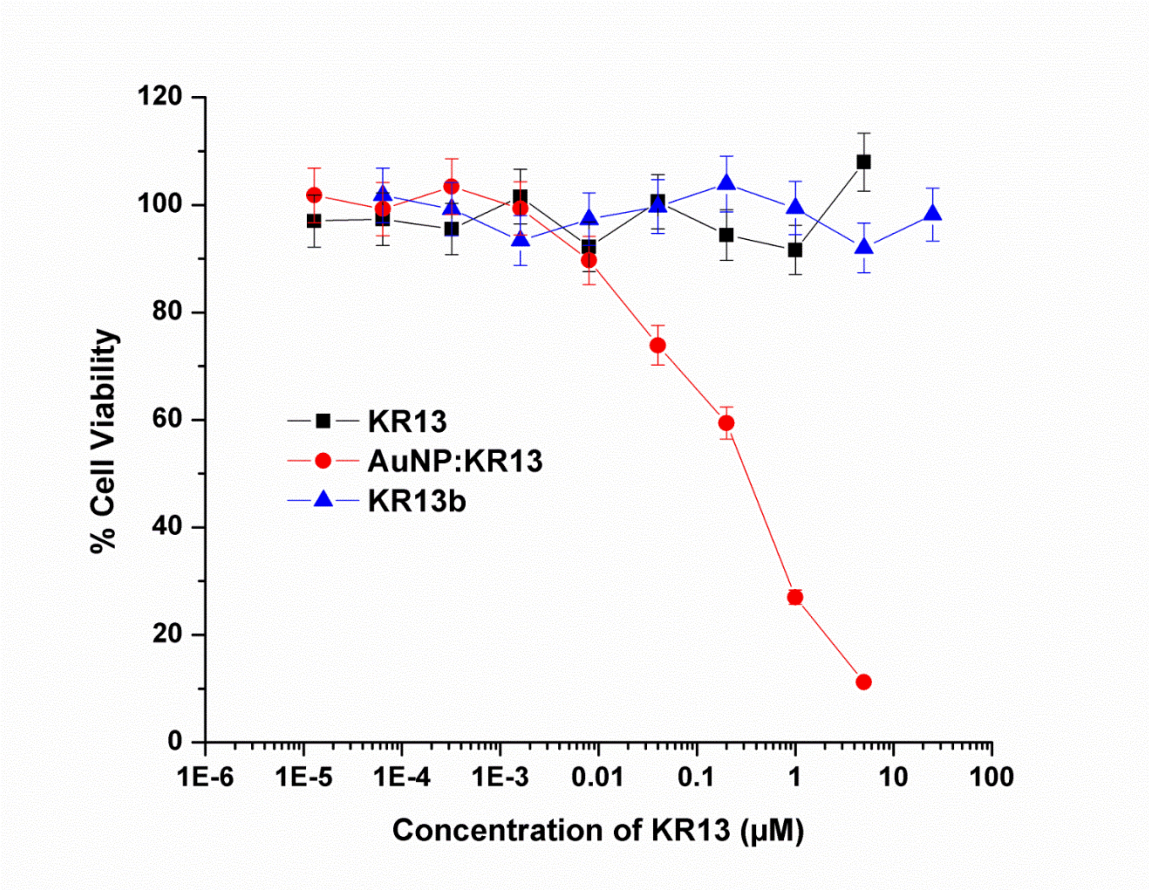

Figure 40: Cell viability of transfected 293T cells which are incubated with KR13 (black), KR13b (blue) and AuNP-KR13 (red). The samples were tested using WST-1 reagent and the absorbance measured at 450 nm. The samples were compared to control which is PBS treated virus producer 293T cells. Error bars represent the standard deviation of the mean, n = 3.

4.1.3.3 Peptide triazoles and gold nanoparticle peptide triazole thiol functions on cells stably expressing gp160 on the surface

To better understand the mechanism of how the KR13 and AuNP-KR13 treatment leads to virions that are non-infectious we tested their effects on cells expressing the HIV env (gp160). This was done with CHO-K1 cells that stable express gp160 trimer. With inhibitor treatment we observed that gp120 was shed from the cell surface in a concentration dependent manner (**Figure 41**). From this result we can confirm that the gp120 also is shed from virion producer cells upon peptide treatment leading to virions that have no gp120 on their surface and thus no infection. Further this also validates that the p24 is not released from the produced virions because the peptide acts on a cellular level. The AuNP-KR13 treatment although not only led to gp120 shedding from the CHO-K1 cell surface but further led to cell lysis and thus cell toxicity (**Figure 41**). The cell viability of CHO-K1 cells –ve gp160 was also conducted in the presence of KR13, KR13b as well as AuNP-KR13. This was a control experiment done in order to test if this gp160 shedding is specific and also whether AuNP-KR13 cell lysis is specific to cells expressing gp160 (**Appendix Fig. 16**). From this experiment it is evident that the AuNP-KR13 induced cell toxicity is specific to cells expressing gp160 on their envelope (**Figure 40 and Figure 41**).

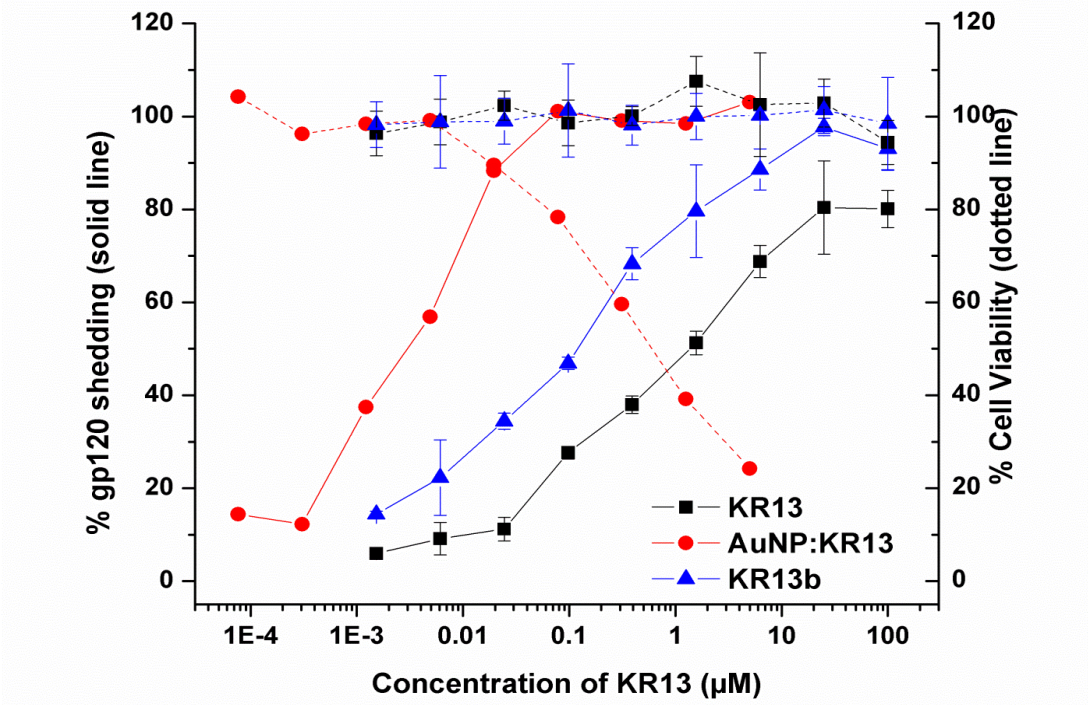

Figure 41: Effects of KR13, AuNP-KR13 and KR13b on CHOK1 cells stably expressing gp160. The dotted lines show the cell viability of the cells when treated for 24 hours with the inhibitors and post a media change. The cell viability was measured using WST_1 Pre-mix reagent and the absorbance read at 450 nm. The samples were normalized from the negative control which was the absorbance measured of cells treated with PBS. The solid lines show the gp120 shedding from the CHOK1 gp160 +ve cells when treated with the inhibitors for 24 hours. The cell supernatants were collected and measured for gp120 using western blot analysis. The positive and negative controls include cells treated with 0.1% triton X and cell treated with PBS respectively. Error bars represent the standard deviation of the mean, n = 3.

.

4.1.3.4 The new virus production inhibition by peptide triazoles and AuNP-KR13 had a broad spectrum against replication HIV-1 competent virions

We used a broad spectrum of HIV-1 virions which include YU2 and JRCSF (clade B, tier 2 and CCR5 tropic); NL4-3 (clade B, tier 1 and dual tropic); HXBC2 (clade B, tier 1 and CXCR4 tropic) and R3A (clade B, tier 2 and dual tropic). The results are summarized in **Figure 42** and we observe that KR13, KR13b as well as AuNP-KR13 all lead to production of non-infectious virions with all the various virions tested. The virions produced in the presence of AuNP-KR13 however had a reduced level of p24 in the supernatant showing that there were fewer virions produced compared to KR13 and KR13b treated virions. The effect of KR13, KR13b and AuNP-KR13 had some very interesting differential effects observed between the different types of virions tested. First of all R3A which is a lab adapted strain had the least effect by the inhibitors compared to other strains and JRCSF had the highest effect by KR13 and AuNP-KR13. Further the inhibitory action by KR13 and AuNP-KR13 was observed with both the dual tropic,NL4-3 and CXCR4 tropic, HXBC2 although AuNP-KR13 action was limited in NL4-3.

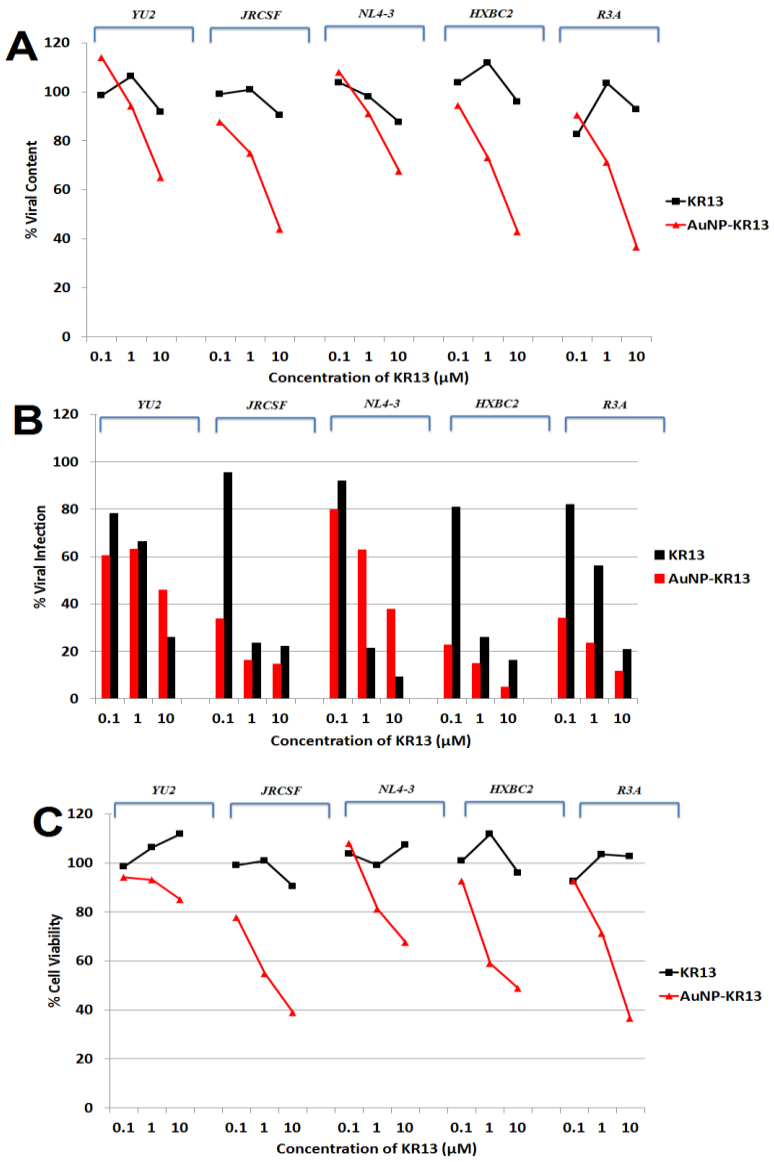

Figure 42: The breadth analysis of KR13 and AuNP-KR13 inhibition of vironeogenesis. (A) Relative the viral content of the cell supernatant post 24 hours of treatment of producer cells measured by p24 quantification. The % p24 was relative to the 100% control which was cells treated with 0.1% triton X and 0% control which was producer cells treated with PBS (B) Viral infection of the produced virions post 24 hours of inhibitor treatment. The p24 levels were normalized prior to addition to HOS $CD4^{+ve}$ $CCR5^{+ve}$ cells. (C) Cell viability of the 293T transfected cells 24 hours post inhibitor addition. Measured using WST-1 Premix and normalized to the untreated cell control incubated for the same time. The samples were quantified using p24 content in the cell supernatant 24 hour post treatment to measure produced viruses. Error bars represent the standard deviation of the mean, n = 3.

4.1.4 Discussion

Previously we have shown that KR13, KR13b and AuNP-KR13 can inhibit viral infection with nM potencies and further we have also shown that KR13 and AuNP-KR13 have an addition virolytic function [6, 8]. In this study we have shown for the first time a class of inhibitors that have multifaceted anti-viral functions that target not only inhibition of viral entry and fusion but further can inhibit viral propagation by targeting new virus production. We showed that KR13 and AuNP-KR13 can target virus producer cells and inhibit new virus production. Further AuNP-KR13 showed an addition effect of cell-lysis or toxicity of cells that are either producing active HIV-1 virions or have stable g160 on the cell surface. This vironeogenesis inhibitory effect of this class of peptide triazoles and conjugate had good breadth of action across the replication competent HIV-1 viruses and also was specific in action. Therefore is a novel inhibitor class that can target multiple stages and hence provide not only protection against HIV-1 initial entry but can even limit propagation of the virus.

The 293T cells that were transfected to produce HIV-1 BaL pseudotyped was treated with KR13 and AuNP-KR13 and this lead to viruses produced that were non-infectious (**Figure 39**). Although KR13, KR13b and AuNP-KR13 treatment led to virions produced with no gp120 on the viral surface only KR13 and AuNP-KR13 led to virions that were non-infectious. In order to explain this effect it is important to know that HIV-1 pseudovirions have nearly 80% of misfolded gp120

that are very weakly tethered to gp41 and can be shed off non-specifically or with a very slight conformational change[267, 320, 321]. From previous work we know that only KR13 and AuNP-KR13 induce virolysis when treated on cell-free HIV-1 BaL pseudotyped. Hence the treatment of virus producer cells with KR13b might be resulting in shedding off of the misfolded Env protein but keeping the functional Env intact which therefore results in infection (**Figure 39B**).

The cell viability studies conducted show that the KR13 and KR13b treated virus producer cells as well as cells that stably express gp160 on their surface had no effect of toxicity. But from the results shown in **Figure 41** we observe that the gp120 is shed from the surface of the CHOK1 cells that stably express gp160, which gives us a mechanistic insight to how these inhibitors produce virions that are non-infectious. The peptide treatment leads to gp120 shedding from the virus producer cells which therefore leads to virions that are budded with no gp120 on their surfaces and thus are non-infectious. But as previously explain KR13b might be shedding off only gp120 that are misfolded from the virus producer cells and thus still leads to budding of virions that are infectious. In order to further test this hypothesis, future studies will be focused on understanding the confirmation of the shed off gp120 using antibody mapping and mutational analysis.

The AuNP-KR13 treatment however had some interesting observations that might give us a better understanding of its mechanism of action. First and foremost AuNP-KR13 treatment resulted in virions with much less p24 content in

their lumen (**Figure 39A**). We also observed that AuNP-KR13 treatment of the virus producer cells led to cell-toxicity with a CC_{50} of 232 ± 53 nM. Since KR13 is decorated in a multivalent fashion around the AuNP, this will result in an increased local concentration of KR13 on the cell surface. Previously we have found that KR13 and AuNP-KR13 result in virolysis of cell free virus, and so this explains why the increased concentration of KR13 on the virus producer cell surface by AuNP conjugation might result in cell membrane stress due to poration and thus lead to cell lysis which will result in cell toxicity[6, 8]. This result is also shown in CHOK1 cells that stably express gp160 on its surface. From **Figure 40** it is evident that the cells start dying only when more than 80% of the gp120 is shed from its surface. Therefore the AuNP-KR13 vironeogenesis inhibition precedes the cell toxicity effect making this a multi-step inhibitory action. Previous studies have found that cells that express gp120 on their surfaces are either producer cells or cells that contain latent HIV-1 population [318, 322]. Therefore finding an inhibitor that targets this latent population is revolutionary and can be extremely advantageous [323].

The KR13 and AuNP-KR13 activity observed in this study is specific as seen in **appendix Fig. 15 and 16**. The breadth analysis conducted showed that these inhibitors are broad acting against HIV-1 replication competent virions (**Figure 42**). Further we also showed the AuNP-KR13 led to virions with less p24 in the replication competent virion lumen as observed in HIV-1 BaL pseudotyped. The R3A virus however was not that sensitive to the inhibitory action by KR13 and

AuNP-KR13 (**Figure 42B**). The R3A virion is a lab adapted viral strain and usually functions very well with lab developed inhibitors but in this study it was the opposite result. This might also be because the inhibitors were developed and tested on BaL virions and thus might be more specific to this viral strain. Studies will be conducted in the future to identify the genetic difference between these viral envelopes that might be showing these differential effects by these inhibitors. But all in all it is important to observe that these inhibitors are able to successfully lead to non-infectious virions across a panel of virions that are otherwise difficult to inhibit. Therefore this study exemplifies the emergence of a new class of inhibitors that can target multiple important stages of HIV-1 infection including; irreversible inactivation of virus, blocking virus entry and, stopping new virus formation.

4.2 Immunogen creation using the peptide triazole thiol treated residual virion

4.2.1 Understanding the potential of a customizable immunogen creation on the HIV-1 epidemic

HIV-1 has been a very difficult virus to completely eradicate due to its high degree of genetic diversity and antigenicity. Although there have been many trials that have been conducted in order to develop a successful vaccine there is still no progress due to the limited neutralizing antibodies developed in this

process[182, 324]. The field has now switched focused on controlling viral load after infection and reduce secondary transmission [325-328]. This is another difficult challenge due to the quick mutations the virus goes through in the host cell post infection. Hence it is very important to design vaccines that target sites on the virion that is highly conserved through the genetic diversity, close to 100% [329]. There have been many recent advances in developing immunogens against gp120 because this is one of the first viral proteins that are encountered by the host immune system [51, 188, 330]. Such an advance is using the new gp120 glycan antibody series PGT, but this is still developing and might take a long time due to the irregularity of the glycans present on the gp120 protein[188, 331]. Hence targeting this protein will lead to antibody leads that can be further developed. But this glycoprotein goes through several conformational changes once in the cell and can hence bypass the immune system attack and reach its target cell. And even though studies are currently being conducted with native gp140 trimers as the immunogen, it is still very limited in developing neutralizing antibodies [332-334].

Our previous studies have shown that KR13, a peptide triazole thiol lead not only to HIV infection inhibition but also to cell-free irreversible virolysis [6, 8]. Further we have also demonstrated that the KR13 treated HIV-1 BaL pseudotyped residual virion has gp41 still on its surface and is immunoactive against the MPER binding site[6]. This therefore has led us to the work in this section which focuses on developing the KR13 residual virion as an immunogen.

In the vaccine development front, MPER site on gp41 is one of the most immunoreactive areas of the virus that has led to several neutralizing antibody development such as 2F5, 4E10 and most recently 10E8 [335-339].

In this study we will be focusing on developing an immunogen which can be a created from the virions present in an infected individual and hence can be tailored to specifically target that viral strain and thus make it custom made for each individual. This novel approach will be the start on a revolutionary approach for vaccine development in the HIV field due to it surpassing the hurdle of HIV genetic diversity by forming a custom immunogen for each individual. This preliminary study might also lead to development of new neutralizing antibodies that target gp41 and can be further developed to find crucial binding sites on gp41 that can be target for creating new microbicides and inhibitors of HIV-1.

4.2.2 Antibody epitope exposure mapping of the residual virion post peptide triazole thiol virolysis

The gp41 epitope exposure was further validated by conducting a gp41 antibody mapping experiment. The peptide treated residual virions were fixed using equal volume of 0.1% paraformaldehyde and loaded onto an ELISA plate. A panel of gp41 antibodies was used in order to test the conformation of gp41 on the

residual virion post KR13 treatment as shown in **Figure 28B**. From this it is clearly evident that the MPER is exposed on virions treated with KR13 specifically. In order to confirm that the immunoactive areas of gp41 are exposed on the KR13 a competition experiment was conducted. HIV-1 BaL pseudovirions were incubated with a constant concentration of KR13 (1 μM) and increasing concentration of 2F5, 4E10 or 10E8 (anti-MPER antibodies) and as control 98-6 (anti-gp41 linear epitope) for 30 minutes at 37°C. The samples were then either loaded onto HOS $CD4^{+ve}CCR5^{+ve}$ cells to test viral infection as explained in section 2.2.2.2 using luciferase reporter gene assay or spun on a table top centrifuge at max speed (15,600 rpm) for 2 hours at 4°C for p24 release analysis. The supernatants were collected and tested for p24 using a p24 capture ELISA as explained in Bastian et al. 2013 [6].

The results are shown in **Figure 43**, and from this we observe that all the three gp41 antibodies that target MPER and are highly neutralizing are able to inhibit the KR13 induced p24 release from the HIV-1 BaL pseudovirions. This shows that the MPER exposure is important for leakage and further also validates that this exposure is specific to KR13 treatment.

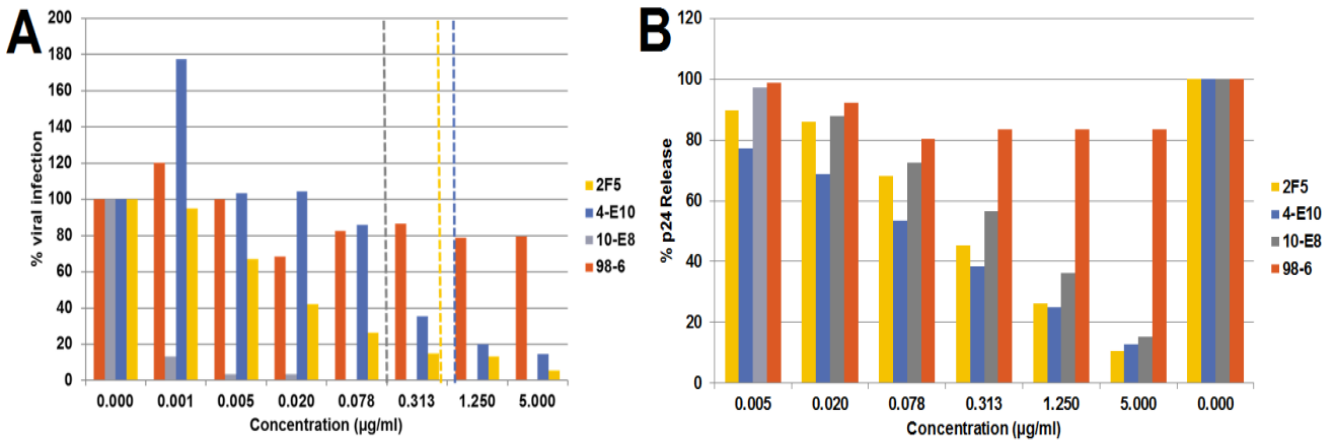

Figure 43: Testing the specificity of KR13 induced MPER exposure. (A) Effect of KR13 on the inhibitory action of the MPER antibodies 2F5, 4E10, 10-E8 and 98-6. The IC_{50} values of the MPER antibodies 2F5, 4E10 and 10E8 are 0.42 µg/ml, 0.78 µg/ml and 0.098 µg/ml and are shown in dotted lines. The samples are normalized to the control 100% infection which is virions treated with PBS and loaded onto HOS $CD4^{+ve}CCR5^{+ve}$ cells. (B) Inhibition of p24 release induced by KR13 (1µM) by 2F5, 4-E10, 10E8 and 98-6. The samples are normalized to 100% release being the p24 released by the HIV-1 BaL pseudotyped treated with 1 µM KR13. . Error bars represent the standard deviation of the mean, n = 3.

4.2.3 The sample preparation and validation of the immunogen for in-vivo studies

In order to start immunogen creation it is important to understand its immunoreactivity in vitro. The immunogen was created as explained above by using KR13 (1μM) and treating with HIV-1 BaL pseudotyped virions that was lab synthesized as explained in section 2.2.2.1. As controls KR13b and PBS treated HIV-1 BaL pseudotyped virions were used to confirm the production of the immunogen. The virions once synthesized using a co-transfection of the HIV-1 BaL envelope plasmid and envelope-deficient pNL4-3-Fluc+env– provirus, was purified using a 6-20% iodixanol gradient as shown in **Figure 16**. The peptide and virus was incubated together for 30 minutes at 37°C and then purified once again in a 6-20% iodixanol gradient to separate the released viral proteins from the residual virion (16-18% iodixanol). The residual virion fraction was pooled and buffer exchanged to PBS. The samples were then fixed with equal volume of 0.1% paraformaldehyde for 30 minutes at 4°C. The treated virus fractions were spun at 16,000 X g for 2 hours at 4°C in an Eppendorf table top centrifuge. The resulting collected virus was loaded onto an ELISA high protein binding 96 well plate and coated at 4°C overnight. The plate was blocked with 3% BSA for 2 hours at room temperature, and then anti-g120 (D7324), anti-gp41 (2F5, 4E10 and 98-6), and anti-p24 (ab 93913 – abcam). The gp120 content and p24 was tested in the residual virion in order to confirm the virus was completely inactive. Further the virion was also tested for viral infection in

HOS $CD4^{+ve}CCR5^{+ve}$ cells as explained above. Further the residual virions was tested to see the exposure of gp41 using 98-6 linear gp41 antibody and specifically MPER in gp41 using conformational gp41 antibodies, 2F5 and 4E10.

The results from two batches prepared are shown in **appendix Fig. 17** and we can clearly see that the KR13 treated virions have very low levels of gp120 and p24 while a good amount of gp41 (~500 μg/ml). The gp41 in the KR13 treated virions was quantified using anti-gp41 2F5 standard curve (for binding to monomeric gp41 protein) and the gp41 in the IV (intact virus) and KR13b treated virions was quantified using anti-gp41 98-6 standard curve (for binding to monomeric gp41 protein). The samples were then transported for immunization in balb/c mice (Jackson Laboratories, Bar harbor, ME) in the Kutzler lab. The mice was acclimatized to the facility and stored in a temperature controlled, light-cycled specific pathogen free facility at Drexel University College of Medicine.

4.2.4 First immunization trial with the peptide triazole treated virions and results

For mouse immunizations, experimental groups (**Figure 44**) contained 100 μl of formulation (Freund's) as negative control (n=3); 100 μl of PBS containing 22 μg of either KR13-treated HIV-1 BaL pseudovirus (n=4) or KR13b-treated HIV-1 BaL pseudovirus (n=4). 100 μl of immunogen was mixed 1:1 with incomplete

freunds adjuvant and injected into the right quadriceps muscle using an insulin syringe needle (28 g). At endpoints designated in the figure legends, animals were sedated using isofluorane, and 200ul of mouse serum was collected on awake mice using the submandibular technique as described in animal protocol 20090. Immunizations will be carried out separated by 2 weeks.

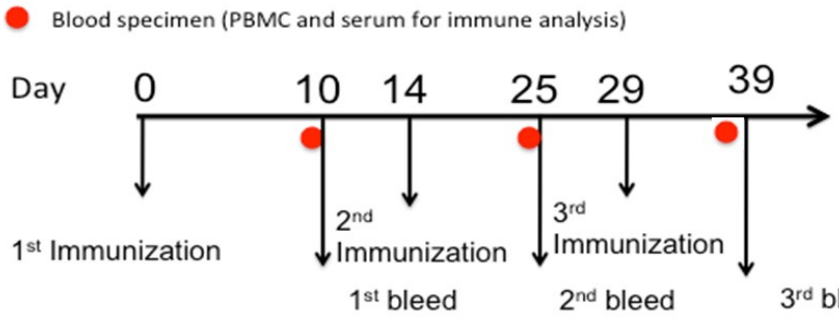

Group	Gp41 (ug)	P24 (ug)	Gp120 (ug)
KR13b	22	3.4	1.6
KR13	22	0.5	1.9
gp41	22	0	0

		Expected immunological reactivity in vivo		
GROUP	# of mice	gp120	p24	gp41
Formulation (HIV-1Bal neg)	3	-	-	-
HIV-Bal+KR13b	4	-	+	+
HIV-Bal+KR13	4	-	-	+
HIV-Bal+gp41	4	-	-	+

Figure 44: The schematic showing the protocol used for the HIV-1 BaL pseudotyped virions deactivated with KR13 or KR13b immunization in BALB/C mice. This also shows in red dots where the blood was collected for further analysis. The table below shows the immunological activities expected in the groups based of on the proteins reactivity of the residual virions. The gp41 used here as control is the monomeric soluble gp41 obtained from NIH aids repository. Data adopted from Michele Kutzler

The sera were collected as described in **figure 44** and they were used to detect gp41, gp120 and p24 antibodies. The respective soluble proteins (gp41, p24 and gp120 – obtained from NIH aids repository) were coated in an ELISA high protein binding overnight at 4°C and the plate was blocked for 2 hours with 3% BSA at room temperature. Sera from immunized mice were diluted in blocking buffer, added to wells in duplicate, and incubated at room temperature for 2 hours or overnight at 4°C. Bound antibodies were detected with horseradish peroxidase–labeled goat antimouse IgG (Santa Cruz Biotechnology) and developed with substrate 3,3′,5,5′-tetramethylbenzidine (TMB) H2O2 (Pierce).

The results are summarized in **figure 45**. And this first batch shows promising results with KR13 residual virions generating anti-gp41 antibodies comparable to control gp41 protein which also generates anti-gp41 antibodies. Although this was promising we did observe that the formulation used did reduce the antigenicity of the residual virions (**Appendix Fig. 18**). And so for the next set of immunizations we switched to footpad injections with no adjuvant addition using PFA fixed virus particles. The sera collected from the 2nd and 3rd immunizations were also tested for antibodies generated for p24, gp120 and gp41 using the capture ELISA as described above. The results are summarized in **Appendix Fig. 19**, and we see that the sera from the mouse immunized with KR13 treated residual virion had binding specific to gp41 even at the 3rd immunization.

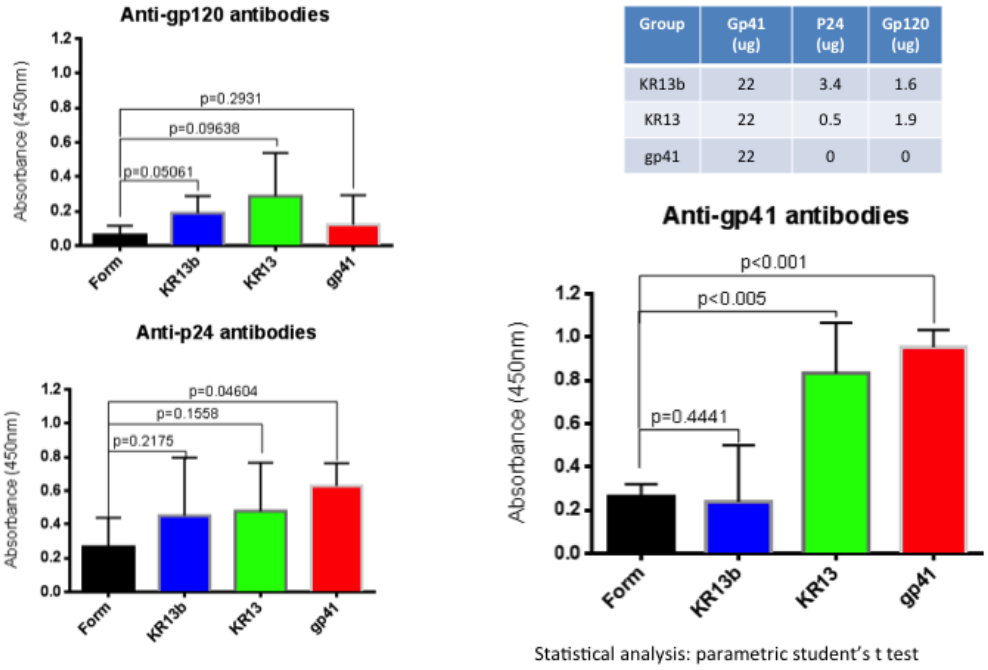

Group	Gp41 (ug)	P24 (ug)	Gp120 (ug)
KR13b	22	3.4	1.6
KR13	22	0.5	1.9
gp41	22	0	0

Figure 45: Delivery of KR13 treated virus generates anti-gp41 antibodies in mice post first immunization. The gp120, p24 and gp41 (1 µg/ml) was coated to an ELISA plate and coated overnight. The plate was blocked with 3% BSA and the sera were added at 1:10 dilution. The antibody binding was detected using horseradish peroxidase–labeled goat anti-mouse IgG. Data obtained from Kutzler lab (Michele Kutzler).

4.2.5 The future directions and importance of the immunogen work

The **figure 45** shows promising results, and currently there is work being done in order to study whether the generated antibodies from the final bleed post the first immunization study is MPER specific and neutralizing. In order to detect the MPER specific epitopes, an assay was developed, in which MPER (2 μg/ml) is coated in a high-protein binding ELISA plate and incubated overnight at 4°C. Following this the plate was blocked for non-specific binding using 3% BSA and incubated for 2 hours at room temperature. Serial dilution of the sera was loaded for 2 hours to the plate and incubated at room temperature. The samples were then detected using anti-mouse HRP (Santa Cruz Biotechnology). The find out whether the MPER antibodies generated is neutralizing two different assays were designed and performed. The first assay was a competition ELISA in which the MPER was coated on an ELISA plate as explained above. The plate was blocked with 3% BSA and serial dilution of the sera was loaded with equal volume of anti-gp41 antibodies, 2F5, 4E10 and 10E8 (MPER specific) at 1μg/ml concentration. The samples were incubated for 1 hour at room temperature, following addition anti-human HRP (EMD Millipore) specific to the MPER antibodies. The preliminary results are shown in **Figure 46**. From this it is clearly evident that the KR13 treated residual HIV-1 BaL pseudotyped immunization in Balb/c mice is able to generate antibodies specific to MPER (**Figure 46A**). The competition assay done with MPER specific antibody 2F5 and the sera generated from the different immunogens showed that the sera from

the gp41 protein and the residual virion post KR13 treatment had competition with 2F5 (**Figure 46B**).

From these results it is evident that the KR13 treated residual virion is a custom made immunogen that leads to generation of MPER specific antibodies. Currently work is being conducted to test the neutralization of HIV-1 BaL infection of HOS $CD4^{+ve}CCR5^{+ve}$ cells. These astounding results can lead to the initiation of a study that can produce immunogens using the virions that are already in patients that are infected and thus stop AIDS progressing and eventually suppression.

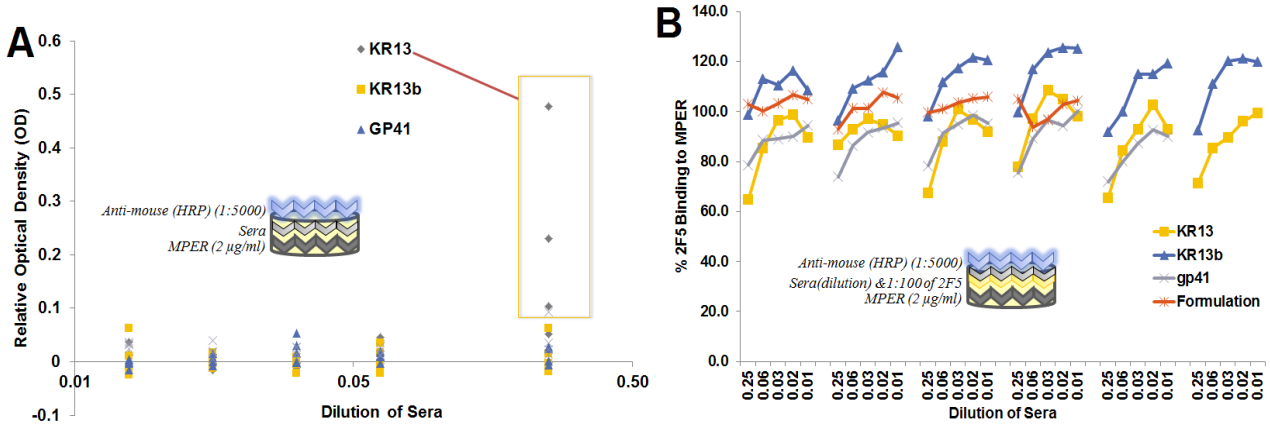

Figure 46: Characterization of the sera obtained post immunization of formulation, gp41 protein, residual virion post KR13 (1 µM) and KR13b (1 µM) treatment. (A) ELISA results showing sera binding to MPER (n=6). (B) ELISA results showing dilution of sera competing with 2F5 anti-gp41 antibody (1ug/ml) to MPER. The number of animals bled for formulation group (n=4), gp41 protein (n=5), KR13 treated residual virion (n=6) and KR13b treated residual virion (n=6). Data obtained in collaboration with Michele Kutzler

4.3 Effect of virolytic agents on capsid mutants and immature virus particles

4.3.1 Effect of capsid stability on the HIV-1 virolytic effect by KR13 and AuNP-KR13

From previous studies and the studies in this thesis we have shown that a class of peptide triazoles known as peptide triazole thiols led to virolysis of HIV-1 which is measured by p24 release from the viral core[6, 8]. Further we also showed that the multivalent conjugate of the peptide triazole thiol, AuNP-KR13 led to the same HIV-1 virolysis but at a much lower concentration of the inhibitor [8]. The mechanism of HIV-1 virolytic activity observed by peptide triazole thiol, KR13, has been shown to follow a pathway in which it hijacks the viral-cell fusion mechanism. The mechanism of virolytic activity observed by AuNP-KR13 however is a much more physical action on the virion that leads to complete obliteration of the virus.

This study was conducted in order to better understand whether the p24 released by KR13 and AuNP-KR13 is from the intra-viral space between the membrane and the viral core or whether it is specifically released from the viral core. The average HIV-1 virion has been shown to have from 1500- 3000 molecules of p24 [340-342]. Previous studies have shown that the viral capsid contains only 10-20% of the total p24 content of the virion and the remaining is in the intra-viral space between the viral matrix and the core[343-345]. The HIV-1 capsid core

(CA) consists of a total of 231 residues of the hexamers of p24 and 6 pentamers that are connected using a flexible linker. Interactions between the N-terminal domains (NTDs) form hexamers through an intersubunit NTD-NTD interface, while the C-terminal domains (CTDs) form dimers that connect adjacent hexamers through a CTD-CTD interface[341, 342, 346, 347].

Therefore in this study we will be using the previously known mutants of the capsid in between the NTD-NTD (E45A) interface and the CTD-NTD interface (E213A) in order to make the capsid core much more stable and thus test the effect of this on the release p24 by KR13 and AuNP-KR13 [343, 344, 348]. From this study we observed that the making the HIV capsid led to a drastic reduction in the p24 released by KR13. This effect however was not observed with AuNP-KR13 which even though had a slight reduction still led to approximately 70% p24 release with both the core stability mutations.

4.3.1.1 Materials and Method

Materials

For peptide triazole thiol preparation, the protocol was followed as previously explained [6, 8]and the reagents were purchased from Chem-Impex International Inc, Ethynylferrocene and Cu(I)I was purchased from

Sigma-Aldrich and used without further purification. Fmoc-cis-4-azidoproline was synthesized starting with commercially available trans-Hyp-OH [22]. Gold (III) chloride hydrate and citric acid were procured obtained from Sigma-Aldrich, Bis (p-sulfonatophenyl) phenylphosphine dehydrate dipotassium salt (BSPP) from Strem Chemicals. Modified human osteosarcoma Cells (HOS $CD4^{+ve}$ $CCR5^{+ve}$) engineered to express CD4 and CCR5, receptor and co-receptor respectively, as well as pNL4-3.Luc R-E-backbone DNA, were obtained from Dr. Nathaniel Landau. The HOS.T4.R5 cells were grown in DMEM supplemented with 10% FBS, 2.5% HEPES, 1% Penicillin- Streptomycin, 2% L-Glutamine and 1 mg of puromycin. 293T cells were obtained from American Type Culture Collection and grown in the same culture medium as the HOS.T4.R5 cells except without puromycin. The plasmids for HIV-1 BaL-01 gp160 and VSV-G Env DNA were from the AIDS Research and Reference Reagent Program (ARRRP). The core mutant plasmids E213A and E45A and the immature virion core plasmids MA/P6, MA/P6 ΔE, NL4-3 ΔPro were obtained from Dr. Christopher Aiken from Vanderbilt University. The antibodies mouse anti-p24, rabbit anti-p24, and the protein p24, were from Abcam. Enhanced chemiluminescence western blot detection system was from Amersham. O-phenylenediamine (OPD) was from Sigma Aldrich. All other materials were from Fisher Scientific.

Methodology

In order to test the effects of the capsid stability, HIV-1 BaL pseudotyped containing the core mutants were produced using the virus production protocol as mentioned above. 4 μg of envelope (BaL-01) and 8 μg of backbone DNA (NL4-3 WT, E213A and E45A were co-transfected into 293T cells using FuGene 6 as the transfection reagent [253]. Fourteen hours post-transfection, the medium was changed, and subsequently the VLP-containing supernatants were collected at 48 hours post transfection. The VLP-containing supernatants were cleared using a 0.45 μm syringe filter and purified further by spinning the sample on an iodixanol gradient, using a Hoefer continuous gradient maker, ranging from 6 - 20 % iodixanol, at 30,000 rpm for 2 hours at 4 °C.

In order to test the effect of the core stability, serial dilution of the peptide KR13 and AuNP-KR13 were incubated with a known concentration of the virions for 30 minutes at 37°C. The samples were then spun at max speed on a table top centrifuge for 2 hours at 4°C. The supernatant was collected and quantified for p24 using a capture ELISA as explained in section 2.2.3. As negative and positive controls the viruses are treated with PBS alone and 0.1% triton X respectively. In order to validate this effect is specific, the effect of VSV-G virions produced with the core mutants were also tested for p24 release with KR13 and AuNP-KR13.

4.3.1.2 Results

The effect of the capsid mutation on the KR13 and AuNP-KR13 p24 release are summarized in **Figure 47**. From this we observe that the p24 release induced by KR13 on the HIV-1 virions is severely affected by both the E45A and the E213A. While for the p24 release by AuNP-KR13 was not affected as much by the E213A mutation compared to E45A. The VSV-G enveloped virions with the core mutants and WT had no effect and did not lead to p24 release with KR13 or AuNP-KR13 treatment. Further we also saw that the mutants had very minimal levels of viral infection which is concurrent with the data observed previously with these mutants due to the stability of the cores [343, 344].

4.3.1.3 Discussion

From the results we observe that the core mutants of HIV-1 which make the core more stable leads to reduction in levels of p24 released. The interesting factor is that the core is made up of only approximately 10-20% of the total p24 content in a virion and the core mutants E213A and E45A lead to the core containing 30% and 40% of the total p24 content[343, 344]. As observed by **Figure 47A**, the p24 release in the virion with the E45A mutant is much more stabilizing compared to E213A of the core. While the AuNP-

KR13 induced p24 release is not that affected by the E213A mutant compared to the E45A mutant (**Figure 46B**).

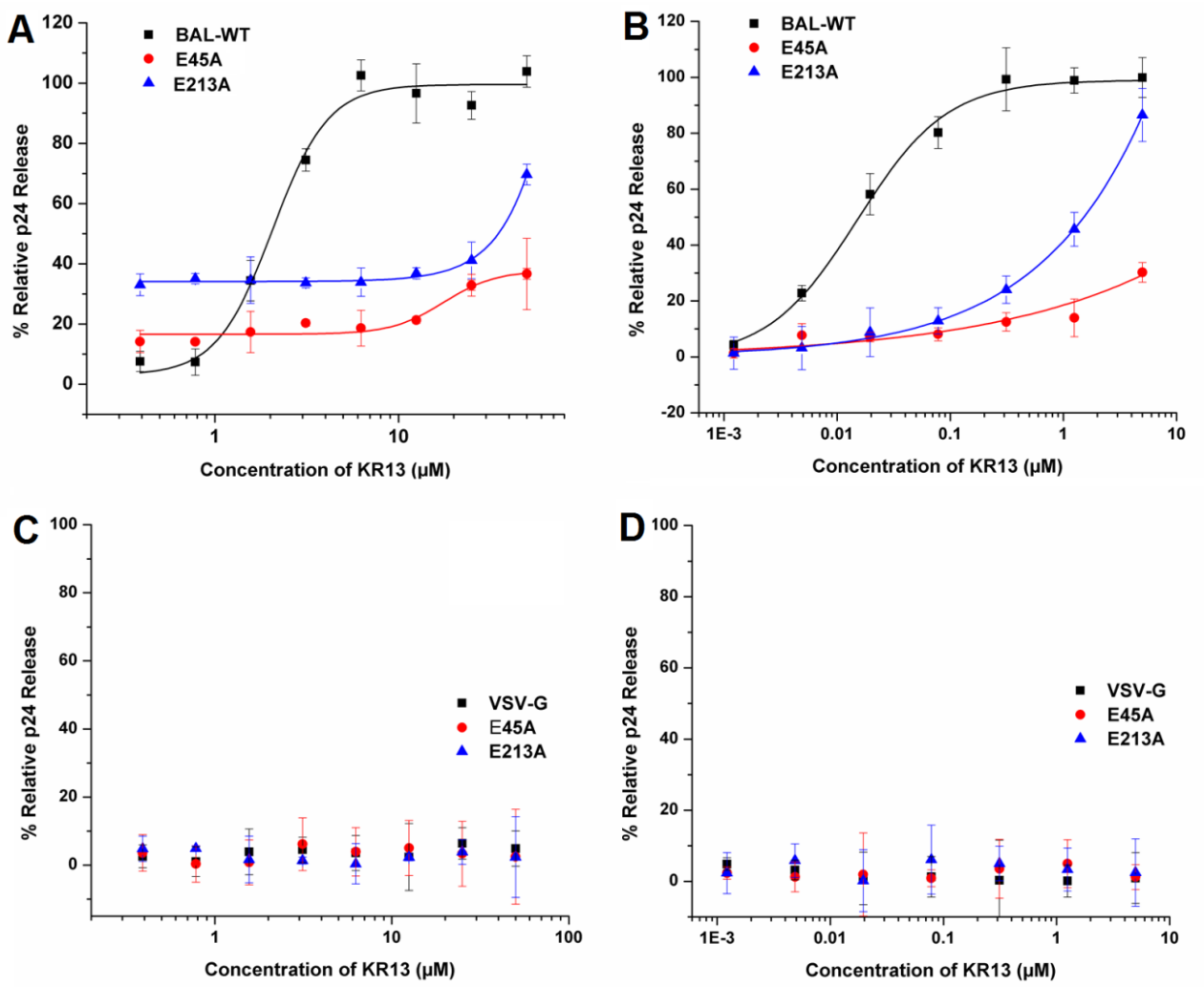

Figure 47: The effects of core stability on KR13 and AuNP KR13 induced p24 release on HIV-1 BaL pseudotyped. The p24 release induced by KR13 (A) and AuNP-KR13 (B) on HIV-1 BaL WT compared to the core mutant virions E45A and E213A. The VSV-G enveloped WT virus and its core mutants were also tested for KR13 (C) and AuNP KR13 (D) induced p24 release. The controls used was 100% release which was virions treated with 1% triton X and 0% release as virions treated with PBS alone.

The E213A mutation is in the helix 10 of the CTD of the capsid dimer and leads to a stronger bond between the two dimers in the hexameric lattice which E45A is a mutation in the helix 2 of the NTD of the capsid hexamer and this makes the interactions between the hexamers much more stronger keeping the core structure hyperstable[343, 344]. From the results it is clearly visible that the stability between the dimers of p24 protein in the hexameric lattice is much more important than the stability of the core itself. Further this effect is specific as seen by the VSV-G controls in which the KR13 and AuNP-kR13 treatment has no effect on the p24 release (**Figure 47C and D**).

4.3.2 Peptide triazole thiol effects on immature HIV-1pseudotyped virions

In a HIV-1 virus lifecycle, post budding of new virions from the host cell, the virus undergoes a maturation process in order to become completely infectious. The immature virion is much thicker and has a hard gag shell that makes the virion much stiffer and will not be able to infect a new cell [295, 341, 349, 350]. The **Figure 48** shows the structure of the immature compared to the WT and shows how much stronger the viral shell of the immature virus is (3.1 N/m stiffness) compared to the mature virus (0.2 N/m stiffness)[295].

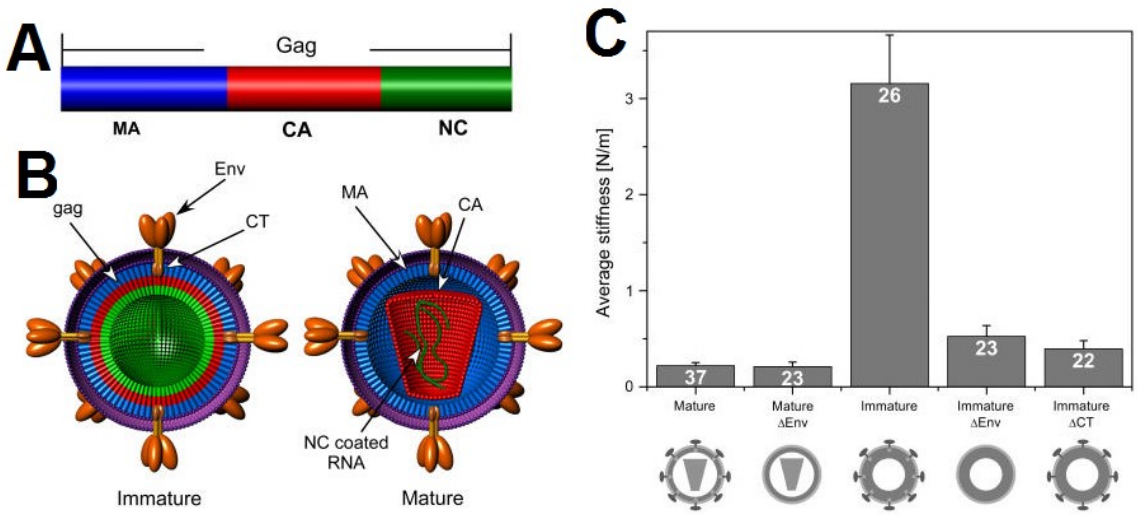

Figure 48: The characteristics of immature HIV-1. (A) Schematic representation of the HIV gag with matrix protein (MA) in blue, capsid protein (CA) in red and nucleocapsid (NC) in green. (B) The model of the immature (left) and mature (right) virion and the location of the gag proteins in both these virions. (C) Average point stiffness of different variation of HIV-1. The stiffness is a mean value (~100 FD curves) of the total number of virions analyzed per sample (number shown in the bars).

In order to produce these immature particles there are two plasmids that were given to us as a gift from Dr. Christopher Aiken. These were the NL4-3 MA/P6 core plasmid and the NL4-3 ΔPro. The MA/P6 contains substitutions preventing cleavage of the major Pr55Gag cleavage sites but encoding a wild-type PR sequence. This mutation has shown to produce immature particles that are non-infectious and have a defective gag preventing correct protease cleavage action [351-353]. The other plasmid NL4-3 ΔPro is the core plasmid with no protease gene and thus will lead to production of immature particles [354-356]. Therefore both these mutants lead to virions that are immature with very rigid viral shells and are non-infectious.

In this study we will be testing whether these immature HIV-1 particles are lysed by KR13 or AuNP-KR13 just like the regular wild type BaL virion. This was conducted in order to understand whether the virus leakage induced by these virolytic agents depends on the stiffness of the viral membrane. The results show that this effect is indeed dependent on the virus stiffness for both KR13 treatment and AuNP-KR13 treatment. Further this gives us insight on viral envelope incorporation on immature virus and how this affects the amount of leakage observed with KR13 and AuNP-KR13 treatment.

4.3.2.1 Materials and Methodology

4.3.2.1.1 Production and validation of the immature HIV-1 virions

The virions are produced as previously described by using co-transfection of 4 µg of HIV-1 BaL-01 envelope plasmid DNA and 8 µg of backbone DNA (NL4-3 WT, NL4-3 MA/P6, NL4-3 MA/P6 Δenv, NL4-3 ΔPro, NL4-3 ΔPro ΔEnv). The cells used for virus production was the 293T cells seeded at 3 million cells in a T75 flask. The cell supernatant were collected 48 hours post incubation at 37°C and purified using 6-20% iodixanol gradient as explained above. The viruses were collected in the virion fraction (16-18% iodixanol) and the buffer was transferred to DMEM. The virions were then validated by testing its p24 content using a capture ELISA as explained above, and tested for virus infection of TZMB1 cells. Since the backbone DNA plasmid used to produce the virions did not contain the luciferase reporter gene we used TZMB1 cells which contains a tat promoter gene that provides luminescence upon HIV-1 infection to quantify infection[357].

4.3.2.1.2 KR13 and AuNP-KR13 treatment of immature HIV-1 virions

The produced virions were normalized for their p24 content and a serial dilution of KR13 or AuNP-KR13 were incubated with the virus for 30 minutes at 37°C. The samples were then spun on a table top centrifuge at max speed (15,600 rpm) for 2 hours at 4°C. The supernatants were collected and tested for p24 using a capture ELISA method. The controls included 100% release which was virions treated with 0.1% triton X and 0% release which was virions treated with PBS alone. The values were calculated and plotted using Origin Pro. 8.

4.3.2.1.3 Testing the amount of Env incorporation and its dependence on p24 leakage induced by KR13 and AuNP-KR13

From the results we observed that the p24 release induced by KR13 and AuNP-KR13 was reduced by the immature virions. Hence we conducted a western blot analysis of the amount of gp120 present in these immature virus particles. The virions were normalized to their p24 content and loaded into an SDS page gel (10%) and detected using anti-gp120 D7324 and secondary antibody anti-sheep HRP. Therefore we produced regular wild type virus particles with reduced amounts of Env incorporation by reducing the concentration of Env plasmid DNA used during transfection. This therefore resulted in virions with reduced level of spikes (**Figure 50A**).

4.3.2.2 Results

4.3.2.2.1 P24 release induced by KR13 and AuNP-KR13 on immature HIV-1 virus particles

Figure 49 shows that the p24 release induced by both KR13 and AuNP-KR13 is completely suppressed in the both the MA/P6 and NL4-3 ΔPro immature HIV-1. The virions were normalized for the p24 content prior to the leakage assay. From this it is clearly evident that the immature virions are too stiff for the virolytic action of both KR13 and AuNP-KR13. AuNP-KR13 does have a low amount of release (20%) at the highest concentration (5 μM KR13). Therefore this shows that the AuNP-KR13 action is much more vigorous that the KR13 alone leading to poration of the immature viral membrane which is nearly 10 times stiffer that the regular WT HIV-1 membrane (**Figure 48C**).

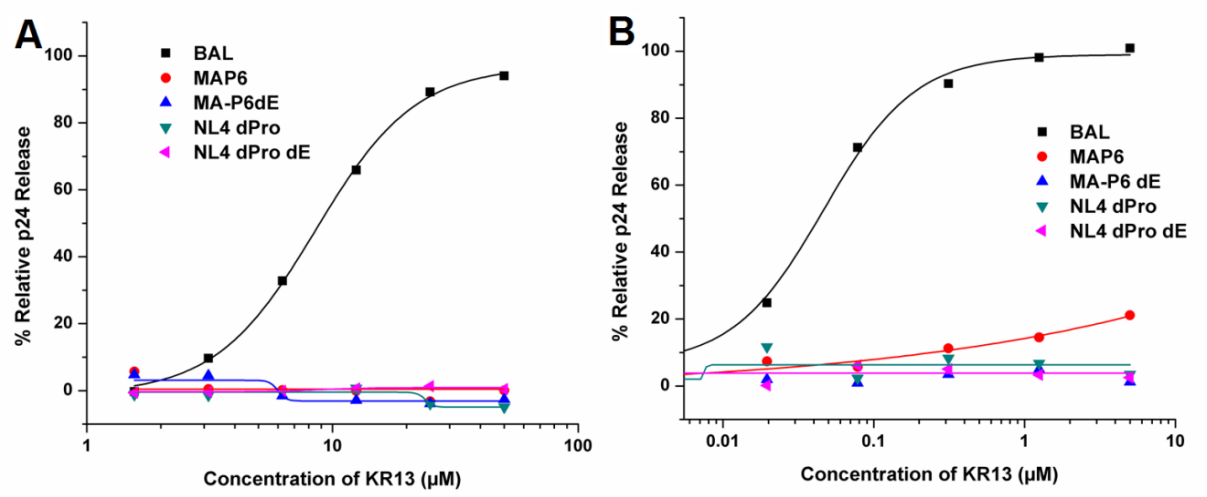

Figure 49: The p24 release induced by KR13 (A) and AuNP-KR13 (B) on immature virions compared to BaL-01 wild type control. The p24 content of the virions are normalized prior to experiment. The 100% p24 release control is virions treated with 0.1% triton X and 0% control is virions treated with PBS alone. n=-1

4.3.2.2.2 HIV-1 Env incorporation in the viral membrane and its dependence on virolysis induced by KR13 and AuNP-KR13

The gp120 content in the immature virions are quantified using western blot analysis and the results are summarized in **figure 49A**. This shows that there are very low levels of gp120 in the immature virions. Since KR13 and AuNP-KR13 binds to gp120 and then proceeds to p24 release, if the level of gp120 is lower this might impact the p24 release profile. In order to test this, we produced HIV-1 BaL WT with reduced levels of gp160 by reducing the Env DNA. The **Figure 50B** shows the characterization of the HIV-1 BaL WT with reduced levels of spikes. The amount of spike incorporation was validated from the gp120 content and compared to a standard curve of monomeric gp120. The **Figure 50C** shows that the virolytic activity of the KR13 and AuNP-KR13 on the HIV-1 virion reduces with reducing level of with the spike incorporation.

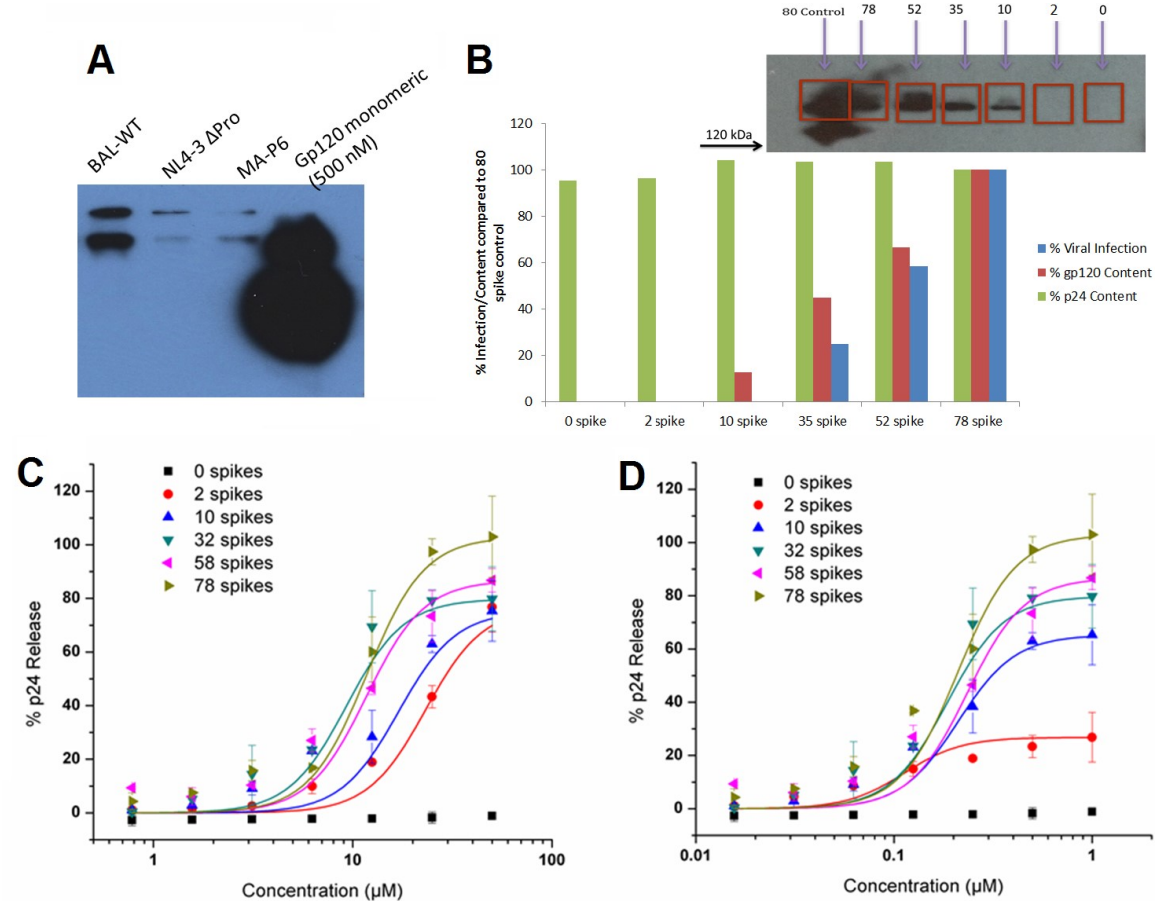

Figure 50: gp120 quantification and spike density variation of BAL-01 WT HIV-1. (A) The gp120 quantification of the gp120 on the viral surface of BAL-WT compared to NL4-3 ΔPro and MA-P6 mutant. The antibody used for gp120 detection was D7324 and secondary antibody, anti-sheep HRP. (B) The characterization of the HIV-1 BaL virions with varying spike density which was quantified based on the western blot analysis from the inset shown. The p24 was quantified using anti-p24 (ab9313) and gp41 using anti-gp41 (98-6) and their respective secondary antibodies using ELISA analysis. p24 release profiles of KR13 (C) and AuNP-KR13 (D) treatment with HIV-1 with varying spike density. The values were plotted using Origin Pro 8.0 and the error bars represent standard deviations of n=3.

4.3.3 Discussion

The results in this study have shown several important characteristics of the virloytic activity observed by KR13 and AuNP-KR13 that will give more insight to the mechanism of this activity. The results show that KR13 and AuNP-KR13 p24 release is diminished with the p24 core mutants as well as immature virions. This shows that the p24 release by KR13 and AuNP-KR13 depends on the stability of the viral core and stiffness of the viral membrane. Previously we have shown that the KR13 induced p24 release is caused by hijacking the viral-cell fusion mechanism, and previous studies have shown that the immature virions and hyper stable core mutants have no infection[6, 344, 349, 351, 357]. Therefore since these mutants limit viral entry to host cell and also inhibits KR13 dependent virolysis this confirms that both these actions are correlated.

The results of the core mutants show that KR13 induced virolysis has a different mechanism compared to the AuNP-KR13 induced virolysis. The AuNP-KR13 virolysis is not affected when the dimers in the capsid is mutated to have an electrostatic bond making it hyperstable, while when the capsid has a mutation to make the bond between the hexamers stronger, this led to reduction in p24 release. But for KR13 induced virolysis both the mutants that made the capsid core stable reduced the p24 release dramatically. It is known that capsid core contains only around 20% of the total p24 content in the virus, and when the core is hyperstable the core contains max 40% of p24 [343-345, 351]. Therefore

from this we can conquer that the AuNP-KR13 poration is much larger than the pore formed with KR13 on the HIV-1 viral membrane. This can be further explored by studying mutants in the core like L203A and Q219A which are capsid destabilizing and L49D which disrupts the interaction between gp120 and gp41[343-345, 358].

The stiffness of the immature HIV virions is 10-20 fold more stiff than the HIV-1 BaL wildtype. The MA-P6 mutation still has the protease enzyme but has a defective gag protein and thus cannot lead to complete protease digest and hence will not form mature infectious virions[351-353]. The NL4-3 ΔPro virions are completely immature because with the protease enzyme they will not be able to mature [351, 354, 356]. The slight activity of AuNP-KR13 with MA-P6 shows that the gag deficiency is not as effective as the protease deletion to inhibit virolysis. Previous studies have shown that the defective gag MA-P6 mutation is not as stiff as the protease deleted virus but both of these mutations are much stiffer than the regular HIV WT [350, 359]. Hence AuNP-KR13 virolytic process is stronger and can induce a pore even on viral membranes that can be much stiffer. Future work will be focused on testing mutations that alter the viral membrane rigidity such as the cytoplasmic tail deletion of gp41 and also using protease inhibitors to test their effect on AuNP-KR13 induced virolysis [350, 360, 361].

This unique action by KR13 can be used to study several unknown aspects of fusion as well as maturation that still need a lot attention. Further the virolysis by AuNP-KR13 is so strong that it forms much larger pores making it a much more effective inhibitor. This design therefore can be emulated on other inhibitors that have low inhibitory effects and can be used to enhance their effect by conjugating to AuNP. This therefore provides new insight into understanding the virolytic activity by peptide triazole thiols and further lead to potent microbicide development that can target multiple stages of the virus lifecycle making this a different form of combination therapy.

CHAPTER 5: FUTURE DIRECTIONS

5 Introduction

The work elaborated in this thesis has led to several novel discoveries and further several methodologies that are very valuable for the virology field. The discoveries in this work have led to 5 research grant proposal of which 3 grants that have awarded as well as the Schlumberger Fellowship which I obtained to complete my work. One of the most novel discoveries in this work was the discovery of a new class of peptide triazoles that have additional virus breakdown effects including gp120 shedding and p24 release leading to complete virus lysis. The other discovery was the development of a multivalent construct of the peptide triazole that led to several rules that can be translational in the biology and engineering field. The AuNP-KR13 size and density dependent analysis led to the layout of rules necessary for developing one of the most potent inhibitors by using multivalent displays. This work has also led to the one of a kind immunogen that is the first immunogen that can be custom made for each infected individual that can lead to generation of antibodies specific to the immunodominant viral protein, gp41. Further the inhibitors developed here can target multiple stages of the HIV-1 lifecycle involving entry, fusion, vironeogenesis as well as latent population of the virus. This composition of work therefore has led to microbicide, immunogen as well as multivalent drug like construct development that can help reduce the viral load and further lead towards eradication of HIV-1. Even though several interesting projects that have high potential have been developed in this thesis, there is still a lot of work to be done in order to lead these projects in the right direction to further develop them into innovative products and methodologies

that can be great contributions toward one ultimate goal, hinder HIV spread and eventually eradicate this life threatening disease.

This section therefore is dedicate to giving suggestions and ideas for each of the discoveries made through this thesis work in order to direct it in the right direction it further.

5.1 Peptide triazole thiols

Peptide triazole thiol was first developed as one of my projects with the help of Dr. Kantharaju Kammana a post doc in our lab. This was initially synthesized in order to conjugate to gold nanoparticles (AuNPs) in order to form a multivalent construct and thus enhance its potency. Although this was eventually achieved and we obtained over 20 fold enhancement of potency by using 20 nm AuNP, we also discovered the unique feature of this peptide. This was the irreversible lysis of the HIV-1 virion leading to p24 release from the virus core. This opened up the pathway to several other discoveries that are spelled out in this thesis. So far we have come to several conclusions a) the p24 release by KR13 is specific to HIV and irreversible. b) the thiol on the peptide is very important for its virolytic activity c) the peptide dependent HIV virus lysis follows a kinetic and biochemical pathway very similar to HIV-cell fusion (Table 5). d) This action is broad and is also effective for founder virions, and e) The residual virion post peptide induced lysis is highly immunoactive.

The future directions that can be envisioned for peptide triazole thiols are as follows:

5.1.1 Structural understanding of the importance of thiol on peptide triazole thiol for HIV-1 virolysis

This involves understanding specifically where the peptide triazole thiol (PTT) binds on gp120 and how it triggers this cascade action on the viral spike that later on translates to the viral membrane leading to poration. Also it is important to track the peptide thiol during this virolysis event in order to study the fate of the peptide which might help with the understanding the mechanism of action. Structural docking studies alongside mutational studies altering the disulfide on gp120 and studying the binding of PTT to gp120 will help better understand the importance of thiol.

5.1.2 Study the 6 helix bundle formation post peptide triazole thiol induced lysis and compare it to virus-cell fusion

The next important work to be conducted is to understand the 6 helix bundle formation during virolysis and compare it to virus-cell fusion. This will not only give us a better understanding of the virolysis mechanism but also shed light on how the virus-cell fusion takes place. This can be achieved by conducting mutational analysis on the different regions of gp41 that are important for the fusion process and are known to help with this process and see how this affects peptide induced virolysis. The next step would be to understand how fusion inhibitors that target different

established sites on gp41 and test how they affect peptide induced virolysis. Temperature arrest studies can be conducted in order to freeze the virolytic process at different stages and use antibody mapping and fusion inhibitors to understand the conformational changes of gp41 to breakdown the virolytic/poration process.

5.1.3 The role of the HIV-1 membrane during peptide triazole thiol induced virolysis:

Post PTT treatment, HIV-1 goes through a sophisticated breakdown process, and the least explored arena is the alterations in the HIV-1 membrane during this. Hence it is important to focus on the viral membrane, alter the membrane properties and study how this affects the poration process. Studies need to be conducted to test how the virion goes through the energy barrier required for the poration process [362, 363].

5.1.4 Breadth of action of the peptide triazole thiol induced virolysis

The breadth of the PTT induced virolytic event not only on replication competent but also primary isolates as well as patient samples at different stages of AIDS need to be conducted in order to better understand the overall breadth of this unique effect. This work therefore will not only provide a complete mechanistic breakdown of the virolytic process induced by KR13 but also give critical information of the HIV-1 – cell fusion which will be very important and valued by the scientific community.

The **Figure 51** shows a breakdown of the studies that can be conducted in the future in order to better understand KR13 induced HIV-1 virolysis.

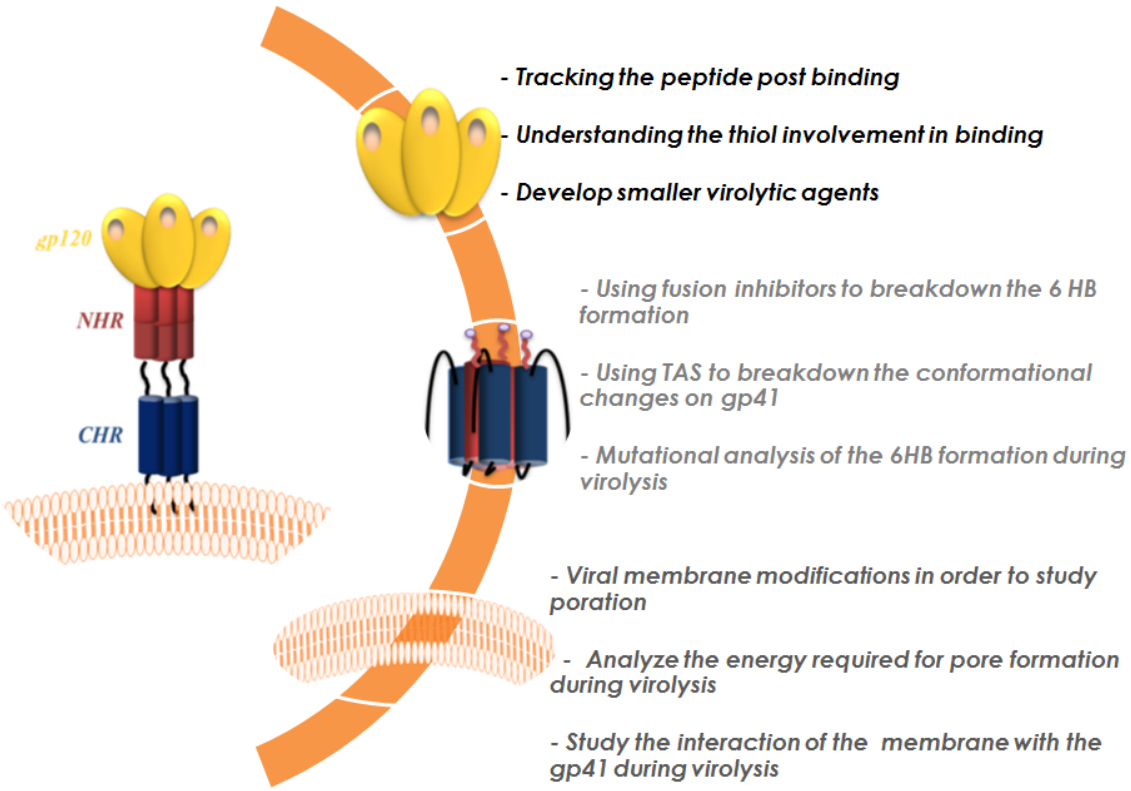

Figure 51: Schematic showing the future directions of peptide triazole thiols. TAS- Temperature arrest state, 6HB- 6 helix bundle.

5.2 Gold Nanoparticle peptide triazole thiol

The gold nanoparticle peptide triazole thiol was developed to create a multivalent conjugate in order to enhance the potency of the peptide triazoles. The multivalent conjugate was first created with 20 nm AuNPs and KR13 and this led to approximately 20 fold enhancement of KR13 antiviral potency. But in this work we discovered that AuNP-KR13 conjugate can also lead to p24 release and complete destruction of the HIV-1 virion. The mechanism by which the AuNP-KR13 leads to virolysis is completely different from the mechanism of KR13 dependent virolysis (Table 10). This therefore made me further explore this multivalent effect, which led to one of the most potent inhibitors ever created in our lab with a low picomolar IC_{50} and EC_{50} of viral infection inhibition and viral p24 release respectively. The multivalent gold nanoparticle could be a prototype for enhancing other inhibitors that target virus or cell surface. This therefore led to a revolutionary discovery that can now guide future nanomedicine and develop nanocarriers that are efficient and can maximize their potential.

5.2.1 Changing the nanoparticle backbone to a more biocompatible design

For future work on the development of the gold nanoparticle peptide triazole thiol, it is important to identify a more biocompatible nanoparticle core that maintains the same rigidly gold. Previous studies in our lab have shown that soft core nanoparticle do not lead to the potent p24 release but still have infection inhibition enhancement when peptides are decorated around its surface. Therefore

materials like chitosan or stiff polymers can be used as alternatives to create nanoparticle-peptide conjugates so that it can be as potent as gold nanoparticles but can be used in clinical trials. It is also important to better understand the mechanism of action of AuNP-KR13. Since AuNP has an advantage of high electron density, it can be used as a marker in electron microscopy studies in order to study the transformations of the virions post AuNP-KR13 treatment in super resolution.

5.2.2 HIV-1 membrane changes post AuNP-KR13 treatment

Further understand the membrane disruptions the virion goes through and the stress induced on the viral membrane surface that leads to poration and complete irreversible lysis.

5.2.3 Further development of other anti-viral effects of AuNP-KR13

Another very interesting development in this thesis was the cell toxicity effect by the AuNP-KR13 on cells expressing gp120. This might be very advantageous because this could be used to target one of the most difficult HIV-1 populations – the latent virions [364-366] which should be further explored. Mutational analysis as well as breadth analysis is also important in order to further understand the mechanism by which the AuNP-KR13 leads to poration of the virion.

5.2.4 Future of AuNP-KR13

The work developed here is the preliminary steps for the creation of a preventative drug design that can target the virion at the entry site. Therefore this once this effect is reproduced in a much more biocompatible nanoparticle construct with a much more efficient PTT (eg. peptidomimetic), it can be developed into a preventative drug. For this it is best to be put the nanoparticle construct in either a gel or film construct that is pH sensitive, and can lead to a slow release of the nanoparticle conjugates during entry of the virion [367].

Figure 52 has summarized the future directions of AuNP-peptide triazole thiol

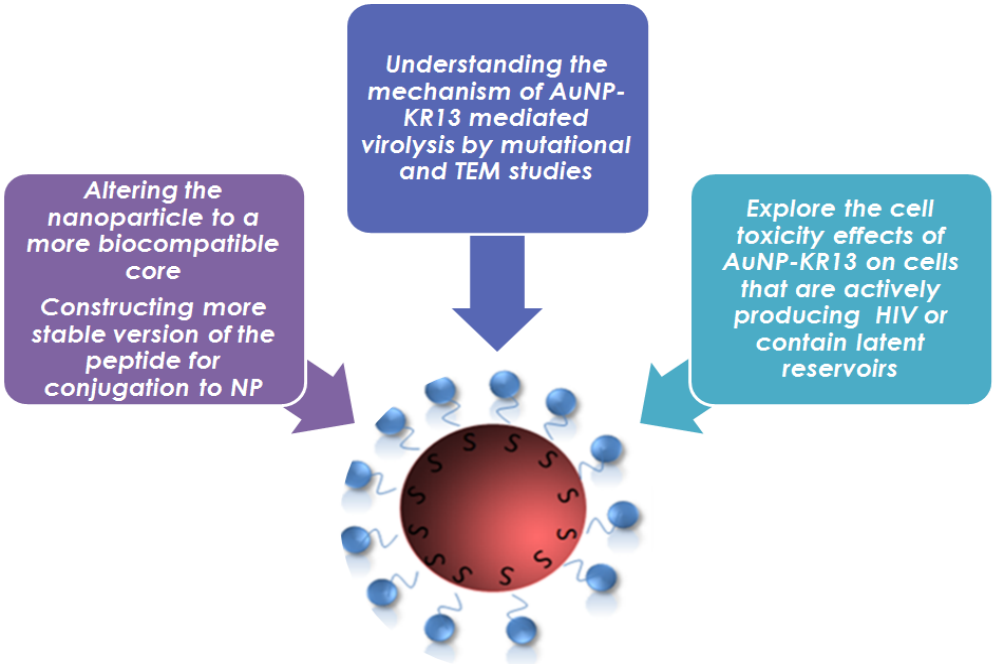

Figure 52: Schematic showing the future directions of AuNP-KR13. NP-nanoparticle

5.3 The immunogen creation with the peptide triazole thiol

The results from the peptide triazole thiol treatment of HIV-1 also lead to an striking result, the antigenicity of the residual virion. The residual virion post KR13 treatment had gp41 on the viral membrane that was immunologically active. Initially this the observation of this activity was set aside in order to better understand the mechanism of virolysis, but once the high binding of the gp41 to already known neutralizing antibodies of gp41 2f5 and 4E10 this had to be further explored. There are very few

immunogens that are currently being created in order to be used to generate antibodies that can target this high genetically variant virus [368]. Therefore there is an urgent need to develop an immunogen that can generate broadly active neutralizing antibodies in humans against infection of a broad range of HIV-1 subtypes. This project is still taking in its preliminary stages but the results are very promising. Hence it is important to explore further the immunoreactivity of the residual virion post peptide triazole treatment. This study introduces the concept of custom made immunogen in which the infected host's virions are used to boost their immune reaction against the disease progression. In order to confirm that we are generating neutralizing antibodies it is important to explore the exact site to which these antibodies are generated. DNA priming is another technique that is currently initiated in the third set of immunization studies to boost the immune response against the residual virion and thus generate larger titers as well as a broad range of antibodies against the native gp41 on the virion with no modifications.

To summarize, the scheme below represents the future directions of each individual concept revealed in this thesis. The peptide triazole thiols and the gold nanoparticle peptide triazole thiol conjugates are the first generation of virolytic agents that are broadly active, can inhibit multiple stages of the virus lifecycle and are highly potent. These agents can be used as leads for developing more stable versions which can be sustained in the body and can be used either as microbicides or as preventatives for PreP (Pre-exposure prophylaxis). The immunogen creation is still in development but

once the preliminary data is established, it is a project with high potential for the future of HIV-1 infection prevention (**Figure 53**).

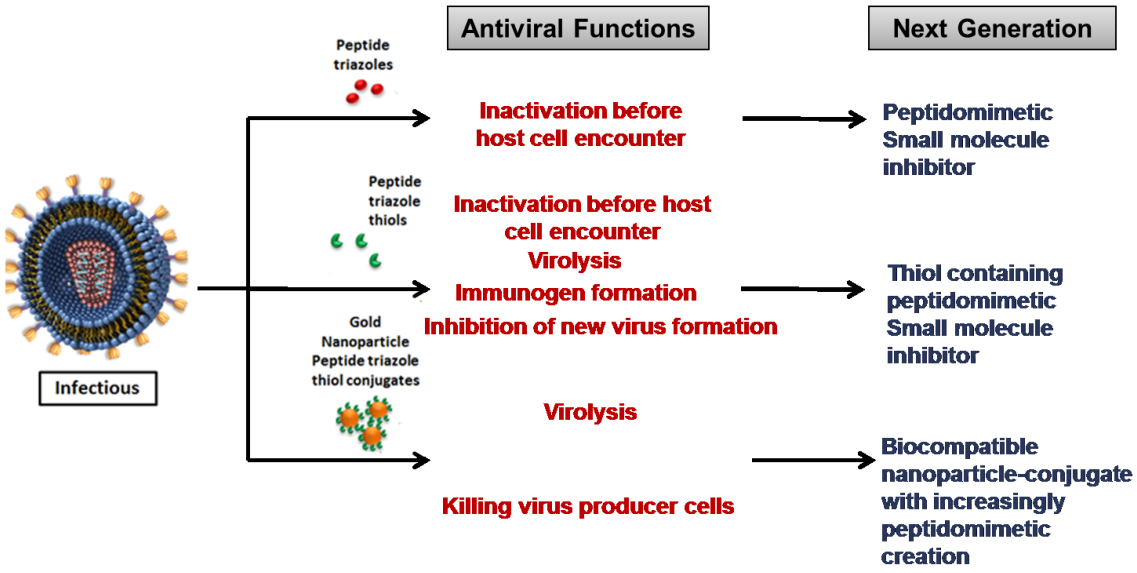

Figure 53: Schematic summarizing the potential future directions of the lead drug candiadates developed in this thesis against HIV-1 infection

BIBLIOGRAPHY

1. Xiang, S.H., et al., *A V3 loop-dependent gp120 element disrupted by CD4 binding stabilizes the human immunodeficiency virus envelope glycoprotein trimer.* J Virol, 2010. **84**(7): p. 3147-61.
2. Mao, Y., et al., *Molecular architecture of the uncleaved HIV-1 envelope glycoprotein trimer.* Proc Natl Acad Sci U S A, 2013. **110**(30): p. 12438-43.
3. Baldwin, C. and B. Berkhout, *Mechanistic studies of a T20-dependent human immunodeficiency virus type 1 variant.* J Virol, 2008. **82**(15): p. 7735-40.
4. Blattner, W., R.C. Gallo, and H.M. Temin, *HIV causes AIDS.* Science, 1988. **241**(4865): p. 515-6.
5. Weiss, R.A., *How does HIV cause AIDS?* Science, 1993. **260**(5112): p. 1273-9.
6. Bastian, A.R., et al., *Interactions of peptide triazole thiols with Env gp120 induce irreversible breakdown and inactivation of HIV-1 virions.* Retrovirology, 2013. **10**: p. 153.
7. McKeating, J.A., et al., *Characterization of HIV-1 neutralization escape mutants.* AIDS, 1989. **3**(12): p. 777-84.
8. Bastian, A.R., et al., *Cell-free HIV-1 virucidal action by modified peptide triazole inhibitors of Env gp120.* ChemMedChem, 2011. **6**(8): p. 1335-9, 1318.
9. Cocklin, S., et al., *Broad-spectrum anti-human immunodeficiency virus (HIV) potential of a peptide HIV type 1 entry inhibitor.* J Virol, 2007. **81**(7): p. 3645-8.
10. McFadden, K., et al., *Antiviral breadth and combination potential of peptide triazole HIV-1 entry inhibitors.* Antimicrob Agents Chemother, 2012. **56**(2): p. 1073-80.
11. Moore, J.P., et al., *Characterization of recombinant gp120 and gp160 from HIV-1: binding to monoclonal antibodies and soluble CD4.* AIDS, 1990. **4**(4): p. 307-15.
12. Moore, J.P., et al., *Dissociation of gp120 from HIV-1 virions induced by soluble CD4.* Science, 1990. **250**(4984): p. 1139-42.
13. Morikawa, Y., et al., *Expression of HIV-1 gp120 and human soluble CD4 by recombinant baculoviruses and their interaction in vitro.* AIDS Res Hum Retroviruses, 1990. **6**(6): p. 765-73.
14. Qiu, S., et al., *The binding mode of fusion inhibitor T20 onto HIV-1 gp41 and relevant T20-resistant mechanisms explored by computational study.* Curr HIV Res, 2012. **10**(2): p. 182-94.
15. Kromdijk, W., A.D. Huitema, and J.W. Mulder, *Treatment of HIV infection with the CCR5 antagonist maraviroc.* Expert Opin Pharmacother, 2010. **11**(7): p. 1215-23.
16. Henrich, T.J. and D.R. Kuritzkes, *HIV-1 entry inhibitors: recent development and clinical use.* Curr Opin Virol, 2013. **3**(1): p. 51-7.
17. Debnath, A.K., *Rational design of HIV-1 entry inhibitors.* Methods Mol Biol, 2013. **993**: p. 185-204.
18. Nettles, R.E., et al., *Pharmacodynamics, safety, and pharmacokinetics of BMS-663068, an oral HIV-1 attachment inhibitor in HIV-1-infected subjects.* J Infect Dis, 2012. **206**(7): p. 1002-11.
19. Zhang, H., et al., *Dual-acting stapled peptides target both HIV-1 entry and assembly.* Retrovirology, 2013. **10**: p. 136.

20. Jacobson, J.M., et al., *Safety, pharmacokinetics, and antiretroviral activity of multiple doses of ibalizumab (formerly TNX-355), an anti-CD4 monoclonal antibody, in human immunodeficiency virus type 1-infected adults.* Antimicrob Agents Chemother, 2009. **53**(2): p. 450-7.
21. Matz, J., et al., *Straightforward selection of broadly neutralizing single-domain antibodies targeting the conserved CD4 and coreceptor binding sites of HIV-1 gp120.* J Virol, 2013. **87**(2): p. 1137-49.
22. Gopi, H.N., et al., *Click chemistry on azidoproline: high-affinity dual antagonist for HIV-1 envelope glycoprotein gp120.* ChemMedChem, 2006. **1**(1): p. 54-7.
23. Gopi, H., et al., *Structural determinants for affinity enhancement of a dual antagonist peptide entry inhibitor of human immunodeficiency virus type-1.* J Med Chem, 2008. **51**(9): p. 2638-47.
24. Emileh, A., et al., *A model of peptide triazole entry inhibitor binding to HIV-1 gp120 and the mechanism of bridging sheet disruption.* Biochemistry, 2013. **52**(13): p. 2245-61.
25. Tuzer, F., et al., *HIV-1 Env gp120 structural determinants for peptide triazole dual receptor site antagonism.* Proteins, 2013. **81**(2): p. 271-90.
26. WHO/UNAIDS, *Joint United Nations Programme on HIV/AIDS/World Health Organization AIDS epidemic update.* 2009.
27. Cohen, O.J. and A.S. Fauci, *Current strategies in the treatment of HIV infection.* Adv Intern Med, 2001. **46**: p. 207-46.
28. Potthoff, A.V. and N.H. Brockmeyer, *Current therapy of HIV.* J Dtsch Dermatol Ges, 2010. **8**(1): p. 45-56; quiz 57-8.
29. Dau, B. and M. Holodniy, *Novel targets for antiretroviral therapy: clinical progress to date.* Drugs, 2009. **69**(1): p. 31-50.
30. Myszka, D.G., et al., *Energetics of the HIV gp120-CD4 binding reaction.* Proc Natl Acad Sci U S A, 2000. **97**(16): p. 9026-31.
31. Gopi, H., et al., *Introducing metallocene into a triazole peptide conjugate reduces its off-rate and enhances its affinity and antiviral potency for HIV-1 gp120.* J Mol Recognit, 2009. **22**(2): p. 169-74.
32. Umashankara, M., et al., *The active core in a triazole peptide dual-site antagonist of HIV-1 gp120.* ChemMedChem, 2010. **5**(11): p. 1871-9.
33. Sattentau, Q.J., *CD4 activation of HIV fusion.* Int J Cell Cloning, 1992. **10**(6): p. 323-32.
34. Kassa, A., et al., *Transitions to and from the CD4-bound conformation are modulated by a single-residue change in the human immunodeficiency virus type 1 gp120 inner domain.* J Virol, 2009. **83**(17): p. 8364-78.
35. Finzi, A., et al., *Topological layers in the HIV-1 gp120 inner domain regulate gp41 interaction and CD4-triggered conformational transitions.* Mol Cell, 2010. **37**(5): p. 656-67.
36. Sattentau, Q.J. and J.P. Moore, *Conformational changes induced in the human immunodeficiency virus envelope glycoprotein by soluble CD4 binding.* J Exp Med, 1991. **174**(2): p. 407-15.
37. Wyatt, R. and J. Sodroski, *The HIV-1 envelope glycoproteins: fusogens, antigens, and immunogens.* Science, 1998. **280**(5371): p. 1884-8.

38. Eckert, D.M. and P.S. Kim, *Mechanisms of viral membrane fusion and its inhibition.* Annu Rev Biochem, 2001. **70**: p. 777-810.
39. Emileh, A., et al., *Covalent conjugation of a peptide triazole to HIV-1 gp120 enables intramolecular binding site occupancy.* Biochemistry, 2014.
40. Weiss, R.A., *Special anniversary review: twenty-five years of human immunodeficiency virus research: successes and challenges.* Clin Exp Immunol, 2008. **152**(2): p. 201-10.
41. (UNAIDS), J.U.N.P.o.H.A., *Global Report: UNAIDS report on the global AIDS epidemic 2013*, in *p.v., Joint United Nations Programme on HIV/AIDS*2013. p. 198.
42. Hammer, S.M., et al., *A trial comparing nucleoside monotherapy with combination therapy in HIV-infected adults with CD4 cell counts from 200 to 500 per cubic millimeter. AIDS Clinical Trials Group Study 175 Study Team.* N Engl J Med, 1996. **335**(15): p. 1081-90.
43. Hammer, S.M., et al., *A controlled trial of two nucleoside analogues plus indinavir in persons with human immunodeficiency virus infection and CD4 cell counts of 200 per cubic millimeter or less. AIDS Clinical Trials Group 320 Study Team.* N Engl J Med, 1997. **337**(11): p. 725-33.
44. Palella, F.J., Jr., et al., *Declining morbidity and mortality among patients with advanced human immunodeficiency virus infection. HIV Outpatient Study Investigators.* N Engl J Med, 1998. **338**(13): p. 853-60.
45. Vella, S. and L. Palmisano, *The global status of resistance to antiretroviral drugs.* Clin Infect Dis, 2005. **41 Suppl 4**: p. S239-46.
46. Frankel, A.D. and J.A. Young, *HIV-1: fifteen proteins and an RNA.* Annu Rev Biochem, 1998. **67**: p. 1-25.
47. Kohlstaedt, L.A., et al., *Crystal structure at 3.5 A resolution of HIV-1 reverse transcriptase complexed with an inhibitor.* Science, 1992. **256**(5065): p. 1783-90.
48. Holm, K., et al., *Human immunodeficiency virus type 1 assembly and lipid rafts: Pr55(gag) associates with membrane domains that are largely resistant to Brij98 but sensitive to Triton X-100.* J Virol, 2003. **77**(8): p. 4805-17.
49. Brugger, B., et al., *The HIV lipidome: a raft with an unusual composition.* Proc Natl Acad Sci U S A, 2006. **103**(8): p. 2641-6.
50. Chan, R., et al., *Retroviruses human immunodeficiency virus and murine leukemia virus are enriched in phosphoinositides.* J Virol, 2008. **82**(22): p. 11228-38.
51. Thomson, M.M., L. Perez-Alvarez, and R. Najera, *Molecular epidemiology of HIV-1 genetic forms and its significance for vaccine development and therapy.* Lancet Infect Dis, 2002. **2**(8): p. 461-71.
52. Coffin, J.M., *HIV population dynamics in vivo: implications for genetic variation, pathogenesis, and therapy.* Science, 1995. **267**(5197): p. 483-9.
53. Hemelaar, J., et al., *Global and regional distribution of HIV-1 genetic subtypes and recombinants in 2004.* AIDS, 2006. **20**(16): p. W13-23.
54. Julien, J.P., et al., *Crystal structure of a soluble cleaved HIV-1 envelope trimer.* Science, 2013. **342**(6165): p. 1477-83.
55. Helseth, E., et al., *Human immunodeficiency virus type 1 gp120 envelope glycoprotein regions important for association with the gp41 transmembrane glycoprotein.* J Virol, 1991. **65**(4): p. 2119-23.

56. Clavel, F. and A.J. Hance, *HIV drug resistance.* N Engl J Med, 2004. **350**(10): p. 1023-35.
57. Pancera, M., et al., *Structure of HIV-1 gp120 with gp41-interactive region reveals layered envelope architecture and basis of conformational mobility.* Proc Natl Acad Sci U S A, 2010. **107**(3): p. 1166-71.
58. Haim, H., et al., *Soluble CD4 and CD4-mimetic compounds inhibit HIV-1 infection by induction of a short-lived activated state.* PLoS Pathog, 2009. **5**(4): p. e1000360.
59. Poignard, P., et al., *gp120: Biologic aspects of structural features.* Annu Rev Immunol, 2001. **19**: p. 253-74.
60. Joyce, M.G., et al., *Outer domain of HIV-1 gp120: antigenic optimization, structural malleability, and crystal structure with antibody VRC-PG04.* J Virol, 2013. **87**(4): p. 2294-306.
61. Kwong, P.D., et al., *Structure of an HIV gp120 envelope glycoprotein in complex with the CD4 receptor and a neutralizing human antibody.* Nature, 1998. **393**(6686): p. 648-59.
62. Wyatt, R., et al., *The antigenic structure of the HIV gp120 envelope glycoprotein.* Nature, 1998. **393**(6686): p. 705-11.
63. Rizzuto, C.D., et al., *A conserved HIV gp120 glycoprotein structure involved in chemokine receptor binding.* Science, 1998. **280**(5371): p. 1949-53.
64. Huang, C.C., et al., *Structure of a V3-containing HIV-1 gp120 core.* Science, 2005. **310**(5750): p. 1025-8.
65. Chen, H., et al., *Mapping the immune response to the outer domain of a human immunodeficiency virus-1 clade C gp120.* J Gen Virol, 2008. **89**(Pt 10): p. 2597-604.
66. Merk, A. and S. Subramaniam, *HIV-1 envelope glycoprotein structure.* Curr Opin Struct Biol, 2013. **23**(2): p. 268-76.
67. Meyerson, J.R., et al., *Molecular structures of trimeric HIV-1 Env in complex with small antibody derivatives.* Proc Natl Acad Sci U S A, 2013. **110**(2): p. 513-8.
68. Khayat, R., et al., *Structural characterization of cleaved, soluble HIV-1 envelope glycoprotein trimers.* J Virol, 2013. **87**(17): p. 9865-72.
69. Lyumkis, D., et al., *Cryo-EM structure of a fully glycosylated soluble cleaved HIV-1 envelope trimer.* Science, 2013. **342**(6165): p. 1484-90.
70. Blattner, C., et al., *Structural Delineation of a Quaternary, Cleavage-Dependent Epitope at the gp41-gp120 Interface on Intact HIV-1 Env Trimers.* Immunity, 2014.
71. Schiffner, T., et al., *Immune focusing and enhanced neutralization induced by HIV-1 gp140 chemical cross-linking.* J Virol, 2013. **87**(18): p. 10163-72.
72. Kong, L., et al., *Supersite of immune vulnerability on the glycosylated face of HIV-1 envelope glycoprotein gp120.* Nat Struct Mol Biol, 2013. **20**(7): p. 796-803.
73. Kumar, R., et al., *Elicitation of broadly reactive antibodies against glycan-modulated neutralizing V3 epitopes of HIV-1 by immune complex vaccines.* Vaccine, 2013. **31**(46): p. 5413-21.

74. Yu, F., et al., *Approaches for identification of HIV-1 entry inhibitors targeting gp41 pocket.* Viruses, 2013. **5**(1): p. 127-49.
75. Bartesaghi, A., et al., *Prefusion structure of trimeric HIV-1 envelope glycoprotein determined by cryo-electron microscopy.* Nat Struct Mol Biol, 2013. **20**(12): p. 1352-7.
76. Pan, C., S. Liu, and S. Jiang, *HIV-1 gp41 fusion intermediate: a target for HIV therapeutics.* J Formos Med Assoc, 2010. **109**(2): p. 94-105.
77. Buzon, V., et al., *Crystal structure of HIV-1 gp41 including both fusion peptide and membrane proximal external regions.* PLoS Pathog, 2010. **6**(5): p. e1000880.
78. Chan, D.C., et al., *Core structure of gp41 from the HIV envelope glycoprotein.* Cell, 1997. **89**(2): p. 263-73.
79. Weissenhorn, W., et al., *Atomic structure of the ectodomain from HIV-1 gp41.* Nature, 1997. **387**(6631): p. 426-30.
80. Melikyan, G.B., et al., *Evidence that the transition of HIV-1 gp41 into a six-helix bundle, not the bundle configuration, induces membrane fusion.* J Cell Biol, 2000. **151**(2): p. 413-23.
81. Buzon, V., E. Padros, and J. Cladera, *Interaction of fusion peptides from HIV gp41 with membranes: a time-resolved membrane binding, lipid mixing, and structural study.* Biochemistry, 2005. **44**(40): p. 13354-64.
82. John-Stewart, G., et al., *Breast-feeding and Transmission of HIV-1.* J Acquir Immune Defic Syndr, 2004. **35**(2): p. 196-202.
83. Garg, H., et al., *Site-specific mutations in HIV-1 gp41 reveal a correlation between HIV-1-mediated bystander apoptosis and fusion/hemifusion.* J Biol Chem, 2007. **282**(23): p. 16899-906.
84. Garg, H. and R. Blumenthal, *Role of HIV Gp41 mediated fusion/hemifusion in bystander apoptosis.* Cell Mol Life Sci, 2008. **65**(20): p. 3134-44.
85. Gallo, S.A., et al., *The HIV Env-mediated fusion reaction.* Biochim Biophys Acta, 2003. **1614**(1): p. 36-50.
86. Walker, L.M., et al., *Broad neutralization coverage of HIV by multiple highly potent antibodies.* Nature, 2011. **477**(7365): p. 466-70.
87. Sok, D., et al., *The effects of somatic hypermutation on neutralization and binding in the PGT121 family of broadly neutralizing HIV antibodies.* PLoS Pathog, 2013. **9**(11): p. e1003754.
88. Kwong, P.D., et al., *HIV-1 evades antibody-mediated neutralization through conformational masking of receptor-binding sites.* Nature, 2002. **420**(6916): p. 678-82.
89. Kwong, P.D., J.R. Mascola, and G.J. Nabel, *Broadly neutralizing antibodies and the search for an HIV-1 vaccine: the end of the beginning.* Nat Rev Immunol, 2013. **13**(9): p. 693-701.
90. Liao, H.X., et al., *Vaccine induction of antibodies against a structurally heterogeneous site of immune pressure within HIV-1 envelope protein variable regions 1 and 2.* Immunity, 2013. **38**(1): p. 176-86.
91. Granich, R., et al., *Highly active antiretroviral treatment as prevention of HIV transmission: review of scientific evidence and update.* Curr Opin HIV AIDS, 2010. **5**(4): p. 298-304.

92. Baggaley, R.F., R.G. White, and M.C. Boily, *HIV transmission risk through anal intercourse: systematic review, meta-analysis and implications for HIV prevention.* Int J Epidemiol, 2010. **39**(4): p. 1048-63.
93. Attia, S., et al., *Sexual transmission of HIV according to viral load and antiretroviral therapy: systematic review and meta-analysis.* AIDS, 2009. **23**(11): p. 1397-404.
94. Cann, A.J. and J. Karn, *Molecular biology of HIV: new insights into the virus life-cycle.* AIDS, 1989. **3 Suppl 1**: p. S19-34.
95. Freed, E.O., *HIV-1 gag proteins: diverse functions in the virus life cycle.* Virology, 1998. **251**(1): p. 1-15.
96. Perelson, A.S., et al., *HIV-1 dynamics in vivo: virion clearance rate, infected cell life-span, and viral generation time.* Science, 1996. **271**(5255): p. 1582-6.
97. Geijtenbeek, T.B., et al., *DC-SIGN, a dendritic cell-specific HIV-1-binding protein that enhances trans-infection of T cells.* Cell, 2000. **100**(5): p. 587-97.
98. Moulard, M. and E. Decroly, *Maturation of HIV envelope glycoprotein precursors by cellular endoproteases.* Biochim Biophys Acta, 2000. **1469**(3): p. 121-32.
99. Parren, P.W., et al., *Neutralization of human immunodeficiency virus type 1 by antibody to gp120 is determined primarily by occupancy of sites on the virion irrespective of epitope specificity.* J Virol, 1998. **72**(5): p. 3512-9.
100. Allan, J.S., et al., *Major glycoprotein antigens that induce antibodies in AIDS patients are encoded by HTLV-III.* Science, 1985. **228**(4703): p. 1091-4.
101. Earl, P.L., S. Koenig, and B. Moss, *Biological and immunological properties of human immunodeficiency virus type 1 envelope glycoprotein: analysis of proteins with truncations and deletions expressed by recombinant vaccinia viruses.* J Virol, 1991. **65**(1): p. 31-41.
102. Robey, W.G., et al., *Characterization of envelope and core structural gene products of HTLV-III with sera from AIDS patients.* Science, 1985. **228**(4699): p. 593-5.
103. Mondor, I., et al., *Interactions among HIV gp120, CD4, and CXCR4: dependence on CD4 expression level, gp120 viral origin, conservation of the gp120 COOH- and NH2-termini and V1/V2 and V3 loops, and sensitivity to neutralizing antibodies.* Virology, 1998. **248**(2): p. 394-405.
104. Truneh, A., et al., *A region in domain 1 of CD4 distinct from the primary gp120 binding site is involved in HIV infection and virus-mediated fusion.* J Biol Chem, 1991. **266**(9): p. 5942-8.
105. Liu, J., et al., *Molecular architecture of native HIV-1 gp120 trimers.* Nature, 2008. **455**(7209): p. 109-13.
106. Mao, Y., et al., *Subunit organization of the membrane-bound HIV-1 envelope glycoprotein trimer.* Nat Struct Mol Biol, 2012. **19**(9): p. 893-9.
107. Tuen, M., et al., *Characterization of antibodies that inhibit HIV gp120 antigen processing and presentation.* Eur J Immunol, 2005. **35**(9): p. 2541-51.
108. Tilton, J.C. and R.W. Doms, *Entry inhibitors in the treatment of HIV-1 infection.* Antiviral Res, 2010. **85**(1): p. 91-100.

109. Frey, G., et al., *Distinct conformational states of HIV-1 gp41 are recognized by neutralizing and non-neutralizing antibodies.* Nat Struct Mol Biol, 2010. **17**(12): p. 1486-91.
110. Tran, E.E., et al., *Structural mechanism of trimeric HIV-1 envelope glycoprotein activation.* PLoS Pathog, 2012. **8**(7): p. e1002797.
111. Gustchina, E., C.A. Bewley, and G.M. Clore, *Sequestering of the prehairpin intermediate of gp41 by peptide N36Mut(e,g) potentiates the human immunodeficiency virus type 1 neutralizing activity of monoclonal antibodies directed against the N-terminal helical repeat of gp41.* J Virol, 2008. **82**(20): p. 10032-41.
112. Gallo, S.A., et al., *Theta-defensins prevent HIV-1 Env-mediated fusion by binding gp41 and blocking 6-helix bundle formation.* J Biol Chem, 2006. **281**(27): p. 18787-92.
113. Este, J.A. and A. Telenti, *HIV entry inhibitors.* Lancet, 2007. **370**(9581): p. 81-8.
114. Greenberg, M., et al., *HIV fusion and its inhibition in antiretroviral therapy.* Rev Med Virol, 2004. **14**(5): p. 321-37.
115. Gallo, S.A., A. Puri, and R. Blumenthal, *HIV-1 gp41 six-helix bundle formation occurs rapidly after the engagement of gp120 by CXCR4 in the HIV-1 Env-mediated fusion process.* Biochemistry, 2001. **40**(41): p. 12231-6.
116. Chan, D.C. and P.S. Kim, *HIV entry and its inhibition.* Cell, 1998. **93**(5): p. 681-4.
117. Palmisano, L. and S. Vella, *A brief history of antiretroviral therapy of HIV infection: success and challenges.* Ann Ist Super Sanita, 2011. **47**(1): p. 44-8.
118. Fischl, M.A., et al., *The efficacy of azidothymidine (AZT) in the treatment of patients with AIDS and AIDS-related complex. A double-blind, placebo-controlled trial.* N Engl J Med, 1987. **317**(4): p. 185-91.
119. Gulick, R.M., et al., *Treatment with indinavir, zidovudine, and lamivudine in adults with human immunodeficiency virus infection and prior antiretroviral therapy.* N Engl J Med, 1997. **337**(11): p. 734-9.
120. Bartlett, J.A., et al., *An updated systematic overview of triple combination therapy in antiretroviral-naive HIV-infected adults.* AIDS, 2006. **20**(16): p. 2051-64.
121. Data, W.L.C.-i.-P., *Global update on hiv treatment 2013: results, impact and opportunities*, I.W.H. Organization, Editor 2013, World Health Organization 2013: Printed in Kuala Lumpur (Malaysia).
122. Volberding, P.A. and S.G. Deeks, *Antiretroviral therapy and management of HIV infection.* Lancet, 2010. **376**(9734): p. 49-62.
123. Thompson, M.A., et al., *Antiretroviral treatment of adult HIV infection: 2010 recommendations of the International AIDS Society-USA panel.* JAMA, 2010. **304**(3): p. 321-33.
124. Rathbun, R.C., *HIV consensus guideline recommends antiretroviral treatment regardless of CD4 count, new regimens and possible regimen change for chronic low level viraemia.* Evid Based Med, 2013. **18**(4): p. 149-50.
125. Lodi, S., et al., *Time from human immunodeficiency virus seroconversion to reaching CD4+ cell count thresholds <200, <350, and <500 Cells/mm(3): assessment of need following changes in treatment guidelines.* Clin Infect Dis, 2011. **53**(8): p. 817-25.

126. Mills, E.J., et al., *Adherence to HAART: a systematic review of developed and developing nation patient-reported barriers and facilitators.* PLoS Med, 2006. **3**(11): p. e438.
127. Simoni, J.M., et al., *Self-report measures of antiretroviral therapy adherence: A review with recommendations for HIV research and clinical management.* AIDS Behav, 2006. **10**(3): p. 227-45.
128. Kanters, S., et al., *Antiretroviral therapy for initial human immunodeficiency virus/AIDS treatment: critical appraisal of the evidence from over 100 randomized trials and 400 systematic reviews and meta-analyses.* Clin Microbiol Infect, 2014. **20**(2): p. 114-22.
129. Vandenhende, M.A., et al., *Prevalence and evolution of low frequency HIV drug resistance mutations detected by ultra deep sequencing in patients experiencing first line antiretroviral therapy failure.* PLoS One, 2014. **9**(1): p. e86771.
130. Kanters, S., et al., *CD4(+) T-cell recovery after initiation of antiretroviral therapy in a resource-limited setting: a prospective cohort analysis.* Antivir Ther, 2014. **19**(1): p. 31-9.
131. Link-Gelles, R., et al., *Tuberculosis Immune Reconstitution Inflammatory Syndrome in Children Initiating Antiretroviral Therapy for HIV Infection: A Systematic Literature Review.* Pediatr Infect Dis J, 2014. **33**(5): p. 499-503.
132. Short, C.E., et al., *Preterm delivery risk in women initiating antiretroviral therapy to prevent HIV mother-to-child transmission.* HIV Med, 2014. **15**(4): p. 233-8.
133. Miller, C.J., et al., *Adjudicated Morbidity and Mortality Outcomes by Age among Individuals with HIV Infection on Suppressive Antiretroviral Therapy.* PLoS One, 2014. **9**(4): p. e95061.
134. Jin, Y., et al., *A systematic review of cohort studies of the quality of life in HIV/AIDS patients after antiretroviral therapy.* Int J STD AIDS, 2014.
135. Yost, R., T.R. Pasquale, and E.G. Sahloff, *Maraviroc: a coreceptor CCR5 antagonist for management of HIV infection.* Am J Health Syst Pharm, 2009. **66**(8): p. 715-26.
136. Clotet, B., et al., *Clinical management of treatment-experienced, HIV-infected patients with the fusion inhibitor enfuvirtide: consensus recommendations.* AIDS, 2004. **18**(8): p. 1137-46.
137. Wild, C., T. Greenwell, and T. Matthews, *A synthetic peptide from HIV-1 gp41 is a potent inhibitor of virus-mediated cell-cell fusion.* AIDS Res Hum Retroviruses, 1993. **9**(11): p. 1051-3.
138. Steger, H.K. and M.J. Root, *Kinetic dependence to HIV-1 entry inhibition.* J Biol Chem, 2006. **281**(35): p. 25813-21.
139. Desmezieres, E., et al., *Human immunodeficiency virus (HIV) gp41 escape mutants: cross-resistance to peptide inhibitors of HIV fusion and altered receptor activation of gp120.* J Virol, 2005. **79**(8): p. 4774-81.
140. Eggink, D., et al., *Resistance of human immunodeficiency virus type 1 to a third-generation fusion inhibitor requires multiple mutations in gp41 and is accompanied by a dramatic loss of gp41 function.* J Virol, 2011. **85**(20): p. 10785-97.

141. Carmona, R., et al., *Natural resistance-associated mutations to Enfuvirtide (T20) and polymorphisms in the gp41 region of different HIV-1 genetic forms from T20 naive patients.* J Clin Virol, 2005. **32**(3): p. 248-53.
142. Perez-Alvarez, L., et al., *Long-term monitoring of genotypic and phenotypic resistance to T20 in treated patients infected with HIV-1.* J Med Virol, 2006. **78**(2): p. 141-7.
143. Hawkins, T., *HIV drug resistance and you. The limitations of drug resistance testing. Many factors influence the results.* Posit Aware, 2006. **Spec No**: p. 13-6.
144. Hawkins, T., *Appearance-related side effects of HIV-1 treatment.* AIDS Patient Care STDS, 2006. **20**(1): p. 6-18.
145. Church, J.A., et al., *Safety and antiretroviral activity of chronic subcutaneous administration of T-20 in human immunodeficiency virus 1-infected children.* Pediatr Infect Dis J, 2002. **21**(7): p. 653-9.
146. Ruxrungtham, K., et al., *Lack of interaction between enfuvirtide and ritonavir or ritonavir-boosted saquinavir in HIV-1-infected patients.* J Clin Pharmacol, 2004. **44**(7): p. 793-803.
147. Hirsch, E., *[HIV-AIDS: ethics in healthcare, research, and access to treatments]*. Med Sci (Paris), 2003. **19**(6-7): p. 753-60.
148. Dorr, P., et al., *Maraviroc (UK-427,857), a potent, orally bioavailable, and selective small-molecule inhibitor of chemokine receptor CCR5 with broad-spectrum anti-human immunodeficiency virus type 1 activity.* Antimicrob Agents Chemother, 2005. **49**(11): p. 4721-32.
149. Rosario, M.C., et al., *A pharmacokinetic-pharmacodynamic disease model to predict in vivo antiviral activity of maraviroc.* Clin Pharmacol Ther, 2005. **78**(5): p. 508-19.
150. Dean, M., et al., *Genetic restriction of HIV-1 infection and progression to AIDS by a deletion allele of the CKR5 structural gene. Hemophilia Growth and Development Study, Multicenter AIDS Cohort Study, Multicenter Hemophilia Cohort Study, San Francisco City Cohort, ALIVE Study.* Science, 1996. **273**(5283): p. 1856-62.
151. Dragic, T., et al., *HIV-1 entry into CD4+ cells is mediated by the chemokine receptor CC-CKR-5.* Nature, 1996. **381**(6584): p. 667-73.
152. Pasi, K.J., et al., *The effects of the 32-bp CCR-5 deletion on HIV transmission and HIV disease progression in individuals with haemophilia.* Br J Haematol, 2000. **111**(1): p. 136-42.
153. Taylor, J.M., et al., *Causal pathways for CCR5 genotype and HIV progression.* J Acquir Immune Defic Syndr, 2000. **23**(2): p. 160-71.
154. Tan, Q., et al., *Structure of the CCR5 chemokine receptor-HIV entry inhibitor maraviroc complex.* Science, 2013. **341**(6152): p. 1387-90.
155. Emmelkamp, J.M. and J.K. Rockstroh, *CCR5 antagonists: comparison of efficacy, side effects, pharmacokinetics and interactions--review of the literature.* Eur J Med Res, 2007. **12**(9): p. 409-17.
156. Stephenson, J., *Researchers buoyed by novel HIV drugs: will expand drug arsenal against resistant virus.* JAMA, 2007. **297**(14): p. 1535-6.
157. Haqqani, A.A. and J.C. Tilton, *Entry inhibitors and their use in the treatment of HIV-1 infection.* Antiviral Res, 2013. **98**(2): p. 158-70.

158. Perry, C.M., *Maraviroc: a review of its use in the management of CCR5-tropic HIV-1 infection.* Drugs, 2010. **70**(9): p. 1189-213.
159. Hughes, A., T. Barber, and M. Nelson, *New treatment options for HIV salvage patients: an overview of second generation PIs, NNRTIs, integrase inhibitors and CCR5 antagonists.* J Infect, 2008. **57**(1): p. 1-10.
160. Lieberman-Blum, S.S., H.B. Fung, and J.C. Bandres, *Maraviroc: a CCR5-receptor antagonist for the treatment of HIV-1 infection.* Clin Ther, 2008. **30**(7): p. 1228-50.
161. Recordon-Pinson, P., et al., *Evaluation of the genotypic prediction of HIV-1 coreceptor use versus a phenotypic assay and correlation with the virological response to maraviroc: the ANRS GenoTropism study.* Antimicrob Agents Chemother, 2010. **54**(8): p. 3335-40.
162. Maddon, P.J., et al., *The isolation and nucleotide sequence of a cDNA encoding the T cell surface protein T4: a new member of the immunoglobulin gene family.* Cell, 1985. **42**(1): p. 93-104.
163. Sweet, R.W., A. Truneh, and W.A. Hendrickson, *CD4: its structure, role in immune function and AIDS pathogenesis, and potential as a pharmacological target.* Curr Opin Biotechnol, 1991. **2**(4): p. 622-33.
164. Ryu, S.E., et al., *Crystal structure of an HIV-binding recombinant fragment of human CD4.* Nature, 1990. **348**(6300): p. 419-26.
165. Kwong, P.D., et al., *Molecular characteristics of recombinant human CD4 as deduced from polymorphic crystals.* Proc Natl Acad Sci U S A, 1990. **87**(16): p. 6423-7.
166. Daar, E.S., et al., *High concentrations of recombinant soluble CD4 are required to neutralize primary human immunodeficiency virus type 1 isolates.* Proc Natl Acad Sci U S A, 1990. **87**(17): p. 6574-8.
167. Veazey, R.S., et al., *Protection of macaques from vaginal SHIV challenge by vaginally delivered inhibitors of virus-cell fusion.* Nature, 2005. **438**(7064): p. 99-102.
168. Madani, N., et al., *Localized changes in the gp120 envelope glycoprotein confer resistance to human immunodeficiency virus entry inhibitors BMS-806 and #155.* J Virol, 2004. **78**(7): p. 3742-52.
169. Ho, J., et al., *Two overrepresented B cell populations in HIV-infected individuals undergo apoptosis by different mechanisms.* Proc Natl Acad Sci U S A, 2006. **103**(51): p. 19436-41.
170. Zhao, Q., et al., *Identification of N-phenyl-N'-(2,2,6,6-tetramethyl-piperidin-4-yl)-oxalamides as a new class of HIV-1 entry inhibitors that prevent gp120 binding to CD4.* Virology, 2005. **339**(2): p. 213-25.
171. Stricher, F., et al., *Combinatorial optimization of a CD4-mimetic miniprotein and cocrystal structures with HIV-1 gp120 envelope glycoprotein.* J Mol Biol, 2008. **382**(2): p. 510-24.
172. Schon, A., et al., *Thermodynamics of binding of a low-molecular-weight CD4 mimetic to HIV-1 gp120.* Biochemistry, 2006. **45**(36): p. 10973-80.
173. Martin, L., et al., *Rational design of a CD4 mimic that inhibits HIV-1 entry and exposes cryptic neutralization epitopes.* Nat Biotechnol, 2003. **21**(1): p. 71-6.

174. Song, R., et al., *Epitope mapping of ibalizumab, a humanized anti-CD4 monoclonal antibody with anti-HIV-1 activity in infected patients.* J Virol, 2010. **84**(14): p. 6935-42.
175. Wohl, A.R., et al., *Barriers and unmet need for supportive services for HIV patients in care in Los Angeles County, California.* AIDS Patient Care STDS, 2011. **25**(9): p. 525-32.
176. Raja, A., et al., *CD4 binding site antibodies inhibit human immunodeficiency virus gp120 envelope glycoprotein interaction with CCR5.* J Virol, 2003. **77**(1): p. 713-8.
177. Posner, M.R., et al., *Neutralization of HIV-1 by F105, a human monoclonal antibody to the CD4 binding site of gp120.* J Acquir Immune Defic Syndr, 1993. **6**(1): p. 7-14.
178. Hessell, A.J., et al., *Effective, low-titer antibody protection against low-dose repeated mucosal SHIV challenge in macaques.* Nat Med, 2009. **15**(8): p. 951-4.
179. Li, Y., et al., *Mechanism of neutralization by the broadly neutralizing HIV-1 monoclonal antibody VRC01.* J Virol, 2011. **85**(17): p. 8954-67.
180. Wu, X., et al., *Rational design of envelope identifies broadly neutralizing human monoclonal antibodies to HIV-1.* Science, 2010. **329**(5993): p. 856-61.
181. Doria-Rose, N.A., et al., *HIV-1 neutralization coverage is improved by combining monoclonal antibodies that target independent epitopes.* J Virol, 2012. **86**(6): p. 3393-7.
182. Kwong, P.D., J.R. Mascola, and G.J. Nabel, *The changing face of HIV vaccine research.* J Int AIDS Soc, 2012. **15**(2): p. 17407.
183. Pejchal, R., et al., *A potent and broad neutralizing antibody recognizes and penetrates the HIV glycan shield.* Science, 2011. **334**(6059): p. 1097-103.
184. Trkola, A., et al., *Human monoclonal antibody 2G12 defines a distinctive neutralization epitope on the gp120 glycoprotein of human immunodeficiency virus type 1.* J Virol, 1996. **70**(2): p. 1100-8.
185. McLellan, J.S., et al., *Structure of HIV-1 gp120 V1/V2 domain with broadly neutralizing antibody PG9.* Nature, 2011. **480**(7377): p. 336-43.
186. Carter, P.J., *Potent antibody therapeutics by design.* Nat Rev Immunol, 2006. **6**(5): p. 343-57.
187. Madani, N., et al., *CD4-mimetic Small Molecules Sensitize Human Immunodeficiency Virus (HIV-1) to Vaccine-elicited Antibodies.* J Virol, 2014.
188. West, A.P., Jr., et al., *Structural insights on the role of antibodies in HIV-1 vaccine and therapy.* Cell, 2014. **156**(4): p. 633-48.
189. Cocchi, F., et al., *Identification of RANTES, MIP-1 alpha, and MIP-1 beta as the major HIV-suppressive factors produced by CD8+ T cells.* Science, 1995. **270**(5243): p. 1811-5.
190. Alkhatib, G., et al., *HIV-1 coreceptor activity of CCR5 and its inhibition by chemokines: independence from G protein signaling and importance of coreceptor downmodulation.* Virology, 1997. **234**(2): p. 340-8.
191. Veazey, R.S., et al., *Topically applied recombinant chemokine analogues fully protect macaques from vaginal simian-human immunodeficiency virus challenge.* J Infect Dis, 2009. **199**(10): p. 1525-7.

192. Gaertner, H., et al., *Semisynthetic analogues of PSC-RANTES, a potent anti-HIV protein.* Bioconjug Chem, 2008. **19**(2): p. 480-9.
193. Colin, P., et al., *HIV-1 exploits CCR5 conformational heterogeneity to escape inhibition by chemokines.* Proc Natl Acad Sci U S A, 2013. **110**(23): p. 9475-80.
194. Nichols, W.G., et al., *Hepatotoxicity observed in clinical trials of aplaviroc (GW873140).* Antimicrob Agents Chemother, 2008. **52**(3): p. 858-65.
195. Caseiro, M.M., et al., *Vicriviroc plus optimized background therapy for treatment-experienced subjects with CCR5 HIV-1 infection: final results of two randomized phase III trials.* J Infect, 2012. **65**(4): p. 326-35.
196. Klibanov, O.M., S.H. Williams, and C.A. Iler, *Cenicriviroc, an orally active CCR5 antagonist for the potential treatment of HIV infection.* Curr Opin Investig Drugs, 2010. **11**(8): p. 940-50.
197. Marier, J.F., et al., *Pharmacokinetics and pharmacodynamics of TBR-652, a novel CCR5 antagonist, in HIV-1-infected, antiretroviral treatment-experienced, CCR5 antagonist-naive patients.* Antimicrob Agents Chemother, 2011. **55**(6): p. 2768-74.
198. Hendrix, C.W., et al., *Safety, pharmacokinetics, and antiviral activity of AMD3100, a selective CXCR4 receptor inhibitor, in HIV-1 infection.* J Acquir Immune Defic Syndr, 2004. **37**(2): p. 1253-62.
199. Olson, W.C., et al., *Differential inhibition of human immunodeficiency virus type 1 fusion, gp120 binding, and CC-chemokine activity by monoclonal antibodies to CCR5.* J Virol, 1999. **73**(5): p. 4145-55.
200. Shimoni, M., et al., *The isolation of novel phage display-derived human recombinant antibodies against CCR5, the major co-receptor of HIV.* Viral Immunol, 2013. **26**(4): p. 277-90.
201. Weiss, C.D., *HIV-1 gp41: mediator of fusion and target for inhibition.* AIDS Rev, 2003. **5**(4): p. 214-21.
202. Liu, Y., et al., *An amphiphilic conjugate approach toward the design and synthesis of betulinic acid-polyphenol conjugates as inhibitors of the HIV-1 gp41 fusion core formation.* ChemMedChem, 2011. **6**(9): p. 1654-64.
203. Root, M.J. and H.K. Steger, *HIV-1 gp41 as a target for viral entry inhibition.* Curr Pharm Des, 2004. **10**(15): p. 1805-25.
204. Bewley, C.A., et al., *Design of a novel peptide inhibitor of HIV fusion that disrupts the internal trimeric coiled-coil of gp41.* J Biol Chem, 2002. **277**(16): p. 14238-45.
205. Welch, B.D., et al., *Potent D-peptide inhibitors of HIV-1 entry.* Proc Natl Acad Sci U S A, 2007. **104**(43): p. 16828-33.
206. Eckert, D.M., et al., *Inhibiting HIV-1 entry: discovery of D-peptide inhibitors that target the gp41 coiled-coil pocket.* Cell, 1999. **99**(1): p. 103-15.
207. Greenberg, M.L. and N. Cammack, *Resistance to enfuvirtide, the first HIV fusion inhibitor.* J Antimicrob Chemother, 2004. **54**(2): p. 333-40.
208. Welch, B.D., et al., *Design of a potent D-peptide HIV-1 entry inhibitor with a strong barrier to resistance.* J Virol, 2010. **84**(21): p. 11235-44.
209. Platt, E.J., et al., *Rapid dissociation of HIV-1 from cultured cells severely limits infectivity assays, causes the inactivation ascribed to entry inhibitors, and masks the inherently high level of infectivity of virions.* J Virol, 2010. **84**(6): p. 3106-10.

210. Lobritz, M.A., A.N. Ratcliff, and E.J. Arts, *HIV-1 Entry, Inhibitors, and Resistance.* Viruses, 2010. **2**(5): p. 1069-105.
211. Briz, V., E. Poveda, and V. Soriano, *HIV entry inhibitors: mechanisms of action and resistance pathways.* J Antimicrob Chemother, 2006. **57**(4): p. 619-27.
212. Al-Jabri, A.A., et al., *In vitro anti-HIV-1 virucidal activity of tyrosine-conjugated tri- and dihydroxy bile salt derivatives.* J Antimicrob Chemother, 2000. **45**(5): p. 617-21.
213. Wilson, D.P., et al., *The paradoxical effects of using antiretroviral-based microbicides to control HIV epidemics.* Proc Natl Acad Sci U S A, 2008. **105**(28): p. 9835-40.
214. Hillier, S.L., et al., *In vitro and in vivo: the story of nonoxynol 9.* J Acquir Immune Defic Syndr, 2005. **39**(1): p. 1-8.
215. Van Damme, L., et al., *Effectiveness of COL-1492, a nonoxynol-9 vaginal gel, on HIV-1 transmission in female sex workers: a randomised controlled trial.* Lancet, 2002. **360**(9338): p. 971-7.
216. Tripathi, S., et al., *Anti HIV-1 virucidal activity of polyamide nucleic acid-membrane transducing peptide conjugates targeted to primer binding site of HIV-1 genome.* Virology, 2007. **363**(1): p. 91-103.
217. Telwatte, S., et al., *Virucidal activity of the dendrimer microbicide SPL7013 against HIV-1.* Antiviral Res, 2011. **90**(3): p. 195-9.
218. Rosenberg, M.J. and K.K. Holmes, *Virucides in prevention of HIV infection. Research Priorities. World Health Organization Working Group on Virucides.* Sex Transm Dis, 1993. **20**(1): p. 41-4.
219. Al-Jabri, A.A. and F.Q. Alenzi, *Vaccines, virucides and drugs against HIV/AIDS: hopes and optimisms for the future.* Open AIDS J, 2009. **3**: p. 1-3.
220. Ferrer, M. and S.C. Harrison, *Peptide ligands to human immunodeficiency virus type 1 gp120 identified from phage display libraries.* J Virol, 1999. **73**(7): p. 5795-802.
221. Biorn, A.C., et al., *Mode of action for linear peptide inhibitors of HIV-1 gp120 interactions.* Biochemistry, 2004. **43**(7): p. 1928-38.
222. Tuzer, F., et al., *HIV-1 ENV gp120 structural determinants for peptide triazole dual receptor site antagonism.* Proteins, 2012.
223. Emileh, A., et al., *A Model of Peptide Triazole Entry Inhibitor Binding to HIV-1 gp120 and the Mechanism of Bridging Sheet Disruption.* Biochemistry, 2013.
224. Kamanna, K., et al., *Non-natural peptide triazole antagonists of HIV-1 envelope gp120.* ChemMedChem, 2013. **8**(2): p. 322-8.
225. Kovochich, M., M.D. Marsden, and J.A. Zack, *Activation of latent HIV using drug-loaded nanoparticles.* PLoS One, 2011. **6**(4): p. e18270.
226. Vyas, T.K., L. Shah, and M.M. Amiji, *Nanoparticulate drug carriers for delivery of HIV/AIDS therapy to viral reservoir sites.* Expert Opin Drug Deliv, 2006. **3**(5): p. 613-28.
227. Amiji, M.M., T.K. Vyas, and L.K. Shah, *Role of nanotechnology in HIV/AIDS treatment: potential to overcome the viral reservoir challenge.* Discov Med, 2006. **6**(34): p. 157-62.
228. Farokhzad, O.C. and R. Langer, *Impact of nanotechnology on drug delivery.* ACS Nano, 2009. **3**(1): p. 16-20.

229. Nowacek, A. and H.E. Gendelman, *NanoART, neuroAIDS and CNS drug delivery.* Nanomedicine (Lond), 2009. **4**(5): p. 557-74.
230. Nowacek, A.S., et al., *NanoART synthesis, characterization, uptake, release and toxicology for human monocyte-macrophage drug delivery.* Nanomedicine (Lond), 2009. **4**(8): p. 903-17.
231. Baert, L., et al., *Development of a long-acting injectable formulation with nanoparticles of rilpivirine (TMC278) for HIV treatment.* Eur J Pharm Biopharm, 2009. **72**(3): p. 502-8.
232. Spreen, W., et al., *Pharmacokinetics, safety, and monotherapy antiviral activity of GSK1265744, an HIV integrase strand transfer inhibitor.* HIV Clin Trials, 2013. **14**(5): p. 192-203.
233. Spreen, W.R., D.A. Margolis, and J.C. Pottage, Jr., *Long-acting injectable antiretrovirals for HIV treatment and prevention.* Curr Opin HIV AIDS, 2013. **8**(6): p. 565-71.
234. Elechiguerra, J.L., et al., *Interaction of silver nanoparticles with HIV-1.* J Nanobiotechnology, 2005. **3**: p. 6.
235. Bowman, M.C., et al., *Inhibition of HIV fusion with multivalent gold nanoparticles.* J Am Chem Soc, 2008. **130**(22): p. 6896-7.
236. Chithrani, B.D., A.A. Ghazani, and W.C. Chan, *Determining the size and shape dependence of gold nanoparticle uptake into mammalian cells.* Nano Lett, 2006. **6**(4): p. 662-8.
237. Henrich, T.J. and R.T. Gandhi, *Early treatment and HIV-1 reservoirs: a stitch in time?* J Infect Dis, 2013. **208**(8): p. 1189-93.
238. Hertje, M., M. Zhou, and U. Dietrich, *Inhibition of HIV-1 entry: multiple keys to close the door.* ChemMedChem, 2010. **5**(11): p. 1825-35.
239. Champagne, K., A. Shishido, and M.J. Root, *Interactions of HIV-1 inhibitory peptide T20 with the gp41 N-HR coiled coil.* J Biol Chem, 2009. **284**(6): p. 3619-27.
240. Wallace, B.J., et al., *Enfuvirtide injection site reactions: a clinical and histopathological appraisal.* Australas J Dermatol, 2011. **52**(1): p. 19-26.
241. Hicks, C., et al., *Safety, tolerability, and efficacy of KP-1461 as monotherapy for 124 days in antiretroviral-experienced, HIV type 1-infected subjects.* AIDS Res Hum Retroviruses, 2013. **29**(2): p. 250-5.
242. Neffe, A.T., et al., *Rational optimization of the binding affinity of CD4 targeting peptidomimetics with potential anti HIV activity.* J Med Chem, 2007. **50**(15): p. 3482-8.
243. Madani, N., et al., *Small-molecule CD4 mimics interact with a highly conserved pocket on HIV-1 gp120.* Structure, 2008. **16**(11): p. 1689-701.
244. Lalonde, J.M., et al., *Structure-Based Design and Synthesis of an HIV-1 Entry Inhibitor Exploiting X-Ray and Thermodynamic Characterization.* ACS Med Chem Lett, 2013. **4**(3): p. 338-343.
245. Jacobson, J.M., et al., *Phase 2a study of the CCR5 monoclonal antibody PRO 140 administered intravenously to HIV-infected adults.* Antimicrob Agents Chemother, 2010. **54**(10): p. 4137-42.
246. Olson, W.C. and J.M. Jacobson, *CCR5 monoclonal antibodies for HIV-1 therapy.* Curr Opin HIV AIDS, 2009. **4**(2): p. 104-11.

247. McCoy, L.E. and R.A. Weiss, *Neutralizing antibodies to HIV-1 induced by immunization.* J Exp Med, 2013. **210**(2): p. 209-23.
248. Flexner, C. and M. Saag, *The antiretroviral drug pipeline: prospects and implications for future treatment research.* Curr Opin HIV AIDS, 2013. **8**(6): p. 572-8.
249. Sharma, A.K., et al., *Inhibitors of HIV-1 entry and integration: recent developments and impact on treatment.* Recent Pat Inflamm Allergy Drug Discov, 2013. **7**(2): p. 151-61.
250. Klein, F., et al., *Antibodies in HIV-1 vaccine development and therapy.* Science, 2013. **341**(6151): p. 1199-204.
251. Connor, R.I., et al., *Vpr is required for efficient replication of human immunodeficiency virus type-1 in mononuclear phagocytes.* Virology, 1995. **206**(2): p. 935-44.
252. He, J. and N.R. Landau, *Use of a novel human immunodeficiency virus type 1 reporter virus expressing human placental alkaline phosphatase to detect an alternative viral receptor.* J Virol, 1995. **69**(7): p. 4587-92.
253. Montefiori, D.C., *Evaluating neutralizing antibodies against HIV, SIV, and SHIV in luciferase reporter gene assays.* Curr Protoc Immunol, 2005. **Chapter 12**: p. Unit 12 11.
254. Cantin, R., et al., *Discrimination between exosomes and HIV-1: purification of both vesicles from cell-free supernatants.* J Immunol Methods, 2008. **338**(1-2): p. 21-30.
255. Thavarajah, R., et al., *Chemical and physical basics of routine formaldehyde fixation.* J Oral Maxillofac Pathol, 2012. **16**(3): p. 400-5.
256. Morton, T.A., et al., *Analysis of the interaction between human interleukin-5 and the soluble domain of its receptor using a surface plasmon resonance biosensor.* Journal of Molecular Recognition, 1994. **7**(1): p. 47-55.
257. Matthias, L.J., et al., *Disulfide exchange in domain 2 of CD4 is required for entry of HIV-1.* Nat Immunol, 2002. **3**(8): p. 727-32.
258. Ryser, H.J., et al., *Inhibition of human immunodeficiency virus infection by agents that interfere with thiol-disulfide interchange upon virus-receptor interaction.* Proc Natl Acad Sci U S A, 1994. **91**(10): p. 4559-63.
259. Hogg, P.J., *Disulfide bonds as switches for protein function.* Trends Biochem Sci, 2003. **28**(4): p. 210-4.
260. Shen, X., et al., *In vivo gp41 antibodies targeting the 2F5 monoclonal antibody epitope mediate human immunodeficiency virus type 1 neutralization breadth.* J Virol, 2009. **83**(8): p. 3617-25.
261. Covens, K., et al., *The rare HIV-1 gp41 mutations 43T and 50V elevate enfuvirtide resistance levels of common enfuvirtide resistance mutations that did not impact susceptibility to sifuvirtide.* Antiviral Res, 2010. **86**(3): p. 253-60.
262. Wood, M.P., et al., *A Compensatory Mutation Provides Resistance to Disparate HIV Fusion Inhibitor Peptides and Enhances Membrane Fusion.* PLoS One, 2013. **8**(2): p. e55478.
263. Sullivan, N., et al., *Determinants of human immunodeficiency virus type 1 envelope glycoprotein activation by soluble CD4 and monoclonal antibodies.* J Virol, 1998. **72**(8): p. 6332-8.

264. Lackman-Smith, C., et al., *Development of a comprehensive human immunodeficiency virus type 1 screening algorithm for discovery and preclinical testing of topical microbicides.* Antimicrob Agents Chemother, 2008. **52**(5): p. 1768-81.
265. Bobardt, M.D., et al., *Hepatitis C virus NS5A anchor peptide disrupts human immunodeficiency virus.* Proc Natl Acad Sci U S A, 2008. **105**(14): p. 5525-30.
266. Ruprecht, C.R., et al., *MPER-specific antibodies induce gp120 shedding and irreversibly neutralize HIV-1.* J Exp Med, 2011. **208**(3): p. 439-54.
267. Thali, M., et al., *Lack of correlation between soluble CD4-induced shedding of the human immunodeficiency virus type 1 exterior envelope glycoprotein and subsequent membrane fusion events.* J Virol, 1992. **66**(9): p. 5516-24.
268. Baldwin, C. and B. Berkhout, *HIV-1 drug-resistance and drug-dependence.* Retrovirology, 2007. **4**: p. 78.
269. Lalezari, J.P., et al., *A phase II clinical study of the long-term safety and antiviral activity of enfuvirtide-based antiretroviral therapy.* AIDS, 2003. **17**(5): p. 691-8.
270. Nameki, D., et al., *Mutations conferring resistance to human immunodeficiency virus type 1 fusion inhibitors are restricted by gp41 and Rev-responsive element functions.* J Virol, 2005. **79**(2): p. 764-70.
271. Jiang, S., Q. Zhao, and A.K. Debnath, *Peptide and non-peptide HIV fusion inhibitors.* Curr Pharm Des, 2002. **8**(8): p. 563-80.
272. Liu, S., et al., *HIV gp41 C-terminal heptad repeat contains multifunctional domains. Relation to mechanisms of action of anti-HIV peptides.* J Biol Chem, 2007. **282**(13): p. 9612-20.
273. Chien, M.P., S. Jiang, and D.K. Chang, *The function of coreceptor as a basis for the kinetic dissection of HIV type 1 envelope protein-mediated cell fusion.* FASEB J, 2008. **22**(4): p. 1179-92.
274. Dimitrov, A.S., et al., *Exposure of the membrane-proximal external region of HIV-1 gp41 in the course of HIV-1 envelope glycoprotein-mediated fusion.* Biochemistry, 2007. **46**(5): p. 1398-401.
275. Shen, X., et al., *Prolonged exposure of the HIV-1 gp41 membrane proximal region with L669S substitution.* Proc Natl Acad Sci U S A, 2010. **107**(13): p. 5972-7.
276. Kahle, K.M., H.K. Steger, and M.J. Root, *Asymmetric deactivation of HIV-1 gp41 following fusion inhibitor binding.* PLoS Pathog, 2009. **5**(11): p. e1000674.
277. Hermann, F.G., et al., *Mutations in gp120 contribute to the resistance of human immunodeficiency virus type 1 to membrane-anchored C-peptide maC46.* J Virol, 2009. **83**(10): p. 4844-53.
278. Park, E.J., et al., *Mutations in both gp120 and gp41 are responsible for the broad neutralization resistance of variant human immunodeficiency virus type 1 MN to antibodies directed at V3 and non-V3 epitopes.* J Virol, 1998. **72**(9): p. 7099-107.
279. Johnson, V.A., et al., *Update of the drug resistance mutations in HIV-1: March 2013.* Top Antivir Med, 2013. **21**(1): p. 6-14.
280. Nichols, W.K., et al., *3-methylindole-induced toxicity to human bronchial epithelial cell lines.* Toxicol Sci, 2003. **71**(2): p. 229-36.
281. Nasrolahi Shirazi, A., et al., *Surface decorated gold nanoparticles by linear and cyclic peptides as molecular transporters.* Mol Pharm, 2013. **10**(8): p. 3137-51.

282. Date, A.A. and C.J. Destache, *A review of nanotechnological approaches for the prophylaxis of HIV/AIDS.* Biomaterials, 2013. **34**(26): p. 6202-28.
283. Frens, G., *Controlled nucleation for the regulation of the particle size in monodisperse gold suspensions.* Nature, 1973. **241**: p. 2.
284. Haiss, W., et al., *Determination of size and concentration of gold nanoparticles from UV-vis spectra.* Anal Chem, 2007. **79**(11): p. 4215-21.
285. Xie, H., et al., *Critical flocculation concentrations, binding isotherms, and ligand exchange properties of peptide-modified gold nanoparticles studied by UV-visible, fluorescence, and time-correlated single photon counting spectroscopies.* Anal Chem, 2003. **75**(21): p. 5797-805.
286. He, J., et al., *Human immunodeficiency virus type 1 viral protein R (Vpr) arrests cells in the G2 phase of the cell cycle by inhibiting p34cdc2 activity.* J Virol, 1995. **69**(11): p. 6705-11.
287. Crooks, E.T., et al., *Enzyme digests eliminate nonfunctional Env from HIV-1 particle surfaces, leaving native Env trimers intact and viral infectivity unaffected.* J Virol, 2011. **85**(12): p. 5825-39.
288. Chojnacki, J., et al., *Maturation-dependent HIV-1 surface protein redistribution revealed by fluorescence nanoscopy.* Science, 2012. **338**(6106): p. 524-8.
289. Muranyi, W., et al., *Super-resolution microscopy reveals specific recruitment of HIV-1 envelope proteins to viral assembly sites dependent on the envelope C-terminal tail.* PLoS Pathog, 2013. **9**(2): p. e1003198.
290. Kim, T., et al., *Control of gold nanoparticle aggregates by manipulation of interparticle interaction.* Langmuir, 2005. **21**(21): p. 9524-8.
291. Johnson, K.L. and J.A. Greenwood, *An Adhesion Map for the Contact of Elastic Spheres.* J Colloid Interface Sci, 1997. **192**(2): p. 326-33.
292. Kanjanaboos, P., et al., *Strain patterning and direct measurement of Poisson's ratio in nanoparticle monolayer sheets.* Nano Lett, 2011. **11**(6): p. 2567-71.
293. Wampler, H.P. and A. Ivanisevic, *Nanoindentation of gold nanoparticles functionalized with proteins.* Micron, 2009. **40**(4): p. 444-8.
294. Sun, S.X. and D. Wirtz, *Mechanics of enveloped virus entry into host cells.* Biophys J, 2006. **90**(1): p. L10-2.
295. Kol, N., et al., *A stiffness switch in human immunodeficiency virus.* Biophys J, 2007. **92**(5): p. 1777-83.
296. Friedman, E.J., et al., *Prediction of protein-protein interfaces on G-protein beta subunits reveals a novel phospholipase C beta2 binding domain.* J Mol Biol, 2009. **392**(4): p. 1044-54.
297. Ivanovska, I.L., et al., *Discrete fracture patterns of virus shells reveal mechanical building blocks.* Proc Natl Acad Sci U S A, 2011. **108**(31): p. 12611-6.
298. Xu, Y., et al., *A novel approach to inhibit HIV-1 infection and enhance lysis of HIV by a targeted activator of complement.* Virol J, 2009. **6**: p. 123.
299. Nakamura, M., et al., *Virolysis and in vitro neutralization of HIV-1 by humanized monoclonal antibody hNM-01.* Hybridoma, 2000. **19**(6): p. 427-34.
300. Contarino, M., et al., *Chimeric Cyanovirin-MPER recombinantly engineered proteins cause cell-free virolysis of HIV-1.* Antimicrob Agents Chemother, 2013. **57**(10): p. 4743-50.

301. Zhang, L., et al., *Nanoparticles in medicine: therapeutic applications and developments.* Clin Pharmacol Ther, 2008. **83**(5): p. 761-9.
302. Hamidi, M., et al., *A pharmacokinetic overview of nanotechnology-based drug delivery systems: an ADME-oriented approach.* Crit Rev Ther Drug Carrier Syst, 2013. **30**(5): p. 435-67.
303. Heidel, J.D. and M.E. Davis, *Clinical developments in nanotechnology for cancer therapy.* Pharm Res, 2011. **28**(2): p. 187-99.
304. Jiang, W., et al., *Nanoparticle-mediated cellular response is size-dependent.* Nat Nanotechnol, 2008. **3**(3): p. 145-50.
305. Mamo, T., et al., *Emerging nanotechnology approaches for HIV/AIDS treatment and prevention.* Nanomedicine (Lond), 2010. **5**(2): p. 269-85.
306. Mahmoud, K.A. and J.H. Luong, *Impedance method for detecting HIV-1 protease and screening for its inhibitors using ferrocene-peptide conjugate/Au nanoparticle/single-walled carbon nanotube modified electrode.* Anal Chem, 2008. **80**(18): p. 7056-62.
307. Poignard, P., et al., *Heterogeneity of envelope molecules expressed on primary human immunodeficiency virus type 1 particles as probed by the binding of neutralizing and nonneutralizing antibodies.* J Virol, 2003. **77**(1): p. 353-65.
308. Mannheimer, S.B., et al., *Quality of life in HIV-infected individuals receiving antiretroviral therapy is related to adherence.* AIDS Care, 2005. **17**(1): p. 10-22.
309. Ferguson, T.F., et al., *Patient-perceived barriers to antiretroviral adherence: associations with race.* AIDS Care, 2002. **14**(5): p. 607-17.
310. Douek, D.C., P.D. Kwong, and G.J. Nabel, *The rational design of an AIDS vaccine.* Cell, 2006. **124**(4): p. 677-81.
311. McGowan, I., *The development of rectal microbicides for HIV prevention.* Expert Opin Drug Deliv, 2014. **11**(1): p. 69-82.
312. D'Cruz, O.J. and F.M. Uckun, *Vaginal microbicides and their delivery platforms.* Expert Opin Drug Deliv, 2014. **11**(5): p. 723-40.
313. Checkley, M.A., B.G. Luttge, and E.O. Freed, *HIV-1 envelope glycoprotein biosynthesis, trafficking, and incorporation.* J Mol Biol, 2011. **410**(4): p. 582-608.
314. Dadachova, E., et al., *Targeted killing of virally infected cells by radiolabeled antibodies to viral proteins.* PLoS Med, 2006. **3**(11): p. e427.
315. McHugh, L., et al., *Increased affinity and stability of an anti-HIV-1 envelope immunotoxin by structure-based mutagenesis.* J Biol Chem, 2002. **277**(37): p. 34383-90.
316. Brooks, D.G., et al., *Molecular characterization, reactivation, and depletion of latent HIV.* Immunity, 2003. **19**(3): p. 413-23.
317. Coleman, C.M. and L. Wu, *HIV interactions with monocytes and dendritic cells: viral latency and reservoirs.* Retrovirology, 2009. **6**: p. 51.
318. Briant, L., et al., *Binding of HIV-1 virions or gp120-anti-gp120 immune complexes to HIV-1-infected quiescent peripheral blood mononuclear cells reveals latent infection.* J Immunol, 1996. **156**(10): p. 3994-4004.
319. Gopi, H., et al., *Introducing metallocene into a triazole peptide conjugate reduces its off-rate and enhances its affinity and antiviral potency for HIV-1 gp120.* Journal of Molecular Recognition, 2009. **22**(2): p. 169-174.

320. Sullivan, N., et al., *CD4-Induced conformational changes in the human immunodeficiency virus type 1 gp120 glycoprotein: consequences for virus entry and neutralization.* J Virol, 1998. **72**(6): p. 4694-703.
321. Moore, P.L., et al., *Nature of nonfunctional envelope proteins on the surface of human immunodeficiency virus type 1.* J Virol, 2006. **80**(5): p. 2515-28.
322. Blankson, J.N., D. Persaud, and R.F. Siliciano, *The challenge of viral reservoirs in HIV-1 infection.* Annu Rev Med, 2002. **53**: p. 557-93.
323. Kent, S.J., et al., *The search for an HIV cure: tackling latent infection.* Lancet Infect Dis, 2013. **13**(7): p. 614-21.
324. Burton, D.R., et al., *HIV vaccine design and the neutralizing antibody problem.* Nat Immunol, 2004. **5**(3): p. 233-6.
325. McMichael, A.J., *HIV vaccines.* Annu Rev Immunol, 2006. **24**: p. 227-55.
326. Shiver, J.W. and E.A. Emini, *Recent advances in the development of HIV-1 vaccines using replication-incompetent adenovirus vectors.* Annu Rev Med, 2004. **55**: p. 355-72.
327. Thorner, A.R. and D.H. Barouch, *HIV-1 vaccine development: progress and prospects.* Curr Infect Dis Rep, 2007. **9**(1): p. 71-5.
328. Sekaly, R.P., *The failed HIV Merck vaccine study: a step back or a launching point for future vaccine development?* J Exp Med, 2008. **205**(1): p. 7-12.
329. Kwong, P.D., J.R. Mascola, and G.J. Nabel, *Rational design of vaccines to elicit broadly neutralizing antibodies to HIV-1.* Cold Spring Harb Perspect Med, 2011. **1**(1): p. a007278.
330. Moore, J.P., P.W. Parren, and D.R. Burton, *Genetic subtypes, humoral immunity, and human immunodeficiency virus type 1 vaccine development.* J Virol, 2001. **75**(13): p. 5721-9.
331. Balzarini, J., *Targeting the glycans of gp120: a novel approach aimed at the Achilles heel of HIV.* Lancet Infect Dis, 2005. **5**(11): p. 726-31.
332. Harris, A., et al., *Trimeric HIV-1 glycoprotein gp140 immunogens and native HIV-1 envelope glycoproteins display the same closed and open quaternary molecular architectures.* Proc Natl Acad Sci U S A, 2011. **108**(28): p. 11440-5.
333. Sattentau, Q.J., *Envelope Glycoprotein Trimers as HIV-1 Vaccine Immunogens.* Vaccines, 2013. **1**(4): p. 497-512.
334. Walker, L.M. and D.R. Burton, *Rational antibody-based HIV-1 vaccine design: current approaches and future directions.* Current opinion in immunology, 2010. **22**(3): p. 358-366.
335. Zwick, M.B., et al., *Anti-human immunodeficiency virus type 1 (HIV-1) antibodies 2F5 and 4E10 require surprisingly few crucial residues in the membrane-proximal external region of glycoprotein gp41 to neutralize HIV-1.* J Virol, 2005. **79**(2): p. 1252-1261.
336. Hessell, A.J., et al., *Broadly neutralizing monoclonal antibodies 2F5 and 4E10 directed against the human immunodeficiency virus type 1 gp41 membrane-proximal external region protect against mucosal challenge by simian-human immunodeficiency virus SHIVBa-L.* J Virol, 2010. **84**(3): p. 1302-1313.
337. Huang, J., et al., *Broad and potent neutralization of HIV-1 by a gp41-specific human antibody.* Nature, 2012. **491**(7424): p. 406-12.

338. Ofek, G., et al., *Structure and mechanistic analysis of the anti-human immunodeficiency virus type 1 antibody 2F5 in complex with its gp41 epitope.* J Virol, 2004. **78**(19): p. 10724-37.
339. Zwick, M.B., et al., *Anti-human immunodeficiency virus type 1 (HIV-1) antibodies 2F5 and 4E10 require surprisingly few crucial residues in the membrane-proximal external region of glycoprotein gp41 to neutralize HIV-1.* J Virol, 2005. **79**(2): p. 1252-61.
340. Summers, M.F., et al., *Nucleocapsid zinc fingers detected in retroviruses: EXAFS studies of intact viruses and the solution-state structure of the nucleocapsid protein from HIV-1.* Protein Sci, 1992. **1**(5): p. 563-74.
341. Briggs, J.A., et al., *Structural organization of authentic, mature HIV-1 virions and cores.* EMBO J, 2003. **22**(7): p. 1707-15.
342. Ganser-Pornillos, B.K., A. Cheng, and M. Yeager, *Structure of full-length HIV-1 CA: a model for the mature capsid lattice.* Cell, 2007. **131**(1): p. 70-9.
343. Forshey, B.M., et al., *Formation of a human immunodeficiency virus type 1 core of optimal stability is crucial for viral replication.* J Virol, 2002. **76**(11): p. 5667-77.
344. Byeon, I.J., et al., *Structural convergence between Cryo-EM and NMR reveals intersubunit interactions critical for HIV-1 capsid function.* Cell, 2009. **139**(4): p. 780-90.
345. Davis, M.R., et al., *A mutation in the human immunodeficiency virus type 1 Gag protein destabilizes the interaction of the envelope protein subunits gp120 and gp41.* J Virol, 2006. **80**(5): p. 2405-17.
346. Gamble, T.R., et al., *Crystal structure of human cyclophilin A bound to the amino-terminal domain of HIV-1 capsid.* Cell, 1996. **87**(7): p. 1285-94.
347. Momany, C., et al., *Crystal structure of dimeric HIV-1 capsid protein.* Nat Struct Biol, 1996. **3**(9): p. 763-70.
348. Yang, R., et al., *Second-site suppressors of HIV-1 capsid mutations: restoration of intracellular activities without correction of intrinsic capsid stability defects.* Retrovirology, 2012. **9**: p. 30.
349. Briggs, J.A., et al., *Structure and assembly of immature HIV.* Proc Natl Acad Sci U S A, 2009. **106**(27): p. 11090-5.
350. Pang, H.B., et al., *Virion stiffness regulates immature HIV-1 entry.* Retrovirology, 2013. **10**: p. 4.
351. Forshey, B.M., J. Shi, and C. Aiken, *Structural requirements for recognition of the human immunodeficiency virus type 1 core during host restriction in owl monkey cells.* J Virol, 2005. **79**(2): p. 869-75.
352. Jiang, J. and C. Aiken, *Maturation-dependent human immunodeficiency virus type 1 particle fusion requires a carboxyl-terminal region of the gp41 cytoplasmic tail.* J Virol, 2007. **81**(18): p. 9999-10008.
353. Wyma, D.J., et al., *Coupling of human immunodeficiency virus type 1 fusion to virion maturation: a novel role of the gp41 cytoplasmic tail.* J Virol, 2004. **78**(7): p. 3429-35.
354. Campbell, S. and V.M. Vogt, *In vitro assembly of virus-like particles with Rous sarcoma virus Gag deletion mutants: identification of the p10 domain as a*

morphological determinant in the formation of spherical particles. J Virol, 1997. **71**(6): p. 4425-35.
355. Fuller, S.D., et al., *Cryo-electron microscopy reveals ordered domains in the immature HIV-1 particle.* Curr Biol, 1997. **7**(10): p. 729-38.
356. Peng, C., et al., *Role of human immunodeficiency virus type 1-specific protease in core protein maturation and viral infectivity.* J Virol, 1989. **63**(6): p. 2550-6.
357. Hu, Q., et al., *Blockade of attachment and fusion receptors inhibits HIV-1 infection of human cervical tissue.* J Exp Med, 2004. **199**(8): p. 1065-75.
358. Schwieters, C.D., et al., *The Xplor-NIH NMR molecular structure determination package.* J Magn Reson, 2003. **160**(1): p. 65-73.
359. Wang, C.T., Y.C. Chou, and C.C. Chiang, *Assembly and processing of human immunodeficiency virus Gag mutants containing a partial replacement of the matrix domain by the viral protease domain.* J Virol, 2000. **74**(7): p. 3418-22.
360. Flexner, C., *HIV-protease inhibitors.* N Engl J Med, 1998. **338**(18): p. 1281-92.
361. Wensing, A.M., N.M. van Maarseveen, and M. Nijhuis, *Fifteen years of HIV Protease Inhibitors: raising the barrier to resistance.* Antiviral Res, 2010. **85**(1): p. 59-74.
362. Markosyan, R.M., F.S. Cohen, and G.B. Melikyan, *HIV-1 envelope proteins complete their folding into six-helix bundles immediately after fusion pore formation.* Mol Biol Cell, 2003. **14**(3): p. 926-38.
363. Blumenthal, R., S. Durell, and M. Viard, *HIV entry and envelope glycoprotein-mediated fusion.* J Biol Chem, 2012. **287**(49): p. 40841-9.
364. Archin, N.M. and D.M. Margolis, *Emerging strategies to deplete the HIV reservoir.* Curr Opin Infect Dis, 2014. **27**(1): p. 29-35.
365. Chun, T.W. and A.S. Fauci, *Latent reservoirs of HIV: obstacles to the eradication of virus.* Proc Natl Acad Sci U S A, 1999. **96**(20): p. 10958-61.
366. Zaikos, T.D. and K.L. Collins, *Long-lived reservoirs of HIV-1.* Trends Microbiol, 2014. **22**(4): p. 173-5.
367. Gupta, K.M., et al., *Temperature and pH sensitive hydrogels: an approach towards smart semen-triggered vaginal microbicidal vehicles.* J Pharm Sci, 2007. **96**(3): p. 670-81.
368. Verkoczy, L., G. Kelsoe, and B.F. Haynes, *HIV-1 envelope gp41 broadly neutralizing antibodies: hurdles for vaccine development.* PLoS Pathog, 2014. **10**(5): p. e1004073.

TABLES

Table 1: Potencies of inactivation and breakdown of BaL HIV-1 pseudotyped and replication competent virions by peptide triazoles. The extents of loss of cell infection, p24 release and gp120 shedding were measured for KR13, KR13b, KR13s and HNG156 treatment of BaL pseudovirus. * Designates the EC50 and IC50 values of the viral infection inhibition, gp120 shedding and p24 release, respectively, obtained for fully infectious HIV-1 BaL virions induced by KR13 and HNG156. All of the IC50 and EC50

values were determined from dose response profiles (Figure 17 and Appendix Fig.1) using Origin Pro.8 (Origin Lab). ± designates the standard deviation of the mean, n > 3.

Peptide	**Viral Inactivation** EC_{50} **(nM)**	**p24 Release** IC_{50} **(nM)**	**gp120 Shedding** IC_{50} **(nM)**
HNG156	803 ± 120 *5500 ± 1100	>500,000 *>200,000	500 ± 230 *1800 ± 1000
KR13	23 ± 45 *639 ± 71	500 ± 80 *4400 ± 930	32 ± 20 *1200 ± 930
KR13s	>500,000	>500,000	>500,000
KR13b	52 ± 35	>100,000	120 ± 43

Table 2: Potencies of effects of fusion inhibitors on inactivation and breakdown of BaL HIV-1 pseudotypedvirions by peptide triazoles. The extents of loss of cell infection and p24 release for T20, C34, C37, N36 and 5 Helix treatment of BaL pseudovirus with or without KR13 are summarized. All of the IC50 and EC50 values were determined from dose response profiles (Figure 26) using Origin Pro.8 (Origin Lab). ± designates the standard deviation of the mean, n > 3.

Fusion Inhibitors	IC_{50} of Viral Infection Inhibition		EC_{50} of P24 Release	
	Without KR13 (nM)	With 500 nM KR13 (nM)	Without KR13 (nM)	With 1 μM KR13 (nM)
T20	8.2 ± 1.2	< 0.001	> 5000	0.5 ± 0.2
C34	NA	NA	> 5000	7.84 ± 1.8
C37	65.7 ± 4.6	~ 0.001	> 5000	3230 ± 800
N36	107.3 ± 24.2	~ 0.01	> 5000	3.23 ± 0.8
5 Helix	4.5 ± 0.4	<0.001	> 5000	0.26 ± 0.8

Table 3: Antibody panel against gp120 and their binding sites. The dilution that is specified in the third column is the dilution used for the antibody mapping in Figure 28.

Ab	Binding site	Dilution/conc
CD4	CD4	60nM
F105	CD4	1:1000
F425A1g8	CD4i epitope	1:1000
17b	coreceptor	40µM
VRC03	CD4	1:1000
B12	CD4	1:1000
2D7	coreceptor	1:500
F425B4e8	Base of V3	1:1000
19b	V3 tip	1:1000
39F	V3 N-terminus	1:1000
2G12	V3 mannose	1:1000
447-52D	linear	1:500
ID6	First 204 amino acids of gp120	1:20
D7324	Linear	1:1000
697-30D	V1/V2	1:100

Table 4: Antibody panel against gp41 and their binding sites. The dilution that is specified in the fourth column is the dilution used for the antibody mapping in figure 25.

Antibody Name	Site	Linear/conformational	Dilution Factor
240-D	240D cloning site (644-663)	Conf (Cluster I)	1:1000
246-D	specificity against QQLGIWG with the core being LLGI	Conf (Cluster I)	1:1000
50-69	aa 560-641	Linear Cluster I)	1:500
NC-1	Specific to 6HB	Conf	1:2500
T32	Region 597-613: immunodominant region containing two Cys residues	Conf	1:1000
98-6	SLIEESQNQQEKNEQELLEL with the core being IWG	Linear (Cluster II)	1:500
126-6	Recognized exclusively the trimeric form of envelope glycoproteins (644-663)	Conf (Cluster II)	1:100
D50	642-665 - CHR	Linear (Cluster II)	1:500
167-D	Two immunodominant domain cluster	Conf (Cluster II)	1:100
644-663	Aa 644-663	Conf (Cluster III)	1:2000
2F5	membrane-proximal external region	Conf (Cluster III)	1:2000
Z13e1	membrane-proximal external region	Conf (Cluster III)	1:1000
10-E8	membrane-proximal external region	Conf (Cluser III)	1:2000
4-E10	membrane-proximal external region	Conf (Cluser III)	1:1000

Table 5: A table showing the similarities between KR13 induced virolysis and virus-cell fusion

Peptide triazole thiol (PTT) Induced Virolysis	HIV – Cell fusion	Supporting Data
The steps of HIV-1 virolysis by PTT include gp120 shedding followed by a slower rate limiting p24 release from the viral lumen	**During virus cell fusion the rate limiting step is the relative content mixing of the virion and cell membrane release of the p24 core of the virion into the cell lumen**	**Figure 20 and Figure 21, Chien et al. 2008**
Gp120 is shed off from the virion surface post PTT binding	**Gp120 is shed off from the virion post CD4 binding**	**Figure 17, 18 and 20 Moore et al. 1990 and Haim et al. 2009**
The gp41 on the HIV virion post PTT treatment leads to MPER exposure	**The gp41 on the HIV virion post CD4 and coreceptor binding leads to MPER exposure**	**Figure 21, Dimitrov et al. 2007, Monetro et al. 2008**
Fusion Inhibitors inhibit PTT induced virolysis	**Fusion inhibitors inhibit HIV-cell fusion**	**Figure 22 and Figure 26, Chan et al. 1998**

Table 6: Potencies of inactivation and breakdown of BaL HIV-1 pseudotyped AuNP-KR13 conjugates of different diameters. The extents of loss of cell infection and p24 release AuNP-KR13 treatment of BaL pseudovirus. The average numbers of peptides per AuNP were measured using amino acid analysis and the peptide coverage per nm^2 was calculated. All of the IC_{50} and EC_{50} values were determined from dose response profiles (Figure 31) using Origin Pro.8 (Origin Lab). ± designates the standard deviation of the mean, n > 3.

Diameter	**Viral infection inhibition IC_{50} (nM)**	**p24 release EC_{50} (nM)**	**Average Number of peptides per AuNP**	**Peptide density per nm^2**
13.2nm	60 ± 10	10.94735 ± 1.66	34	0.062
19.9nm	0.9 ±0.2	14.1626 ± 1.52	73	0.059
42.8nm	0.18 ± 0.1	12.09586 ± 0.83	139	0.024
92.6nm	0.02 ± 0.01	9.85039 ± 0.61	220	0.008
123.4nm	0.01 ± 0.01	5.70828 ± 0.60	652	0.014

Table 7: Potencies of inactivation and breakdown of BaL HIV-1 pseudotyped AuNP-KR13 conjugates with varying peptide coverage density. The extents of loss of cell infection and p24 release AuNP-KR13 treatment of BaL pseudovirus. The average number of peptides per AuNP were measured using amino acid analysis and the peptide coverage per nm^2 was calculated. All of the IC_{50} and EC_{50} values were determined from dose response profiles (Figure 33) using Origin Pro.8 (Origin Lab). ± designates the standard deviation of the mean, n > 3.

No of KR13 Per AuNP	**Viral infection inhibition IC50 (nM)**	**p24 release EC50 (nM)**	**Peptide density per nm^2**
68.6	0.42 nM	1.64 nM	0.055
28.8	1.1 nM	6.2 nM	0.023
10.9	8.1 nM	19.5 nM	0.009
0	>50 nM AuNP	>50 nM AuNP	NA

Table 8: Potencies of inactivation and breakdown of BaL HIV-1 pseudotyped AuNP-KR13 conjugates of different diameters with same amount of peptide per nm^2. The extents of loss of cell infection and p24 release AuNP-KR13 treatment of BaL pseudovirus. The average number of peptides per AuNP were measured using amino acid analysis and the peptide coverage per nm^2 was calculated. All of the IC_{50} and EC_{50} values were determined from dose response profiles (Figure 33) using Origin Pro.8 (Origin Lab). ± designates the standard deviation of the mean, n > 3.

Inhibitor Used	Viral Infection Inhibtion IC50 (nM)	P24 release EC50 (nM)	Coverage density (no. of peptides)	Peptide density per nm^2
KR13	196.6 ± 36.29	3250 ± 567	1	1
AuNP-KR13 (20.2 nm)	5.3 ± 1.14	9.7 ± 1.07	96	0.075
AuNP-KR13 (42.3 nm)	0.7 ± 0.14	1.2 ± 2.5	430	0.077
AuNP-KR13 (80.2 nm)	0.05 ± 0.06	0.2 ± 0.4	1387	0.069

Table 9: Potencies of inactivation and breakdown of BaL HIV-1 pseudotyped AuNP-KR13 (20.2 nm) conjugate (left) and KR13 alone (right) with HIV-1 pseudotyped with increasing amount of mutant spikes (S375W). The extents of loss of cell infection and p24 release AuNP-KR13 treatment of BaL pseudovirus. The amount of spike density was calculated as shown in methods section 4.1 and summarized in figure 36. All of the IC50 and EC50 values were determined from dose response profiles (Figure 36) using Origin Pro.8 (Origin Lab). ± designates the standard deviation of the mean, n > 3.

AuNP-KR13

µg of DNA BAL01 WT-S375W	IC50 of Viral Infection Inhibition (nM)	EC50 of p24 Release (nM)
0-4	NA	NA
0.5-3.5	2930 ± 316	215.1 ± 89.6
1-3	469.6 ± 67	159.9 ± 39.5
2-2	151.4 ± 60	22.5 ± 1.6
3-1	40.6 ± 4.3	10.2 ± 0.8
3.5-0.5	16.5 ± 2.2	1.8 ± 0.3
4-0	10.4 ± 2.6	1.3 ± 0.1

KR13

µg of DNA BAL01 WT-S375W	IC50 of Viral Infection Inhibition (nM)	EC50 of p24 Release (µM)
0-4	NA	NA
0.5-3.5	22800 ± 3191	NA
1-3	1412.8 ± 213.3	NA
2-2	614.1 ± 89.4	4.26 ± 0.32
3-1	243.4 ± 32.1	6.03 ± 0.54
3.5-0.5	119.2 ± 45.6	6.74 ± 1.31
4-0	53.2 ± 12.8	3.10 ± 2.5

Table 10: A table summarizing the differences between KR13 and AuNP-KR13

Similarities	Differences	Supporting Data
Both p24 and gp120 is released from the HIV-1 virion post treatment	**AuNP-KR13 treatment has a faster rate of both p24 and gp120 release from the virion compared to KR13**	**Figure 35**
Lead to morphological alteration to the virion	**The physical effect of AuNP-KR13 on the virion is more dramatic and irregular compared to KR13 which gives more shrunken particles**	**Appendix Fig. 4 and Appendix Fig. 13**
The gp41 remains on the virion post treatment	**AuNP-KR13 treatment does not expose MPER on gp41**	**Figure 21 and Figure 35**
Both result in gp120 shedding from the HIV-1 producer cells leading to inactive virus production	**AuNP-KR13 treatment also leads to cytotoxicity and eventually death of these virus producer cells**	**Figure 39, Figure 40**
The p24 release is only observed with peptide triazoles with thiol	**The free thiol on KR13 is important for virolysis only for KR13 alone and not AuNP-KR13. The p24 release by KR13 is inhibited by DTNB and 2G12, blocking free thiols as well as disufide rich regions of gp120.**	**Figure not shown The thiol for KR13 is important for function**

6 APPENDIX

Control optical biosensor analysis to rule out non-specific T20-KR13 interaction:
As part of confirmation of the specificity of the T20 inhibition of HIV-1 lytic deformation by KR13, a competition surface plasmon resonance experiment was conducted. Since T20 requires a small amount of DMSO for adequate solubility, all of the SPR experiments with T20 were conducted in PBS + 0.005% Tween-20 containing 2% DMSO as running buffer. Direct binding of KR13 and T20 respectively was also conducted separately by injecting 0.3 nM to 156 nM of the above peptides in 2% DMSO-containing buffer over the gp120 surface. This was done to monitor the binding of the peptides in the presence of 2% DMSO (**Appendix Fig. 5**). For KR13/T20 competition experiments, serial dilutions of the T20 (starting from 5 μM) with a constant concentration of KR13 (300 nM) were pre-mixed for 30 minutes and injected over the gp120 surface. Controls included buffer alone, KR13s (300 nM) alone and T20 (5 μM) alone. Data were fit to the Langmuir 1:1 binding equation to estimate steady state affinity in BiaEvaluation version 4.0 (GE) (direct binding) as noted above. The sensorgrams obtained (**Appendix Fig. 5**) demonstrated lack of interference of KR13 binding to gp120 by T20. This is consistent with lack of nonspecific binding of T20 to KR13.

Cell-Culture and Cytotoxicity Test:

The AuNP-KR13 conjugates were tested for stability in physiological conditions (**Appendix Fig. 9A**), as well as cytotoxicity test in vitro using the using the tetrazolium salt premix reagent, WST-1 from Takara Bio Inc. following the manufacturer's protocol. The formazan product was measured using the microplate reader at absorbance wavelenght 460 nm (Molecular Devices) (**Appendix Fig. 9B**).

APPENDIX FIGURES

Figure 1: Western blot gel images showing gp120 shedding from HIV-1_{BaL} pseudovirus as a function of dose of KR13, HNG156, KR13b and KR13s. The western blots were stained using the primary anti-gp120 antibody D7324 and secondary anti-sheep HRP. Controls shown were intact virus (IV, treated with PBS) and recombinant gp120(200 ng/ml). The gp120 control was the YU2 recombinant gp120 obtained by 293F cell expression and contains monomeric and aggregate bands as observed previously [25]. The gp120 from the virions ran at a different size compared to the monomeric gp120 most likely due to a different extent of glycosylation on the surface of these proteins when expressed in 293T cells.

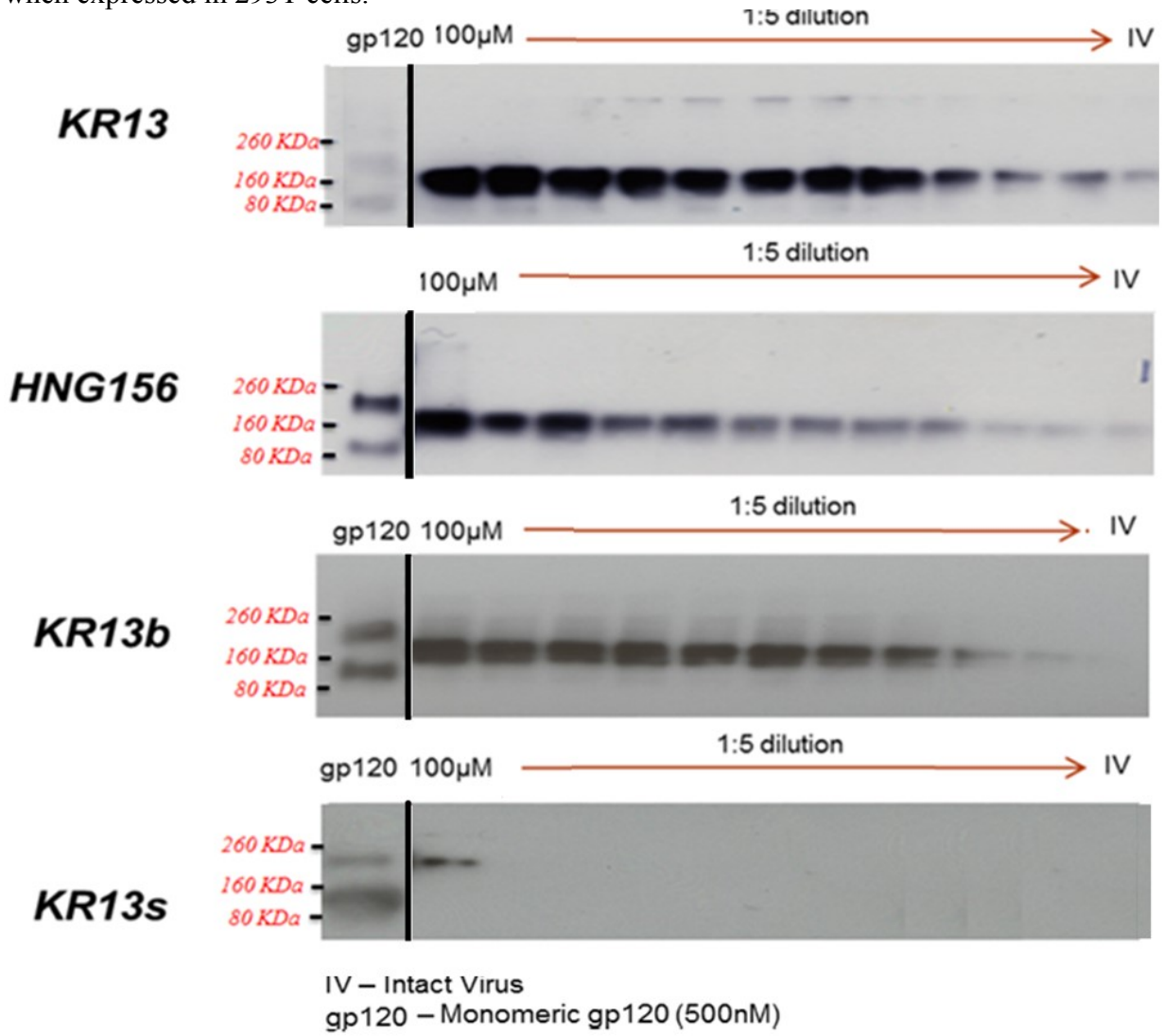

Figure 2: Inhibition of infection of HOS $CD4^{+ve}$ $CCR5^{+ve}$ cells by recombinant viruses pseudotyped with the envelope for VSV-G (**a**) and AMLV (**b**) by the peptides HNG156, KR13, KR13b and KR13s at concentrations ranging from 250µM to 0.01 nM. The data were normalized to 100% infection activity in the absence of peptide triazole.

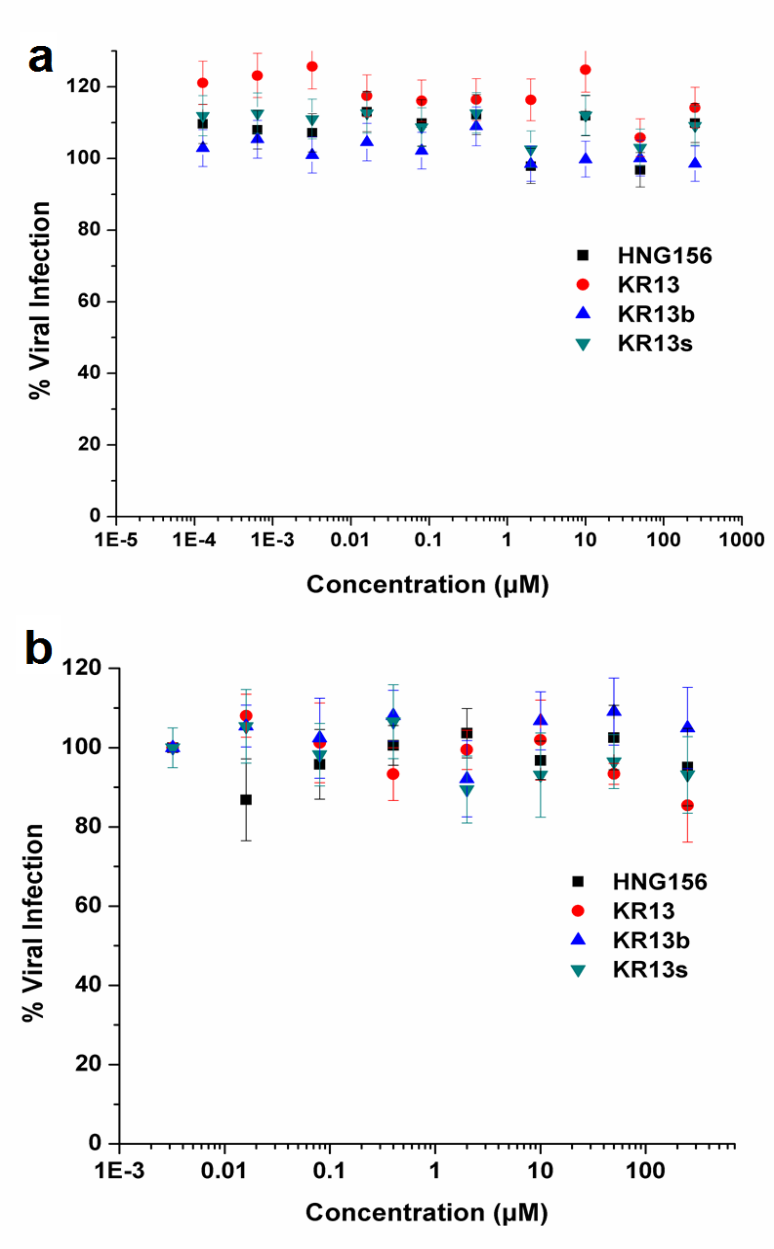

Figure 3: Measurement of gp41 content in HIV-1 BaL pseudotype treated with KR13 and HNG156, respectively, as detected by mAb 98-6. Soluble protein (6% Optiprep) and residual virion (18.2 - 19% Optiprep) fractions of the gradient purified, peptide treated virus (HIV-1 BaL pseudotyped) were separated by polyacrylamide gel electrophoresis and transferred to a PVDF membrane. Bands were detected with anti-gp41 mAb 98-6. Band intensities were normalized to total gp41 content present in intact virus control (virus treated with PBS). Error bars represent the standard deviation of the mean, n = 3.

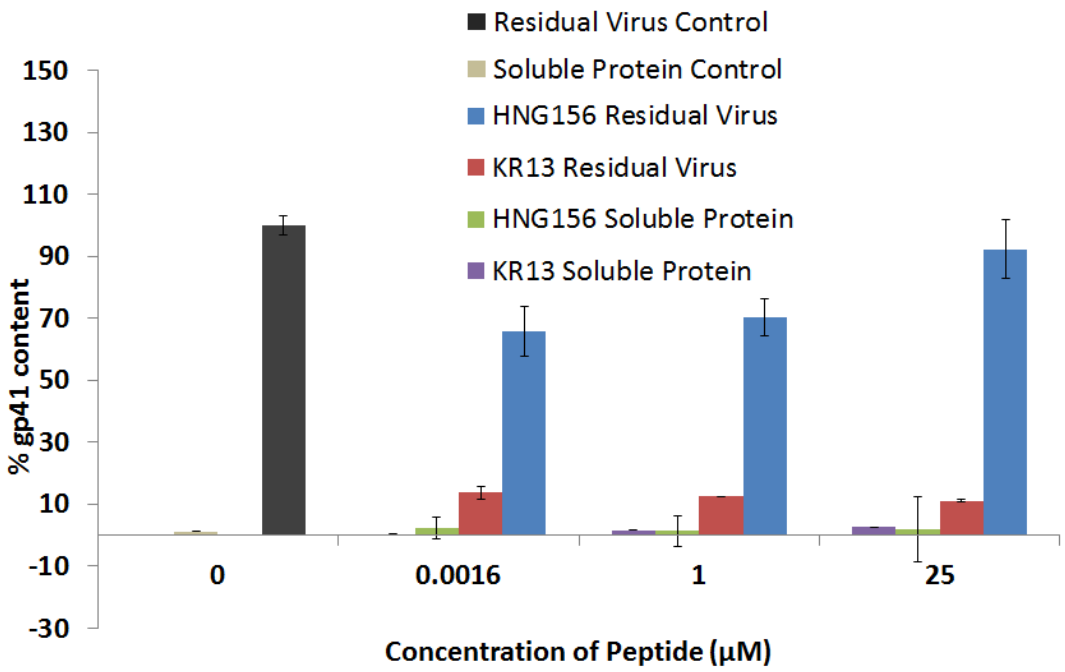

Figure 4: Raw TEM images used to determine the diameter distributions in Figure 21. The intact virus field was obtained for viruses treated with PBS for 30 minutes at 37 °C before fixing the virions with 0.1% paraformaldehyde and loading on epoxy for TEM analysis. Separate samples of virions were treated for 30, 720 and 1440 minutes with KR13 at 37 °C before fixing with paraformaldehyde. The epoxy samples were cut into 100 nm thick slices using a Leica EM UC6 Cryo-ultramicrotome and loaded onto a holey carbon TEM 200 mesh grid for TEM analysis. The grids were stained with 1% uranyl acetate and loaded onto the JEM 2100 microscope system (JEOL, Japan) operated at 120 kV.

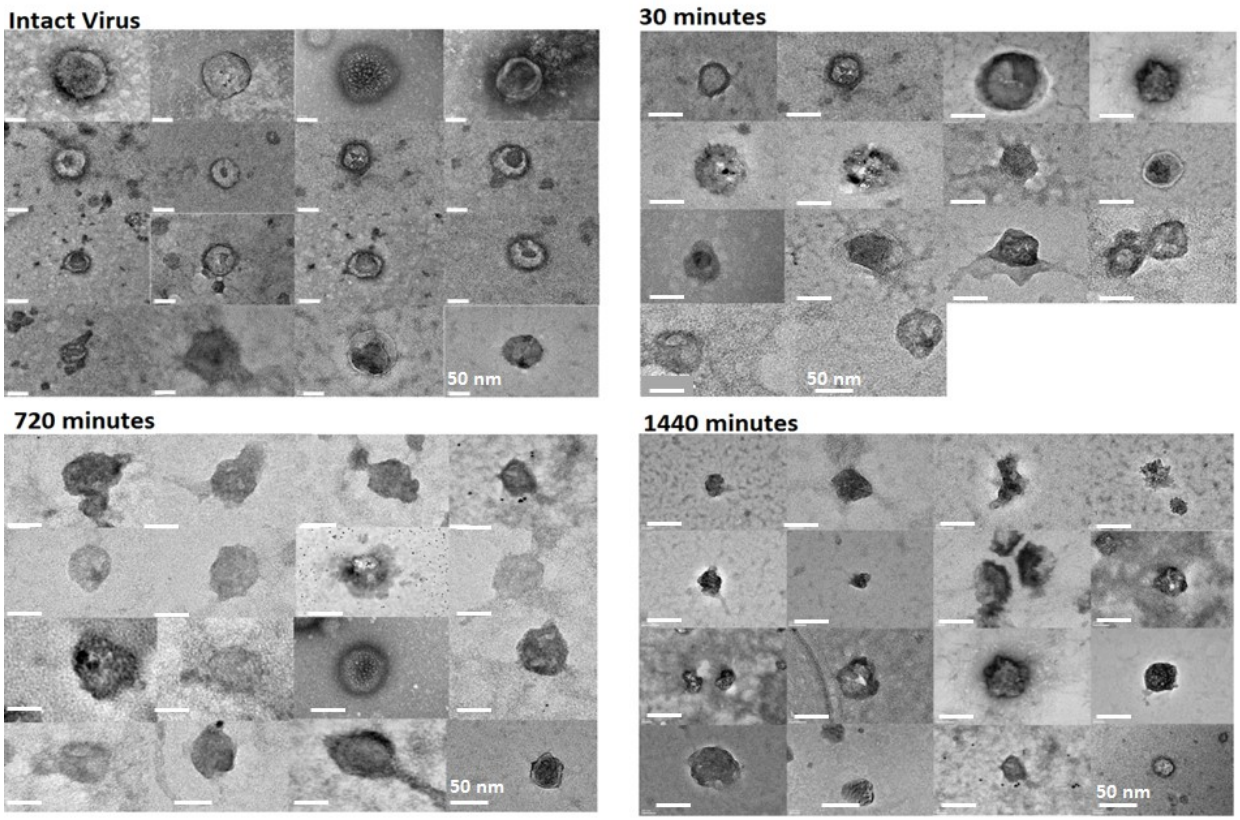

Figure 5: SPR analysis to test for possible artifactual binding of T20 to KR13. All the samples were diluted in buffer that contained 2% DMSO and 0.005% tween 20 due to the low solubility of T20 in SPR buffer alone. (a) Sensorgrams for direct binding of KR13 to chip-immobilized soluble WT YU2 gp120. Data show proportionally increasing binding responses to immobilized gp120 at increasing concentrations of KR13. (b) Steady state fit analysis of the R_{eq} values for each concentration of the peptide from (a) calculated using the BiaEvaluation software, with separate k_{on} and k_{off} fit analysis using the Langmuir equation described in Appendix Text section (c) Sensorgrams for direct KR13 binding to chip-immobilized gp120 in the presence of T20. Samples of T20 (0 µM to 5 µM – shown in the legend) and constant concentration of KR13 (300 nM) were pre-mixed (30 min) and injected into the sensor flow cell. The binding profiles were observed on the same WT monomeric gp120 chip as in (a). As a baseline control, PBS (Buffer) alone was injected, T20 at 5 µM and KR13s at 300 nM were used as a negative controls. Data show lack of significant dose-dependent effect of T20 on KR13 binding to gp120. The negative control surface used was chip immobilized with non-specific EGFR antibody cetuximab. All curves were plotted using Biaevaluation 4.0 software (GE).

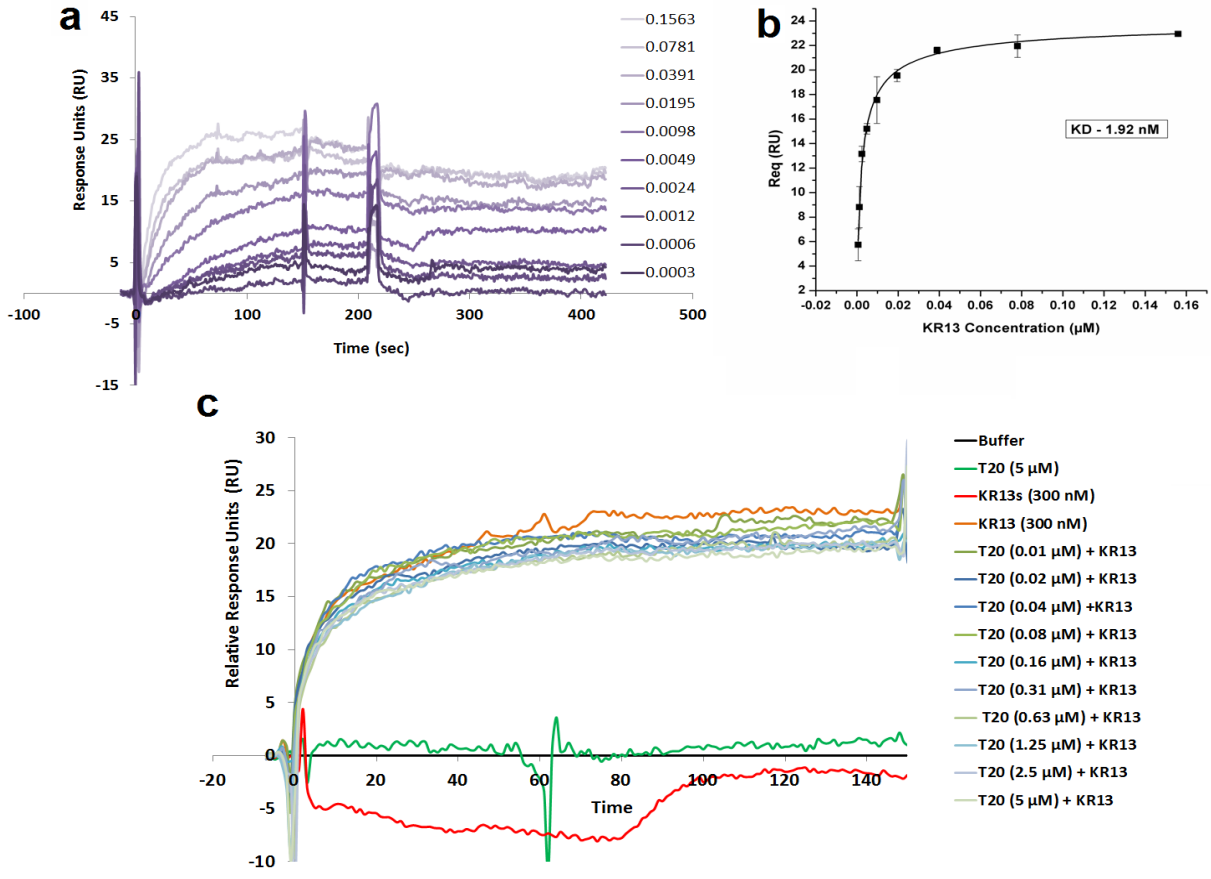

Figure 6: Dose responses of the effects of peptide triazoles, KR13 and HNG156 on HIV-1 BaL pseudovirus induced infection inhibition of HOS $CD4^{+ve}$ $CCR5^{+ve}$ and HOS $CD4^{-ve}$ $CCR5^{+ve}$ cells. Extent of cell infection was measured using a single round infection assay. Origin Pro. 8 was used for sigmoidal curve fitting, n=3. The x-axis represents Relative Luminescence Units (RLU) which was calculated by subtracting the background signal (approximately 120 RLU).

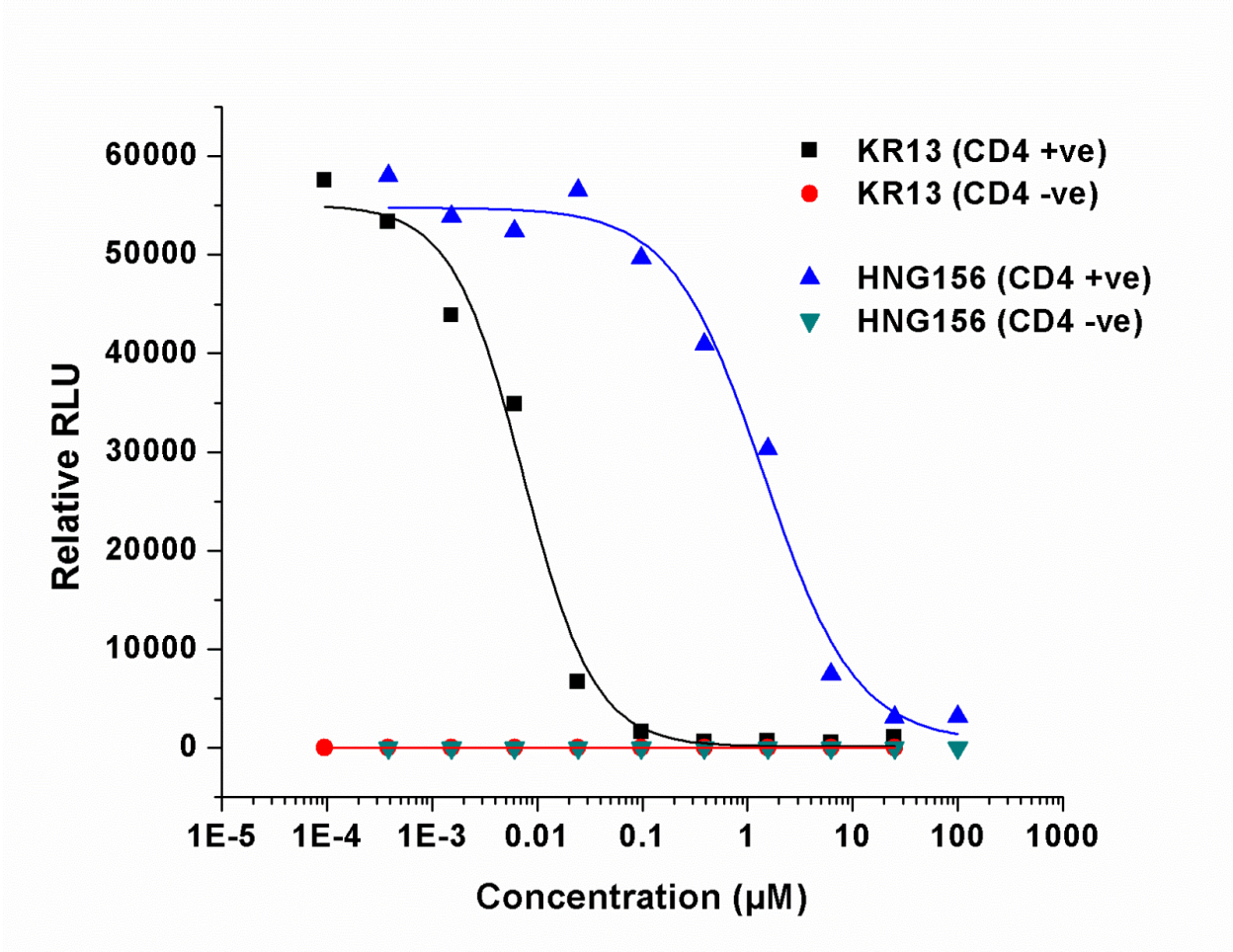

Figure 7: Viral infection inhibition of the T20 resistant mutant viruses by (A) T20 and (B) KR13. The data were normalized to 100% infection activity in the absence of peptide triazole. Origin Pro. 8 was used for sigmoidal curve fitting, n=3.

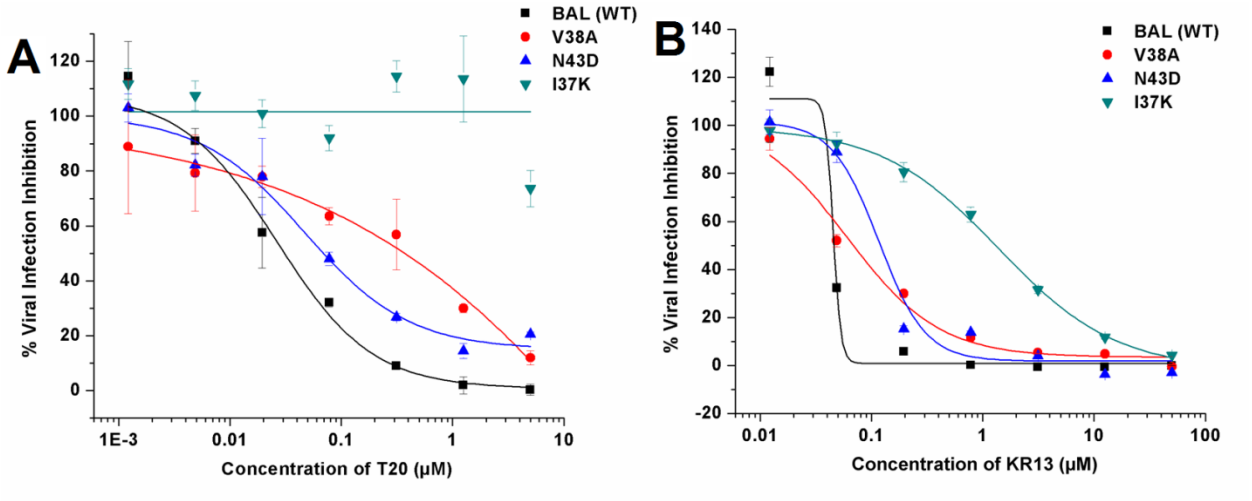

Figure 8: (A) Stability of the gold and gold conjugates in physiological conditions shown in x-axis. The absorbance peak of the AuNP, AuNP-KR13 (20 nm diameter) as well as AuNP:BSPP at different physiological conditions, Phosphate Buffer (PB), DI-water, PBS, NaCl (17 mM) and HOS $CD4^{+ve}$ $CCR5^{+ve}$ growth media. **(B)** Cell toxicity assay using WST-1 reagent for the effect of AuNP-KR13 (20 nm diameter) and KR13 alone on HOS $CD4^{+ve}$ $CCR5^{+ve}$ 48 hours post addition.; no statistically significant differences measured, P<<<0.05, n =3 using a t test.

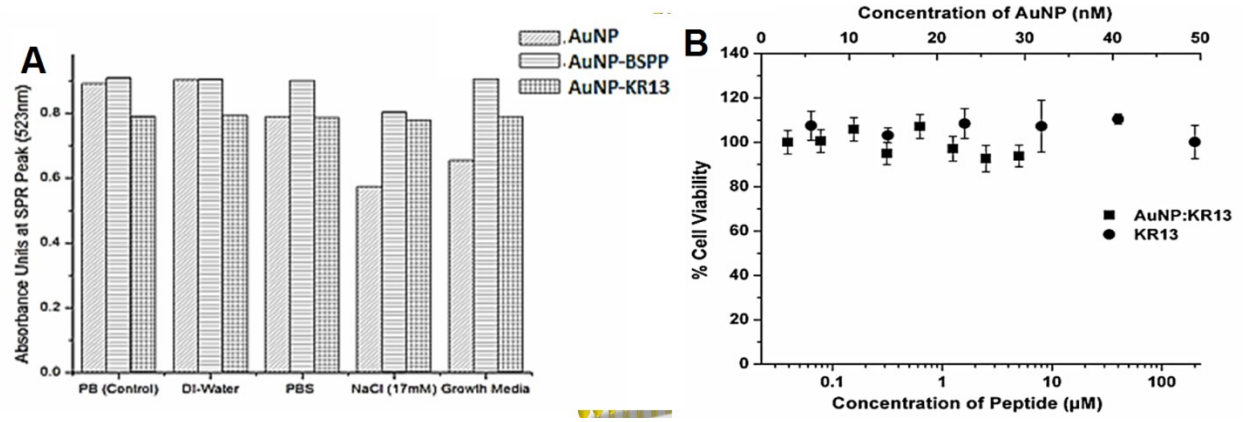

Figure 9: Flocculation assay of the AuNP in order to estimate the amount of peptide (KR13) required for stable conjugation. Equal concentration of AuNP is vigorously stirred with increasing concentration of KR13 for 30 minutes at room temperature. Following 1 M NaCl is added to the mixture and the absorbance at the surface plasmon resonance absorbance of AuNP (532 nm) is measured using a spectrophotometer. When the absorbance is stabilized, this shows that the conjugate is stable and no longer leads to aggregation, that concentration of the peptide to AuNP ratio is used for conjugation.

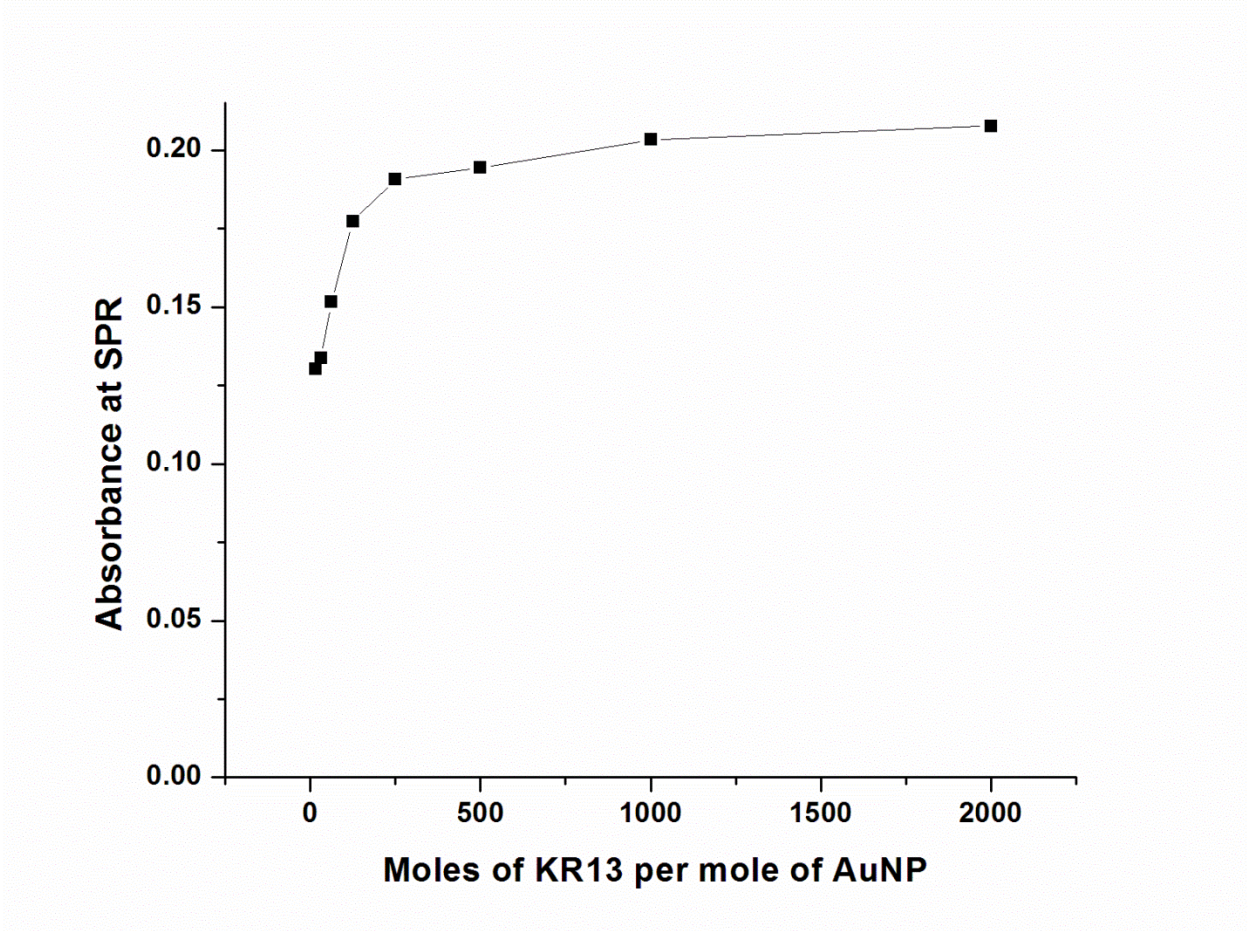

Figure 10: Zeta potential measurements from the zetasizer of the AuNP prior and post to KR13 addition. The diameters that are on the x-axis of the AuNP-KR13 is based off on the TEM and DLS measurements.

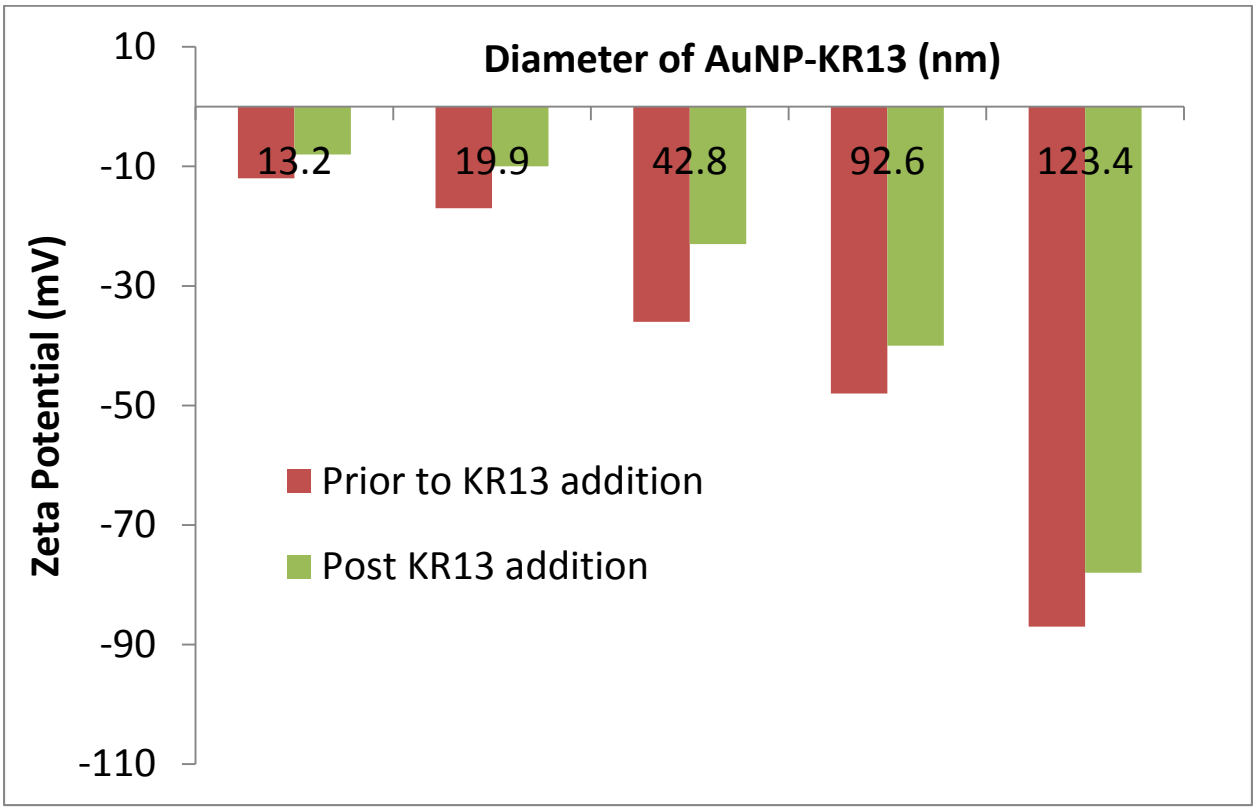

Figure 11: (A) Shows the activity of the HIV-1 BaL pseudotyped that have different levels of S375W mutant incorporated. The No. of spikes on the y-axis (red) is calculated from the gel image in the inset, assuming that one virus has 2500 molecules of p24 (Thali et al. 1994) and also that all spikes have three monomers incorporated. The gp120 content was measured using western blot analysis, the p24 release was measured using p24 ELISA and virus infection was measured using single round luciferase reporter gene assay as explained in detail in the methods. **(B)** Shows the gp120 monomer standard curve from the western blot analysis and the linear fit equation in the inset which was used to calculate the gp120 monomers in the HIV-1 BaL pseudotyped that have different levels of S375W mutant incorporated.

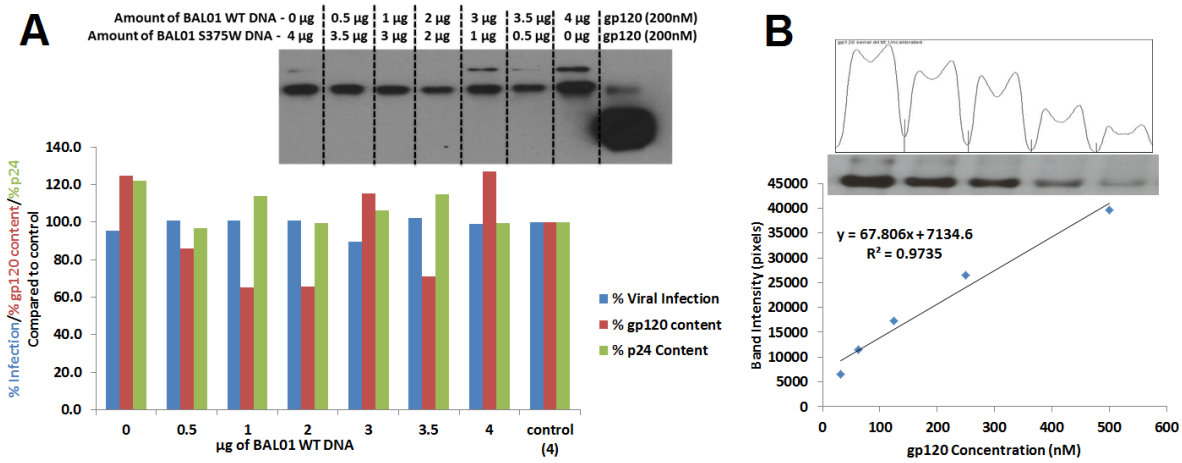

Figure 12: Comparing the anti-viral effects of KR13 **(A)** versus AuNP-KR13 (20 nm) **(B)**. This data is summarized from the raw data plots of viral infection inhibiton and p24 release of KR13 and AuNP-KR13 presented in figure 34 respectively. This shows that the higher the value of the hills coefficient the sharper the slope of the curve and the lower the anti-viral effect on the virion.

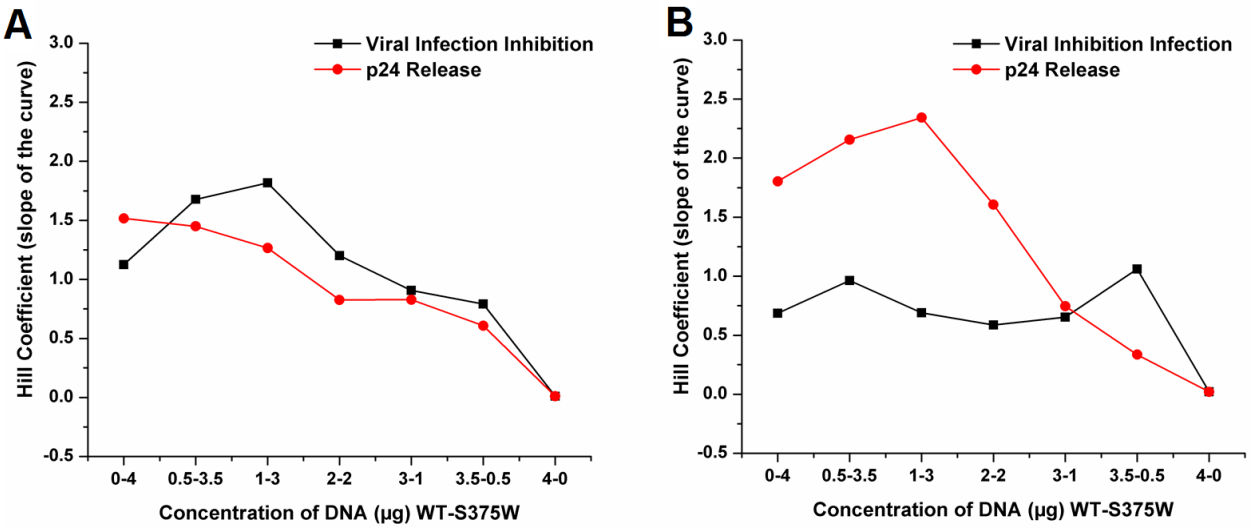

Figure 13: Representative images of the TEM images taken for intact virus, AuNP-KR13 (20 nm) and AuNP-KR13 (80 nm) at 50 nM concentration and treated with the HIV-1 BaL pseudotyped for 10 minutes at 37°C and fixed as explained in the methods. The samples are stained with 1% uranyl acetate and loaded onto a TEM copper grid and imaged using the JEM 2100 operated at 120 kV (JEOL, Japan).

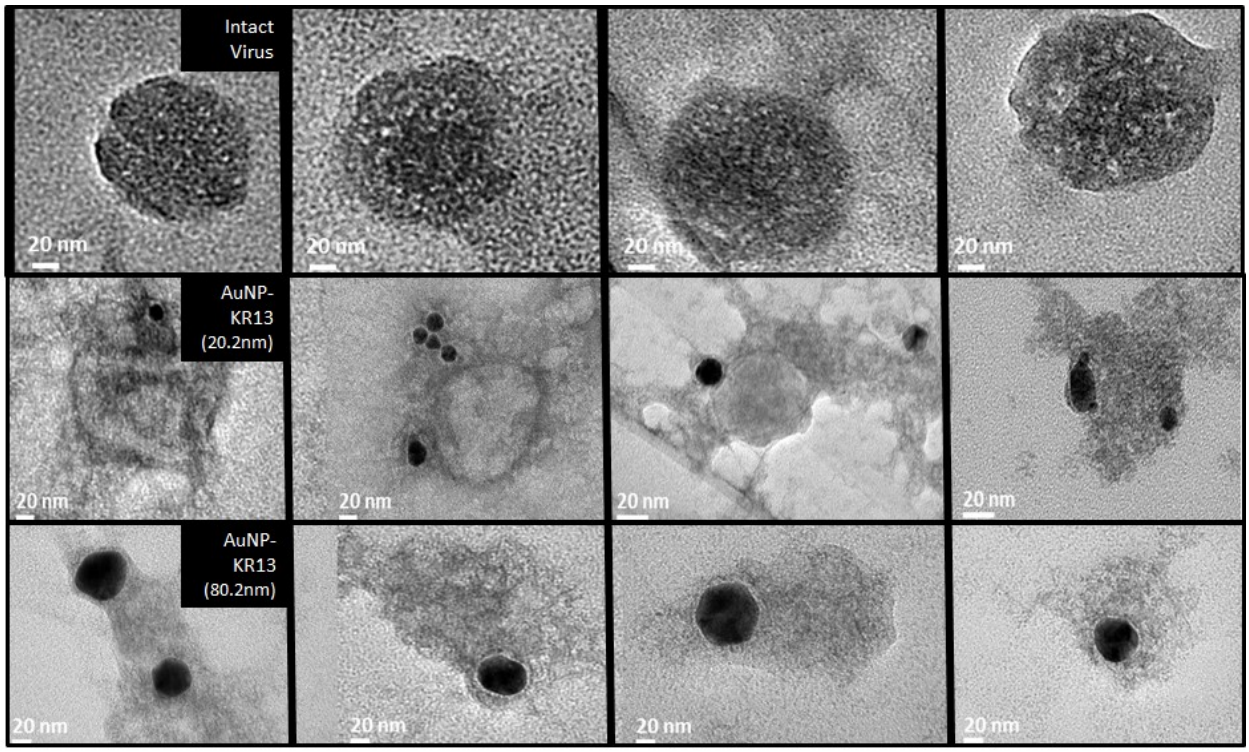

Figure 14: (A) KR13 and KR13b structure and bottom right shows how KR13 is conjugated on 20 nm AuNP. (B) Viral infection inhibition of HOS $CD4^{+ve}CCR5^{+ve}$ cells by KR13 (black) KR13b (red) and AuNP-KR13 (blue) and the IC_{50} values are 52.1 ± 3.4 nM, 147.3 ± 6.4 nM and 1.2 ± 2.4 nM respectively (C) p24 release from KR13, KR13b and AuNP-KR13 treated HIV-1 BaL pseudovirions. The samples are plotted using 100% as virions treated with 1% triton X and 0% as PBS treated virions. The EC_{50} values of the p24 release caused by KR13 and AuNP-KR13 are 3.15 ± 1.5 µM and 6.3 ± 5.1 nM. Origin Pro. 8 was used for sigmoidal curve fitting, n=3. Error bars represent standard deviation of n=3.

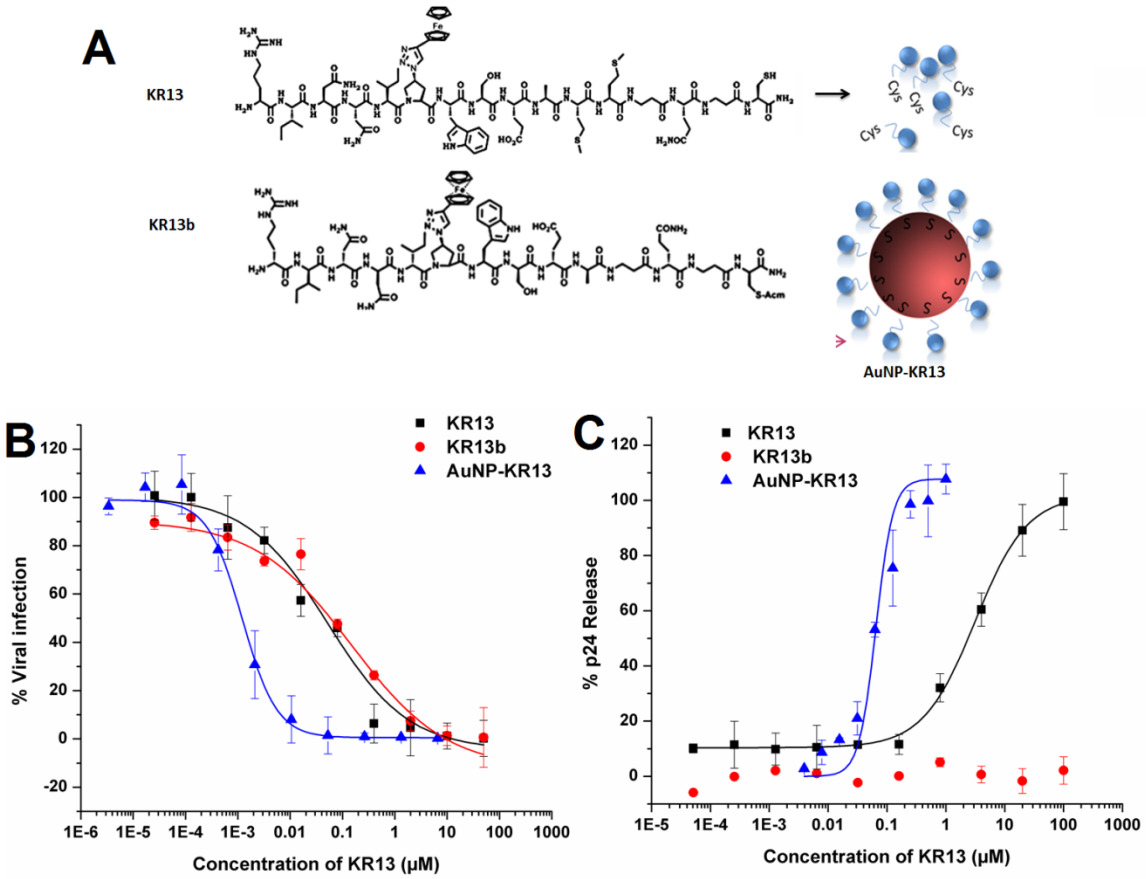

Figure 15: Testing the viral infection of the virions collected from producer 293T cells that are incubated with increasing concentrations of AuNP alone or AuNP-KR13s. The virions were collected and purified using a 6-20% iodixanol gradient and loaded onto a HOS $CD4^{+ve}CCR5^{+ve}$ and tested for infection 48 hours post addition. Error bars represent the standard deviation of the mean, n = 3.

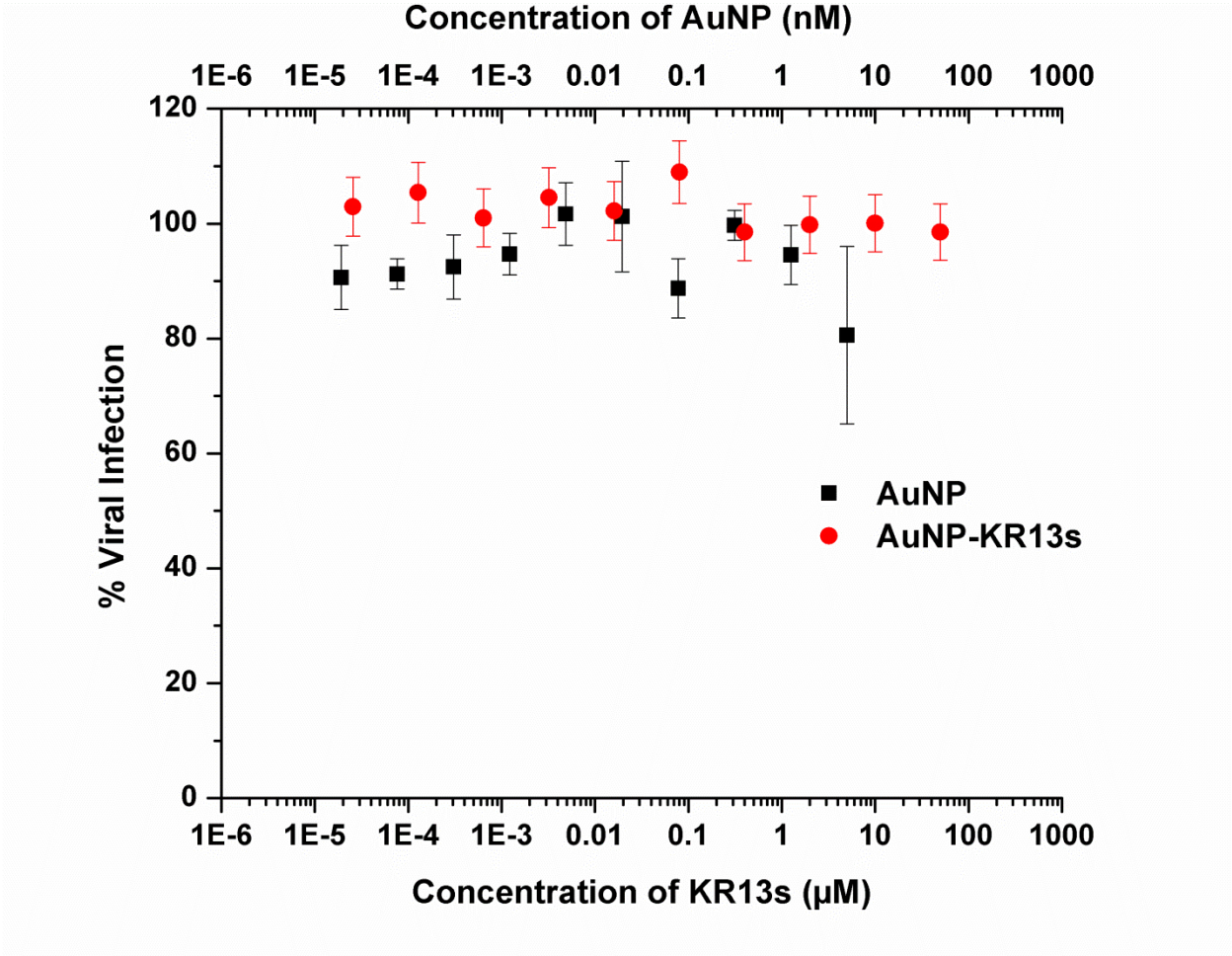

Figure 16: Cell viability of CHOK1 cells after 24 hours post KR13, KR13b and AuNP-KR13 treatment. The WST-1 pre-mix was used in order to test the cell viability and the absorbance was measured at 450 nm. CHOK1 cells treated with PBS for 24 hours were used as the 100% viability control. Error bars represent the standard deviation of the mean, n = 3.

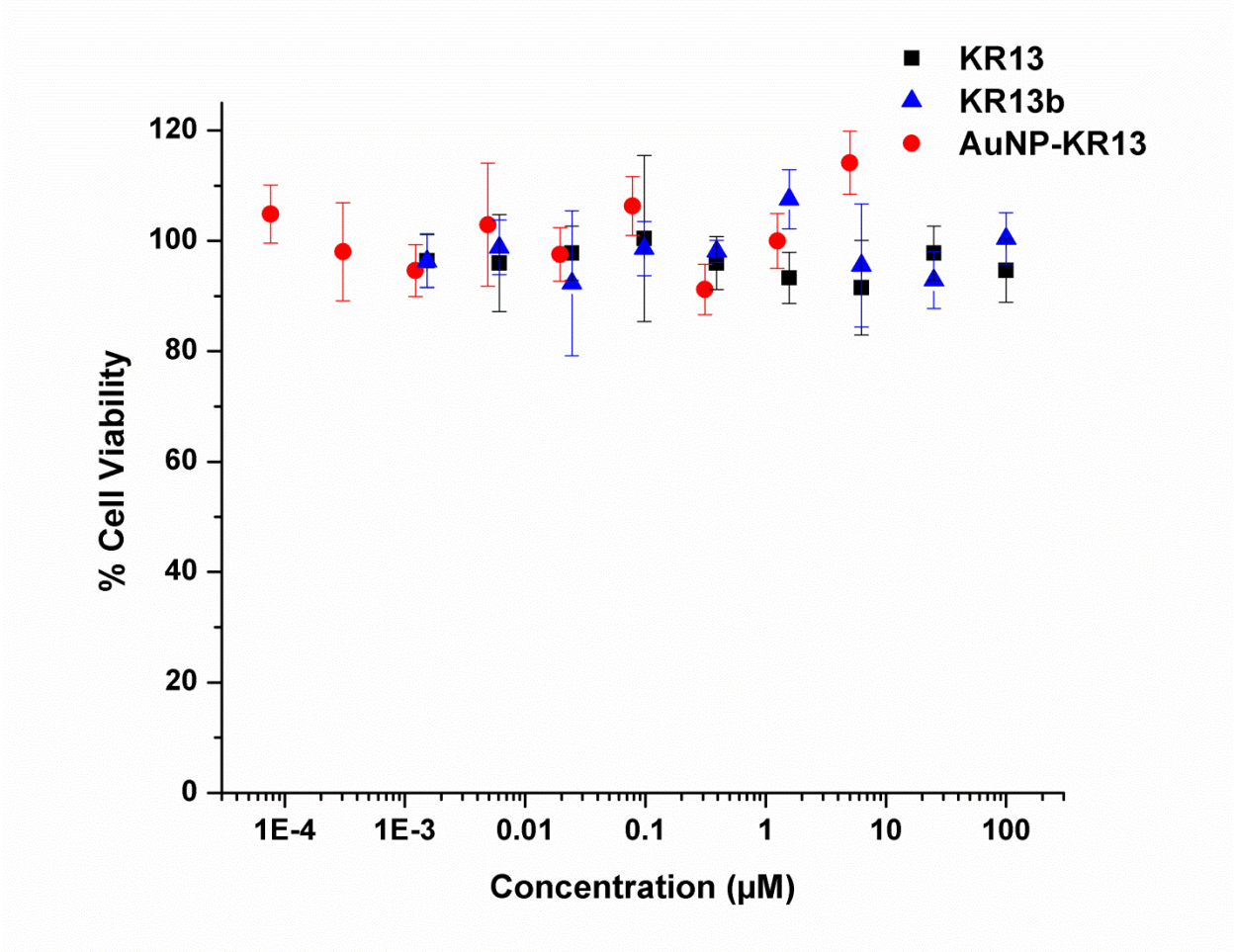

Figure 17: Cell viability of 293T cells transfected with S375W virion DNA and BAL-WT DNA, in the presence of KR13 and AuNP-KR13. 24 hours post KR13 and AuNP-KR13 treatment WST-1 pre-mix was used in order to test the cell viability and the absorbance was measured at 450 nm. 293T cells treated with PBS for 24 hours were used as the 100% viability control. Error bars represent the standard deviation of the mean, n = 3.